

# **Symmetrical and unsymmetrical donor–acceptor benzothiadiazoles**

**Ph.D. Thesis**

By  
**PRABHAT GAUTAM**



**DISCIPLINE OF CHEMISTRY  
INDIAN INSTITUTE OF TECHNOLOGY INDORE  
FEBRUARY, 2016**



# Symmetrical and unsymmetrical donor–acceptor benzothiadiazoles

A THESIS

*Submitted in partial fulfillment of the  
requirements for the award of the degree*

*of*

**DOCTOR OF PHILOSOPHY**

*by*

**PRABHAT GAUTAM**



**DISCIPLINE OF CHEMISTRY  
INDIAN INSTITUTE OF TECHNOLOGY INDORE  
FEBRUARY, 2016**





# INDIAN INSTITUTE OF TECHNOLOGY INDORE

## CANDIDATE'S DECLARATION

I hereby certify that the work which is being presented in the thesis entitled **Symmetrical and unsymmetrical donor–acceptor benzothiadiazoles** in the partial fulfillment of the requirements for the award of the degree of **DOCTOR OF PHILOSOPHY** and submitted in the **DISCIPLINE OF CHEMISTRY, Indian Institute of Technology Indore**, is an authentic record of my own work carried out during the time period from January, 2011 to January, 2016 under the supervision of Dr. Rajneesh Misra, Associate Professor.

The matter presented in this thesis has not been submitted by me for the award of any other degree of this or any other institute.

**Signature of the student with date  
(PRABHAT GAUTAM)**

-----  
This is to certify that the above statement made by the candidate is correct to the best of my/our knowledge.

**Signature of Thesis Supervisor with date  
(Dr. RAJNEESH MISRA)**

-----  
**PRABHAT GAUTAM** has successfully given his/her Ph.D. Oral Examination held on.....

Signature of Thesis Supervisor  
Date:

Convener, DPGC  
Date:

Signature of PSPC Member #1  
Date:

Signature of PSPC Member #1  
Date:

Signature of External Examiner  
Date:

-----



## ACKNOWLEDGEMENTS

The work described in this thesis would not have been possible without my close association with numerous people who were always there when I required them the most. I take this opportunity to acknowledge them and extend my sincere gratitude for helping me make this Ph.D. thesis a possibility.

I would like to begin with the person who made the biggest difference in my life, my mentor and supervisor, Dr. Rajneesh Misra. He has been there, in front of my eyes throughout my Ph.D., motivating and inspiring every bit of me towards new possibilities in life. He has been a living role model to me, taking up new challenges every day, tackling them with all his grit and determination and always thriving to come out victorious. It's his vigor and hunger to perform in adverse situation, which has inspired me to thrive for excellence and nothing less. His excellent supervision, advice and guidance from the very early stage made the completion of this study possible. I am indebted to him for his support, motivation and better understanding.

I express my heart-felt gratitude to Dr. Shaikh M. Mobin for single crystal X-ray support and his valuable guidance. I would also like to extend my gratitude to my PSPC members Dr. Tushar Kanti Mukherjee and Dr. Amit Kumar for their valuable suggestions and guidance.

With great pleasure, I express my respect to Prof. Pradeep Mathur (Director, Indian Institute of Technology Indore) for his unending encouragement and providing all the facilities at Indian Institute of Technology Indore.

I am grateful to Dr. Satya S. Bulusu (Head, Discipline of Chemistry, Indian Institute of Technology Indore) for his suggestions and guidance in various aspects. I am also grateful to Dr. Apurba Kumar Das, Dr. Suman Mukhopadhyay, Dr. Tridib K. Sarma, Dr. Anjan Chakraborty, Dr. Sampak Samanta, Dr. Biswarup Pathak, Dr. Sanjay Singh and Dr. Chelvam Venkatesh for their guidance and help during various activities.

I would like to acknowledge all the teachers I learnt from since my childhood, I would not have been here without their guidance, blessing and support.

I extend my profound thanks to my group members, Dr. Bhausahab, Ramesh, Thaksen, Rekha, Yuvraj, Mandeep, and Madhurima, Yogajivan, Bijesh, and Jeevan for their generous co-operation and help to make my work successful.

It has been wonderful to work with many friends and labmates together during my Ph.D., and I would like to record my thanks to Dr. Dnyaneshwar, Ms. Manideepa, Ms. Tamalika, Mr. N. Rajendra, Mr. Bhagwati. Dr. Indrajit, Mr. Shivendra, Ms. Anvita, Mrs. Veenu, Mr. Anupam, Ms. Sonam and Mr. Maruthi.

My heart-felt thanks to my splendid juniors at IIT Indore for their generous co-operation and help.

I am also thankful to all my friends who helped me directly-indirectly during my Ph. D. I am thankful to Ms. Sarita Batra, Mr. Kinney Pandey, Mr. Ghanshyam Bhavsar and Mr. Manish Kushwaha for their technical help and support.

I would like to express my thanks to IIT Indore for infrastructure and Council of Scientific and Industrial Research (CSIR), New Delhi for my Fellowship and all others who helped and supported me directly or indirectly.

I thank the Almighty for giving me the strength and patience to work through all these years.

Finally, I would like to acknowledge the people who mean world to me, my parents, uncle, aunty, my brothers, sisters and Upasana. I don't imagine a life without their love and blessings.

**Prabhat Gautam**



**DEDICATED TO  
MY TEACHERS, FAMILY AND  
FRIENDS**

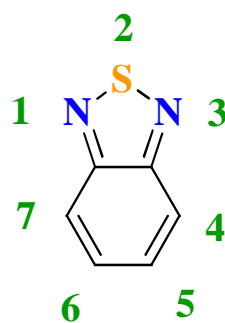
**–Prabhat**



## SYNOPSIS

In recent years research on benzothiadiazole (BTD) based molecular system with enhanced  $\pi$ -electron delocalization has gained significant attention of the scientific community due to their diverse photonic, and electronic applications. BTD is strong acceptor and its donor–acceptor (D–A) derivatives exhibit strong absorption, high fluorescence quantum yield, and excellent thermal and photochemical stability. The electronic and photonic properties of BTD based D–A system is a function of their HOMO–LUMO gap. The HOMO–LUMO gap of D– $\pi$ –A systems can be tuned either by altering the strength of D/A units or by varying the  $\pi$ -bridge. The D–A molecules with strong intramolecular charge-transfer and low HOMO–LUMO gap are potential candidates for organic photovoltaics.

A wide variety of donors (triphenylamine, carbazole, ferrocene, *etc.*) and acceptors (TCNE, TCNQ, BODIPY, *etc.*) have been explored in the design and synthesis of donor–acceptor systems.



**Figure 1.** 2,1,3-Benzothiadiazole (BTD).

Substitution of the donors and acceptors at 4- and 7-position of the BTD perturbs the photonic properties of these molecular systems significantly. In order

to tune the HOMO–LUMO gap, the BTD unit was functionalized with various donors, acceptors and linkers in symmetrical and unsymmetrical fashion. The effect of substitution of various D/A units on the photonic, thermal and electrochemical properties were studied.

The main objectives of present study are:

- To synthesize donor-substituted symmetrical BTDs of the type D– $\pi$ –A– $\pi$ –D and to study the effect of extension of  $\pi$ -conjugation length on the photophysical properties.
- To design and synthesize ferrocenyl-substituted symmetrical and unsymmetrical benzothiadiazoles by modulation of the  $\pi$ -spacer and acceptor units, and to compare their properties.
- To study the effect of systematic variation of D/A units on photophysical, thermal and electrochemical properties.
- To develop a smart strategy for tuning the HOMO–LUMO gap of donor-substituted symmetrical and unsymmetrical BTDs.
- To study the effect of the planar and non-planar orientation of the pyridyl and dipyridyl units on the mechanochromic behavior of unsymmetrical BTDs.

## **Chapter 1: Introduction.**

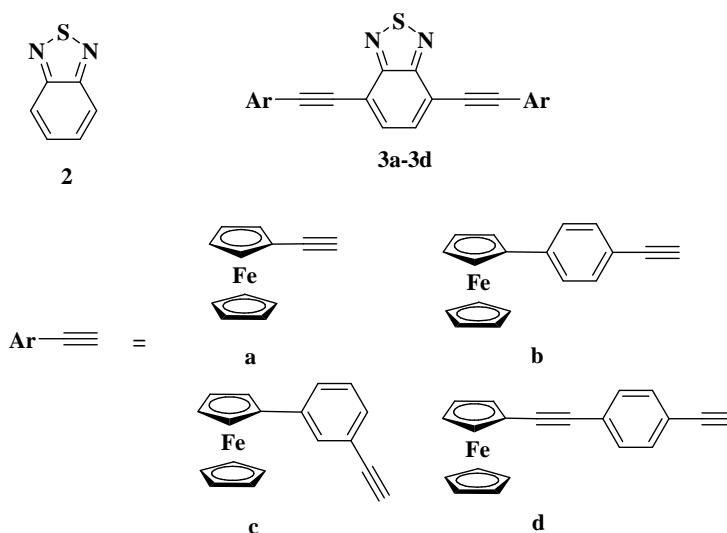
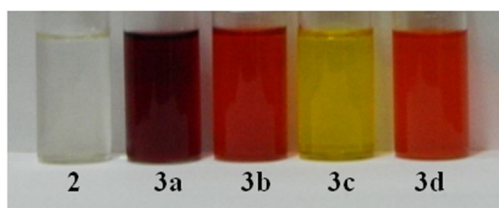
This chapter describes the synthesis and functionalization strategies of BTD derivatives, and their applications in diverse fields.

## **Chapter 2: Materials and experimental techniques.**

Chapter 2 summarizes the general experimental methods, characterization techniques and details of instruments used for characterization.

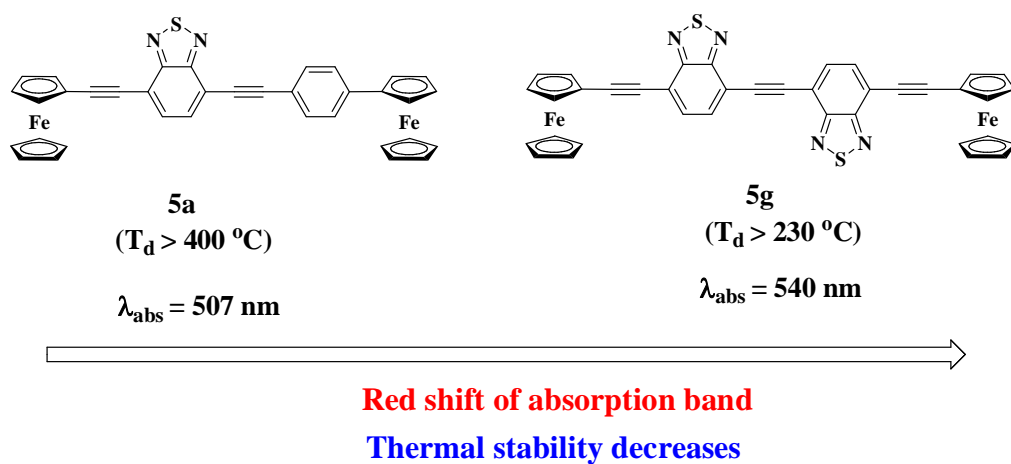
### Chapter 3: Donor- $\pi$ -acceptor- $\pi$ -donor benzothiadiazoles.

Chapter 3 describes a series of ferrocenyl-substituted symmetrical benzothiadiazole of the type D- $\pi$ -A- $\pi$ -D which were synthesized by the Pd-catalyzed Sonogashira cross-coupling reaction. Photonic, electrochemical, and thermal properties of these BTD systems have been explored. The UV-visible absorption results indicate strong intramolecular charge-transfer from ferrocene to BTD.



## Chapter 4: Donor–acceptor ferrocenyl-substituted benzothiadiazoles.

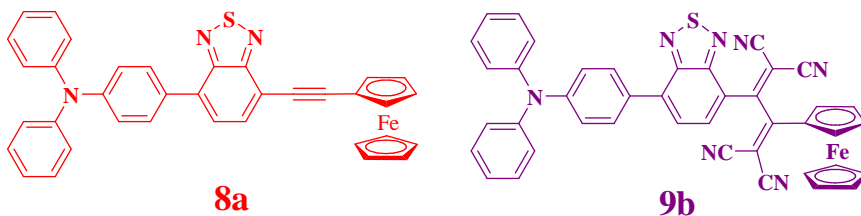
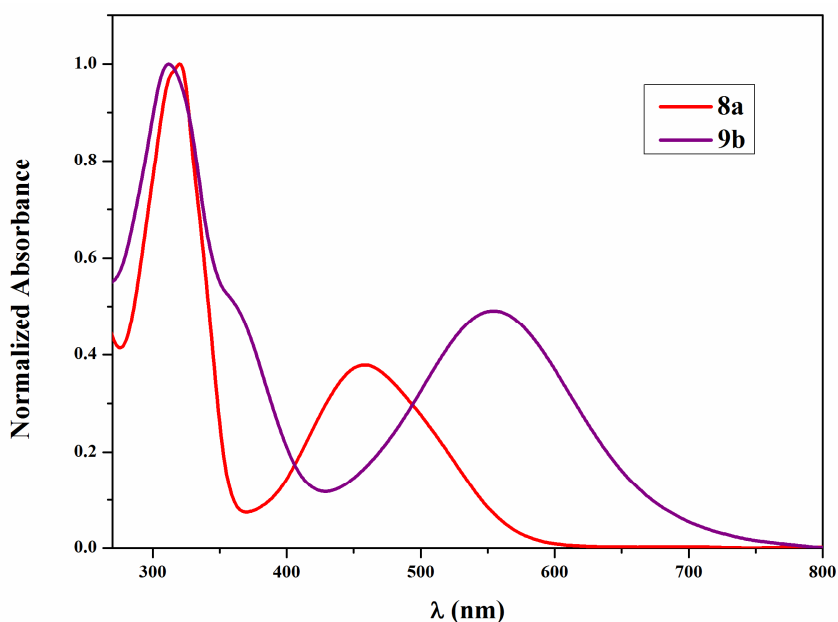
This chapter describes work on the design and synthesis of D– $\pi_1$ –A– $\pi_2$ –D unsymmetrical, and D– $\pi_1$ –A– $\pi_2$ –A– $\pi_1$ –D symmetrical type of ferrocenyl-substituted BTDs. Photophysical and electrochemical behavior of the ferrocenyl-substituted benzothiadiazoles show strong donor–acceptor interaction. Modulation of the  $\pi$ -spacer group between the donor and the acceptor units, and increasing the number of acceptor units results in significant perturbation in the photonic properties. An increase in the number of acceptor BTD unit results in the lowering of energy gap, which leads to the bathochromic shift of the absorption spectrum. Single crystal X-ray structures of ferrocenyl-substituted benzothiadiazoles show interesting supramolecular interactions.



## Chapter 5: Aryl-substituted unsymmetrical benzothiadiazoles.

Chapter 5 describes, a family of unsymmetrical donor–acceptor ferrocenyl substituted benzothiadiazoles of type D<sub>1</sub>– $\pi$ –A– $\pi$ –D<sub>2</sub>, D<sub>1</sub>– $\pi$ –A<sub>1</sub>– $\pi$ –A<sub>2</sub>, D<sub>1</sub>–A– $\pi$ –D<sub>2</sub> and D<sub>1</sub>–A<sub>1</sub>–A<sub>2</sub>–D<sub>2</sub> bearing a variety of electron donating and electron withdrawing groups, were designed and synthesized. Their

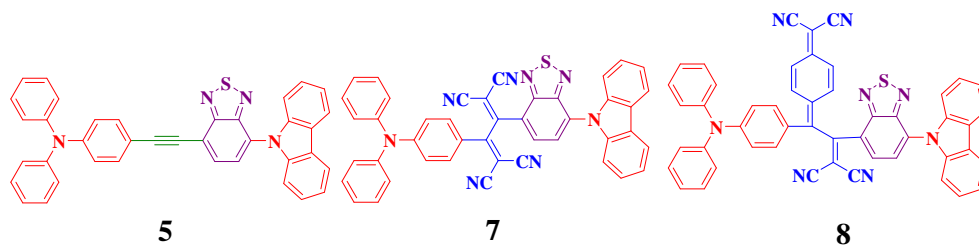
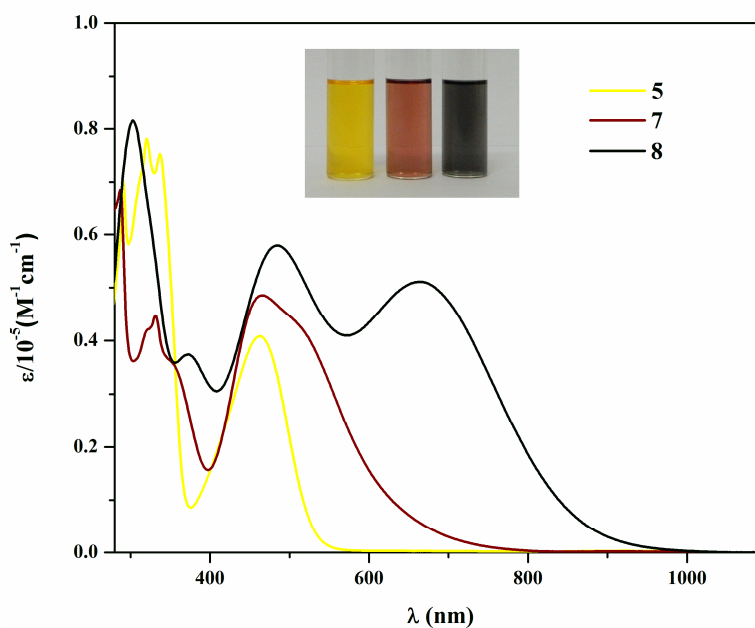
photophysical, electrochemical and computational properties were explored, which show strong donor–acceptor interaction. The presence of electron rich unit anthracene and triphenylamine, and electron deficient unit 1,1,4,4-tetracyanobuta-1,3-diene (TCBD) result in lowering of HOMO–LUMO gap, which leads to red shift of the absorption spectrum in these BTD based systems. The modulation of the donor and acceptor strength results in significant lowering of the HOMO–LUMO gap.



## **Chapter 6: Tuning of the HOMO–LUMO gap of symmetrical and unsymmetrical benzothiadiazoles.**

Chapter 6 reports the design and synthesis of donor-substituted symmetrical and unsymmetrical benzothiadiazoles (BTDs) of type D– $\pi$ –A–D, D<sub>1</sub>– $\pi$ –A–D<sub>2</sub>, D<sub>1</sub>–A<sub>1</sub>–A<sub>2</sub>–D<sub>2</sub>, D–A<sub>1</sub>–A<sub>2</sub>–D and D–A<sub>1</sub>–A<sub>2</sub>–A<sub>1</sub>–D by the Ullmann, Suzuki and [2 + 2] cycloaddition–retroelectrocyclization reactions. Photophysical, electrochemical and computational properties were studied which show substantial donor–acceptor interaction. Their single-photon absorption show strong charge-transfer bands in the near-infrared (NIR) region and the electrochemical reduction show multiple reduction waves. The dicyanoquinodimethane (DCNQ) and tetracyanobutadiene (TCBD) linkage of donor-substituted benzothiadiazole facilitates the reduction of the acceptor BTD unit and results in non-emissive nature of these molecular systems, which confirms the strong donor–acceptor interaction. Optical HOMO–LUMO gap of BTDs was found to be a function of the number and nature of the acceptors. The computational studies reveal that strong cyano-based acceptors, DCNQ and TCBD lower the LUMO level in these BTDs, which results in low HOMO–LUMO gap compared to acetylene linked BTDs. The BTDs having carbazole, and single DCNQ and TCBD acceptor show better thermal stability. These results clearly indicate that the number and nature of acceptor units perturbs the photonic properties, HOMO–LUMO gap and thermal stability of the BTDs.

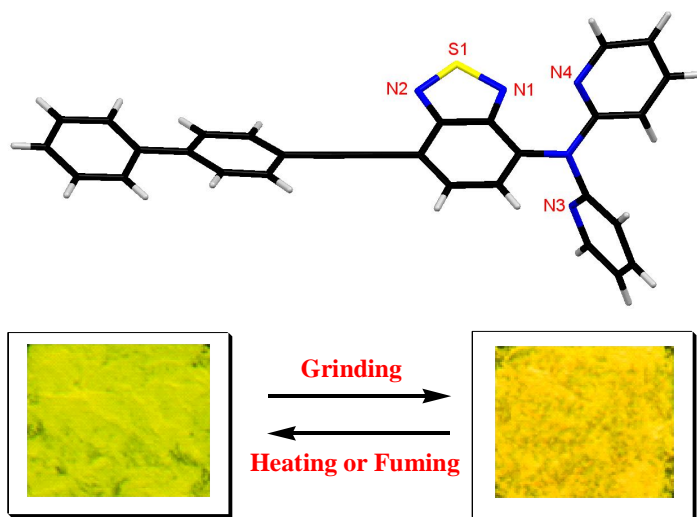




## Chapter 7: Reversible mechanochromism in unsymmetrical benzothiadiazole.

In this chapter we report the design and synthesis of unsymmetrical push–pull benzothiadiazoles (BTDs) of type  $D_1-\pi-A-\pi-D_2$  and  $D_1-\pi-A-D_2$  by the Pd-catalyzed Sonogashira, and Cu-catalyzed Ullmann coupling reactions. These BTDs show strong charge-transfer interaction. The photophysical, computational and single crystal X-ray studies reveal that the planar and non-planar orientation of pyridyl and dipyridyl units with respect to the benzothiadiazole core effectively alters the mechanochromic behavior. The planar orientation of pyridyl and BTD unit results no change in solid state emission whereas non-planar orientation of dipyridylamine and BTD unit results in efficient mechanochromism. The

dipyridylamine-substituted BTD show reversible mechanochromism with color contrast between yellow (crystalline state) and orange (amorphous state).



## Chapter 8: Conclusions and future scope.

Chapter 8 summarizes the salient features of the work and its future prospects.

## LIST OF PUBLICATIONS

1. Misra R.,\* **Gautam P.**, Jadhav T., Mobin S. M. (2013), Donor–acceptor ferrocenyl-substituted benzothiadiazoles: synthesis, structure, and properties, *J. Org. Chem.*, 78, 4940-4948 (DOI: 10.1021/jo4005734). †
2. Misra R.,\* **Gautam P.**, Mobin S. M. (2013), Aryl-substituted unsymmetrical benzothiadiazoles: synthesis, structure, and properties, *J. Org. Chem.*, 78, 12440-12452 (DOI: 10.1021/jo402111q). †
3. **Gautam P.**, Misra R.,\* Siddiqui S. A., Sharma G. D. (2015), Unsymmetrical donor–acceptor–acceptor– $\pi$ –donor type benzothiadiazole-based small molecule for a solution processed bulk heterojunction organic solar cell, *ACS Appl. Mater. Interfaces*, 7, 10283-10292 (DOI: 10.1021/acsami.5b02250)
4. Misra R.,\* **Gautam P.** (2014), Tuning of the HOMO–LUMO gap of donor-substituted symmetrical and unsymmetrical benzothiadiazoles, *Org. Biomol. Chem.*, 12, 5448-5457 (DOI: 10.1039/c4ob00629a). †
5. **Gautam P.**, Maragani, R., Mobin S. M., Misra R.\* (2014), Reversible mechanochromism in dipyridylamine-substituted unsymmetrical benzothiadiazoles, *RSC Adv.*, 4, 52526-52529 (DOI: 10.1039/C4RA09921D). †
6. **Gautam P.**, Misra R.,\* Koukaras E. N., Sharma A., Sharma G. D. (2015), Donor–acceptor–acceptor–donor small molecules for solution processed bulk heterojunction solar cells, *Org. Electron.*, 27, 72-83 (DOI: 10.1016/j.orgel.2015.09.006)
7. **Gautam P.**, Misra R.,\* Siddiqui S. A., Sharma G. D. (2015), Donor–acceptor– $\pi$ –acceptor based charge transfer chromophore as electron donors for solution processed small molecule organic bulk heterojunction solar cells, *Org. Electron.*, 19, 76-82 (DOI: 10.1016/j.orgel.2015.01.032)

8. **Gautam P.**, Maragani, R., Misra R.,\* (2015), Aryl-substituted symmetrical and unsymmetrical benzothiadiazoles, *RSC Adv.*, 5, 18288- 18294 (DOI: 10.1039/c4ra15424j)
9. **Gautam P.**, Dhokale B., Mobin S. M., Misra R.,\* Ferrocenyl BODIPYs: synthesis, structure and properties, *RSC Adv.*, 2, 12105-12107 (DOI: 10.1039/c2ra21964f)
10. Misra R.,\* **Gautam P.**, Sharma R., Mobin S. M. (2013), Donor– $\pi$ –acceptor– $\pi$ –donor ferrocenyl benzothiadiazoles: synthesis, structure, and properties, *Tetrahedron Lett.*, 54, 381-383 (DOI: 10.1016/j.tetlet.2012.11.016). †
11. Misra R.,\* **Gautam P.**, Maragani R. (2015) Ferrocenyl thiazoles: synthesis and properties, *Tetrahedron Lett.*, 56, 1664-1666 (DOI: 10.1016/j.tetlet.2015.02.031)
12. Misra R.,\* **Gautam P.** (2015), *Meso*-tetrakis(ferrocenylethynylphenyl) porphyrins: Synthesis and properties, *J. Organomet. Chem.*, 776, 83-88 (DOI: 10.1016/j.jorganchem.2014.11.006)
13. **Gautam P.**, Maragani R., Misra R.\* (2014), Tuning the HOMO–LUMO gap of donor-substituted benzothiazoles, *Tetrahedron Lett.*, 55, 6827-6830 (DOI: 10.1016/j.tetlet.2014.10.094)
14. **Gautam P.**, Dhokale B., Shukla V., Singh, C. P., Bindra K. S., Misra, R.\* (2012), Optical limiting performance of *meso*-tetraferrocenyl porphyrin and its metal derivatives, *J Photochem Photobiol A Chem*, 239, 24-27 (DOI: 10.1016/j.jphotochem.2012.04.020).
15. Misra R.,\* Maragani R., Pathak B., **Gautam P.**, Mobin S. M. (2015), Star shaped ferrocenyl substituted triphenylamines, *RSC Adv.*, 5, 71046-71051 (DOI: 10.1039/C5RA13400E)

16. Sharma R., **Gautam P.**, Misra R.,\* Shukla S. K. (2015),  $\beta$ -Substituted triarylborane appended porphyrins: photophysical properties and anion sensing, *RSC Adv.*, 5, 27069-27074 (DOI: 10.1039/C5RA03931B)
17. Misra, R.,\* Jadhav T., Dhokale B., **Gautam, P.**, Sharma R., Maragani R., Mobin S. M. (2015), Carbazole-BODIPY conjugates: design, synthesis, structure and properties, *Dalton Trans.*, 43, 13076-13086 (DOI: 10.1039/C4DT00983E)
18. Sharma R., **Gautam P.**, Mobin S. M., Misra R.\* (2013),  $\beta$ -Substituted ferrocenyl porphyrins: synthesis, structure, and properties *Dalton Trans.*, 42, 5539-5545 (DOI: 10.1039/C3DT00003F)
19. Dhokale B., **Gautam P.**, Mobin S. M., Misra R.\* (2013), Donor–acceptor, ferrocenyl substituted BODIPYs with marvelous supramolecular interactions Journal Article *Dalton Trans.*, 42, 1512-1518 (DOI: 10.1039/C2DT31632C)
20. Maragani R., **Gautam, P.**, Mobin S. M., Misra R.\* (2015), Tetracyanoethylene substituted triphenylamine analogues, *Tetrahedron Lett.*, 55, 7102-7105 (DOI: 10.1016/j.tetlet.2014.10.148)
21. Dhokale B., **Gautam P.**, Misra R.\* (2012) Donor–acceptor perylenediimide–ferrocene conjugates: synthesis, photophysical, and electrochemical properties, *Tetrahedron Lett.*, 53, 2352-2354 (DOI: 10.1016/j.tetlet.2012.02.107)

†Papers pertaining to the thesis.

## CONFERENCE PRESENTATION

1. Gautam P., Misra R.\* “Symmetrical and Unsymmetrical Benzothiadiazoles”, National Organic Symposium Trust, 10<sup>th</sup> J-NOST Conference for Research Scholars, IIT Madras, Chennai (04<sup>th</sup>–06<sup>th</sup> December 2014) Oral Presentation.....



# TABLE OF CONTENTS

<b>1. List of Figures</b>	xxvii
<b>2. List of Schemes</b>	xxxix
<b>3. List of Tables</b>	xxxix
<b>4. Acronyms</b>	xxxv
<b>5. Nomenclature</b>	xxxvii

## **Chapter 1: Introduction**

1.1. Background	1
1.2. Benzothiadiazole (BTD)	3
1.2.1. Classification of symmetrical and unsymmetrical benzothiadiazoles	4
1.2.2. Synthesis of 2,1,3-benzothiadiazole	5
1.3. Synthesis of other 2,1,3-thiadiazole derivatives	6
1.3.1. From 1,2-diamines and related compounds	6
1.3.2. Transformation of other heterocycles	6
1.3.3. Cross-coupling of 2,1,3 thiadiazoles	7
1.4. Applications of benzothiadiazoles	13
1.4.1. Nonlinear optics (NLO)	13
1.4.2. Two-photon absorption cross section	14
1.4.3. Dye sensitized solar cells (DSSCs)	15
1.4.4. Bulk heterojunction (BHJ) solar cells	15
1.4.5. Organic light emitting diodes (OLEDs)	17
1.4.6. Reversible mechanochromism	18
1.4.7. Sensing	20
1.5. Organization of thesis	21
1.6. References	22

## **Chapter 2: Materials and experimental techniques**

2.1. Introduction	33
2.2. Chemicals for synthesis	33
2.3. Spectroscopic measurements	33
2.3.1. Mass spectrometry	33

2.3.2.	NMR spectroscopy	33
2.3.3.	UV–vis spectroscopy	34
2.3.4.	Fluorescence spectroscopy	34
2.4	Electrochemical studies	34
2.5.	Single crystal X-ray diffraction studies	35
2.6	Powder X-ray diffraction (PXRD) studies	35
2.7	Computational calculations	35
2.8.	References	35
<b>Chapter 3:</b>	<b>Donor–<math>\pi</math>–acceptor–<math>\pi</math>–donor benzothiadiazoles</b>	
3.1.	Introduction	37
3.2.	Results and discussion	37
3.3.	Thermal properties	38
3.4.	Photophysical properties	39
3.5.	Electrochemical properties	40
3.6.	Single crystal X-ray diffraction studies	42
3.7.	Experimental section	44
3.8.	Conclusions	46
3.9.	References	46
<b>Chapter 4:</b>	<b>Donor-acceptor ferrocenyl-substituted benzothiadiazoles</b>	
4.1.	Introduction	51
4.2.	Results and discussion	52
4.3.	Thermogravimetric analysis	54
4.4.	X-ray analysis	55
4.5.	Photophysical properties	60
4.6.	Electrochemical properties	61
4.7.	Theoretical calculations	64
4.8.	Experimental section	65
4.9.	Conclusions	70
4.10.	References	71



<b>Chapter 5:</b>	<b>Aryl-substituted unsymmetrical benzothiadiazoles</b>	
5.1.	Introduction	79
5.2.	Results and discussion	80
5.3.	Thermogravimetric analysis	83
5.4.	Photophysical properties	84
5.5.	Theoretical calculations	88
5.6.	Electrochemical properties	91
5.7.	X-ray analysis	94
5.8.	Experimental details	100
5.9.	Conclusions	106
5.10.	References	107
<b>Chapter 6:</b>	<b>Tuning of the HOMO–LUMO gap of symmetrical and unsymmetrical benzothiadiazoles</b>	
6.1.	Introduction	115
6.2.	Results and discussion	116
6.3.	Photophysical properties	120
6.4.	Theoretical calculations	123
6.5.	Electrochemical properties	126
6.6.	Thermal stability	129
6.7.	Experimental section	131
6.8.	Conclusions	135
6.9.	References	136
<b>Chapter 7:</b>	<b>Reversible mechanochromism in unsymmetrical benzothiadiazoles</b>	
7.1.	Introduction	145
7.2.	Results and discussion	145
7.3.	Thermal properties	146
7.4.	Photophysical properties	147
7.5.	Theoretical calculations	148
7.6.	Mechanochromic properties	149
7.7.	X-ray Analysis	152

7.8.	PXRD analysis	155
7.9.	Experimental section	156
7.10.	Conclusions	158
7.11.	References	159
<b>Chapter 8:</b>	<b>Conclusions and future scope</b>	
8.1.	Conclusions	163
8.2.	Future scope	164
8.3.	References	165

## LIST OF FIGURES

<b>Chapter 1.</b>	<b>Introduction</b>	
<b>Figure 1.1.</b>	Structure of conjugated polymer (CP) and small molecule (SM).	1
<b>Figure 1.2.</b>	Structure of donors (red) and acceptors (blue).	2
<b>Figure 1.3.</b>	Effect of orbital couplings of donor and acceptor on HOMO–LUMO gap.	2
<b>Figure 1.4.</b>	Molecular structure of 2,1,3-Benzothiadiazole (BTD).	3
<b>Figure 1.5.</b>	Numbering system for 2,1,3-benzothiadiazol.	3
<b>Figure 1.6.</b>	Classification of symmetrical and unsymmetrical benzothiadiazoles in this work.	4
<b>Figure 1.7.</b>	Structure of two-photon absorbing BTD derivatives.	14
<b>Figure 1.8.</b>	Synthesis of BTD based donor–acceptor molecules for OLEDs.	18
<b>Chapter 3.</b>	<b>Donor–<math>\pi</math>–acceptor–<math>\pi</math>–donor benzothiadiazoles</b>	
<b>Figure 3.1.</b>	TGA plots of compounds <b>3a–3d</b> .	39
<b>Figure 3.2.</b>	Normalized absorption spectra of ferrocenyl benzothiadiazole <b>3a–3d</b> in dichloromethane at $4 \times 10^{-6}$ M concentration.	40
<b>Figure 3.3.</b>	Ferrocenyl benzothiadiazoles <b>3a–3d</b> in dichloromethane at $10^{-4}$ M concentration.	40
<b>Figure 3.4.</b>	Cyclic voltammogram of ferrocenyl benzothiadiazole <b>3a–3d</b> at 0.01 M concentration in 0.1 M $\text{Bu}_4\text{NPF}_6$ in dichloromethane recorded at $100 \text{ mVs}^{-1}$ scan speed.	41
<b>Figure 3.5.</b>	Single crystal X-ray structure of ferrocenyl benzothiadiazole <b>3a</b> . (a) Front view, and (b) Side view.	42
<b>Chapter 4.</b>	<b>Donor-acceptor ferrocenyl-substituted benzothiadiazoles</b>	
<b>Figure 4.1.</b>	TGA plots of ferrocenyl BTDs <b>5a–5h</b> at a heating rate of $10 \text{ }^\circ\text{C min}^{-1}$ , under nitrogen atmosphere.	55
<b>Figure 4.2.</b>	Single crystal X-ray structure of ferrocenyl BTDs <b>3a</b> , <b>5a</b> , and <b>5g</b> . (i) Top view, and (ii) side view.	57
<b>Figure 4.3.</b>	Packing diagram of ferrocenyl BTD <b>3a</b> forming 2D-network along the <i>a</i> -axis.	58
<b>Figure 4.4.</b>	Packing diagram of ferrocenyl BTD <b>5a</b> along the <i>b</i> -axis.	58

<b>Figure 4.5.</b>	Packing diagram of ferrocenyl BTD <b>5g</b> along the <i>c</i> -axis.	59
<b>Figure 4.6.</b>	Normalized electronic absorption spectra of ferrocenyl BTD <b>5a-5h</b> in dichloromethane at $1.0 \times 10^{-6}$ M concentration.	60
<b>Figure 4.7.</b>	Ferrocenyl BTDs <b>5a-5h</b> at $10^{-4}$ M concentration in DCM.	61
<b>Figure 4.8.</b>	Cyclic voltammogram of ferrocenyl BTDs <b>5f</b> , and <b>5h</b> at 0.01 M concentration in 0.1 M TBAPF <sub>6</sub> in dichloromethane recorded at a scan rate of $100 \text{ mVs}^{-1}$ .	63
<b>Figure 4.9.</b>	Cyclic voltammogram of ferrocenyl BTDs <b>5a-5e</b> , and <b>5g</b> at 0.01 M concentration in 0.1 M TBAPF <sub>6</sub> in dichloromethane recorded at a scan rate of $100 \text{ mVs}^{-1}$ .	64
<b>Figure 4.10.</b>	Correlation diagram showing the HOMO, and LUMO wave functions and energies of the BTDs <b>5a</b> (left), and <b>5g</b> (right), as determined at the B3LYP/6-31G** level for C, N, S, and H, and the Lanl2DZ level for Fe (Isovalue = 0.02).	65
<b>Chapter 5.</b>	<b>Aryl-substituted unsymmetrical benzothiadiazoles</b>	
<b>Figure 5.1.</b>	TGA plots of unsymmetrical BTDs <b>6a-6h</b> , <b>7a-7c</b> , <b>8a-8c</b> , and <b>9a-9b</b> at a heating rate of $10 \text{ }^{\circ}\text{C min}^{-1}$ , under nitrogen atmosphere.	84
<b>Figure 5.2.</b>	Normalized electronic absorption spectra of (i) benzothiadiazoles <b>6a-6h</b> , and (ii) benzothiadiazoles <b>7a-7c</b> , <b>8a-8c</b> , and <b>9a-9b</b> in dichloromethane at $1.0 \times 10^{-6}$ M concentration.	86
<b>Figure 5.3.</b>	Unsymmetrical benzothiadiazoles <b>6a-6h</b> , <b>7a-7c</b> , <b>8a-8c</b> , and <b>9a-9b</b> at $1 \times 10^{-4}$ M concentration in dichloromethane.	86
<b>Figure 5.4.</b>	HOMO and LUMO frontier orbitals of unsymmetrical benzothiadiazoles <b>6a-6h</b> at the B3LYP/6-31G** level for C, N, S, H, and Lanl2DZ level for Fe.	88
<b>Figure 5.5.</b>	HOMO and LUMO frontier orbitals of unsymmetrical benzothiadiazoles <b>7a-7c</b> , <b>8a-8c</b> , <b>9a</b> , and <b>9b</b> at the B3LYP/6-31G** level for C, N, S, H, and Lanl2DZ level for Fe.	90
<b>Figure 5.6.</b>	Cyclic voltammogram of unsymmetrical benzothiadiazoles <b>6a-6h</b> , <b>7a-7c</b> , <b>8a-8c</b> , <b>9a</b> , and <b>9b</b> representing the reduction wave (i, ii, and iii), and the oxidation wave (iv, v, and vi) at 0.01 M concentration in 0.1 M TBAPF <sub>6</sub> in dichloromethane recorded at a scan rate of $100 \text{ mVs}^{-1}$ .	91

<b>Figure 5.7.</b>	Cyclic voltammogram of BTD <b>9a</b> and <b>9b</b> representing the complete reduction waves at 0.01 M concentration in 0.1 M Bu <sub>4</sub> NPF <sub>6</sub> in dichloromethane recorded at 100 mVs <sup>-1</sup> scan speed.	92
<b>Figure 5.8.</b>	Single-crystal X-ray structure of ferrocenyl BTDs <b>6c</b> , <b>6g</b> , <b>7a</b> , and <b>7b</b> ; (i) front view and (ii) side view. Solvent molecule (Chloroform) is omitted from <b>7a</b> for clarity.	95
<b>Figure 5.9.</b>	Packing diagram of ferrocenyl BTD <b>6c</b> forming 2D zigzag chain along <i>a</i> -axis.	96
<b>Figure 5.10.</b>	Packing diagram of ferrocenyl BTD <b>6g</b> forming 2D zigzag chain along <i>a</i> -axis.	96
<b>Figure 5.11.</b>	Packing diagram of ferrocenyl BTD <b>7a</b> forming 2D sheet along <i>a</i> -axis	97
<b>Figure 5.12.</b>	Packing diagram of ferrocenyl BTD <b>7b</b> forming 2D sheet along <i>b</i> -axis.	98
<b>Chapter 6.</b>	<b>Tuning of the HOMO–LUMO gap of symmetrical and unsymmetrical benzothiadiazoles</b>	
<b>Figure 6.1.</b>	Electronic absorption spectra of benzothiadiazoles <b>5–12</b> in dichloromethane at $1.0 \times 10^{-5}$ M concentration.	120
<b>Figure 6.2.</b>	Benzothiadiazoles <b>5–12</b> at $1 \times 10^{-5}$ M concentration in dichloromethane.	121
<b>Figure 6.3.</b>	Emission spectra of BTD <b>5</b> and <b>6</b> at 0.1 absorption, excited at 462 nm and 473 nm respectively in dichloromethane (recorded at T = 293 K).	121
<b>Figure 6.4.</b>	HOMO and LUMO frontier orbitals of benzothiadiazoles <b>5–12</b> at the B3LYP/6-31G** level for C, N, S, and H.	123
<b>Figure 6.5.</b>	HOMO and LUMO frontier orbitals of benzothiadiazoles <b>5–12</b> at the B3LYP/6-31G** level for C, N, S, and H.	124
<b>Figure 6.6.</b>	Energy diagram of the frontier orbitals of benzothiadiazole <b>5–12</b> estimated by DFT calculations.	125
<b>Figure 6.7.</b>	Simulated UV-visible optical absorption spectra of BTD <b>7</b> at the TDDFT/CAM-B3LYP/6-31G** level for C, N, H, and S in dichloromethane.	125
<b>Figure 6.8.</b>	Cyclic voltammograms of benzothiadiazoles <b>5–12</b> at 0.01 M concentration in 0.1 M TBAPF <sub>6</sub> in dichloromethane recorded	

	at a scan rate of 100 mV s <sup>-1</sup> .	127
<b>Figure 6.9.</b>	Differential pulse voltammogram of benzothiadiazoles <b>5–12</b> at 0.01 M concentration in 0.1 M TBAPF <sub>6</sub> in dichloromethane (representing the oxidation waves).	128
<b>Figure 6.10.</b>	TGA plots of benzothiadiazoles <b>5–12</b> at a heating rate of 10 °C min <sup>-1</sup> , under nitrogen atmosphere.	130
<b>Chapter 7.</b>	<b>Reversible mechanochromism in unsymmetrical benzothiadiazoles</b>	
<b>Figure 7.1.</b>	TGA plots of <b>2</b> and <b>3</b> at a heating rate of 10 °C min <sup>-1</sup> , under nitrogen atmosphere.	147
<b>Figure 7.2.</b>	Electronic absorption and emission spectra of BTD <b>2</b> and <b>3</b> .	147
<b>Figure 7.3.</b>	HOMO and LUMO frontier orbitals of BTD <b>2</b> and <b>3</b> .	149
<b>Figure 7.4.</b>	DFT optimized structure of BTDs <b>2</b> (top) and <b>3</b> (bottom).	149
<b>Figure 7.5.</b>	Normalized absorbance of the solid sample of BTD <b>2</b> and <b>3</b> as prepared.	150
<b>Figure 7.6.</b>	Normalized absorbance of the sample of BTD <b>3</b> after grinding.	150
<b>Figure 7.7.</b>	Normalized emission of the solid sample of BTD <b>2</b> .	150
<b>Figure 7.8.</b>	Solid state emission spectra and fluorescence colour change induced upon grinding the solid sample of BTD <b>3</b> .	151
<b>Figure 7.9.</b>	<b>BTD 3</b> as prepared (Ap) and repeated switching of the solid-state fluorescence by repeated grinding (G) and heating (H) cycles.	152
<b>Figure 7.10.</b>	<b>BTD 3</b> as prepared (Ap) and repeated switching of the solid-state fluorescence by repeated grinding (G) and fuming (V) cycles.	152
<b>Figure 7.11.</b>	Crystal structure of <b>3</b> side view (above) and top view (below).	154
<b>Figure 7.12.</b>	Packing diagram of BTD <b>3</b> along the <i>b</i> -axis.	155
<b>Figure 7.13.</b>	Powder-XRD patterns of BTD <b>3</b> .	156

## LIST OF SCHEMES

<b>Chapter 1.</b>	<b>Introduction</b>	
<b>Scheme 1.1.</b>	Synthesis of 2,1,3-benzothiadiazole (BTD).	5
<b>Scheme 1.2.</b>	Synthesis of dibromo-BTD.	5
<b>Scheme 1.3.</b>	Mechanism of bromination of BTD.	5
<b>Scheme 1.4.</b>	Synthesis of BTD derivatives <i>via</i> 1,2-diamines and related	

	compounds.	6
<b>Scheme 1.5.</b>	Synthesis of BTB derivatives <i>via</i> transformation of other heterocycles.	7
<b>Scheme 1.6.</b>	Synthesis of BTB derivatives <i>via</i> Suzuki cross-coupling reaction of dibromo-BTB.	8
<b>Scheme 1.7.</b>	Synthesis of BTB derivatives <i>via</i> Suzuki cross-coupling reaction of pinacol esters of BTB.	8
<b>Scheme 1.8.</b>	Synthesis of BTB derivatives <i>via</i> Stille coupling of dibromo-BTB.	9
<b>Scheme 1.9.</b>	Synthesis of BTB derivatives <i>via</i> Sonogashira cross-coupling reaction of dibromo-BTB.	10
<b>Scheme 1.10.</b>	Synthesis of tetra-substituted BTB derivative <i>via</i> Sonogashira cross-coupling reaction.	10
<b>Scheme 1.11.</b>	Synthesis of linear and star shaped BTB derivatives <i>via</i> Heck coupling.	11
<b>Scheme 1.12.</b>	Synthesis of BTB derivatives <i>via</i> Heck coupling of dibromo-BTB.	12
<b>Scheme 1.13.</b>	Synthesis of carbazole-substituted BTB derivative.	13
<b>Scheme 1.14.</b>	Synthesis of BTB-substituted porphyrins for DSSCs.	15
<b>Scheme 1.15.</b>	Synthesis of BTB-based small molecule for BHJ solar cell.	16
<b>Scheme 1.16.</b>	Synthesis of [1,2,5]thiadiazolo[3,4- <i>c</i> ]pyridine (PT) based small molecule for (BHJ) solar cell.	17
<b>Scheme 1.17.</b>	Synthesis of trifluoromethyl-substituted BTB-cored phenylene vinylene fluorophore.	19
<b>Scheme 1.18.</b>	Synthesis of benzothiadiazole-cored cyano-substituted diphenylethene derivatives.	19
<b>Scheme 1.19.</b>	Synthesis of tetraphenylethene-substituted benzothiadiazoles.	20
<b>Scheme 1.20.</b>	Synthesis of water soluble bis-triazolyl BTB.	20
<b>Scheme 1.21.</b>	Synthesis of aryl or heteroaryl 5-substituted imidazo-benzothiadiazole derivatives.	21
<b>Chapter 3.</b>	<b>Donor-<math>\pi</math>-acceptor-<math>\pi</math>-donor benzothiadiazoles</b>	
<b>Scheme 3.1.</b>	Synthesis of ferrocenyl benzothiadiazoles <b>3a-3d</b> .	38
<b>Chapter 4.</b>	<b>Donor-acceptor ferrocenyl-substituted benzothiadiazoles</b>	
<b>Scheme 4.1.</b>	Synthetic route for BTB precursors <b>3a-3c</b> .	52

<b>Scheme 4.2.</b>	Synthetic route for ferrocenyl BTDs <b>5a-5c</b> , <b>5g</b> and <b>5h</b> .	53
<b>Scheme 4.3.</b>	Synthetic route for ferrocenyl BTDs <b>5d-5f</b> .	54
<b>Chapter 5.</b>	<b>Aryl-substituted unsymmetrical benzothiadiazoles</b>	
<b>Scheme 5.1.</b>	Synthetic route for mono-bromobenzothiadiazoles <b>3a</b> , <b>4a</b> , and <b>5a</b> .	80
<b>Scheme 5.2.</b>	Synthesis of unsymmetrical benzothiadiazoles <b>6a-6h</b> .	81
<b>Scheme 5.3.</b>	Synthesis of benzothiadiazoles <b>7a-7c</b> , and <b>8a-8c</b> .	82
<b>Scheme 5.4.</b>	Synthesis of benzothiadiazoles <b>9a</b> , and <b>9b</b> .	83
<b>Chapter 6.</b>	<b>Tuning of the HOMO–LUMO gap of symmetrical and unsymmetrical benzothiadiazoles</b>	
<b>Scheme 6.1.</b>	Synthesis of benzothiadiazoles <b>3</b> and <b>4</b> .	117
<b>Scheme 6.2.</b>	Synthesis of benzothiadiazoles <b>5</b> and <b>6</b> .	117
<b>Scheme 6.3.</b>	Synthesis of benzothiadiazoles <b>7</b> , <b>9</b> and <b>11</b> .	118
<b>Scheme 6.4.</b>	Synthesis of benzothiadiazoles <b>8</b> , <b>10</b> and <b>12</b> .	119
<b>Chapter 7.</b>	<b>Reversible mechanochromism in unsymmetrical benzothiadiazoles.</b>	
<b>Scheme 7.1.</b>	Synthesis of BTD <b>1</b> .	146
<b>Scheme 7.2.</b>	Synthesis of BTDs <b>2</b> and <b>3</b> .	146

## LIST OF TABLES

<b>Chapter 3.</b>	<b>Donor–<math>\pi</math>–acceptor–<math>\pi</math>–donor benzothiadiazoles.</b>	
<b>Table 3.1.</b>	Photophysical and electrochemical data of ferrocenyl benzothiadiazole <b>3a–3d</b> .	42
<b>Table 3.2.</b>	Crystal data and refinement parameters for <b>3a</b> .	43
<b>Table 3.3.</b>	Selected bond length and bond angle of <b>3a</b> .	44
<b>Chapter 4.</b>	<b>Donor-acceptor ferrocenyl-substituted benzothiadiazoles.</b>	
<b>Table 4.1.</b>	Crystal data and structure refinement for <b>3a</b> , <b>5a</b> and <b>5g</b> .	56
<b>Table 4.2.</b>	Photophysical, and electrochemical data of the ferrocenyl BTDs <b>5a–5h</b> .	62
<b>Chapter 5.</b>	<b>Aryl-substituted unsymmetrical benzothiadiazoles.</b>	
<b>Table 5.1.</b>	Photophysical, and thermal properties of the benzothiadiazoles <b>6a–6h</b> , <b>7a–7c</b> , <b>8a–8c</b> , <b>9a</b> , and <b>9b</b> .	87
<b>Table 5.2.</b>	Electrochemical data of unsymmetrical BTDs <b>6a–6h</b> , <b>7a-7c</b> , <b>8a-8c</b> , <b>9a</b> , and <b>9b</b> .	94



<b>Table 5.3.</b>	Crystal data and structure refinement for <b>6c</b> , <b>6g</b> , <b>7a</b> and <b>7b</b> .	99
<b>Chapter 6.</b>	<b>Tuning of the HOMO–LUMO gap of symmetrical and unsymmetrical benzothiadiazoles.</b>	
<b>Table 6.1.</b>	Photophysical, electrochemical and thermal stability data of benzothiadiazoles <b>5–12</b> .	122
<b>Table 6.2.</b>	Electrochemical data of benzothiadiazoles <b>5–12</b> .	129
<b>Chapter 7.</b>	<b>Reversible mechanochromism in unsymmetrical benzothiadiazoles.</b>	
<b>Table 7.1.</b>	Photophysical data of BTD <b>2</b> and <b>3</b> .	148
<b>Table 7.2.</b>	Crystal data and structure refinement for BTD <b>3</b> .	153
<b>Table 7.3.</b>	Selected bond length and bond angle of BTD <b>3</b> .	154



## ACRONYMS

D–A	Donor–acceptor
NLO	Nonlinear Optical
pH	The negative logarithm of hydronium-ion concentration ( $-\log_{10} [\text{H}_3\text{O}^+]$ )
SCXRD	Single Crystal X-ray diffraction
PXRD	Powder X-ray diffraction
NMR	Nuclear Magnetic Resonance
PPh <sub>3</sub>	Triphenylphosphine
DMF	Dimethylformamide
DCM	Dichloromethane
TGA	Thermogravimetric Analysis
Ph	phenyl
IR	Infrared
UV-Vis	UV-Visible Spectroscopy
...	Represents interaction
Calcd.	Calculated
CDCl <sub>3</sub>	Chloroform-d
ESI-MS	Electrospray Ionization- Mass Spectrometry
EtOH	Ethanol
MeOH	Methanol
THF	Tetrahydrofuran
TFA	Trifluoroacetic Acid
TLC	Thin Layer Chromatography
TEA	Triethylamine

DIEPA	<i>N,N</i> -Di-isopropyl-ethylamine
DIPA	<i>N,N</i> -Di-isopropylamine
DBU	1,8-Diazabicyclo[5.4.0]undec-7-ene

## NOMENCLATURE

$\lambda$	Wavelength
$\varepsilon$	Extinction coefficient
$\alpha$	Alfa
$\beta$	Beta
$\gamma$	Gamma
$\pi$	Pi
$\Phi$	Fluorescence quantum yield
$\sigma$	Sigma
$\text{\AA}$	Angstrom
nm	Nanometer
cm	Centimeter
$^{\circ}$	Degree
$^{\circ}\text{C}$	Degree Centigrade
mmol	Millimol
mL	Milliliter
$\mu\text{L}$	Microliter
a. u.	Arbitrary Unit

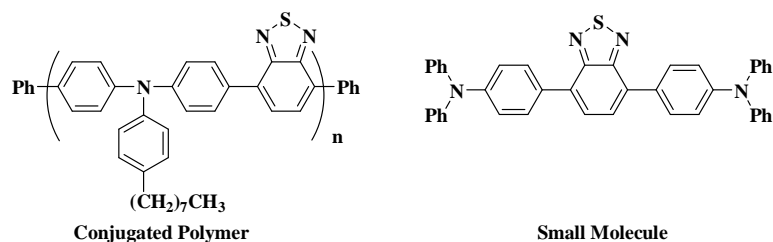


# Chapter 1

## Introduction

### 1.1. Background

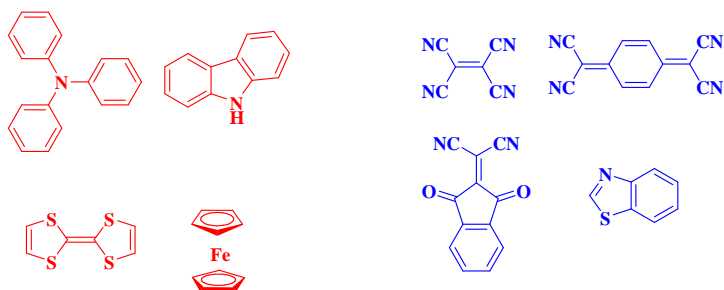
The systematic tuning of electronic and photonic properties of  $\pi$ -conjugated donor–acceptor (D–A) molecular systems has attracted the attention of scientific community due to their applications in organic electronics and organic photonics.<sup>[1]</sup> The electronic and photonic properties of the D–A system is a function of their HOMO–LUMO gap.<sup>[2,3]</sup> The HOMO–LUMO gap in D– $\pi$ –A systems can be tuned either by altering the strength of D/A units or by varying the  $\pi$ -bridge.<sup>[4]</sup> A variety of donors (triphenylamine, carbazole, *etc.*) have been attached to the electron acceptors (benzothiadiazole, diketopyrrolopyrrole, *etc.*) to design low HOMO–LUMO gap molecular systems.<sup>[5]</sup>



**Figure 1.1.** Structure of conjugated polymer (CP) and small molecule (SM).

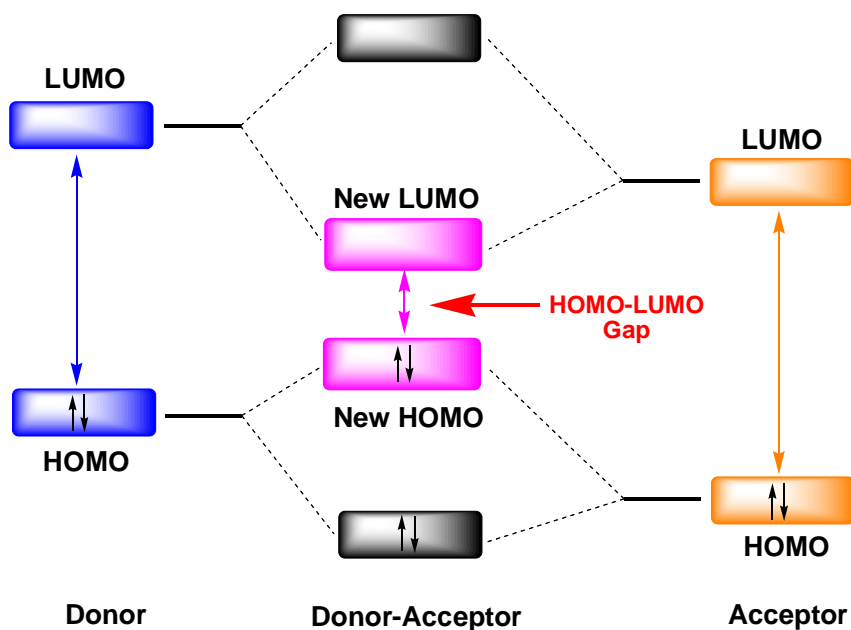
The design and synthesis of low HOMO–LUMO gap conjugated polymers and small molecules are of significant interest because of their potential applications in organic light emitting diodes (OLEDs) and organic photovoltaics (OPVs) (Figure 1.1.).<sup>[6]</sup> The small molecules have several advantages such as, high purity, definite molecular weight, well-defined molecular structure, and ease of purification that eliminate the disadvantages associated with their polymeric analogs.<sup>[7,8]</sup>

The linkage of an electron rich donor (D) and an electron deficient acceptor (A) either directly or through a  $\pi$ -linker is the most common approach to tune the HOMO–LUMO gap of small molecules. (Figure 1.2).<sup>[9]</sup>



**Figure 1.2.** Structure of donors (red) and acceptors (blue).

The effect of orbital couplings of donor and acceptor on HOMO–LUMO gap is well-described by the molecular orbital (MO) theory (Figure 1.3). The hybridization of the energy levels of the donor and acceptor raises the energy level of the HOMO, and lowers the energy level of the LUMO in the D–A system. This leads to low HOMO–LUMO gap and new molecular system with a broad absorption across the solar spectrum. This interesting feature has attracted many groups to develop new absorbing materials using D–A approach.<sup>[10]</sup>

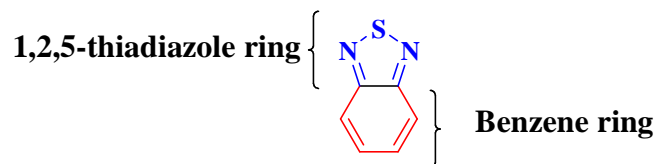


**Figure 1.3.** Effect of orbital couplings of donor and acceptor on HOMO–LUMO gap.



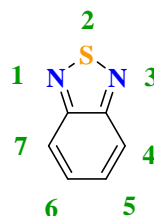
## 1.2. Benzothiadiazole (BTD)

2,1,3-Benzothiadiazole (BTD) is widely studied heterocyclic core in the field of organic electronics and photonics. As the name suggests “Benzo+thia+diazole”, the BTD core comprises of a benzene ring fused with diazole ring (azole ring containing two nitrogen atoms), where one of the C atom in the diazole ring is replaced by an S atom (Figure. 1.4.).



**Figure 1.4.** Molecular structure of 2,1,3-Benzothiadiazole (BTD).

Two different numberings of the thiadiazoles ring systems, 1,2,5- and 2,1,3- (for benzofused), have been used in the literature. The numbering system for 2,1,3-benzothiadiazole is shown below (Figure 1.5).<sup>[11,12]</sup>



**Figure 1.5.** Numbering system for 2,1,3-benzothiadiazole.

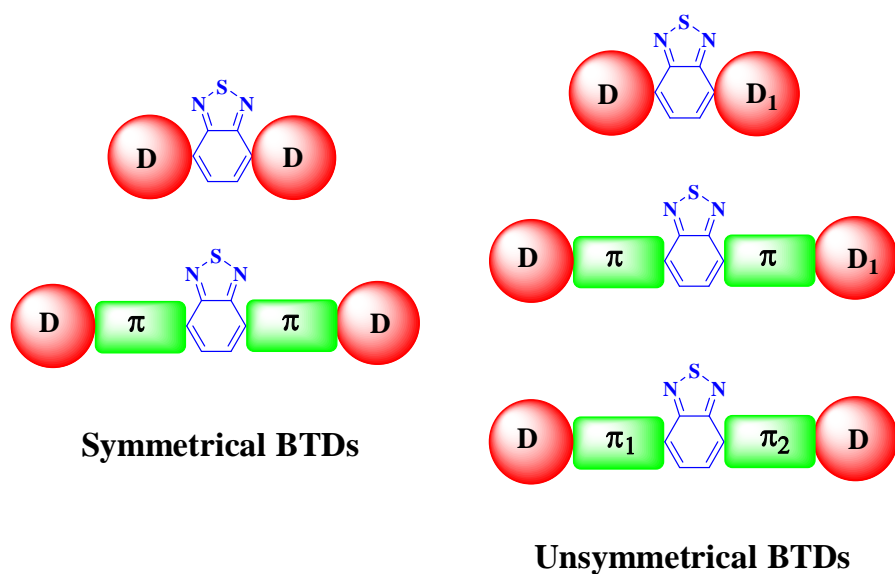
BTD is efficient electron acceptor and show high electron affinity due to the imine functionalities. The molecule can be better considered as a quasi-quinoidal structure as compared to a  $10\pi$  electron heteroaromatic system. The quasi-quinoidal structure with localized and relatively short  $\pi$ -bonds in the benzo ring tend to increase electronic coupling between substituents at the 4- and 7-positions.<sup>[2]</sup> Therefore the BTD unit is mostly substituted at the 4- and 7-positions. BTD and its derivatives possess several spectacular features like:<sup>[7,12]</sup>

(1) The heterocyclic five-membered ring ( $C=N-S-N=C$ ) is a strong acceptor and show high electron affinity.

- (2) BTD derivatives exhibit strong absorption throughout the visible region with high molar extinction coefficient.
- (3) D–A BTDs are efficient fluorophores.
- (4) BTD derivatives show well-ordered crystal structures with intermolecular interactions such as heteroatom contacts and  $\pi$ – $\pi$  interactions.
- (5) D–A BTDs exhibit excellent photochemical and thermal stability.
- (6) BTD derivatives exhibit tunable photonic properties and ease of synthetic functionalization.

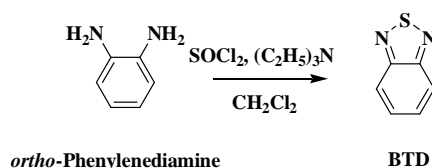
### 1.2.1. Classification of symmetrical and unsymmetrical benzothiadiazoles:

The classification of symmetrical and unsymmetrical benzothiadiazoles in this work is based on the substituents at the 4- and 7- positions. The substitution of same donor or linker units at both the positions on the BTD core result in symmetrical BTDs, whereas the substitution of different donor units (D and D<sub>1</sub>) or linkers ( $\pi$  and  $\pi_1$ ) at the 4- and 7-positions results in unsymmetrical BTDs (Figure 1.6).



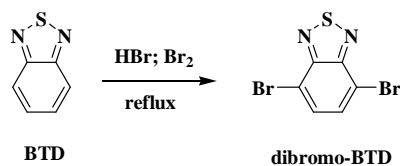
**Figure 1.6.** Classification of symmetrical and unsymmetrical benzothiadiazoles in this work.

**1.2.2. Synthesis of 2,1,3-benzothiadiazole:** The formation of a 1,2,5-thiadiazole ring from compounds containing two amino groups in *ortho*-positions is the most popular pathway. *ortho*-Phenylenediamine was treated with freshly distilled thionyl chloride in the presence of a base in the appropriate solvent which resulted 2,1,3-benzothiadiazoles after steam distillation (Scheme 1.1).<sup>[13]</sup>

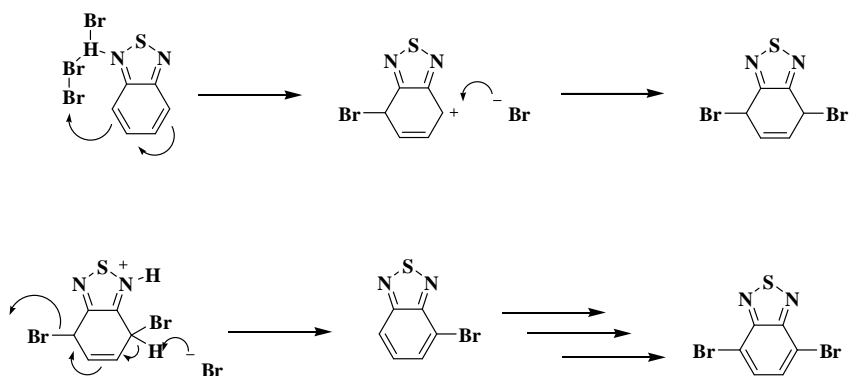


**Scheme 1.1.** Synthesis of 2,1,3-benzothiadiazole (BTB).

4,7-Dibromo-2,1,3-benzothiadiazole (**dibromo-BTB**) is the most commonly used intermediate for the synthesis of  $\pi$ -extended benzothiadiazole derivatives. The dibromo-BTB intermediate can be easily prepared by bromination of 2,1,3-benzothiadiazole in high yields (Scheme 1.2).<sup>[14]</sup>



**Scheme 1.2.** Synthesis of dibromo-BTB.



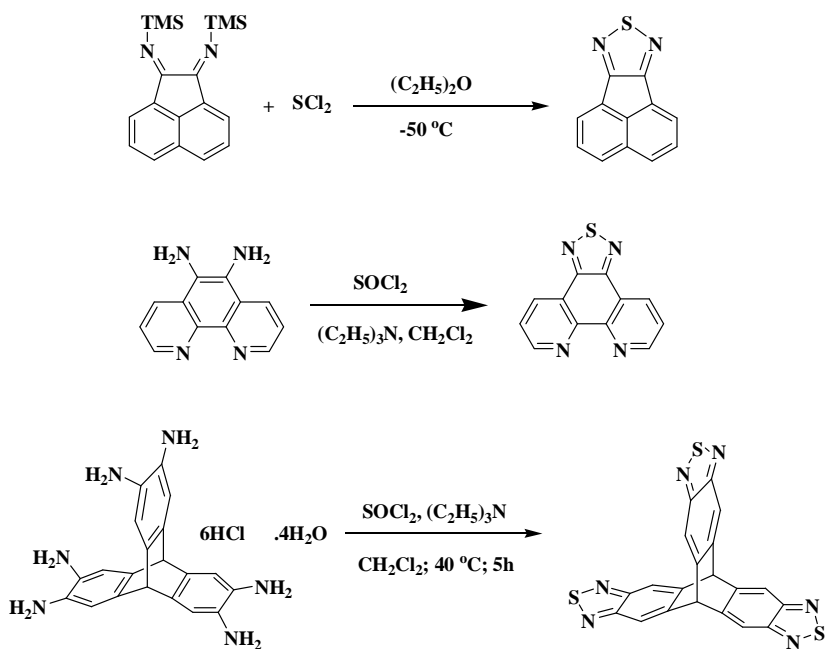
**Scheme 1.3.** Mechanism of bromination of BTB.

The dropwise slow addition of molecular bromine in hydrobromic acid, to a mixture of BTD in hydrobromic acid results 4,7-disubstituted dibromo-BTD regioisomer in high yields. The proposed mechanism is shown in Scheme 1.3.<sup>[13]</sup>

### 1.3. Synthesis of other 2,1,3-thiadiazole derivatives

The common synthetic methodology for the synthesis of 2,1,3-thiadiazole based derivatives are summarized in the following sections.

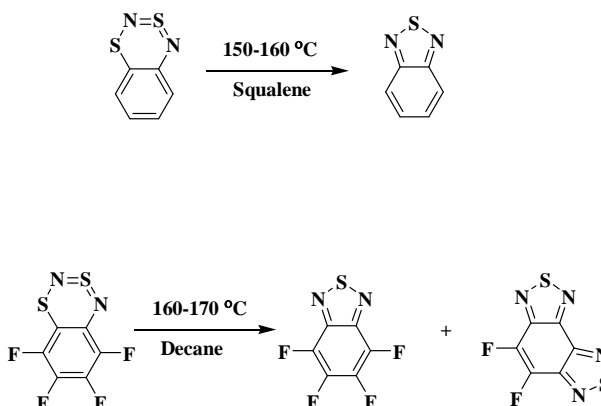
**1.3.1. From 1,2-diamines and related compounds:** The most widely used protocol for the preparation of 2,1,3-thiadiazole derivatives involves the introduction of a sulphur atom between the two *ortho*-amine groups. The reaction of *vicinal* diamine derivatives with thionyl chloride (SOCl<sub>2</sub>) in presence of an organic base is most general method for the synthesis of 2,1,3-thiadiazole derivatives. Usually the base employed is trimethylamine or pyridine (Scheme 1.4).<sup>[15]</sup>



**Scheme 1.4.** Synthesis of BTD derivatives *via* 1,2-diamines and related compounds.

**1.3.2. Transformation of other heterocycles:** The synthesis of BTD derivatives have also been achieved by transformation of other heterocycles by extrusion of

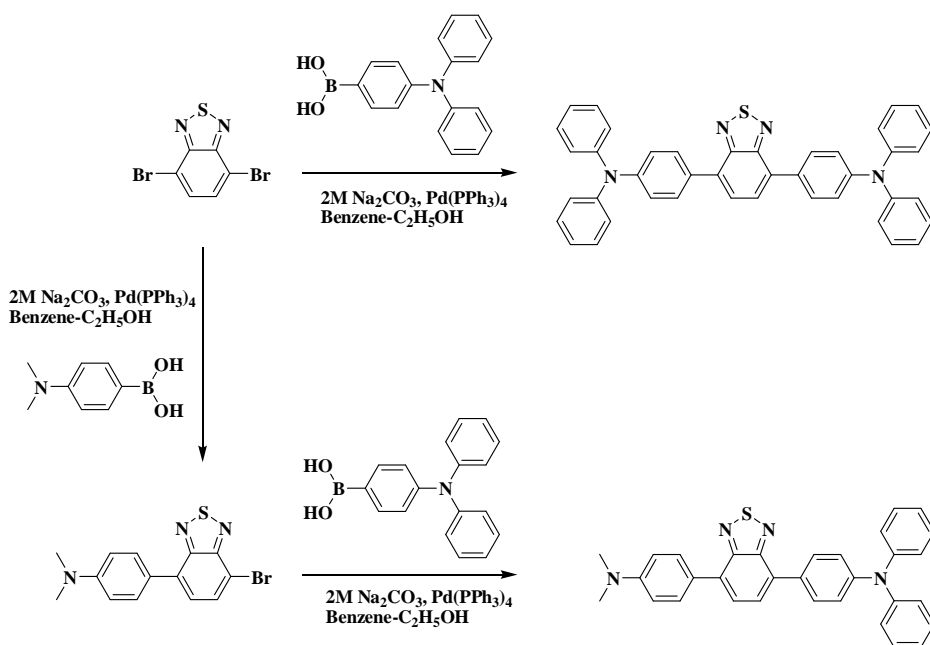
sulfur atom. The thermolysis of 1,3,4,8-tetrafluoro-2,4-benzodithiadiazine and its perfluoro-derivative resulted in complex mixtures of heterocycles along with compounds containing one or two 2,1,3-thiadiazole rings (Scheme 1.5).<sup>[16]</sup>



**Scheme 1.5.** Synthesis of BTB derivatives *via* transformation of other heterocycles.

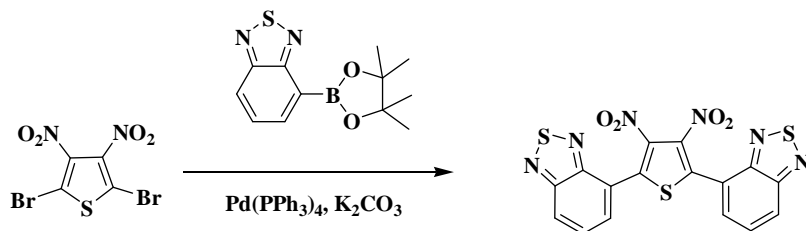
**1.3.3. Cross-coupling of 2,1,3-thiadiazoles:** The most common pathway for the design and synthesis of benzothiadiazole derivatives involves the Pd-catalyzed cross-coupling reaction of the BTB unit with the other aryl units.

**Suzuki Coupling:** The design and synthesis of donor–acceptor BTB derivatives *via* the Pd-catalyzed Suzuki cross-coupling reaction is one of the most commonly used protocol. This methodology usually involves the reaction of 4,7-dibromo-BTBs and arylboronic acids or esters in the presence of palladium catalysts such as *tetrakis*(triphenylphosphine)palladium(0) [Pd(PPh<sub>3</sub>)<sub>4</sub>] in the presence of a sodium and potassium carbonates as base. The reaction yields are generally high. Mataka *et al.* synthesized donor-substituted BTB derivatives by the reaction of 4,7-dibromo-BTB with arylboronic acids (Scheme 1.6).<sup>[17]</sup>



**Scheme 1.6.** Synthesis of BTD derivatives *via* Suzuki cross-coupling reaction of dibromo-BTD.

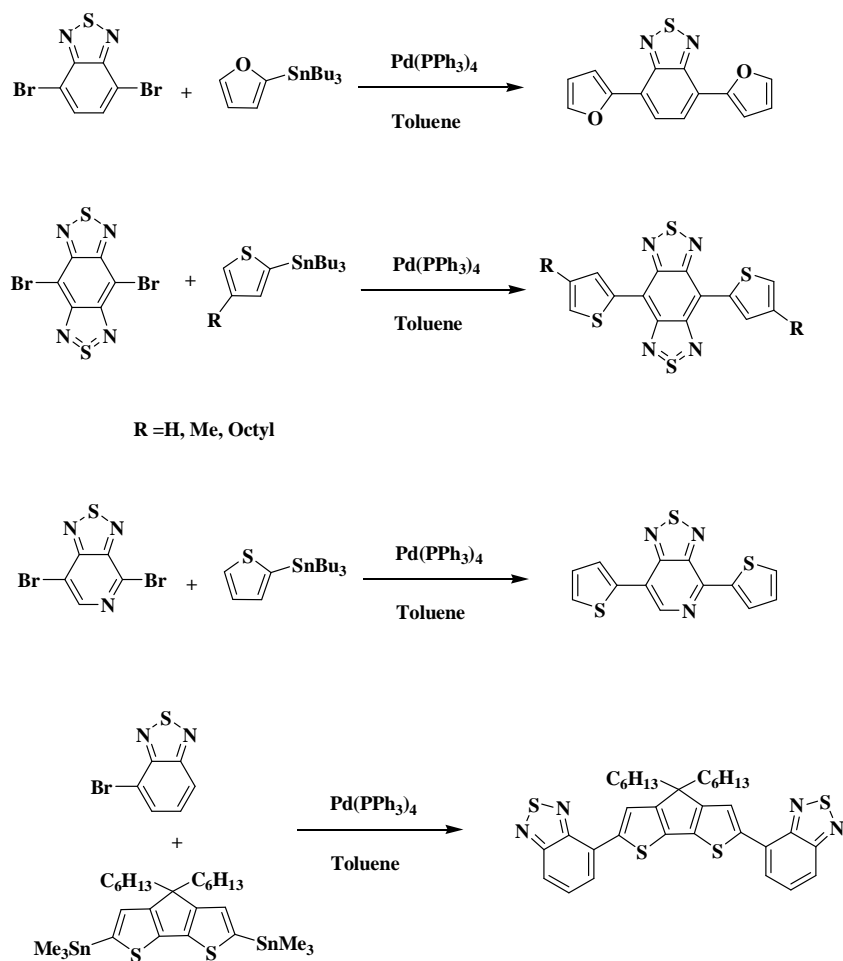
Alternatively the Suzuki cross-coupling reaction have also been carried out with the pinacol esters of BTD in moderate yields (Scheme 1.7).<sup>[18, 19]</sup>



**Scheme 1.7.** Synthesis of BTD derivatives *via* Suzuki cross-coupling reaction of pinacol esters of BTD.

**Stille Coupling:** The synthesis of BTD derivatives *via* the Pd-catalyzed Stille coupling reaction is another common protocol for the synthesis of donor–acceptor benzothiadiazoles. A variety of BTD derivatives have been prepared using the palladium catalysts such as *bis*(triphenylphosphine)palladium(II) dichloride [ $\text{Pd}(\text{PPh}_3)_2\text{Cl}_2$ ], *tetrakis*(triphenylphosphine)palladium(0) [ $\text{Pd}(\text{PPh}_3)_4$ ], and

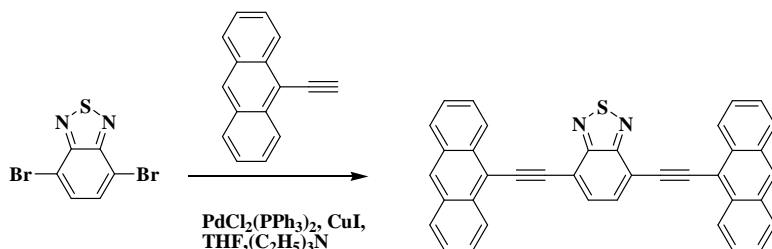
*tris*(dibenzylideneacetone)dipalladium(0) [Pd<sub>2</sub>(dba)<sub>3</sub>] with *tris*(*o*-tolylphosphine) ligand. The commonly used alkylstannanes are either tributyl- or trimethylstannanes. These reactions exhibit moderate to high yield. Some of the examples are shown below in Scheme 1.8.<sup>[20]</sup>



**Scheme 1.8.** Synthesis of BTD derivatives *via* Stille coupling of dibromo-BTD.

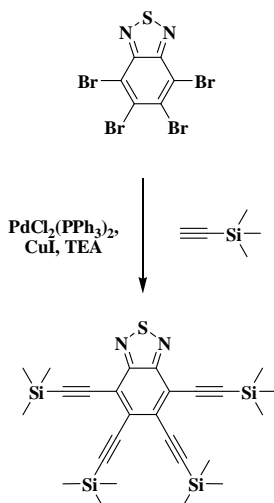
**Sonogashira Coupling:** The Pd-catalyzed Sonogashira cross-coupling is also an important protocol for the design and synthesis of donor–acceptor  $\pi$ -conjugated benzothiadiazoles. The standard conditions for Sonogashira reaction involves the treatment of the 4,7-dibromo-2,1,3-benzothiadiazole and the alkyne derivative with catalytic amounts of *bis*(triphenylphosphine)palladium(II) dichloride

[Pd(PPh<sub>3</sub>)<sub>2</sub>Cl<sub>2</sub>], and copper(I) iodide in the presence of an organic base (triethylamine or diisopropylamine). Some common example are shown in Scheme 1.9.<sup>[21]</sup>



**Scheme 1.9.** Synthesis of BTB derivatives *via* Sonogashira cross-coupling reaction of dibromo-BTD.

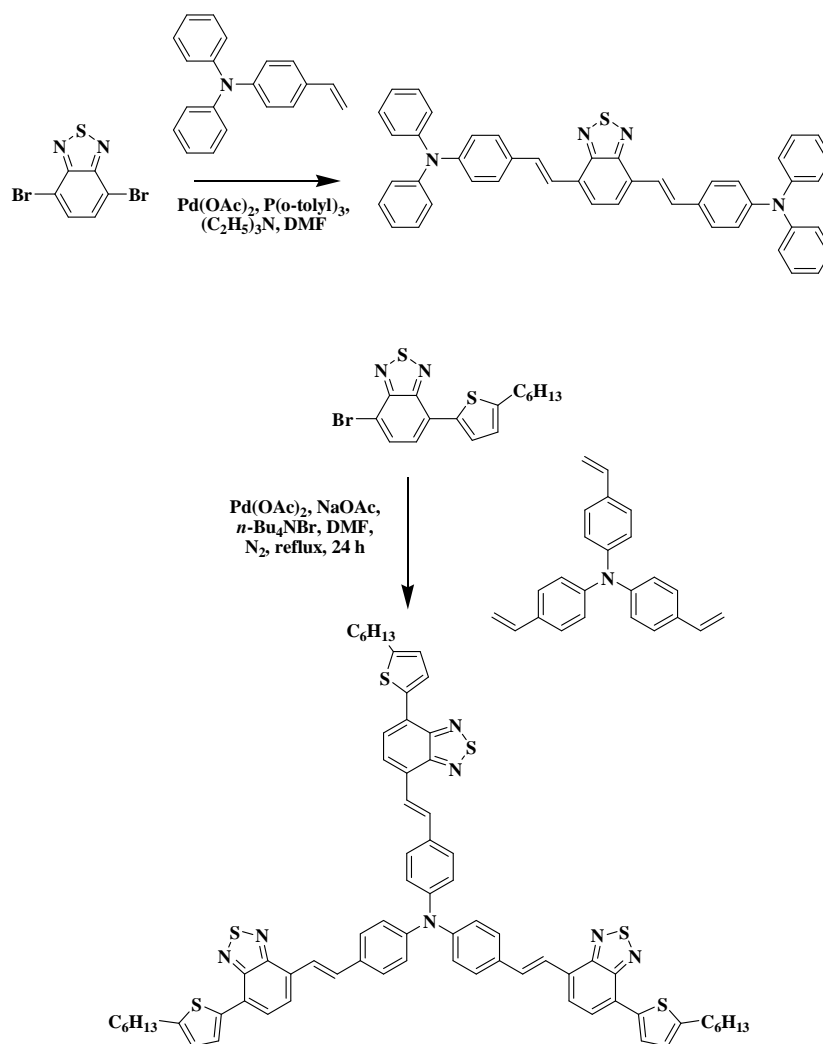
The Sonogashira cross-coupling has also been utilized for the synthesis of tetra-substituted BTB derivative by the reaction of tetrabromobenzothiadiazole. (Scheme 1.10).<sup>[22]</sup>



**Scheme 1.10.** Synthesis of tetra-substituted BTB derivative *via* Sonogashira cross-coupling reaction.

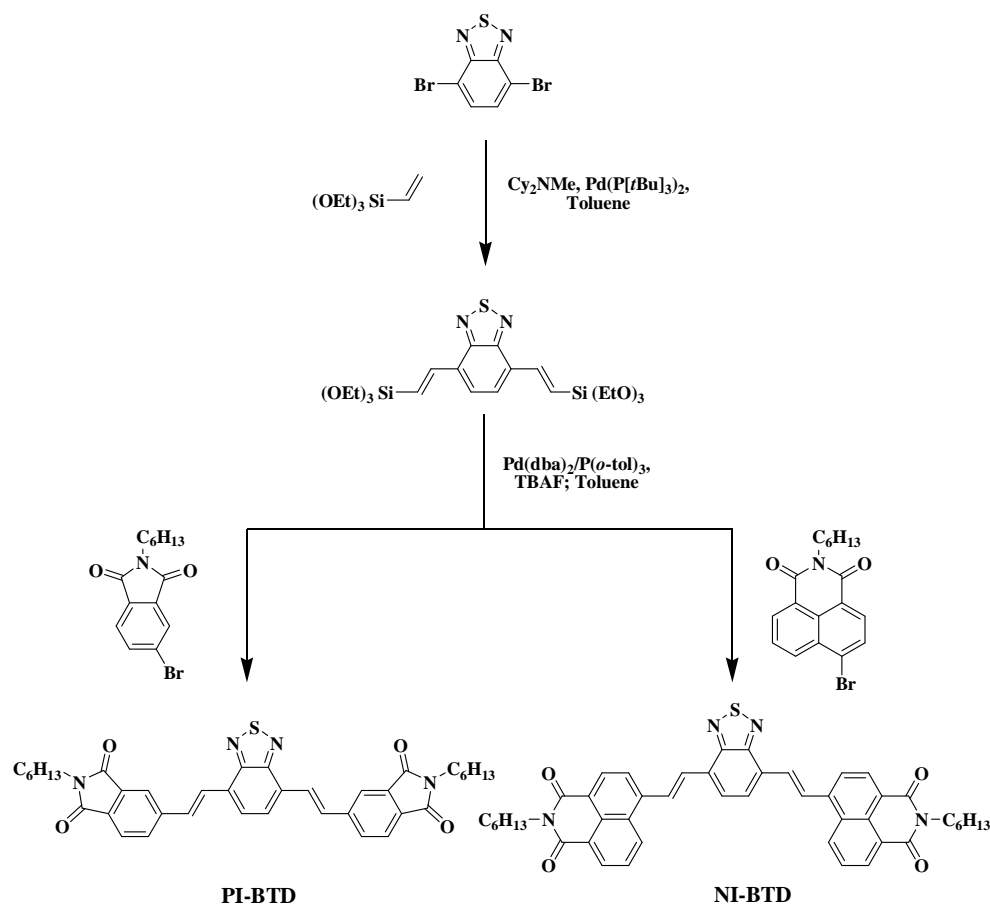


**Heck Coupling:** The Heck cross-coupling of 4,7-dibromo-BTD is a less frequently used protocol for the design of donor–acceptor BTDs as compared to the Suzuki, Stille or Sonogashira cross-coupling reactions. However it is an important methodology for incorporation of C=C bond for various optoelectronic applications. This methodology usually involves the reaction of 4,7-dibromo-BTD with alkenes catalyzed by palladium(II) acetate/tris(aryl)phosphine in the presence of a tertiary amine such as triethylamine or dicyclohexylmethylamine (Cy<sub>2</sub>NMe) as shown in Scheme 1.11. [23]



**Scheme 1.11.** Synthesis of linear and star shaped BTD derivatives *via* Heck coupling.

Alan Sellinger group designed and synthesized 4,7-bis(4-(*N*-hexylphthalimide)vinyl)benzo[*c*]1,2,5-thiadiazole (PI-BTD) and 4,7-bis(4-(*N*-hexylnaphthalimide)vinyl)benzo[*c*]1,2,5-thiadiazole (NI-BTD) through Heck coupling reactions (Scheme 1.12). The initial step involved the synthesis of silicon-based intermediate (BTD-Si) *via* the Heck reaction. The reaction of 4,7-dibromo-BTD with vinyltriethoxysilane in the presence of (Pd[P(*t*Bu)<sub>3</sub>]<sub>2</sub>) as a catalyst resulted silicon-based intermediate (BTD-Si). The final step involved the deprotection of the triethoxysilyl group to generate 4,7-divinylbenzo[*c*][1,2,5]thiadiazole *in situ* which reacted with *N*-hexyl-4-bromophthalimide and *N*-hexyl-4-bromo-naphthalimide in the presence of bis-(dibenzylideneacetone)palladium(0) (Pd(dba)<sub>2</sub>)/(P(*o*-tol)<sub>3</sub>) to give PI-BTD and NI-BTD (Scheme 1.12).<sup>[24]</sup>

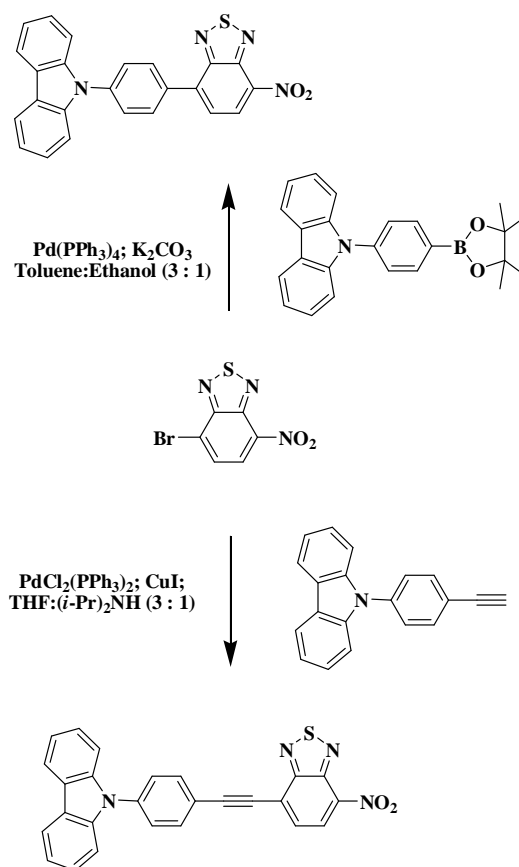


**Scheme 1.12.** Synthesis of BTD derivatives *via* Heck coupling of dibromo-BTD.

#### 1.4. Applications of benzothiadiazoles

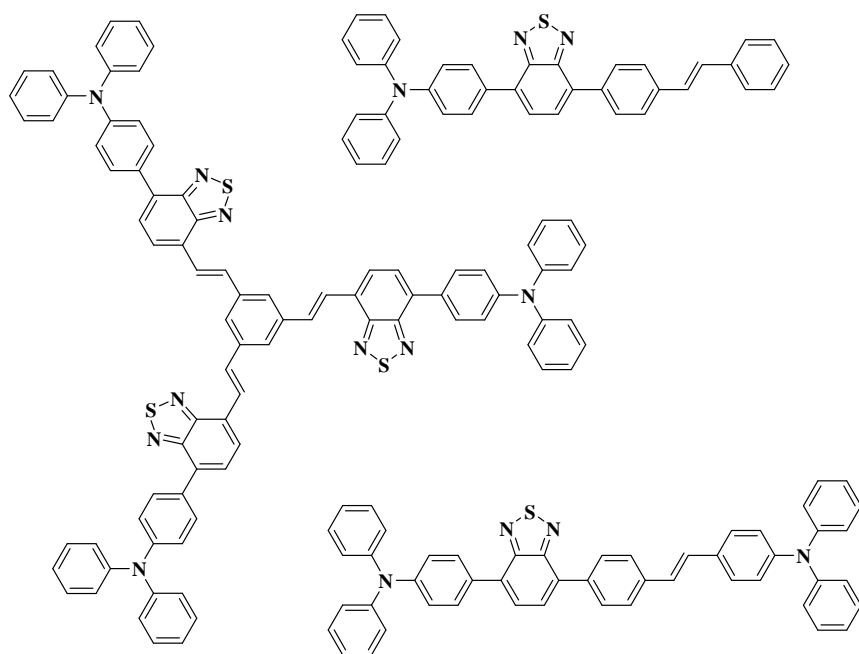
The donor–acceptor benzothiadiazole based molecular systems have been explored for a wide variety of application. Some of the common applications are discussed below:

**1.4.1. Nonlinear optics (NLO):** There has been considerable interest in the development of organic nonlinear optical materials. The benzothiadiazole (BTD) moiety is an important building block for NLO materials due to its large reduction potential and electron affinity. Yuliang Li group has designed a variety of donor-substituted BTDs as efficient NLO materials (Scheme 1.13).<sup>[25,26]</sup>



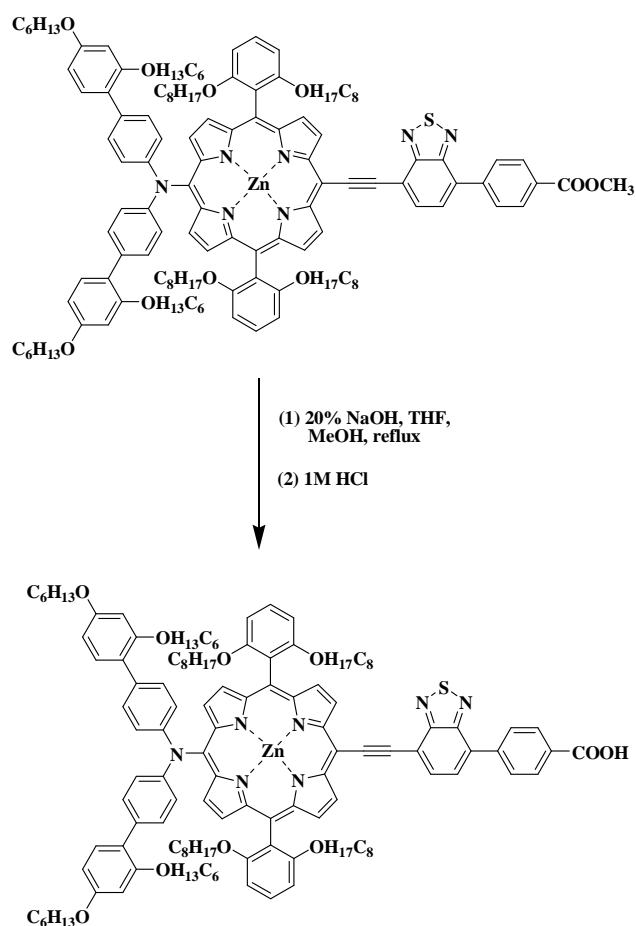
**Scheme 1.13.** Synthesis of carbazole-substituted BTD derivative.

**1.4.2. Two-photon absorption cross-section:** Donor–acceptor  $\pi$ -conjugated organic molecules with large two-photon absorption (TPA) cross-sections are potential candidate for various applications such as optical limiting, microfabrication, three-dimensional optical data storage, photodynamic therapy, and two-photon laser scanning fluorescence imaging. Fluorophores with large TPA cross-sections and high fluorescence quantum yields in the NIR region are required, in order to image at an increased penetration depth in tissues with less photodamage. Benzothiadiazole based D–A molecular systems exhibit enhanced intramolecular charge-transfer (ICT) and large stokes shift and hence beneficial for two-photon laser scanning fluorescence imaging (Figure 1.7). Mataka *et al.* designed and synthesized a variety of triphenylamine substituted BTDs and explored their two photon absorption properties. The TPA cross-sections was significantly high in three branched star-burst-type BTD as compared to the corresponding one-dimensional sub-units.<sup>[27,28]</sup>



**Figure 1.7.** Structure of two-photon absorbing BTD derivatives.

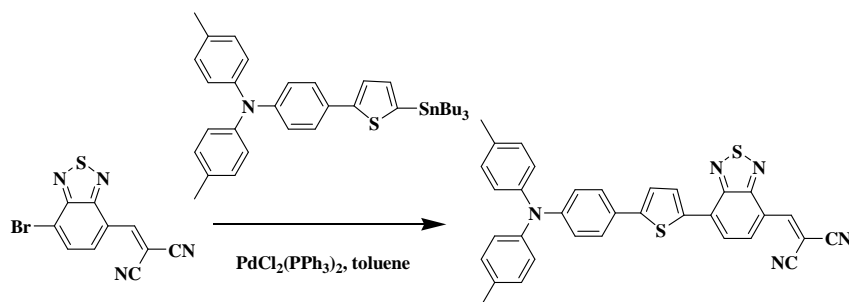
**1.4.3. Dye sensitized solar cells (DSSCs):** Increasing energy demands have prompted research on dye-sensitized solar cells (DSSCs) for efficient utilization of solar energy. DSSCs provides a promising potential because of their low production cost, tunable features, easy fabrication, and relatively high solar energy conversion efficiency. The strong acceptor BTD unit have been effectively utilized by Grätzel group to synthesize BTD-substituted porphyrins with over 13% efficiency (Scheme 1.14).<sup>[29,30]</sup>



**Scheme 1.14.** Synthesis of BTD-substituted porphyrins for DSSCs.

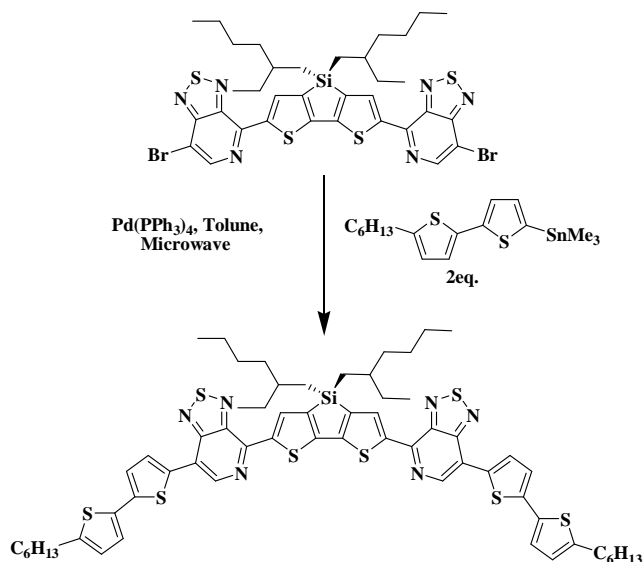
**1.4.4. Bulk heterojunction (BHJ) solar cells:** Organic solar cell (OSC) based on bulk heterojunction active layer is efficient approach to convert solar energy into electrical energy because of their advantages such of low cost, light weight

and flexibility. Solution-processed bulk-heterojunction (BHJ) solar cell was first reported by Friend *et al.* and followed by Heeger *et al.* in 1995.<sup>[31,32]</sup> Low band gap polymers are usually used as the donor materials with fullerene derivatives as acceptors for BHJ solar cells. Recently small molecules with low HOMO–LUMO gap have also been used as donor materials in BHJ solar cells. A variety of low HOMO–LUMO gap D–A molecular systems based on BTB acceptor unit have been designed and synthesized owing to its strong electron affinity. Wong *et al.* reported a novel D–A–A-type donor molecule, 2-([7-(5-*N,N*-ditolylaminothiophen-2-yl)-2,1,3-benzothiadiazol-4-yl]methylene)malononitrile (DTDCTB) based on the electron-accepting BTB unit (Scheme 1.15). The organic solar cells employing DTDCTB as donor and C<sub>70</sub> as acceptor achieved a high power conversion efficiency (PCE) of 5.81%.<sup>[33]</sup>



**Scheme 1.15.** Synthesis of BTB-based small molecule for (BHJ) solar cell.

Bazan and Heeger *et al.* utilized [1,2,5]thiadiazolo[3,4-*c*]pyridine (PT) unit, a more efficient acceptor based on the BTB unit to synthesize low HOMO–LUMO gap small molecule. The BHJ solar cells based on the PT-derivative showed a record PCE of 6.7% (Scheme 1.16).<sup>[34]</sup>



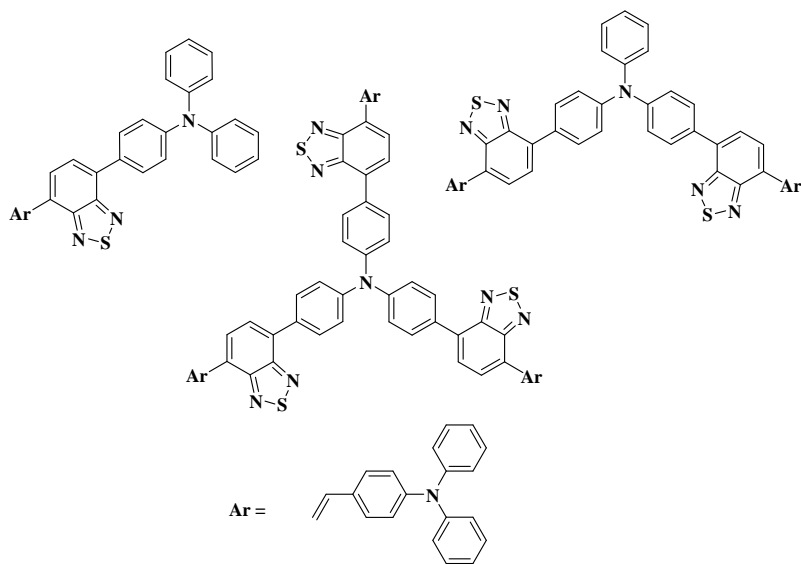
**Scheme 1.16.** Synthesis of [1,2,5]thiadiazolo[3,4-*c*]pyridine (PT) based molecule for (BHJ) solar cell.

#### 1.4.5. Organic light emitting diodes (OLEDs)

Organic Light Emitting Diodes (OLEDs) have become another major interest in the field of organic electronics. Organic light emitting diodes (OLEDs) was initially introduced by Tang *et al.* who used a vacuum deposited layer of molecular organic material.<sup>[35]</sup> Later in 1990 Friend and co-workers reported an OLED in which the active light-emitting material consisted of a  $\pi$ -conjugated polymer.<sup>[36]</sup> 2,1,3-Benzothiadiazole (BTD) is a strong electron acceptor and widely used for the synthesis of low band gap  $\pi$ -conjugated systems. The BTD based fluorophores exhibit high electron affinity, reversible electrochemical reduction, high emission quantum yields and tunable photoluminescence (PL) emission spectra in solution which make them potential candidates for OLEDs.

A variety of triphenylamine-substituted BTDs were synthesized and their OLED property was explored (Figure 1.8). The highest device efficiency was

observed for mono-BTD derivative, whereas the di- and tri-BTD derivatives exhibited substantially lower efficiencies.<sup>[37]</sup>

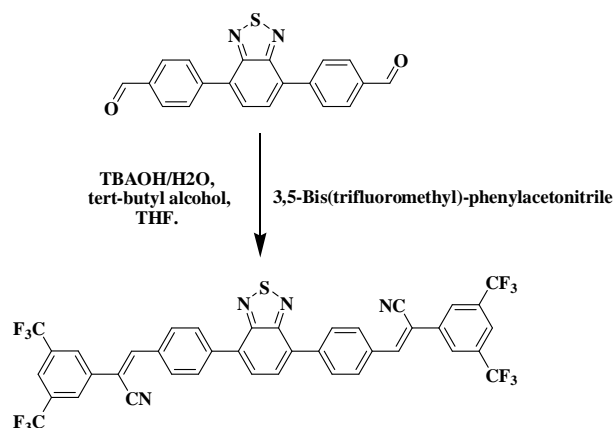


**Figure 1.8.** Synthesis of BTD based donor–acceptor molecules for OLEDs.

**1.4.6. Reversible Mechanochromism.** Mechanochromic luminescent materials change their emission color in response to mechanical stimuli such as pressing, grinding, or rubbing. The development of mechanochromic luminescent materials has gained attention due to their applications in mechano-sensors, security papers, and data storage. High contrast and solid state emission is essential for mechanochromic luminescent materials. The donor–acceptor benzothiadiazole based molecules show strong solid state emission, which can be utilized to design mechanofluorochromic materials.<sup>[38]</sup>

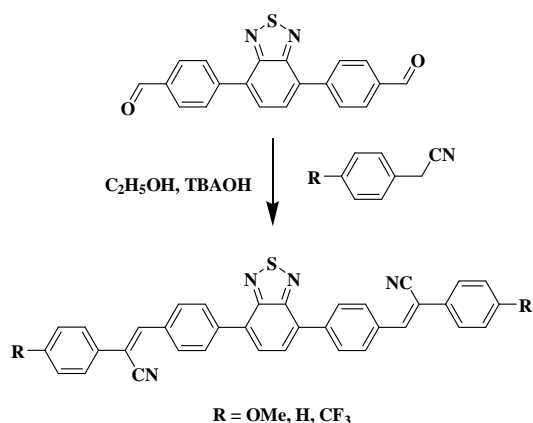
Recently reversible mechanochromism has been reported in trifluoromethyl-substituted benzothiadiazole-cored phenylene vinylene fluorophore, which upon grinding shows orange emission in the amorphous state and switches back to its green emission in the crystalline state upon heating (Scheme 1.17).<sup>[39]</sup>





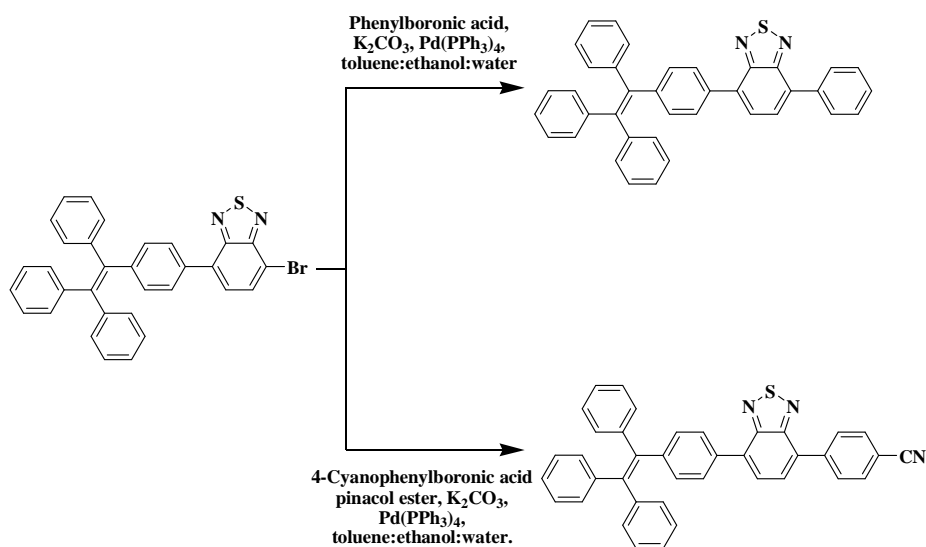
**Scheme 1.17.** Synthesis of trifluoromethyl-substituted BTD-cored phenylene vinylene fluorophore.

In another report the mechanofluorochromic properties of benzothiadiazole-cored cyano-substituted diphenylethene derivatives were fine-tuned through D–A approach (Scheme 1.18).<sup>[40]</sup> The end groups in these molecules resulted in different donor–acceptor (D–A) effects, and resulted in completely opposite mechanofluorochromic property. The D–A molecules with -OMe and -H end groups exhibit red-shifted mechanofluorochromic property whereas -CF<sub>3</sub> end groups showed blue-shifted mechanofluorochromic property.



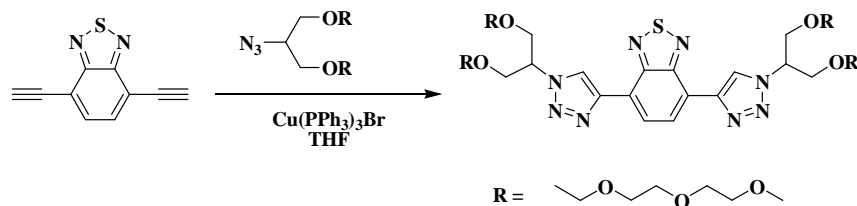
**Scheme 1.18.** Synthesis of benzothiadiazole-cored cyano-substituted diphenylethene derivatives.

Our group has synthesized two unsymmetrical tetraphenylethene (TPE) substituted Donor–Acceptor (D–A) benzothiadiazoles (BTDs). The derivative with cyano-group exhibits strong reversible mechanochromic behavior (Scheme 1.19).<sup>[41]</sup>



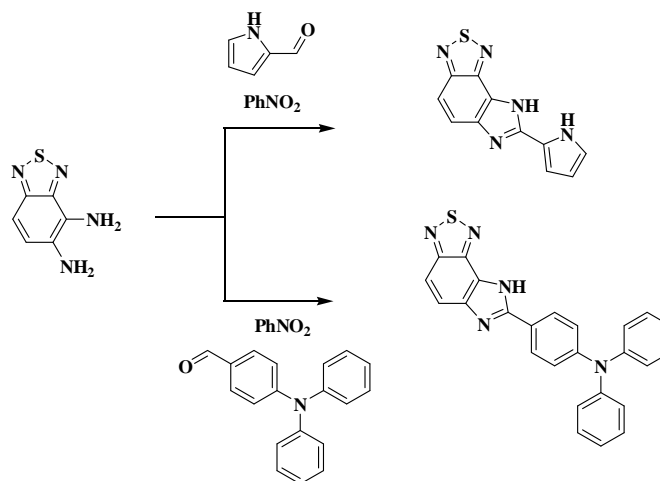
**Scheme 1.19.** Synthesis of tetraphenylethene-substituted benzothiadiazoles.

**1.4.7. Sensing:** In the recent years the design and synthesis of benzothiadiazole-based molecules for development metal ion sensors has gained attention. Bunz *et al.* has synthesized water soluble *bis*-triazolyl benzothiadiazole and investigated their metal-binding capabilities (Scheme 1.20).<sup>[42]</sup>



**Scheme 1.20.** Synthesis of water soluble *bis*-triazolyl BTD.

In another report aryl or heteroaryl 5-substituted imidazo-benzothiadiazole derivatives have been synthesized (Scheme 1.21). These multifunctional molecules selectively sense mercury(II) cations and acetate anions, and to discriminate between nitroaromatic derivatives such as *p*-nitrophenol and picric acid. <sup>[43]</sup>



**Scheme 1.21.** Synthesis of aryl or heteroaryl 5-substituted imidazo-benzothiadiazole derivatives

## 1.5. Organization of thesis

**Chapter 1:** This chapter gives an outline of the special features, classification and various synthetic strategies for the design of BTD and its derivatives, and their applications in diverse fields.

**Chapter 2:** This chapter summarizes the instrumentation and general methods used for the present study.

**Chapter 3:** In this chapter, we describe a series of ferrocene-substituted symmetrical BTDs and extended the conjugation length between the donor and the acceptor to tune the photonic properties.

**Chapter 4:** In this chapter, a series of symmetrical and unsymmetrical ferrocenyl-substituted BTD derivatives were designed and synthesized via Pd-catalyzed Sonogashira and Stille coupling reaction and the effect of altering the  $\pi$ -linker and

number of acceptor unit on the photonic properties and thermal stability was explored.

**Chapter 5:** In this chapter, a series of aryl-substituted unsymmetrical benzothiadiazole based small molecules of the type  $D_1-\pi-A-\pi-D_2$ ,  $D_1-A-\pi-D_2$ , and  $D_1-A_1-A_2-D_2$  were designed and synthesized, and the effect of substitution of different aryl-donor and acceptor units on photonic, electrochemical and thermal properties was investigated.

**Chapter 6:** In this chapter we have utilized a smart strategy to tune the photonic properties and improve the thermal stability of benzothiadiazole based molecular systems. We have synthesized a series of tetracyanoethylene (TCNE) and 7,7,8,8-tetracyanoquinodimethane (TCNQ) substituted symmetrical and unsymmetrical BTDs.

**Chapter 7:** Mechanochromic materials exhibit reversible solid-state emission in response to external stimuli such as grinding, pressing, fuming and annealing. In this chapter we have designed and synthesized dipyridylamine substituted unsymmetrical BTD and explored its reversible mechanochromic properties.

**Chapter 8:** This Chapter summarizes the salient features of the work and addressed the future prospects.

## 1.6. References

- [1] (a) Liangwab M., Chen J. (2013), Arylamine organic dyes for dye-sensitized solar cells, *Chem. Soc. Rev.*, 42, 3453-3488 (DOI: 10.1039/C3CS35372A). (b) Mishra A., Fischer M. K. R., Bauerle P. (2009), Metal-free organic dyes for dye-sensitized solar cells: from structure: property relationships to design rules, *Angew. Chem., Int. Ed.*, 48, 2474-2499 (DOI: 10.1002/anie.200804709). (c) Thomas K. R. J., Lin J. T., Velusamy M., Tao Y. T., Chuen C. H. (2004), Color tuning in benzo[1,2,5]thiadiazole-based small molecules by amino conjugation/deconjugation: bright red-light-emitting diodes, *Adv. Funct. Mater.*, 14, 83-90 (DOI: 10.1002/adfm.200304486). (d) Omer K. M., Ku S. Y., Wong K. T., Bard A. J. (2009), Green electrogenerated chemiluminescence of highly fluorescent benzothiadiazole and fluorene

- derivatives, *J. Am. Chem. Soc.*, 131, 10733-10741 (DOI: 10.1021/ja904135y).
- [2] Parker T. C., Patel D. G., Moudgil K., Barlow S., Risko C., Brédas, J.-L., Reynolds J. R., Marder S. R. (2015), Heteroannulated acceptors based on benzothiadiazole, *Mater. Horiz.*, 2, 22-36 (DOI: 10.1039/c4mh00102h).
- [3] Zhang Q. T., Tour J. M. (1998), Alternating donor/acceptor repeat units in polythiophenes. Intramolecular charge transfer for reducing band gaps in fully substituted conjugated polymers, *J. Am. Chem. Soc.*, 120, 5355-5362 (DOI: 10.1021/ja972373e).
- [4] (a) Štefko M., Tzirakis M. D., B. Breiten, M.-O. Ebert, O. Dumele, Schweizer W. B., Gisselbrecht J.-P., Boudon C., Beels M. T., Biaggio I., Diederich F. (2013), Donor–acceptor (D–A)-substituted polyynes chromophores: modulation of their optoelectronic properties by varying the length of the acetylene spacer, *Chem. –Eur. J.*, 19, 12693-12704 (DOI: DOI: 10.1002/chem.201301642 ). (b) van Mullekom H. A. M., Vekemans J. A. J. M., Meijer E. W. (1998), Band-Gap Engineering of Donor–Acceptor-Substituted  $\pi$ -Conjugated Polymers, *Chem. –Eur. J.*, 4, 1235-1243 (DOI: 10.1002/(SICI)1521-3765(19980710)4:7<1235::AID-CHEM1235>3.0.CO;2-4). (c) Wang J.-L., Xiao Q., Pei J. (2010), Benzothiadiazole-based D– $\pi$ -A– $\pi$ -D organic dyes with tunable band gap: synthesis and photophysical properties, *Org. Lett.*, 12, 4164-4167 (DOI: 10.1021/ol101754q). (e) Moonen N. N. P., Pomerantz W. C., Gist R., Boudon C., Gisselbrecht J.-P., Kawai T., Kishioka A., Gross M., Irie M., Diederich F. (2005), Donor-substituted cyanoethynylethenes:  $\pi$ -conjugation and band-Gap tuning in strong charge-transfer chromophores, *Chem. –Eur. J.*, 11, 3325-3341 (DOI: 10.1002/chem.200500082).
- [5] (a) Wang J.-L., Tang Z.-M., Xiao Q., Ma Y., Pei J. (2010), Benzothiadiazole-based D– $\pi$ -A– $\pi$ -D organic dyes with tunable band gap: synthesis and photophysical properties, *Org. Lett.*, 10, 4271-4274 (DOI: 10.1021/ol101754q). (b) Dou L., Gao J., Richard E., You J., Chen C. -C., Cha K. C., He Y., Li G., Yang, Y. (2012), Systematic investigation of

- benzodithiophene- and diketopyrrolopyrrole-based low-bandgap polymers designed for single junction and tandem polymer solar cells, *J. Am. Chem. Soc.*, 134, 10071-10079 (DOI: 10.1021/ja301460s). (c) Blouin N., Michaud A., Leclerc M. (2007), A low-bandgap poly(2,7-Carbazole) derivative for use in high-performance solar cells *Adv. Mater.*, 19, 2295–2300 (10.1002/adma.200602496). (d) Sonar P., Ng G. -M., Lin G. T. T., Dodabalapur A., Chen Z.-K. (2010), Solution processable low bandgap diketopyrrolopyrrole (DPP) based derivatives: novel acceptors for organic solar cells, *J. Mater. Chem.*, 20, 3626-3636 (DOI: 10.1039/B924404B).
- [6] Yasuda T., Shinohara Y., Matsuda T., Han L., Ishi-i. T. (2012), Improved power conversion efficiency of bulk-heterojunction organic solar cells using a benzothiadiazole–triphenylamine polymer, *J. Mater. Chem.*, 22, 2539-2544 (DOI: 10.1039/c2jm14671a).
- [7] Gautam P., Misra R., Siddiqui S. A., Sharma G. D. (2015), Unsymmetrical donor–acceptor–acceptor– $\pi$ –donor type benzothiadiazole-based small molecule for a solution processed bulk heterojunction organic solar cell, *ACS Appl. Mater. Interfaces*, 7, 10283-10292 (DOI: 10.1021/acsami.5b02250).
- [8] Walker B., Kim C., Nguyen T. -Q. (2011), Small molecule solution-processed bulk heterojunction solar cells, *Chem. Mater.*, 23, 470-482 (DOI: 10.1021/cm102189g).
- [9] Bureš F. (2014), Fundamental aspects of property tuning in push–pull molecules, *RSC Adv.*, 4, 58826-58851 (DOI: 10.1039/c4mh00102h)
- [10] (a) Qian G., Wang Z. Y. (2010), Near-infrared organic compounds and emerging applications, *Chem. Asian J.*, 5, 1006-1029 (DOI: 10.1002/asia.200900596). (b) Roncali, J. (2007), Molecular engineering of the band gap of  $\pi$ -conjugated systems: facing technological applications, *Macromol. Rapid Commun.*, 28, 1761-1775 (DOI: 10.1002/marc.200700345)

- [11] Neto B. A. D., Lapis A. A. M., Júnior E. N., da S., Dupont J. (2013), 2,1,3-Benzothiadiazole and derivatives: synthesis, properties, reactions, and applications in light technology of small molecules, *Eur. J. Org. Chem.*, 228-255 (DOI: 10.1002/ejoc.201201161).
- [12] Konstantinova, L. S. Knyazeva E. A., Rakitin O. A. (2014), Recent developments in the synthesis and applications of 1,2,5-thia- and selenadiazoles. a review, *Org. Prep. Proc. Int.*, 46, 475-544 (DOI: 10.1080/00304948.2014.963454)
- [13] (a) Hinsberg O. (1889), Ueber Piaselenole und Piazthiole *Ber. Dtsch. Chem. Ges.*, 22, 2895-2902 (10.1002/cber.188902202199). (b) Weinstock L. M., Davis P., Handelsman B., Tull R. J. (1967), General synthetic system for 1,2,5-thiadiazoles, *J. Org. Chem.*, 32, 2823-2829 (DOI: 10.1021/jo01284a040). (c) Komim A. P., Street R. W., Carmack M. (1975), Chemistry of 1,2,5-thiadiazoles. III. [1,2,5]thiadiazolo[3,4-c][1,2,5]thiadiazole, *J. Org. Chem.*, 40, 2749-2752.
- [14] Pilgram K., Zupan M., Skiles R. (1970), Bromination of 2,1,3-benzothiadiazoles, *J. Heterocycl. Chem.* 7, 629-633 (DOI: 10.1002/jhet.5570070324).
- [15] (a) Bashirov D. A., Sukhikh T. S., Kuratieva N. V., Naumov D. Y., Konchenko S. N., Semenov N. A., Zibarev A. V. (2012), Iridium complexes with 2,1,3-benzothiadiazole and related ligands, *Polyhedron*, 42, 168-174 (DOI: 10.1016/j.poly.2012.05.015). (b) Conte G., Bortoluzzi A. J., Gallardo H. (2006), [1,2,5]Thiadiazolo[3,4-f][1,10]phenanthroline as a building block for organic materials, *Synthesis*, 3945-3947 (DOI: 10.1055/s-2006-950323). (c) Kohl B., Over, L. C., Lohr T., Vasylyeva M., Rominger F., Mastalerz M. (2014), Selective even-numbered bromination of triptycene tris(thiadiazoles), *Org. Lett.*, 16, 5596-5599 (DOI: 10.1021/ol502639x)
- [16] Zhivonitko V. V., Makarov A. Y., Bagryanskaya I. Y., Gatilov Y. V., Shakirov M. M., Zibarev, A. V. (2005), New polysulfur-nitrogen heterocycles by thermolysis of 1,3 $\lambda^4\delta^2$ ,2,4-benzodithiadiazines in the

hydrocarbon and fluorocarbon series, *Eur. J. Inorg. Chem.*, 4099-4108 (DOI: 10.1002/ejic.200500383).

- [17] (a) Kato S.-i., Matsumoto T., Ishi-I T., Thiemann T., Shigeiwa M., Gorohmaru H., Maeda S., Yamashita Y., Mataka S. (2004), Strongly red-fluorescent novel donor- $\pi$ -bridge-acceptor- $\pi$ -bridge-donor (D- $\pi$ -A- $\pi$ -D) type 2,1,3-benzothiadiazoles with enhanced two-photon absorption cross-sections, *Chem. Commun.*, 2342-2343 (DOI: 10.1039/B410016F). (b) Zhang X., Yamaguchi R., Moriyama K., Kadowaki M., Kobayashi T., Ishi-i T., Thiemann T., Mataka S. (2006), Highly dichroic benzo-2,1,3-thiadiazole dyes containing five linearly  $\pi$ -conjugated aromatic residues, with fluorescent emission ranging from green to red, in a liquid crystal guest-host system, *J. Mater. Chem.*, 16, 736-740 (DOI: 10.1039/B512493J). (c) Balaji G., Shim W. L., Parameswaran M., Valiyaveetil S. (2009), Thiadiazole fused indolo[2,3-a]carbazole based oligomers and polymer, *Org. Lett.*, 11, 4450-4453 (DOI: 10.1021/ol901806q). (d) Zhu W., Yang Y., Metivier R., Zhang Q., Guillot R., Xie Y., Tian H., Nakatani K. (2011), Unprecedented stability of a photochromic bisthienylethene based on benzobisthiadiazole as an ethene bridge, *Angew. Chem., Int. Ed.*, 50, 10986-10990 (DOI: 10.1002/anie.201105136). (e) Fu Y., Kim J., Siva A., Shin W. S., Moon S.-j., Park T. (2011), Parameters influencing the molecular weight of 3,6-carbazole-based D- $\pi$ -A-type copolymers, *J. Polym. Sci., A*, 49, 4368-4378 (DOI: 10.1002/pola.24877). (f) Noujeim N., Zhu K., Vukotic V. N., Loeb S. J. (2012), [2]Pseudorotaxanes from T-shaped benzimidazolium axles and [24]crown-8 wheels, *Org. Lett.*, 14, 2484-2487 (DOI: 10.1021/ol300761q). (g) Fang Q., Xu B., Jiang B., Fu H., Chen X., Cao A. (2005), Bisindoles containing a 2,1,3-benzothiadiazole unit: novel non-doping red organic light-emitting diodes with excellent color purity, *Chem. Commun.*, 1468-1470 (DOI: 10.1039/B417810F).
- [18] (a) Sonar P., Foong T. R. B., Singh S. P., Li Y., Dodabalapur A. (2012), A furan-containing conjugated polymer for high mobility ambipolar organic



- thin film transistors, *Chem. Commun.*, 8383-8385 (DOI: 10.1039/C2CC33093H). (b) Ding X., Chen L., Honsho Y., Feng X., Saengsawang O., Guo J., Saeki A., Seki S., Irie S., Nagase S., Parasuk V., Jiang D. (2011), An n-channel two-dimensional covalent organic framework *J. Am. Chem. Soc.*, 133, 14510-14513 (DOI: 10.1021/ja2052396).
- [19] (a) Cheng Y.-J., Chen C.-H., Ho Y.-J., Chang S.-W., Witek H. A., Hsu C.-S. (2011), Thieno[3,2-*b*]pyrrolo donor fused with benzothiadiazole, benzoselenadiazole and quinoxalino acceptors: synthesis, characterization, and molecular properties, *Org. Lett.*, 13, 5484-5487 (DOI: 10.1021/ol202199v). (b) Tomar M. Lucas N. T., Müllen K., Jacob J. (2013), *Tetrahedron Lett.*, 54, 5883-5885 (DOI:10.1016/j.tetlet.2013.08.107).
- [20] (a) Fan J., Yuen J. D., Wang M., Seifert J., Seo J.-H., Mohebbi A. R., Zakhidov D., Heeger A., Wudl F. (2012), *Adv. Mater.*, 24, 2186-2190 (DOI: 10.1002/adma.201103836). (b) Kawabata K., Takeguchi M., Goto H. (2013), Optical activity of heteroaromatic conjugated polymer films prepared by asymmetric electrochemical polymerization in coelectric liquid crystals: structural function for chiral induction, *Macromolecules*, **46**, 2078-2091 (DOI: 10.1021/ma400302j). (c) Huber J., Jung C., Mecking S. (2012), Nanoparticles of low optical band gap conjugated polymers, *Macromolecules*, 45, 7799-7805 (DOI: 10.1021/ma3013459). (d) Cardone A., Martinelli C., Losurdo M., Dilonardo E., Brunantonio G., Scavia G., Destri S., Cosma P., Salamandra L., Reale A., Carlo A. D., Aguirre A., Milián-Medina B., Gierschner J., Farinola G. M. (2013), Fluoro-functionalization of vinylene units in a polyarylenevinylene for polymer solar cells, *J. Mater. Chem. A*, 1, 715-727 (DOI: 10.1039/C2TA00177B). (e) Patel D. G., Feng F., Ohnishi Y.-y., Abboud K. A., Hirata S., Schanze K. S., Reynolds J. R. (2012), It takes more than an imine: the role of the central atom on the electron-accepting ability of benzotriazole and benzothiadiazole oligomers, *J. Am. Chem. Soc.*, 134, 2599-2612 (DOI:

DOI: 10.1021/ja207978v). (f) Steinberger S., Mishra A., Reinold E., Müller C. M., Uhrich C., Pfeiffer M. and Bäuerle P. (2011), A–D–A–D–A-type oligothiophenes for vacuum-deposited organic solar cells, *Org. Lett.*, **13**, 90-93 (DOI: 10.1021/ol102603n). (g) Peng Q., Liu X., Qin Y., Xu J., Lia M., Dai L. (2011), Pyrazino[2,3-g]quinoxaline-based conjugated copolymers with indolocarbazole coplanar moieties designed for efficient photovoltaic applications, *J. Mater. Chem.*, **21**, 7714-7722 (DOI: 10.1039/C1JM10433K). (h) Unver E. K., Tarkuc S., Baran D., Tanyeli C., Toppare L. (2011), Synthesis of new donor–acceptor polymers containing thiadiazoloquinoxaline and pyrazinoquinoxaline moieties: low-band gap, high optical contrast, and almost black colored materials, *Tetrahedron Lett.*, **52**, 2725-2729 (DOI:10.1016/j.tetlet.2011.03.078). (i) Zhou H., Yang L., Price S. C., Knight K. J., You W. (2010), Enhanced photovoltaic performance of low-bandgap polymers with deep LUMO levels, *Angew. Chem., Int. Ed.*, **49**, 7992-7995 (DOI: 10.1002/anie.201003357). (j) Hemgesberg M., Ohlmann D. M., Schmitt Y., Wolfe M. R., Müller M. K., Erb B., Sun Y., Gooßen L. J., Gerhards M., Thiel W. R. (2012), Simple access to sol–gel precursors bearing fluorescent aromatic core units *Eur. J. Org. Chem.*, 2142-2151 (DOI: 10.1002/ejoc.201200076). (k) Schwartz P.-O., Zaborova E., Bechara R., Leveque P., Heiser T., Mery S., Leclerc N. (2013), Impact of the arrangement of functional moieties within small molecular systems for solution processable bulk heterojunction solar cells, *New J. Chem.*, **37**, 2317-2323 (DOI: 10.1039/C3NJ00218G).

- [21] (a) Gautam, P., Maragani, R., Misra, R. (2015), Aryl-substituted symmetrical and unsymmetrical benzothiadiazoles, *RSC Adv.*, **5**, 18288-18294 (DOI: 10.1039/C4RA15424J). (b) Coombs B. A., Lindner B. D., Edkins R. M., Rominger F., Beeby A., Bunz U. H. F. (2012), Photophysical property trends for a homologous series of bis-ethynyl-substituted benzochalcogendiazoles, *New J. Chem.*, **36**, 550-553 (DOI: 10.1039/C2NJ20847D). (c) Akhtaruzzaman M., Tomura M., Zaman M.

- B., Nishida J.-i., Yamashita Y. (2002), Synthesis and characterization of new linear  $\pi$ -conjugated molecules containing bis(ethynylpyridine) units with a benzothiadiazole spacer, *J. Org. Chem.*, 67, 7813-7818 (DOI: 10.1021/jo0202334).
- [22] Bangcuyo, C. G., Smith M. D., Bunz, U. H. F. (2004), Tetraethynylbenzo[2,1,3]thiadiazole, *Synlett*, 169-172 (DOI: 10.1055/s-2003-43356).
- [23] Zhang J., Yang Y., He C., He Y., Zhao G., Li. Y., (2009), Solution-processable star-shaped photovoltaic organic molecule with triphenylamine core and benzothiadiazole-thiophene arms, *Macromolecules*, 42, 7619–7622 (DOI: 10.1021/ma901896n)
- [24] Bloking J. T., Han X., Higgs A. T., Kastrop J. P., Pandey L., Norton J. E., Risko C., Chen C. E., Bredas J.-L., McGehee M. D., Sellinger A. (2011), Solution-processed organic solar cells with power conversion efficiencies of 2.5% using benzothiadiazole/imide-based acceptors, *Chem. Mater.*, 23, 5484-5490 (DOI: 10.1021/cm203111k).
- [25] Chen S., Li Y., Yang W., Chen N., Liu H. and Li Y. (2010), Synthesis and Tuning optical nonlinear properties of molecular crystals of benzothiadiazole, *J. Phys. Chem. C*, 114, 15109-15115 (DOI: 10.1021/jp103159b).
- [26] Chen S., Qin Z., Liu T., Wu X., Li Y., Liu H., Song Y., Li Y. (2013), Aggregation-induced emission on benzothiadiazole dyads with large third-order optical nonlinearity, *Phys. Chem. Chem. Phys.*, 15, 12660-12666 (DOI: 10.1039/C3CP51273H).
- [27] Kato S.-i., Matsumoto T., Ishi-i T., Shigeiwa M., Gorohmaru H., Maeda S., Ishi-i T., Mataka S. (2006), Novel 2,1,3-benzothiadiazole-based red-fluorescent dyes with enhanced two-photon absorption cross-sections, *Chem. Eur. J.*, **12**, 2303-2317 (DOI: 10.1002/chem.200500921 ).
- [28] Ishi-i T., Taguri Y., Kato S.-i., Shigeiwa M., Gorohmaru H., Maeda S., Mataka S. (2007), Singlet oxygen generation by two-photon excitation of porphyrin derivatives having two-photon-absorbing benzothiadiazole

- chromophores, *J. Mater. Chem.*, 17, 3341-3346 (DOI: 10.1039/B704499B).
- [29] O'regan B., Grätzel M., A low-cost, high-efficiency solar cell based on dye-sensitized colloidal TiO<sub>2</sub> films, *Nature* 353 , 737-740 (DOI: 10.1038/353737a0)
- [30] Mathew S., Yella A., Gao P., Humphry-Baker R., Curchod B. F. E., Ashari-Astani N., Tavernelli I., Rothlisberger U., Nazeeruddin M. K., Grätzel M. (2014), Dye-sensitized solar cells with 13% efficiency achieved through the molecular engineering of porphyrin sensitizers, *Nat. Chem.*, 6, 242–247, (DOI:10.1038/nchem.1861).
- [31] Marks R. N., Halls, J. J. M., Bradley D. D. C., Friend R. H., Holmes A. B. (1994), The photovoltaic response in poly(p-phenylene vinylene) thin-film devices, R. N. Marks, *J. Phys.: Condens. Matter* 6, 1379, (DOI: 10.1088/0953-8984/6/7/009).
- [32] Yu G., Gao J., Hummelen J. C., Wudl F., Heeger A. J. (1995), Polymer Photovoltaic Cells: Enhanced efficiencies via a network of internal donor-acceptor heterojunctions, *Science*, 270, 1789-1791 (DOI: 10.1126/science.270.5243.1789).
- [33] Lin L.-Y., Chen Y.-H., Huang Z.-Y., Lin H.-W., Chou S.-H., Lin F., Chen C.-W., Liu Y.-H., Wong K.-T. (2011), A low-energy-gap organic dye for high-performance small-molecule organic solar cells, *J. Am. Chem. Soc.*, 133, 15822–15825, (DOI: 10.1021/ja205126t).
- [34] Sun Y., Welch G. C., Leong W. L., Takacs C. J., Bazan G. C., Heeger A. J. (2012), Solution-processed small-molecule solar cells with 6.7% efficiency, *Nat. Mater.*, 11, 44–48, (DOI: 10.1038/NMAT3160).
- [35] Tang C. W., VanSlyke S. A. (1987), Organic electroluminescent diodes, *Appl. Phys. Lett.*, 51, 913 (DOI: 10.1063/1.98799)
- [36] Burroughes J. H., Bradley D. D. C., Brown A. R., Marks R. N., Mackay K., Friend R. H., Burn P. L., Holmes A. B. (1990), Light-emitting diodes based on conjugated polymers, *Nature*, 347, 539-541 (DOI: 10.1038/347539a0).

- [37] Yang Y., Zhou Y., He Q.-G., He C. ,Yang C.-H., Bai F.-L., Li Y.-F. (2009), Solution-processable red-emission organic materials containing triphenylamine and benzothiadiazole units: synthesis and applications in organic light-emitting diodes, *J. Phys. Chem. B*, 2009, 113, 7745-7752 (DOI: 10.1021/jp900362f).
- [38] Misra R., Jadhav T., Dhokale B., Mobin S. M. (2014), Reversible mechanochromism and enhanced AIE in tetraphenylethene substituted phenanthroimidazoles, *Chem. Commun.*, 50, 9076-9078 (DOI: 10.1039/c4cc02824d)
- [39] Dou C., Chen D., Iqbal J., Yuan Y., Zhang H., Wang Y. (2011), Multistimuli-responsive benzothiadiazole-cored phenylene vinylene derivative with nanoassembly properties, *Langmuir*, 27, 6323-6329, (DOI: 10.1021/la200382b)
- [40] Zhang X., Ma Z., Yang Y., Zhang X., Jia X., Wei Y. (2014), Fine-tuning the mechanofluorochromic properties of benzothiadiazole-cored cyano-substituted diphenylethene derivatives through D–A effect, *J. Mater. Chem. C*, 2, 8932-8938 (DOI: 10.1039/c4tc01457j).
- [41] Jadhav T., Dhokale B., Misra R. (2015), Effect of the cyano group on solid state photophysical behavior of tetraphenylethene substituted benzothiadiazoles. *J. Mater. Chem. C*, 3, 9063-9068 (DOI: 10.1039/C5TC01871D)
- [42] Bryant J. J., Lindner B. D., Bunz U. H. F. (2013), Water-soluble bis-triazolyl benzochalcogendiazole cycloadducts as tunable metal ion sensors, *J. Org. Chem.*, 78, 1038-1044, (DOI: 10.1021/jo3024889)
- [43] Alfonso M., Espinosa A., Tárraga A., Molina P. (2014), Multifunctional benzothiadiazole-based small molecules displaying solvatochromism and sensing properties toward nitroarenes, anions, and cations, *ChemistryOpen*, 3, 242-249, (DOI: 10.1002/open.201402022).

## Chapter 2

### Materials and experimental techniques

#### 2.1. Introduction

This chapter describes the materials, general synthetic procedures, characterization techniques and the instrumentation employed in this thesis.

#### 2.2. Chemicals for synthesis

The common solvents used for syntheses were purified according to established procedures.<sup>[1]</sup> 2,1,3-Benzothiadiazole, CuI, Pd(PPh<sub>3</sub>)<sub>4</sub>, PdCl<sub>2</sub>(PPh<sub>3</sub>)<sub>2</sub>, ferrocene, tetrabutylammonium hexafluorophosphate (TBAF<sub>6</sub>), 4-ethynylaniline, 3-ethynylaniline, ethynyl ferrocene, triphenylamine, and carbazole, were procured from Aldrich chemicals USA. Silica gel (100–200 mesh and 230–400 mesh) were purchased from Rankem chemicals, India. TLC pre-coated silica gel plates (Kieselgel 60F254, Merck) were obtained from Merck, India. Dry solvents dichloromethane, 1,2-dichloroethane, chloroform, tetrahydrofuran (THF), 1,2-dichlorobenzene, dioxane, triethylamine and methanol were obtained from spectrochem and S. D. Fine chem. Ltd. All the oxygen or moisture sensitive reactions were performed under nitrogen/argon atmosphere using standard schlenk method. The solvents and reagents were used as received unless otherwise indicated. Photophysical and electrochemical studies were performed with spectroscopic grade solvents.

#### 2.3. Spectroscopic measurements

##### 2.3.1. Mass spectrometry

High resolution mass spectra (HRMS) were recorded on Brucker-Daltonics, micrOTOF-Q II mass spectrometer using positive and negative mode electrospray ionizations.

##### 2.3.2. NMR spectroscopy

<sup>1</sup>H NMR (400 MHz), and <sup>13</sup>C NMR (100 MHz) spectra were recorded on the Bruker Avance (III) 400 MHz, using CDCl<sub>3</sub> and acetone-d<sub>6</sub> as solvent. Chemical shifts in <sup>1</sup>H, and <sup>13</sup>C NMR spectra were reported in parts per million

(ppm). In  $^1\text{H}$  NMR chemical shifts are reported relative to the residual solvent peak ( $\text{CDCl}_3$ , 7.26 ppm). Multiplicities are given as: s (singlet), d (doublet), t (triplet), q (quartet), dd (doublet of doublets), m (multiplet), and the coupling constants  $J$ , are given in Hz.  $^{13}\text{C}$  NMR chemical shifts are reported relative to the solvent residual peak ( $\text{CDCl}_3$ , 77.36 ppm).

### 2.3.3. UV-Vis spectroscopy

UV-Vis absorption spectra were recorded using a Varian Cary100 Bio UV-Vis and Perkin Elmer LAMBDA 35 UV/Vis spectrophotometer.

### 2.3.4. Fluorescence spectroscopy

Fluorescence emission spectra were recorded upon specific excitation wavelength on a Horiba Scientific Fluoromax-4 spectrophotometer. The slit width for the excitation and emission was set at 2 nm.

#### *The fluorescence quantum yields ( $\phi_F$ )*

The fluorescence quantum yields ( $\phi_F$ ) of compounds **1-4** were calculated by the steady-state comparative method using following equation,

$$\phi_F = \phi_{st} \times S_u/S_{st} \times A_{st}/A_u \times n_u^2 D_u/n_s^2 D_{st} \dots\dots\dots (\text{Eq. 1})$$

Where  $\phi_F$  is the emission quantum yield of the sample,  $\phi_{st}$  is the emission quantum yield of the standard,  $A_{st}$  and  $A_u$  represent the absorbance of the standard and sample at the excitation wavelength, respectively, while  $S_{st}$  and  $S_u$  are the integrated emission band areas of the standard and sample, respectively, and  $n D_{st}$  and  $n D_u$  the solvent refractive index of the standard and sample, u and st refer to the unknown and standard, respectively.

### 2.4. Electrochemical studies

Cyclic voltamograms (CVs) and Differential Pulse Voltamograms (DPVs) were recorded on CHI620D electrochemical analyzer using Glassy carbon as working electrode, Pt wire as the counter electrode, and Saturated Calomel Electrode (SCE) as the reference electrode. The scan rate was  $100 \text{ mVs}^{-1}$ . A solution of tetrabutylammonium hexafluorophosphate ( $\text{TBAPF}_6$ ) in  $\text{CH}_2\text{Cl}_2$  (0.1 M) was employed as the supporting electrolyte.

## 2.5. Single crystal X-ray diffraction studies.

Single crystal X-ray diffraction studies were performed on SUPER NOVA diffractometer. The strategy for the Data collection was evaluated by using the CrysAlisPro CCD software. The data were collected by the standard 'phi-omega scan techniques, and were scaled and reduced using CrysAlisPro RED software. The structures were solved by direct methods using SHELXS-97, and refined by full matrix least-squares with SHELXL-97, refining on  $F^2$ .<sup>1</sup> The positions of all the atoms were obtained by direct methods. All non-hydrogen atoms were refined anisotropically. The remaining hydrogen atoms were placed in geometrically constrained positions, and refined with isotropic temperature factors, generally 1.2  $U_{eq}$  of their parent atoms. The CCDC numbers contain the respective supplementary crystallographic data. These data can be obtained free of charge via [www.ccdc.cam.ac.uk/conts/retrieving.html](http://www.ccdc.cam.ac.uk/conts/retrieving.html) (or from the Cambridge Crystallographic 42 Data Centre, 12 union Road, Cambridge CB21 EZ, UK; Fax: (+44) 1223-336-033; or [deposit@ccdc.cam.ac.uk](mailto:deposit@ccdc.cam.ac.uk)).

## 2.6. Powder X-ray diffraction (PXRD) studies.

The XRD measurements were performed using Rigaku SmartLab, Automated Multipurpose X-ray diffractometer. The X-rays were produced using a sealed tube and the wavelength of the X-ray was 0.154 nm (Cu K-alpha).

## 2.7. Computational calculations

The density functional theory (DFT) calculation were carried out at the B3LYP/6-31G\*\* level for C, N, S, H, and Lanl2DZ level for Fe in the Gaussian 09 program.<sup>[2]</sup>

## References

- [1] (a) Vogel A. I., Tatchell A. R., Furnis B. S., Hannaford A. J., & Smith, P. W. G. (1996), *Vogel's Textbook of Practical Organic Chemistry (5th Edition)* (5<sup>th</sup> ed.). (b) Wei Ssberger A. Proskraner E. S. Riddick J. A.,



Toppos Jr. E. F. (1970). *Organic Solvents in Techniques of Organic Chemistry*, Vol. IV, 3<sup>rd</sup> Edition, Inc. New York.

- [2] (a) Lee C., Yang W., & Parr R. G. (1988). Development of the Colle-Salvetti correlation-energy formula into a functional of the electron density. *Physical Review B*, 37(2), 785–789 (DOI: 10.1103/PhysRevB.37.785). (b) A. D. Becke (1993), A new mixing of Hartree-Fock and local densityfunctional theories, *J. Chem. Phys.* 98 (2), 1372–377 (DOI: 10.1063/1.464304). (c) Frisch M. J., Trucks G. W., Schlegel H. B., Scuseria G. E., Robb M. A., Cheeseman J. R., Scalmani G., Barone V., Mennucci B., Petersson G. A., Nakatsuji H., Caricato M., Li X., Hratchian H. P., Izmaylov A. F., Bloino J., Zheng G., Sonnenberg J. L., Hada M., Ehara M., Toyota K., Fukuda R., Hasegawa J., Ishida M. Nakajima T., Honda Y., Kitao O., Nakai H., Vreven T., Montgomery J. A. Jr., Peralta J. E., Ogliaro F., Bearpark M., Heyd J. J., Brothers E., Kudin K. N., Staroverov V. N., Kobayashi R., Normand J., Raghavachari K., Rendell A., Burant J. C., Iyengar S. S., Tomasi J., Cossi M., Rega N., Millam N. J., Klene M., Knox J. E., Cross J. B., Bakken V., Adamo C., Jaramillo J., Gomperts R., Stratmann R. E., Yazyev O., Austin A. J., Cammi R., Pomelli C.; Ochterski J. W., Martin R. L., Morokuma K., Zakrzewski V. G., Voth G. A., Salvador P., Dannenberg J. J., Dapprich S., Daniels A. D., Farkas O., Foresman J. B., Ortiz J. V., Cioslowski J., Fox D. J. (2009), *Gaussian 09, revision A.02*; *Gaussian, Inc.*:Wallingford, CT.

## Chapter 3

### Donor- $\pi$ -acceptor- $\pi$ -donor benzothiadiazoles

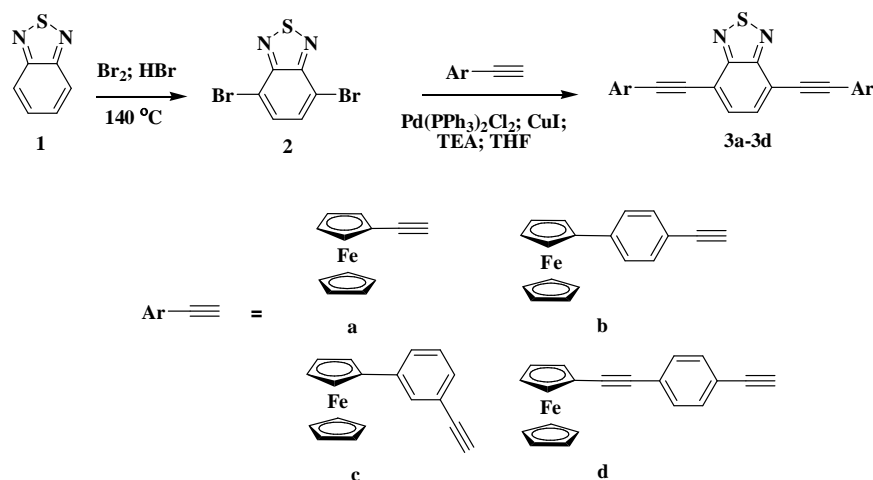
#### 3.1. Introduction

Donor-acceptor (D-A) organic compounds are of great interest, because of their application in various electronic, and photonic devices such as organic light emitting diodes (OLEDs), organic photovoltaic devices (OPVs), organic thin film transistors (OTFTs), and nonlinear optical (NLO) materials.<sup>[1]</sup> The electronic properties of the D-A molecular systems can be tuned by varying the strength of the donor and acceptor group or by varying the  $\pi$ -linker between the donor and the acceptor units. Benzothiadiazole has attracted considerable attention because of its distinguished acceptor property owing to its electron deficient groups C=N, and S=N.<sup>[2]</sup> It has been established that the structural motifs of type D-A-D show promising nonlinear optical (NLO) behavior.<sup>[3]</sup> Therefore we were interested to incorporate the donor groups into the benzothiadiazole, and to explore its photophysical, and electrochemical properties. There are many reports, where the donor groups are attached to the benzothiadiazole.<sup>[4]</sup> Ferrocene is a strong donor, and highly stable.<sup>[5]</sup> In this chapter, we have incorporated the ferrocene group on both the ends of benzothiadiazole, and designed a D- $\pi$ -A- $\pi$ -D type of molecular system. Here our aim was to explore the effect of ferrocene unit on the photophysical, and electrochemical behavior of the benzothiadiazole by enhancing the  $\pi$ -conjugation.

#### 3.2. Results and discussion

The synthetic route for the ferrocenyl substituted benzothiadiazole **3a-3d** is shown in Scheme 3.1. The dibromobenzothiadiazole **2**, was synthesized by the bromination reaction of the benzothiadiazole **1**. The ferrocenyl substituted benzothiadiazole **3a-3d** were synthesised by the Pd-catalyzed Sonogashira cross-coupling reactions of the dibromobenzothiadiazole **2**, with the corresponding ethynyl-ferrocene. The Sonogashira coupling reaction of the dibromobenzothiadiazole **2**, with ethynyl-ferrocene, 4-ferrocenylphenylacetylene,

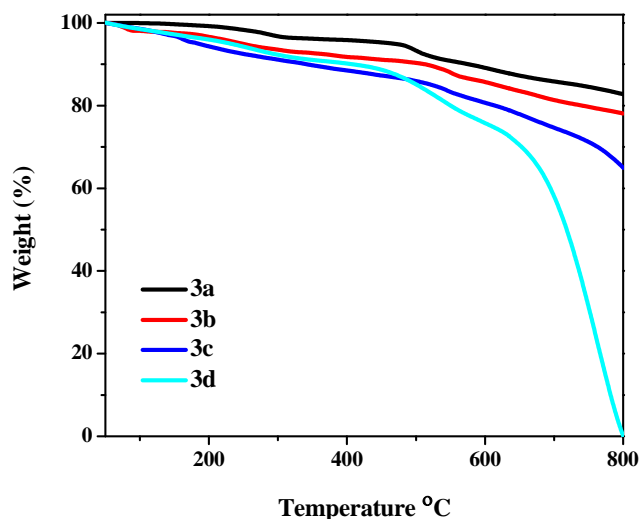
3-ferrocenylphenylacetylene, and 4-ethynyl-phenylethynylferrocene resulted **3a**, **3b**, **3c**, and **3d** in 80%, 70%, 75%, and 80% yield respectively. The benzothiadiazole **3a–3d** were well characterized by  $^1\text{H}$ ,  $^{13}\text{C}$  NMR, and HRMS techniques. The  $^1\text{H}$  NMR spectra of **3a–3d** shows a characteristic singlet between 7.70 and 7.85 ppm corresponding to the two protons of the benzothiadiazole. The benzothiadiazole **3a–3d**, are readily soluble in common organic solvents such as chloroform, dichloromethane, toluene, tetrahydrofuran, *etc.*



**Scheme 3.1.** Synthesis of ferrocenyl benzothiadiazoles **3a–3d**.

### 3.3. Thermal properties

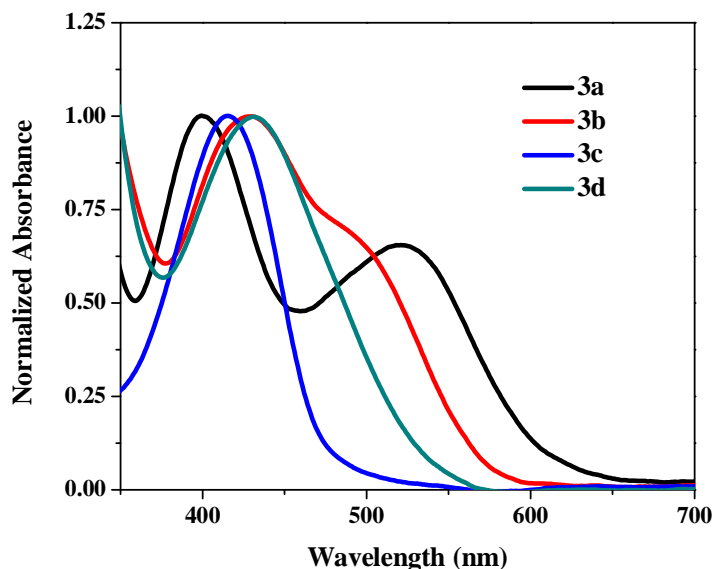
Thermal stability is one of key requirements for practical applications of organic chromophores. The thermal properties of **3a–3d** were investigated by the thermogravimetric analysis (TGA) at a heating rate of  $10\text{ }^\circ\text{C min}^{-1}$ , under nitrogen atmosphere (Figure 3.1.). TGA results show that the benzothiadiazoles **3a–3d** are relatively robust. The decomposition temperatures for compounds **3a–3d** in nitrogen atmosphere are above  $450\text{ }^\circ\text{C}$ . The trend in thermal stability follows the order **3a** > **3b** > **3c** > **3d**.



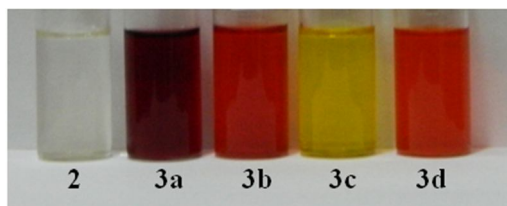
**Figure 3.1.** TGA plots of compounds **3a–3d**.

### 3.4. Photophysical properties

The electronic absorption spectra of the benzothiadiazole **3a–3d** were recorded in dichloromethane at room temperature (Figure 3.2.), and the data are listed in Table 3.1. The benzothiadiazoles **3a–3d** exhibit, strong absorption band between 400–431 nm, corresponding to  $\pi \rightarrow \pi^*$  transition.<sup>[6]</sup> The  $\pi \rightarrow \pi^*$  transition exhibits red shifted absorption with high molar extinction coefficient ( $\epsilon$ ) as the conjugation length was enhanced. This reflects strong electronic communication between the donor, and the acceptor moiety. The absorption spectra of compound **3a**, and **3b** exhibits band at 523 nm and 505 nm due to the charge transfer from ferrocene to the benzothiadiazole unit.<sup>[7]</sup> The presence of distinct CT band was not observed for benzothiadiazole **3c**, and **3d**. This may be due to the overlap of the charge-transfer absorption with the  $\pi \rightarrow \pi^*$  absorption.<sup>[8]</sup> This is also reflected in the dichloromethane solution of compounds **3a–3d** which shows intense red color for benzothiadiazole **3a** compared to red, yellow, and orange colored solutions of compounds **3b**, **3c**, and **3d**, respectively (Figure 3.3.). The compounds **3a–3d** are non-emissive in nature due to the fast non-radiative deactivation of the excited state with intramolecular charge-transfer.<sup>[9]</sup>



**Figure 3.2.** Normalized absorption spectra of ferrocenyl benzothiadiazole **3a–3d** in dichloromethane at  $4 \times 10^{-6}$  M concentration.

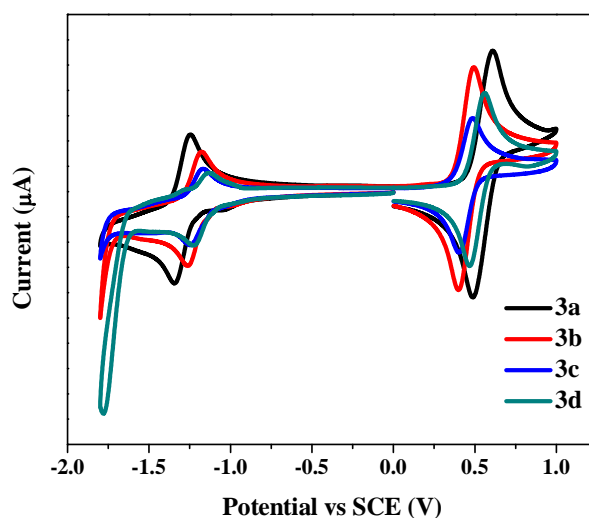


**Figure 3.3.** Ferrocenyl benzothiadiazoles **3a–3d** in dichloromethane at  $10^{-4}$  M concentration.

### 3.5. Electrochemical properties

The electrochemical behavior of the compounds **3a–3d** was explored by cyclic voltammetric analysis in dichloromethane solution using tetrabutylammonium hexafluorophosphate ( $\text{Bu}_4\text{NPF}_6$ ) as supporting electrolyte. The cyclic voltammograms of compounds **3a–3d** are presented in Figure 3.4, and the data is listed in Table 3.1. The ferrocenyl substituted benzothiadiazole **3a–3d**, exhibit one reversible reduction wave in the region  $-1.29$  V to  $-1.19$  V. The reduction potential of **3a–3d** is shifted to lower values compared to unsubstituted benzothiadiazole **1**, indicating that the benzothiadiazole unit is easier to reduce.<sup>[10-12]</sup> The oxidation peaks corresponding to the oxidation of ferrocene to

ferrocenium ion were observed for the compounds **3a–3d** in the region 0.55 V to 0.43 V. The trend in oxidation potential of the ferrocenyl moiety in the benzothiadiazoles **3a–3d** follows the order **3a** > **3d** > **3b** > **3c**. The ferrocene oxidation potential shows high oxidation compared to free ferrocene, confirming the strong electronic communication between the ferrocenyl unit, and the benzothiadiazole core in compounds **3a–3d**.<sup>[13]</sup> The trend observed in the oxidation potential depends upon the nature of the spacer group. The compound **3a** linked by acetylenic spacer shows high oxidation potential compared to compound **3b–3d** due to maximum electronic communication. The *meta* branching in compound **3c** disrupts the extended  $\pi$ -conjugation compared to the other phenylacetylene spacers and thus exhibits lower oxidation potential than **3a**, **3b** and **3d**.<sup>[14]</sup>



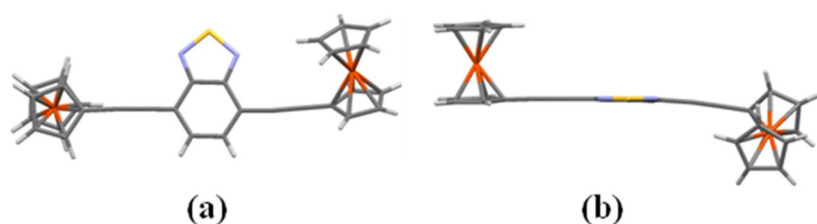
**Figure 3.4.** Cyclic voltammogram of ferrocenyl benzothiadiazole **3a–3d** at 0.01 M concentration in 0.1 M Bu<sub>4</sub>NPF<sub>6</sub> in dichloromethane recorded at 100 mVs<sup>-1</sup> scan speed.

**Table 3.1.** Photophysical and electrochemical data of ferrocenyl benzothiadiazole **3a–3d**.

Compound	Photophysical data <sup>a</sup>	Electrochemical data <sup>b</sup>	
	$\lambda_{\text{max, abs}}$ [nm]/ $\epsilon$ (M <sup>-1</sup> cm <sup>-1</sup> )	E <sub>ox</sub> (V)	E <sub>red</sub> (V)
Ferrocene	–	0.38	–
<b>3a</b>	400 (31200), 523 (20630)	0.55	–1.29
<b>3b</b>	427 (43170), 505 (26778)	0.46	–1.22
<b>3c</b>	415 (50080)	0.43	–1.20
<b>3d</b>	431(55050)	0.52	–1.19

<sup>a</sup> Measured in dichloromethane at  $4 \times 10^{-6}$  M concentration. <sup>b</sup> Recorded by cyclic voltammetry, in 0.1 M solution of Bu<sub>4</sub>NPF<sub>6</sub> in DCM at 100 mV s<sup>-1</sup> scan rate, vs SCE Electrode.

### 3.6. Single crystal X-ray diffraction studies



**Figure 3.5.** Single crystal X-ray structure of ferrocenyl benzothiadiazole **3a**. (a) Front view, and (b) Side view.

The single crystal of the ferrocenyl benzothiadiazole **3a** was obtained via slow diffusion of acetonitrile into dichloromethane solution at room temperature. The benzothiadiazole **3a** crystallizes in the monoclinic space group C2/c. Figure 3.5 shows the single crystal X-ray structure of **3a**. The benzothiadiazole core shows planar structure. The two cyclopentadienyl rings of ferrocene moiety show eclipsed conformation in compound **3a**. The tilt between the benzothiadiazole core, and the cyclopentadienyl ring of one of the ferrocene units is more prominent with the dihedral angle of 60.79° while the other

ferrocene unit shows the dihedral angle of 5.75°. The ferrocene units in compound **3a** lie on the opposite sides of the benzothiadiazole mean plane. The crystal data and refinement parameters, important bond lengths, and bond angles are listed in the Table 3.2 and 3.3.

**Table 3.2.** Crystal data and refinement parameters for **3a**.

<b>Empirical formula</b>	C <sub>12.63</sub> H <sub>8.42</sub> Fe <sub>0.84</sub> N <sub>0.84</sub> S <sub>0.42</sub>
<b>Formula weight (g mol<sup>-1</sup>)</b>	232.52
<b>Temperature</b>	150(2) K
<b>Wavelength</b>	0.71073 Å
<b>Crystal system, space group</b>	Monoclinic, <i>C2/c</i>
<b>Unit cell dimensions</b>	a = 31.052(3) Å   α = 90 ° b = 9.8453(2) Å   β = 134.553(19) ° c = 21.868(2) Å   γ = 90 °
<b>Volume/(Å<sup>3</sup>)</b>	4764.1(7)
<b>Z, Calculated density/ (Mg m<sup>-3</sup>)</b>	19, 1.540
<b>Absorption coefficient /(mm<sup>-1</sup>)</b>	1.328
<b>F(000)</b>	2256
<b>Crystal size (mm)</b>	0.23 × 0.18 × 0.14
<b>θ range for data collection/(°)</b>	2.92 to 25.00
<b>Limiting indices</b>	-36 ≤ h ≤ 36, -11 ≤ k ≤ 11, -26 ≤ l ≤ 26
<b>Reflections collected / unique</b>	22011 / 4196 [R(int) = 0.0263]
<b>Completeness to θmax</b>	θ = 25.00; 99.9 %
<b>Absorption correction</b>	Semi-empirical from equivalents
<b>Max. and min. transmission</b>	0.8359 and 0.7499
<b>Refinement method</b>	Full-matrix least-squares on F <sup>2</sup>
<b>Data / restraints / parameters</b>	4196 / 0 / 316
<b>Goodness-of-fit on F<sup>2</sup></b>	1.047
<b>Final R indices [I &gt; 2σ(I)]</b>	R <sub>1</sub> = 0.0434, wR <sub>2</sub> = 0.1059
<b>R indices (all data)</b>	R <sub>1</sub> = 0.0493, wR <sub>2</sub> = 0.1110
<b>CCDC Number</b>	901492



**Table 3.3.** Selected bond length and bond angle of **3a**

Bond lengths [Å]		Bond angles [°]	
S1-N1	1.612(3)	N1-S1-N2	101.1(2)
S1-N2	1.612(5)	S1-N1-C1	106.1(3)
N1-C1	1.342(7)	S1-N2-C2	106.0(3)
N2-C2	1.335(6)	N1-C1-C2	113.0(3)
C1-C2	1.427(4)	N1-C1-C6	121.0(3)
C1-C6	1.421(6)	N2-C2-C1	113.7(3)
C2-C3	1.427(7)		
C3-C4	1.368(6)		
C4-C5	1.415(5)		
C5-C6	1.365(8)		
C6-C7	1.433(4)		
C7-C8	1.179(5)		
C8-C11	1.430(6)		
C3-C9	1.430(4)		
C9-C10	1.188(4)		
C10-C21	1.427(4)		

### 3.7. Experimental section

All NMR spectra ( $\delta$  values, ppm) were recorded with 400 MHz spectrometers. Tetramethylsilane (TMS) was used as reference for recording  $^1\text{H}$  (of residual proton;  $\delta = 7.26$  ppm) and  $^{13}\text{C}$  ( $\delta = 77.0$  ppm) spectra in  $\text{CDCl}_3$ . Cyclic voltammetric (CV) studies were carried out with an electrochemical system utilizing a three-electrode configuration consisting of a glassy carbon (working) electrode, platinum wire (counter) electrode, and a saturated calomel (reference) electrode. The experiments were performed in dry  $\text{CH}_2\text{Cl}_2$  with 0.1 M tetrabutylammoniumhexafluorophosphate as the supporting electrolyte.

**Synthetic procedure for ferrocenyl substituted benzothiadiazole 3a.** To a stirred solution of ethynylferrocene (107 mg, 0.51 mmol), and 4,7-dibromobenzothiadiazole (50 mg, 0.17 mmol) in THF, and TEA (1:1, v/v) were added  $\text{PdCl}_2(\text{PPh}_3)_2$  (5 mg, 0.007 mmol), and CuI (1 mg, 0.005 mmol) under

an argon flow at room temperature. The reaction mixture was heated to reflux with stirring for 6 h, and then cooled to room temperature. The solvent was then evaporated under reduced pressure, and the mixture was purified by SiO<sub>2</sub> chromatography with CH<sub>2</sub>Cl<sub>2</sub>/hexane (2:3, v/v) to obtain deep-red solid (72 mg, Yield: 80 %). <sup>1</sup>H NMR (400 MHz, CDCl<sub>3</sub>,  $\delta$  in ppm): 7.70 (s, 2H), 4.63 (s, 4H), 4.32-4.30 (m, 14H); <sup>13</sup>C NMR (100 MHz, CDCl<sub>3</sub>,  $\delta$  in ppm): 154.5, 131.9, 117.1, 97.3, 82.0, 71.9, 70.2, 69.4, 64.3; HRMS (C<sub>30</sub>H<sub>20</sub>Fe<sub>2</sub>N<sub>2</sub>S) calcd 552.0041 [M<sup>+</sup>], found 552.0054 [M<sup>+</sup>].

**3b:** Red solid (84 mg, Yield: 70 %). <sup>1</sup>H NMR (400 MHz, CDCl<sub>3</sub>,  $\delta$  in ppm): 7.80 (s, 2H), 7.59 (d, 4H, *J* = 8 Hz), 7.50 (d, 4H, *J* = 8 Hz), 4.70 (s, 4H), 4.38 (s, 4H), 4.05 (s, 10H); <sup>13</sup>C NMR (100 MHz, CDCl<sub>3</sub>,  $\delta$  in ppm): 154.4, 141.0, 132.3, 132.1, 125.8, 119.5, 117.2, 98.1, 85.6, 84.0, 69.8, 69.5, 66.6; HRMS (C<sub>42</sub>H<sub>28</sub>Fe<sub>2</sub>N<sub>2</sub>S) calcd 704.0668 [M<sup>+</sup>], found 704.0701 [M<sup>+</sup>].

**3c:** Yellow-orange solid (90 mg, Yield: 75 %). <sup>1</sup>H NMR (400 MHz, CDCl<sub>3</sub>,  $\delta$  in ppm): 7.85 (s, 2H), 7.75 (s, 2H), 7.53-7.49 (m, 4H), 7.34-7.30 (m, 2H), 4.60 (s, 4H), 4.35 (s, 4H), 4.07 (s, 10H); <sup>13</sup>C NMR (100 MHz, CDCl<sub>3</sub>,  $\delta$  in ppm): 154.4, 139.9, 132.6, 132.1, 129.1, 128.5, 126.5, 122.5, 117.2, 97.8, 85.1, 84.1, 69.7, 69.2, 66.5; HRMS (C<sub>42</sub>H<sub>28</sub>Fe<sub>2</sub>N<sub>2</sub>S) calcd 704.0668 [M<sup>+</sup>], found 704.0623 [M<sup>+</sup>].

**3d:** Orange solid (102 mg, Yield: 80 %). <sup>1</sup>H NMR (400 MHz, CDCl<sub>3</sub>,  $\delta$  in ppm): 7.79 (s, 2H), 7.62 (d, 4H, *J* = 8 Hz), 7.50 (d, 4H, *J* = 8 Hz), 4.51 (s, 4H), 4.26-4.25 (m, 14H); <sup>13</sup>C NMR (100 MHz, CDCl<sub>3</sub>,  $\delta$  in ppm): 154.3, 132.5, 131.9, 131.4, 124.8, 121.5, 117.2, 97.5, 91.3, 86.9, 85.5, 71.5, 70.0, 69.1, 64.8; HRMS (C<sub>48</sub>H<sub>28</sub>Fe<sub>2</sub>N<sub>2</sub>S) calcd 752.0668 [M<sup>+</sup>], found 752.0603 [M<sup>+</sup>].

### 3.8. Conclusions

In summary we have synthesized a series of ferrocenyl substituted benzothiadiazoles by the Pd-catalyzed Sonogashira cross-coupling reaction. The UV-visible absorption, and electrochemical studies of these molecules show strong donor–acceptor interaction. These compounds are non-emissive in nature. The study towards NLO properties of these molecules is currently ongoing in our group.

### 3.9. References

- [1] (a) Ellinger S., Graham K. R., Shi P., Farley R. T., Steckler T. T., Brookins R. N., Taranekar P., Mei J., Padilha L. A., Ensley T. R., Hu H., Webster S., Hagan D. J., Stryland E. W. V., Schanze K. S., Reynolds J. R. (2011), Donor–acceptor–donor-based  $\pi$ -conjugated oligomers for nonlinear optics and near-IR emission, *Chem. Mater.*, 23, 3805-3817 (DOI: 10.1021/cm201424a). (b) Delgado J. L., Bouit P. A., Filippone S., Herranz M. A., Martin N. (2010), Organic photovoltaics: a chemical approach, *Chem. Commun.*, 46, 4853-4865 (DOI: 10.1039/C003088K ). (c) Li Y., Singh S. P., Sonar P. (2010), A high mobility P-Type DPP-thieno[3,2-*b*]thiophene copolymer for organic thin-film transistors, *Adv. Mater.*, 22, 4862-4866 (DOI: 10.1002/adma.201002313). (d) Andersson A. S., Diederich F., Nielsen M. B. (2009), Acetylenic tetrathiafulvalene-dicyanovinyl donor-acceptor chromophores, *Org. Biomol. Chem.*, 7, 3474-3480 (DOI: 10.1039/B909886K). (e) Kivala, M., Diederich, F. (2009), Acetylene-derived strong organic acceptors for planar and nonplanar push–pull chromophores, *Acc. Chem. Res.*, 42, 235-248 (DOI: 10.1021/ar8001238).
- [2] (a) Tambara K., Pantoş G. D. (2012), Supramolecular chemistry of donor–acceptor interactions, *Annu. Rep. Prog. Chem., Sect. B: Org. Chem.*, 108, 186-201 (DOI: 10.1039/C2OC90016E). (b) Polander L. E., Pandey L., Barlow S., Tiwari S. P., Risko C., Kippelen B., Brédas J., Marder S. R. (2011), Benzothiadiazole-dithienopyrrole donor–acceptor–donor and acceptor–donor–acceptor triads: synthesis and optical, electrochemical, and charge-transport properties, *J. Phys. Chem. C*, 115, 23149-23163 (DOI: 10.1021/jp208643k).
- [3] (a) Wang Y., Zhang D., Zhou H., Ding J., Chen Q., Xiao Y., Qian S. (2010), Nonlinear optical properties and ultrafast dynamics of three novel boradiazaindacene derivatives, *J. Appl. Phys.*, 108, 033520 (DOI: 10.1063/1.3457859). (b) Li Y., Wang N., He X., Wang S., Liu H., Li Y.,

Li X., Zhuang J., Zhu D. (2005), Synthesis and characterization of ferrocene-perylenetetracarboxylic diimide–fullerene triad, *Tetrahedron*, 61, 1563-1569 (DOI:10.1016/j.tet.2004.11.078). (c) Yin X., Li Y., Zhu Y., Jing X.; Li Y.; Zhu D. (2010), A highly sensitive viscosity probe based on ferrocene-BODIPY dyads, *Dalton Trans.*, 39, 9929-9935 (DOI: 10.1039/C0DT00309C). (d) Belfield K. D., Morales A. R., Kang B. S., Hales J. M. D., Hagan J., Stryl E. W. V., Chapela V. M., Percino J. (2004), Synthesis, characterization, and optical properties of new two-photon-absorbing fluorene derivatives, *Chem. Mater.*, 16, 4634-4641 (DOI: 10.1021/cm049872g). (c) Hrobarikova V., Hrobarik P., Gajdos P., Fitis I., Fakis M., Persephonis P., Zahradnik P. (2010), Benzothiazole-based fluorophores of donor- $\pi$ -acceptor- $\pi$ -donor type displaying high two-photon absorption, *J. Org. Chem.*, 75, 3053-3068 (DOI: 10.1021/jo100359q). (d) Solntsev V. P., Dudkin S. V., Sabin J. R., Nemykin, V. N. (2011), Electronic communications in (Z)-bis(ferrocenyl)ethylenes with electron-withdrawing substituents, *Organometallics*, 30, 3037-3046 (DOI: 10.1021/om2001266). (e) Nemykin V. N., Makarova E. A., Grosland J. O., Hadt R. G., Koposov A. Y. (2007), Preparation, characterization, molecular and electronic structures, TDDFT, and TDDFT/PCM study of the solvatochromism in cyanovinylferrocenes, *Inorg. Chem.*, 46, 9591–9601 (DOI: 10.1021/ic700558v).

- [4] Kato S., Matsumoto T., Ishi-i T., Thiemann T., Shigeiwa M., Gorohmaru H., Maeda S., Yamashita Y., Mataka S. (2004), Strongly red-fluorescent novel donor- $\pi$ -bridge-acceptor- $\pi$ -bridge-donor (D- $\pi$ -A- $\pi$ -D) type 2,1,3-benzothiadiazoles with enhanced two-photon absorption cross-sections, *Chem. Commun.*, 2342-2343 (DOI: 10.1039/B410016F).
- [5] (a) Green M. L. H., Marder S. R., Thompson M. E., Bandy J. A., Bloor D., Kolinsky P. V., Jones R. J. (1987), Synthesis and structure of (cis)-[1-ferrocenyl-2-(4-nitrophenyl)ethylene], an organotransition metal

- compound with a large second-order optical nonlinearity, *Nature*, 330-362 (DOI:10.1038/330360a0). (b) Gautam P., Dhokale B., Shukla V., Singh C. P., Bindra K. S., Misra R. (2012), Optical limiting performance of meso-tetraferrocenyl porphyrin and its metal derivatives, *J. Photochem. Photobiol. A. Chem.*, 239, 24-27 (DOI:10.1016/j.jphotochem.2012.04.020).
- [6] Vieira A. A., Cristiano R., Bortoluzzi A. J., Gallardo H. (2008), Luminescent 2,1,3-benzothiadiazole-based liquid crystalline compounds, *J. Mol. Struct.*, 875, 364-371 (DOI:10.1016/j.molstruc.2007.05.006).
- [7] (a) Liu H., Zhao Q., Li Y., Liu Y., Lu F., Zhuang J., Wang S., Jiang L., Zhu D., Yu D., Chi L. (2005), Field emission properties of large-area nanowires of organic charge-transfer complexes, *J. Am. Chem. Soc.* **2005**, 127, 1120-1121 (DOI: 10.1021/ja0438359). (b) Cui S., Li Y., Guo Y., Liu H., Song Y., Xu J., Lv J., Zhu M., Zhu D. (2008), Fabrication and field-emission properties of large-area nanostructures of the organic charge-transfer complex Cu-TCNAQ, *Adv. Mater.*, 20, 309-313 (DOI: 10.1002/adma.200701617). (c) Janowska I., Miomandre F., Clavier G., Audebert P., Zakrzewski J., Thi K. H., Ledoux-Rak I. (2006), Donor–acceptor–donor tetrazines containing a ferrocene unit: synthesis, electrochemical and spectroscopic properties, *J. Phys. Chem. A*, 110, 12971-12975 (DOI: 10.1021/jp062186f). (d) Kato S., Matsumoto T., Shigeiwa M., Gorohmaru H., Maeda S., Ishi-i T., Mataka S. (2006), Novel 2,1,3-benzothiadiazole-based red-fluorescent dyes with enhanced two-photon absorption cross-sections, *Chem. Eur. J.*, 12, 2303-2317 (DOI: 10.1002/chem.200500921).
- [8] Ziessel R., Retailleau P., Elliott K. J., Harriman A. (2009), Boron dipyrroin dyes exhibiting “push–pull–pull” electronic signatures, *Chem. Eur. J.*, 15, 10369-10374 (DOI: DOI: 10.1002/chem.200901725).

- [9] (a) Fery-Forgues S., Delavaux-Nicot B. (2000), Ferrocene and ferrocenyl derivatives in luminescent systems, *J. Photochem. Photobiol. A*, 132, 137-159 (DOI:10.1016/S1010-6030(00)00213-6). (b) Dhokale B., Gautam P., Misra, R. (2012), Donor–acceptor perylenediimide–ferrocene conjugates: synthesis, photophysical, and electrochemical properties, *Tetrahedron Lett.*, 53, 2352-2354 (DOI:10.1016/j.tetlet.2012.02.107). (c) Nadtichenko V. A., Denisov N. N., Gak V. Y., Abramova N. V., Loim N. M. (1999), Photochemical and photophysical properties of meso-tetraferrocenylporphyrin. Quenching of meso-tetraphenylporphyrin by ferrocene, *Russ. Chem. Bull.*, 48, 1900-1903 (DOI: 10.1007/BF02494744). (d) Barlow S., Marder S. R. (2000), Electronic and optical properties of conjugated group 8 metallocene derivatives, *Chem. Commun.*, 1555-1562 (DOI: 10.1039/B004907G).
- [10] Zhang H., Wan X., Xue X., Li Y., Yu A., Chen Y. (2010), Selective Tuning of the HOMO–LUMO gap of carbazole-based donor–acceptor–donor compounds toward different emission colors, *Eur. J. Org. Chem.*, 1681-1687 (DOI: 10.1002/ejoc.200901167).
- [11] Watanabe M., Goto K., Shibahara M., Shinmyozu T. (2010), Synthesis, structure, and electronic and photophysical properties of two- and three-layered [3.3]paracyclophane-based donor–acceptor systems (1), *J. Org. Chem.*, 75, 6104-6114 (DOI: 10.1021/jo100688m).
- [12] Rao M. R., Kumar K. V. P., Ravikanth M. (2010), Synthesis of boron-dipyrromethene–ferrocene conjugates, *J. Organomet. Chem.*, 695, 863-869 (DOI: 10.1016/j.jorganchem.2010.01.009).
- [13] Maragani R., Jadhav T., Mobin S. M., Misra R. (2012), Synthesis, structure, photophysical, and electrochemical properties of donor–acceptor ferrocenyl derivatives, *Tetrahedron*, 68, 7302-7308 (DOI: 10.1016/j.tet.2012.06.094).

- [14] (a) Melinger J. S., Pan Y., Kleiman V. D., Peng Z., Davis B. L., McMorro D., Lu M. (2002), Optical and photophysical properties of light-harvesting phenylacetylene monodendrons based on unsymmetrical Branching, *J. Am. Chem. Soc.*, 124, 12002-12012 (DOI: 10.1021/ja020380j). (b) Misra R., Kumar R., Chandrashekar T. K., Suresh C. H., Nag A., Goswami D. (2006),  $22\pi$ -smaragdyrin molecular conjugates with aromatic phenylacetylenes and ferrocenes: syntheses, electrochemical, and photonic properties, *J. Am. Chem. Soc.*, 128, 16083-16091 (DOI: 10.1021/ja0628295).

## Chapter 4

### Donor–acceptor ferrocenyl-substituted benzothiadiazoles

#### 4.1. Introduction

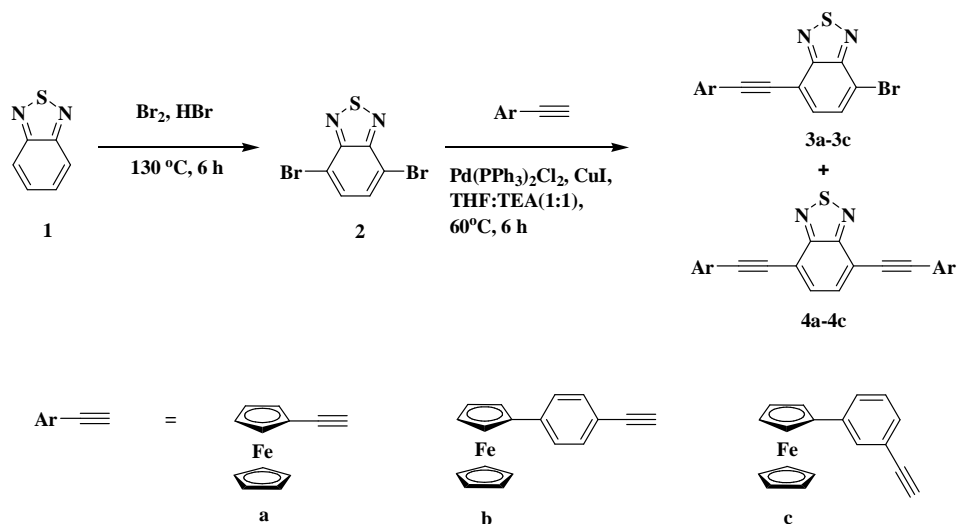
There has been a considerable interest in the design, and synthesis of molecular system with enhanced  $\pi$ -electron delocalization for photonic, and electronic applications.<sup>[1,2]</sup> The linkage of the donor (D) and the acceptor (A) units on the conjugated species results in, D– $\pi$ –A kind of molecular system.<sup>[3]</sup> The photonic properties of the D– $\pi$ –A molecular system can be tuned by either: (a) varying the strength of the donor, or the acceptor group or (b) by changing the  $\pi$ -linker between the donor and the acceptor units.<sup>[4,5]</sup> A variety of acceptors have been exploited for the design, and synthesis of D– $\pi$ –A molecular materials.<sup>[6]</sup> The benzothiadiazole (BTD) with a five-membered heterocyclic ring (C=N-S-N=C) is a strong acceptor, due to its high electron affinity.<sup>[7,8]</sup> Our group has explored ferrocenyl moiety as a strong electron donor, for variety of photonic applications.<sup>[9,10]</sup> Recently, we have synthesized symmetrically substituted ferrocenyl BTDs.<sup>[11]</sup> Our group is interested in modulating the  $\pi$ -bridges between the donor, and the acceptor units, and varying the number of acceptor, in order to explore its photonic, and electronic properties. In this chapter, we wish to report the synthesis of the unsymmetrical D– $\pi_1$ –A– $\pi_2$ –D, and the symmetrical D– $\pi_1$ –A– $\pi_2$ –A– $\pi_1$ –D type of BTD systems. A set of new bromo-BTDs were designed, and synthesized, which serve as the precursors for the synthesis of the ferrocenyl substituted BTDs. The structural, photophysical, and electrochemical properties of these BTD systems were explored.

#### 4.2. Results and discussion

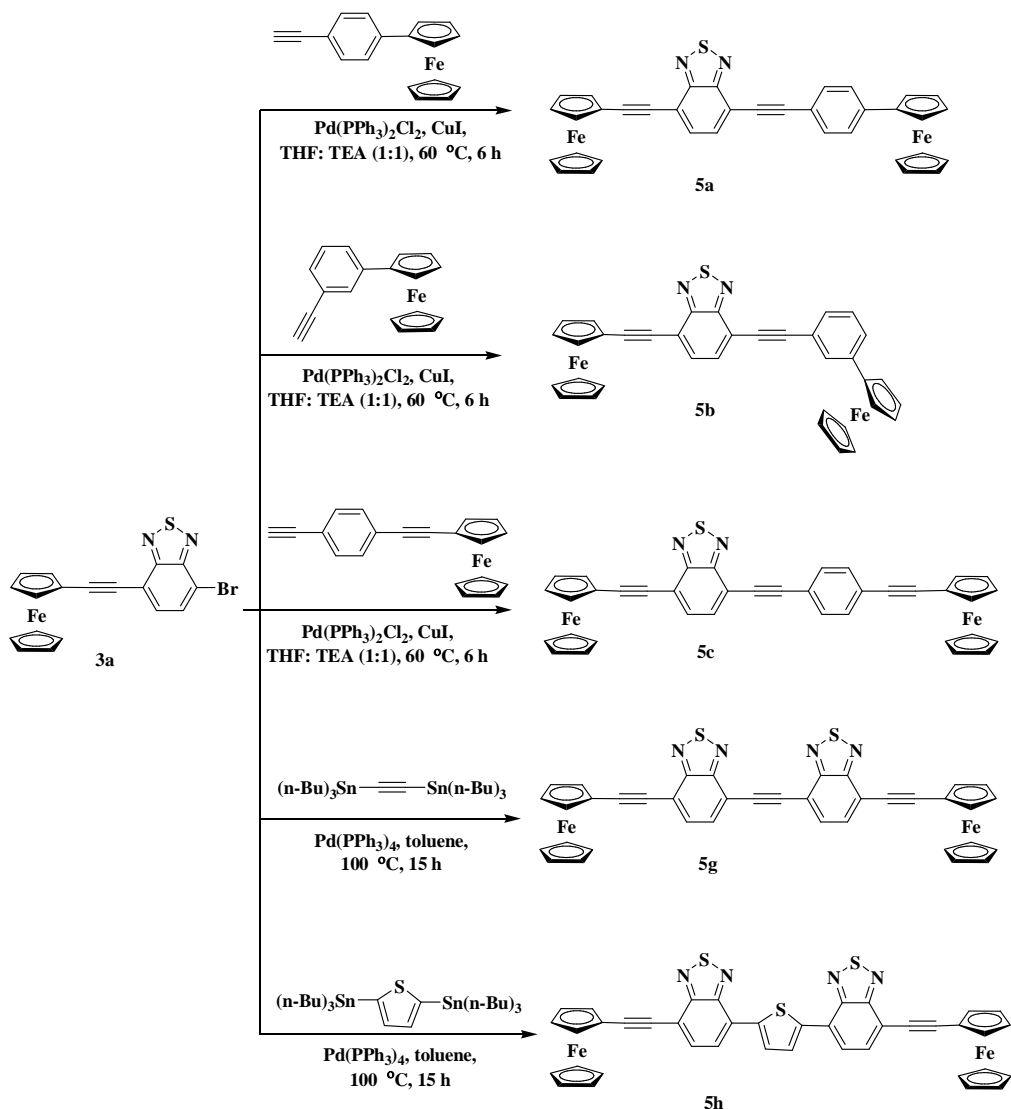
The ferrocenyl substituted BTDs **5a–5h** were synthesized by the Pd-catalyzed Sonogashira, and Stille coupling reactions. The dibromo-BTD **2** was synthesized by the bromination reaction of the BTD **1**.<sup>[12]</sup> The precursors **3a–3c** were synthesized by the Pd-catalyzed Sonogashira coupling reactions of the



dibromo-BTD **2**, with the corresponding ferrocenyl acetylenes (Scheme 4.1.). The reaction of the 1 equivalent of dibromo-BTD **2**, with 1.1 equivalents of ethynyl-ferrocene (**a**), 4-ferrocenylphenylacetylene (**b**), and 3-ferrocenylphenylacetylene (**c**) under the Sonogashira coupling conditions resulted **3a**, **3b**, and **3c** in 60%, 50%, and 55% yield respectively.<sup>[13]</sup> The use of more than 1.1 equivalents of the ferrocenyl acetylenes resulted in the formation of the disubstituted BTDs **4a–4c** in major quantity ( $\geq 40\%$ ), whereas the use of less than 1.1 equivalents of alkynyl-ferrocene left unreacted dibromo-BTD **2**.



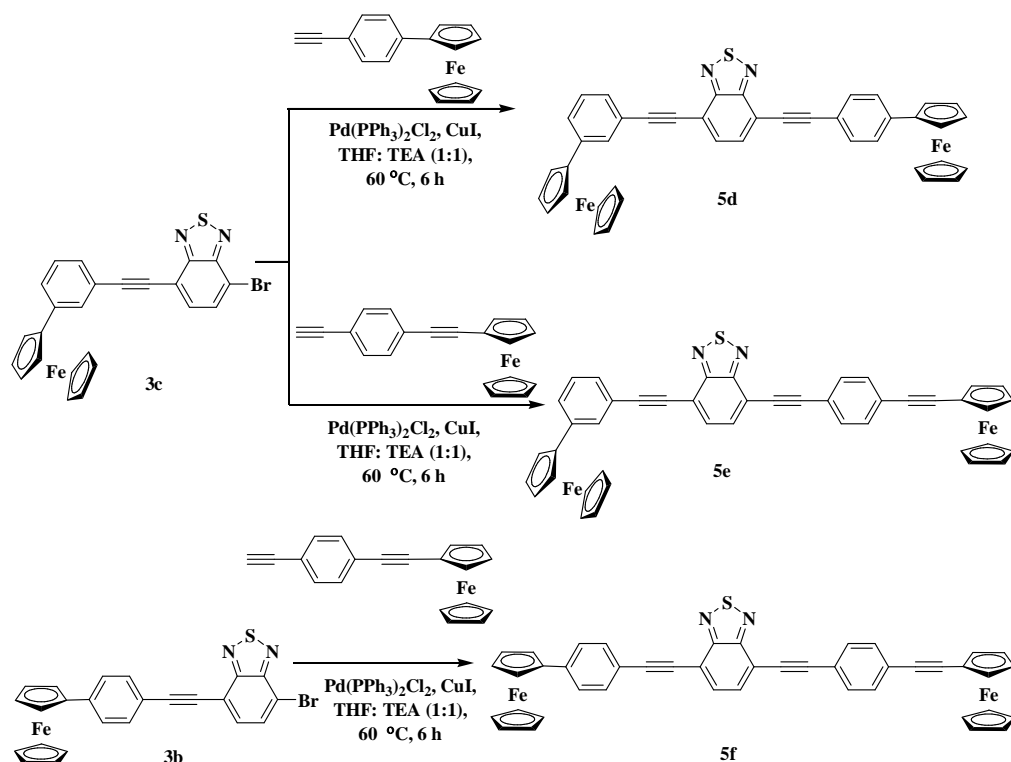
**Scheme 4.1.** Synthetic route for BTD precursors **3a–3c**.



**Scheme 4.2.** Synthetic route for ferrocenyl BTDs **5a-5c**, **5g** and **5h**.

The Sonogashira coupling reaction of the ferrocenyl substituted bromo-BTDs **3a-3c**, and the ferrocenyl acetylenes resulted in BTDs **5a-5f** in 60–70% yield (Scheme 4.2. and Scheme 4.3.). The Stille coupling reaction of the precursor **3a** with bis(tributylstannyl)acetylene, and 2,5-bis(tributylstannyl)thiophene resulted **5g**, and **5h** in 30%, and 25% yield respectively (Scheme 2).<sup>[14]</sup> All the compounds were well characterized by  $^1\text{H}$  NMR,  $^{13}\text{C}$  NMR, and HRMS techniques. The  $^1\text{H}$  NMR spectra of the precursors **3a-3c** show two characteristic doublets between 7.86–7.19 ppm corresponding to the two protons of the BTD.

The BTDs **5a–5d**, **5g**, and **5h** show the characteristic doublet for the BTD protons in the region 7.80–7.50 ppm. The BTD **5e** exhibits a multiplet for the two protons between 7.84–7.80 ppm, whereas the BTD **5f** shows a singlet at 7.79 ppm for the BTD protons. The BTD **3a**, **5a**, and **5g** were also characterized by single crystal X-ray diffraction.

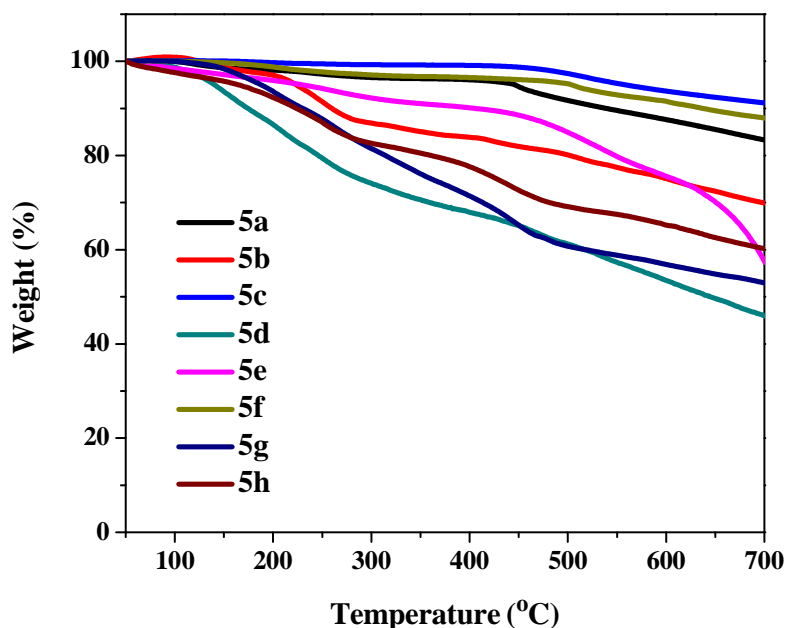


**Scheme 4.3.** Synthetic route for ferrocenyl BTDs **5d–5f**.

### 4.3. Thermogravimetric analysis

The thermal properties of the BTDs **5a–5h** were investigated by the thermogravimetric analysis (TGA) at a heating rate of 10 °C min<sup>-1</sup>, under nitrogen atmosphere (Figure 4.1.). The decomposition temperatures for 10% weight loss in the BTDs **5a**, **5c**, and **5f** was above 400 °C. The BTDs **5b**, **5d**, and **5e** show the decomposition temperature above 200 °C, whereas the BTDs **5g**, and

**5h** with two acceptor units show the decomposition temperature above 230 °C. The thermal stability trend reveals that the ferrocenyl substituted BTDs with two acceptor BTD units have lower thermal stability.



**Figure 4.1.** TGA plots of ferrocenyl BTDs **5a-5h** at a heating rate of 10 °C min<sup>-1</sup>, under nitrogen atmosphere.

#### 4.4. X-ray analysis

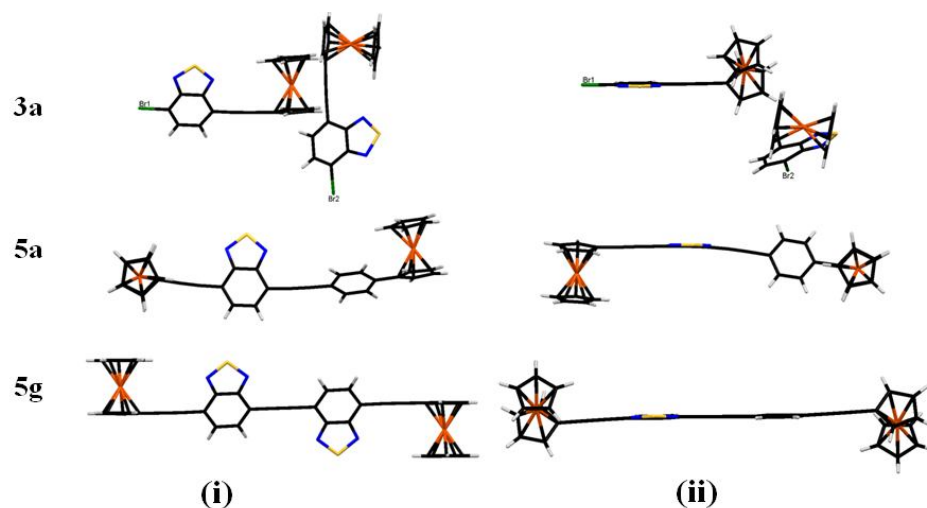
The single crystal of the ferrocenyl BTDs **3a**, **5a**, and **5g** were obtained via slow diffusion of ethanol into the dichloromethane solution at room temperature. The BTDs **3a** and **5a** crystallizes in the triclinic space group  $P\bar{1}$ , whereas the BTD **5g** with two acceptor unit crystallizes in the monoclinic space group  $P2_1/c$ . Figure 4.2 shows the single crystal X-ray structure of **3a**, **5a**, and **5g**.

The BTD core shows planar structure in **3a**, **5a**, and **5g**. The two acceptor units in BTD **5g** are oriented anti to each other. The cyclopentadienyl rings of the ferrocenyl moiety shows eclipsed conformation in BTDs **3a** and **5a**, and eclipsed skew conformation in BTD **5g**. The crystal structure of **3a** consists of two molecules in an asymmetric unit where the Br atom is labeled as Br1, and Br2.

The dihedral angle between the planes containing the BTD core, and the cyclopentadienyl ring of ferrocene units was found to be 60.06° (for Br1), and 58.41° (for Br2) in **3a**, 12.90° (for Fe1), and 87.68° (for Fe2) in **5a**, and 56.66° (Fe1) in **5g**.

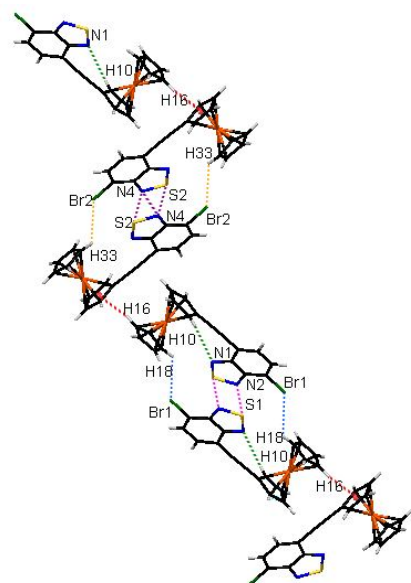
**Table 4.1.** Crystal data and structure refinement for **3a**, **5a** and **5g**.

Parameter	<b>3a</b>	<b>5a</b>	<b>5g</b>
<b>Empirical formula</b>	C <sub>36</sub> H <sub>22</sub> Br <sub>2</sub> Fe <sub>2</sub> N <sub>4</sub> S <sub>2</sub>	C <sub>36</sub> H <sub>24</sub> Fe <sub>2</sub> N <sub>2</sub> S	C <sub>19</sub> H <sub>11</sub> Fe N <sub>2</sub> S
<b>Formula weight</b>	846.22	628.33	355.21
<b>Temperature</b>	150(2) K	150(2) K	150(2) K
<b>Wavelength(Å)</b>	0.71073	0.71073	0.71073
<b>Crystal system, space group</b>	Triclinic, <i>P</i> $\bar{1}$	Triclinic, <i>P</i> $\bar{1}$	Monoclinic, <i>P</i> 2 <sub>1</sub> / <i>c</i>
<b><i>a</i> / (Å)</b>	5.8233(13)	7.8356(3)	5.8557(2)
<b><i>b</i> / (Å)</b>	10.972(3)	13.5503(6)	11.1797(3)
<b><i>c</i> / (Å)</b>	25.131(4)	14.1937(7)	23.0458(7)
<b><math>\alpha</math> / (°)</b>	92.163(16)	101.051(4)	90
<b><math>\beta</math> / (°)</b>	94.088(16)	104.151(4)	96.169(3)
<b><math>\gamma</math> / (°)</b>	90.087(18)	102.601(4)	90
<b>Volume</b>	1600.4(6) Å <sup>3</sup>	1377.45(11) Å <sup>3</sup>	1499.96(8) Å <sup>3</sup>
<b>Z, Calculated density (mg m<sup>-3</sup>)</b>	2, 1.756	2, 1.515	4, 1.573
<b>Absorption coefficient / (mm<sup>-1</sup>)</b>	3.568	1.159	1.143
<b>F(000)</b>	840	644	724
<b>Crystal size</b>	0.33 × 0.26 × 0.21 mm	0.33 × 0.26 × 0.19 mm	0.33 × 0.28 × 0.23 mm
<b><math>\theta</math> range for data collection/(°)</b>	3.12 to 25.00	3.06 to 25.00	3.23 to 25.00
<b>Limiting indices</b>	-6 ≤ <i>h</i> ≤ 6, -13 ≤ <i>k</i> ≤ 13, -29 ≤ <i>l</i> ≤ 29	-9 ≤ <i>h</i> ≤ 9, -16 ≤ <i>k</i> ≤ 15, -16 ≤ <i>l</i> ≤ 16	-6 ≤ <i>h</i> ≤ 6, -13 ≤ <i>k</i> ≤ 13, -27 ≤ <i>l</i> ≤ 27
<b>Reflections collected / unique</b>	11939 / 5600 [R(int) = 0.0270]	11523 / 4838 [R(int) = 0.0296]	11530 / 2620 [R(int) = 0.0243]
<b>Completeness to theta</b>	$\theta$ = 25.00; 99.8%	$\theta$ = 25.00; 99.8%	$\theta$ = 25.00; 99.9%
<b>Absorption correction</b>	Semi-empirical from equivalents	Semi-empirical from equivalents	Semi-empirical from equivalents
<b>Max. and min. transmission</b>	0.5212 and 0.3856	0.8099 and 0.7010	0.7790 and 0.7041
<b>Refinement method</b>	Full-matrix least-squares on F <sup>2</sup>	Full-matrix least-squares on F <sup>2</sup>	Full-matrix least-squares on F <sup>2</sup>
<b>Data / restraints / parameters</b>	5600 / 0 / 415	4838 / 0 / 370	2620 / 0 / 208
<b>Goodness-of-fit on F<sup>2</sup></b>	1.059	1.014	1.129
<b>Final R indices [I &gt; 2σ(I)]</b>	R <sub>1</sub> = 0.0356, wR <sub>2</sub> = 0.0841	R <sub>1</sub> = 0.0396, wR <sub>2</sub> = 0.0920	R <sub>1</sub> = 0.0741, wR <sub>2</sub> = 0.2299
<b>R indices (all data)</b>	R <sub>1</sub> = 0.0456, wR <sub>2</sub> = 0.0904	R <sub>1</sub> = 0.0600, wR <sub>2</sub> = 0.1045	R <sub>1</sub> = 0.0795, wR <sub>2</sub> = 0.2357
<b>Largest diff. peak and hole (eÅ<sup>-3</sup>)</b>	0.541 and -0.520	0.247 and -0.273	0.393 and -1.504
<b>CCDC Number</b>	928342	928343	928341

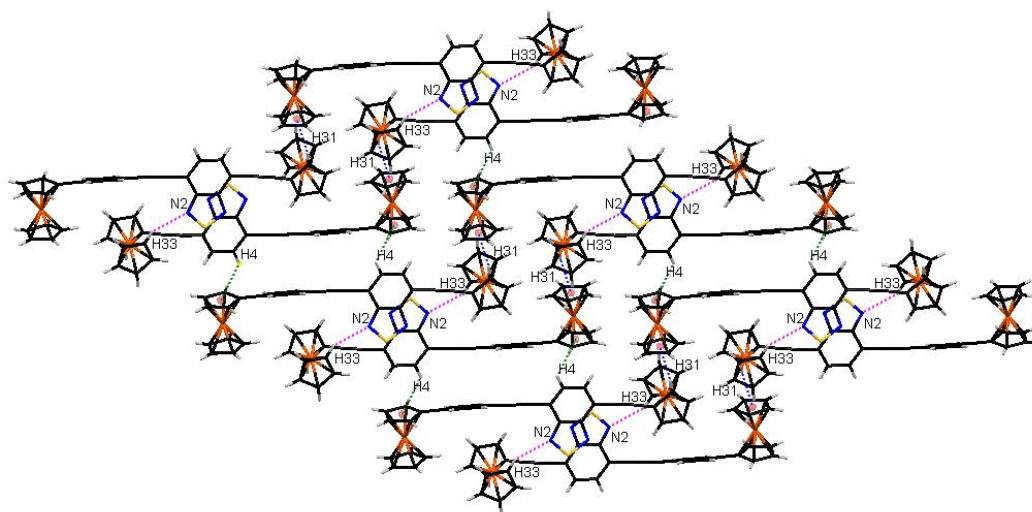


**Figure 4.2.** Single crystal X-ray structure of ferrocenyl BTDs **3a**, **5a**, and **5g**. (i) Top view, and (ii) side view.

The packing diagram of **3a** exhibits short S1...N2 (3.131 Å), S2...N4 (3.154 Å), and N4...N4 (3.080 Å) interthioatom contacts between the BTD rings, which leads to the formation of dimer in head-to-head fashion.<sup>[15]</sup> These dimers are interconnected through hydrogen bonding between N1...H10 (2.640 Å), Br1...H18 (2.934 Å), and Br2...H33 (2.954 Å) to form stacked structures. These stacks are interlinked through CH... $\pi$  interaction C16H16...C27-C31 (3.056 Å) to form 2D zig-zag chain (Figure 4.3.).

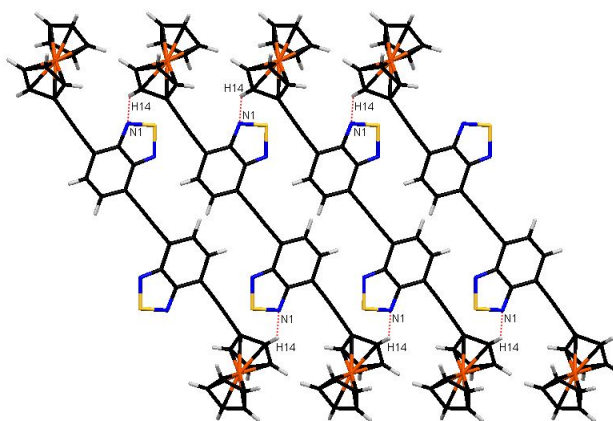


**Figure 4.3.** Packing diagram of ferrocenyl BTD **3a** forming 2D-network along the *a*-axis.



**Figure 4.4.** Packing diagram of ferrocenyl BTD **5a** along the *b*-axis.

The packing diagram of **5a** shows intermolecular C–H $\cdots$ N interaction C33–H33 $\cdots$ N2 (2.665 Å), which leads to the formation of a hydrogen bonded dimers in head-to-head fashion. These dimers are interlinked through C–H $\cdots$  $\pi$  interaction C4H4 $\cdots$ C17–C21 (3.046 Å) to form a 1D polymeric chain. The C–H $\cdots$  $\pi$  interaction C31H31 $\cdots$  C22–C26 (2.803) leads to the cross-linking of the chains, and formation of a 2D sheet like structure (Figure 4.4.).

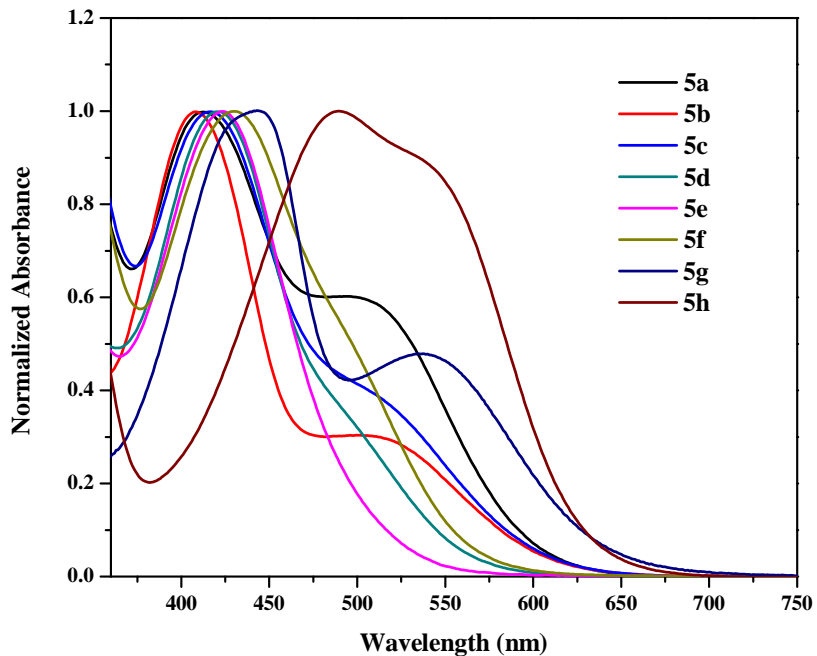


**Figure 4.5.** Packing diagram of ferrocenyl BTB **5g** along the *c*-axis.

The packing diagram of BTB **5g** shows intermolecular C–H $\cdots$  N interaction between the H14 of one BTB molecule, and the N1 of the neighboring BTB molecule at a distance of 2.672 Å (Figure 4.5.), which leads to the formation of 1D polymeric chain.



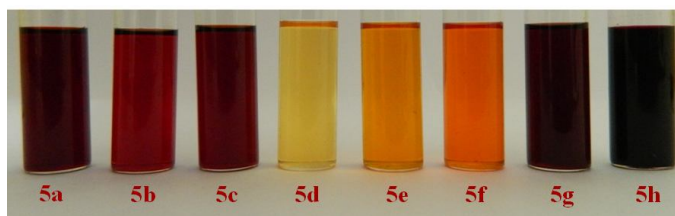
#### 4.5. Photophysical properties



**Figure 4.6.** Normalized electronic absorption spectra of ferrocenyl BTD **5a-5h** in dichloromethane at  $1.0 \times 10^{-6}$  M concentration.

The UV-vis absorption spectra of the benzothiadiazoles **5a-5h** were recorded in dichloromethane at room temperature (Figure 4.6.), and the data are listed in Table 4.2. The BTDs **5a-5h** show strong absorption band between 409–489 nm, corresponding to the  $\pi \rightarrow \pi^*$  transition.<sup>[11]</sup> The  $\pi \rightarrow \pi^*$  transition exhibits red shift in the absorption maxima with the enhancement of the conjugation length. The ferrocenyl BTDs with two acceptor units show substantial bathochromic shift, and higher molar extinction coefficient ( $\epsilon$ ) as compared to the BTDs with one acceptor unit. The red-shift in the absorption maxima follows the order **5h** > **5g** > **5f** > **5e** > **5d** > **5c** > **5a** > **5b**. The linkage of the donor ferrocene at the *meta*-position of the  $\pi$ -spacer in compound **5b**, and **5e** disrupts the extended  $\pi$ -conjugation, and thus results in blue shift in the absorption maxima compared to their isomers **5a**, and **5f** respectively.<sup>[16]</sup> The absorption spectra of BTDs **5a**, **5b**, **5c**, **5g**, and **5h** exhibits band at 507 nm, 504 nm, 515 nm (shoulder), 540 nm, and 542 nm (shoulder), respectively due to the charge-transfer (CT) from ferrocene to the BTD unit. The BTDs **5d-5f** do not show distinct CT band, which

may be due to the overlap of the charge-transfer absorption with the  $\pi \rightarrow \pi^*$  absorption.<sup>[11,17]</sup> The interpretation of the absorption spectra reveals that the charge-transfer is more pronounced, when the donor ferrocene unit is attached to BTD unit by acetylenic linkage. This is also reflected from the intense red colored dichloromethane solution of BTDs **5a–5h** (Figure 4.7.).<sup>[18]</sup> The emission studies of BTDs **5a–5h** shows complete quenching of the fluorescence.<sup>[19]</sup> This further confirms the strong donor–acceptor interaction in these BTD systems.<sup>[20]</sup>



**Figure 4.7.** Ferrocenyl BTDs **5a–5h** at  $10^{-4}$  M concentration in DCM.

#### 4.6. Electrochemical properties

The electrochemical behavior of the BTDs **5a–5h** were explored by the cyclic voltammetric (CV), and differential pulse voltammetric analysis in dry dichloromethane (DCM) solution at room temperature using tetrabutylammonium hexafluorophosphate (TBAPF<sub>6</sub>) as a supporting electrolyte. The electrochemical data of the BTDs **5a–5h** are listed in Table 4.2, and the representative cyclic voltammogram are shown in Figure 4.8 and 4.9. The BTDs **5a** and **5b** exhibit two reversible oxidation waves in the region 0.02 V to 0.12 V, whereas the BTDs **5c–5h** exhibit one reversible oxidation wave in the region 0.07 V to 0.16 V, corresponding to the oxidation of ferrocene to ferrocenium ion. The ferrocenyl moiety in the BTDs **5a–5h** exhibit high oxidation potential compared to free ferrocene, confirming the strong electronic communication between the ferrocene unit, and the BTD core.<sup>[21]</sup> The trend in the oxidation potential of the ferrocenyl moiety in the BTDs **5a–5h** follows the order **5g** > **5h** > **5c** > **5a** > **5f** > **5b** > **5e** >

**5d**, which reveals that the increase in the number of acceptor unit, improves the donor–acceptor interaction.

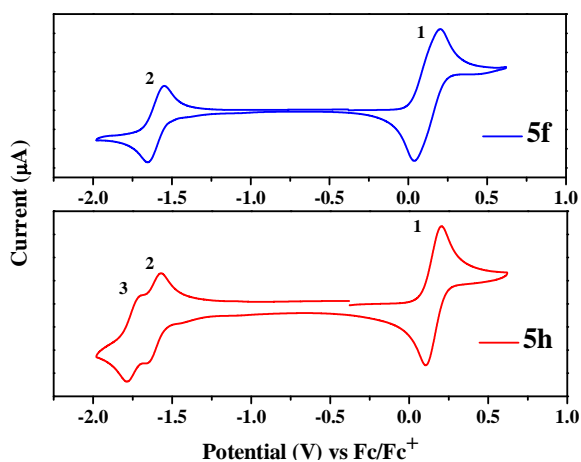
**Table 4.2.** Photophysical and electrochemical data of the ferrocenyl BTDs **5a–5h**.

Compound	Photophysical data <sup>a</sup>		Electrochemical data <sup>b</sup>		
	$\lambda_{\text{abs}}$ (nm)	$\varepsilon$ (M <sup>-1</sup> cm <sup>-1</sup> )	Wave	E°(V)	$i_{\text{pc}}/i_{\text{pa}}$
<b>Ferrocene</b>	-	-	1	0.00	0.94
<b>5a</b>	413	38,250	1 <sup>d</sup>	0.12	-
	507	22,677	2 <sup>d</sup>	0.02	-
			3	-1.66	0.97
<b>5b</b>	409	39,850	1 <sup>d</sup>	0.11	-
	504	12,870	2 <sup>d</sup>	0.02	-
			3	-1.67	0.91
<b>5c</b>	417	52950	1	0.14	0.97 <sup>c</sup>
	515	sh	2	-1.64	0.98 <sup>c</sup>
<b>5d</b>	421	46,400	1	0.07	0.99
	-	-	2	-1.62	0.98 <sup>c</sup>
<b>5e</b>	423	54,630	1	0.09	0.96
	-	-	2	-1.60	0.95
<b>5f</b>	429	52,500	1	0.11	0.98
	-	-	2	-1.59	0.95 <sup>c</sup>
<b>5g</b>	443	69,000	1	0.16	0.98
	540	33,023	2	-1.55	0.91
			3	-1.72	0.89 <sup>c</sup>
<b>5h</b>	489	70,900	1	0.15	0.94 <sup>c</sup>
	542	sh	2	-1.62	0.93 <sup>c</sup>
			3	-1.77	0.84 <sup>c</sup>

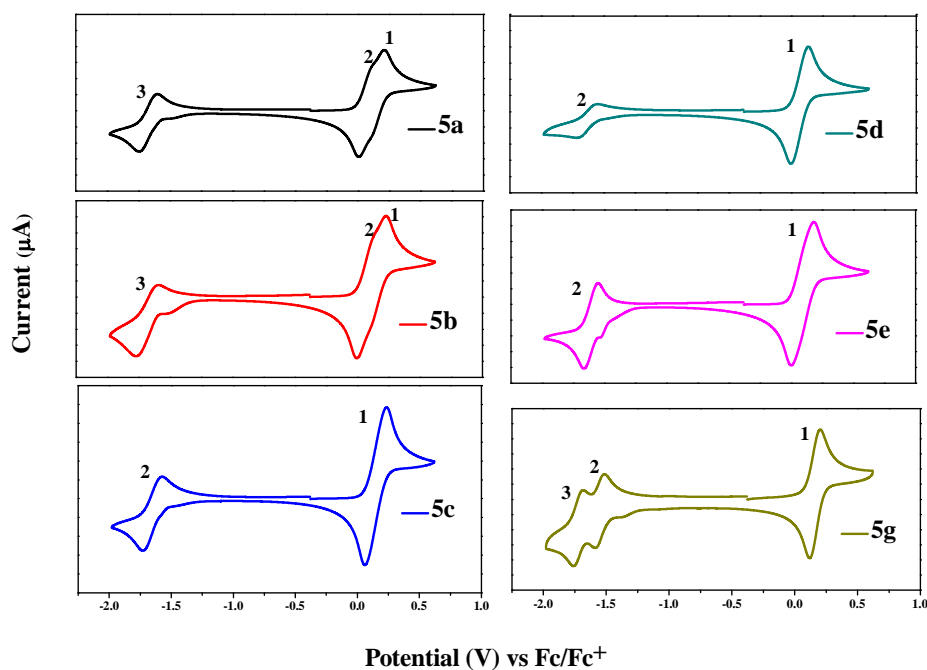
<sup>a</sup>Absorbance measured in dichloromethane at  $4 \times 10^{-6}$  M concentration; sh = shoulder;  $\lambda_{\text{abs}}$ : absorption wavelength;  $\varepsilon$ : extinction coefficient. <sup>b</sup>Recorded by cyclic voltammetry, in 0.1 M solution of TBAPF<sub>6</sub> in DCM at 100 mVs<sup>-1</sup> scan rate, vs Fc/Fc<sup>+</sup> at 25 °C;  $i_{\text{pc}}/i_{\text{pa}}$ = peak current ratio. <sup>c</sup>  $i_{\text{pa}}/i_{\text{pc}}$ ; <sup>d</sup>Recorded by differential pulse voltammetry.

The BTDs **5a–5f**, exhibit one electron reversible reduction wave in the region -1.59 V to -1.67 V corresponding to the BTD acceptor moiety, whereas the BTDs **5g–5h** exhibit two distinct waves in the region -1.55 V to -1.77 V due

to the presence of two acceptor units. This indicates strong intramolecular electronic interaction between the two BTD units in BTDs **5g**, and **5h**, which leads to a decrease of the first reduction potential.<sup>[22,23]</sup> In general, the reduction potential for the BTDs **5a–5h** shows lower values compared to unsubstituted BTD **1** (−1.98 V vs. Fc/Fc<sup>+</sup> in DCM) indicating that the BTD ring in ferrocenyl substituted BTDs is easy to reduce compared to unsubstituted BTD.<sup>[11,24]</sup> The reversibility was observed with peak current ratios close to 1 for all processes, and the deviation from 1 is the result of baseline uncertainty due to the onset of solvent decomposition at these low potentials.<sup>[25]</sup>



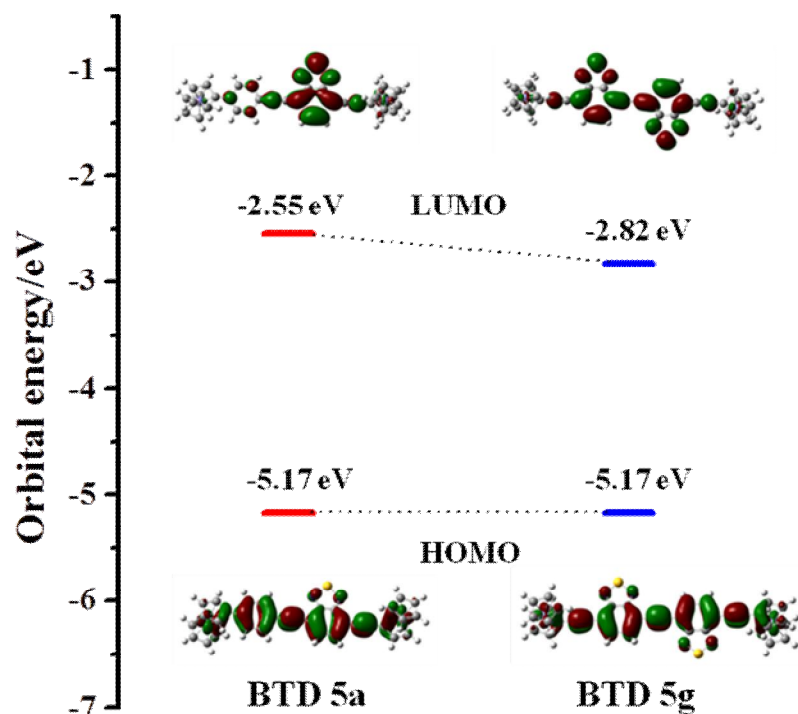
**Figure 4.8.** Cyclic voltammogram of ferrocenyl BTDs **5f**, and **5h** at 0.01 M concentration in 0.1 M TBAPF<sub>6</sub> in dichloromethane recorded at a scan rate of 100 mVs<sup>−1</sup>.



**Figure 4.9.** Cyclic voltammogram of ferrocenyl BTDs **5a–5e**, and **5g** at 0.01 M concentration in 0.1 M TBAPF<sub>6</sub> in dichloromethane recorded at a scan rate of 100 mVs<sup>-1</sup>.

#### 4.7 Theoretical Calculations

In order to explore the electronic structure of the unsymmetrical, and symmetrical BTDs, DFT calculations were performed on the BTDs **5a**, and **5g**. The contours of the HOMO, and LUMO of BTDs **5a**, and **5g** are shown in Figure 4.11, which reveals that the HOMO orbitals are localized over ferrocene, benzene, and benzo of the BTD unit. The HOMOs of BTD **5a**, and **5g** were found to be at almost the same energy level. The LUMO orbitals of BTD **5a**, and **5g** are mainly concentrated on the BTD unit.<sup>[22]</sup> The lowering of the LUMO energy level for BTD **5g** in comparison to BTD **5a** can be attributed to the presence of two acceptor units.<sup>[26]</sup> The lower energy gap in the BTD **5g** as compared to BTD **5a** results in the bathochromic shift in the electronic absorption.



**Figure 4.10.** Correlation diagram showing the HOMO, and LUMO wave functions and energies of the BTDs **5a** (left), and **5g** (right), as determined at the B3LYP/6-31G\*\* level for C, N, S, and H, and the Lanl2DZ level for Fe (Isovalue = 0.02).

#### 4.8. Experimental section

$^1\text{H}$  NMR (400 MHz), and  $^{13}\text{C}$  NMR (100 MHz) spectra were recorded on 400 MHz, using  $\text{CDCl}_3$  as solvent. Tetramethylsilane (TMS) was used as reference for recording  $^1\text{H}$  (of residual proton;  $\delta = 7.26$  ppm), and  $^{13}\text{C}$  ( $\delta = 77.0$  ppm) spectra in  $\text{CDCl}_3$ . The  $^1\text{H}$  NMR splitting patterns have been described as “s, singlet; bs, broad singlet; d, doublet; t, triplet; and m, multiplet”. UV-visible absorption spectra of all compounds were recorded in DCM. Cyclic voltamograms (CVs) and differential pulse voltamograms (DPVs) were recorded on electrochemical analyzer using Glassy carbon as working electrode, Pt wire as the counter electrode, and Saturated Calomel Electrode (SCE) as the reference

electrode. The scan rate was 100 mVs<sup>-1</sup> for CV, and 50 mVs<sup>-1</sup> for DPV. A solution of tetrabutylammoniumhexafluorophosphate (TBAPF<sub>6</sub>) in CH<sub>2</sub>Cl<sub>2</sub> (0.1 M) was employed as the supporting electrolyte. DCM was freshly distilled from CaH<sub>2</sub> prior to use. All potentials were experimentally referenced against the saturated calomel electrode couple but were then manipulated to be referenced against Fc/Fc<sup>+</sup> as recommended by IUPAC.<sup>[27]</sup> Under our conditions, the Fc/Fc<sup>+</sup> couple exhibited  $i_{pc}/i_{pa} = 0.94$ ,  $E^\circ = 0.38$  V versus SCE. HRMS was recorded on TOF-Q mass spectrometer.

**General procedure for the preparation of ferrocenyl bromo-BTDs 3a-3c by Sonogashira coupling reaction.**

To a stirred solution of respective alkynyl ferrocene (0.37 mmol), and 4, 7-dibromo-BTD (0.34 mmol) in THF, and TEA (1:1, v/v) were added PdCl<sub>2</sub>(PPh<sub>3</sub>)<sub>2</sub> (10 mg, 0.014 mmol), and CuI (2 mg, 0.01 mmol) under an argon flow at room temperature. The reaction mixture was stirred for 6 h at 60 °C, and then cooled to room temperature. The solvent was evaporated under reduced pressure, and the mixture was purified by SiO<sub>2</sub> chromatography with DCM/Hexane (1:3, v/v) followed by recrystallization in DCM:methanol (1:1) to obtain colored solid.

**BTD 3a:** Red solid (86.4 mg, Yield: 60 %): mp 170.5-171.2 °C; <sup>1</sup>H NMR (400 MHz, CDCl<sub>3</sub>,  $\delta$  in ppm): 7.65 (d, 1H,  $J = 8.3$  Hz), 7.20 (d, 1H,  $J = 8.0$  Hz), 4.49 (s, 2H), 4.24 (bs, 7H); <sup>13</sup>C NMR (100 MHz, CDCl<sub>3</sub>,  $\delta$  in ppm): 154.2, 153.1, 132.1, 132.0, 117.4, 113.5, 97.0, 81.1, 71.9, 70.2, 69.4, 63.9; HRMS (ESI)  $m/z$  calcd for C<sub>18</sub>H<sub>11</sub>BrFeN<sub>2</sub>S 421.9172 [M<sup>+</sup>], found 421.9168 [M<sup>+</sup>].

**BTD 3b:** Red solid (85 mg, Yield: 50 %): mp 182.2-183.4 °C; <sup>1</sup>H NMR (400 MHz, CDCl<sub>3</sub>,  $\delta$  in ppm): 7.83 (d, 1H,  $J = 7.5$  Hz), 7.66 (d, 1H,  $J = 7.5$  Hz), 7.56 (d, 2H,  $J = 8.5$  Hz), 7.48 (d, 2H,  $J = 8.5$  Hz), 4.68 (t, 2H,  $J = 1.8$  Hz), 4.37 (t, 2H,  $J = 1.8$  Hz), 4.04(s, 5H); <sup>13</sup>C NMR (100 MHz, CDCl<sub>3</sub>,  $\delta$  in ppm): 154.2, 153.1, 141.1, 132.5, 132.0, 125.8, 119.4, 117.0, 114.3, 97.5, 84.7, 83.9, 69.76, 69.75, 69.5, 66.6; HRMS (ESI)  $m/z$  calcd for C<sub>24</sub>H<sub>15</sub>BrFeN<sub>2</sub>S 499.9467 [M<sup>+</sup>], found 499.9464 [M<sup>+</sup>].

**BTD 3c:** Orange solid (93.5 mg, Yield: 55 %): mp 148.2-148.8 °C; <sup>1</sup>H NMR (400 MHz, CDCl<sub>3</sub>, δ in ppm): 7.85 (d, 1H, *J* = 7.5 Hz), 7.73 (t, 1H, *J* = 1.3 Hz), 7.70 (d, 1H, *J* = 7.8 Hz), 7.51-7.47 (m, 2H), 7.31 (t, 1H, *J* = 1.3 Hz), 4.68 (t, 2H, *J* = 1.8 Hz), 4.34 (t, 2H, *J* = 1.8 Hz), 4.06 (s, 5H); <sup>13</sup>C NMR (100 MHz, CDCl<sub>3</sub>, δ in ppm): 154.2, 153.1, 139.9, 132.9, 132.0, 129.4, 129.0, 128.5, 126.9, 122.3, 116.7, 114.6, 97.1, 84.3, 84.0, 69.7, 69.2, 66.5; HRMS (ESI) *m/z* calcd for C<sub>24</sub>H<sub>15</sub>BrFeN<sub>2</sub>S 497.9485 [M<sup>+</sup>], found 497.9515 [M<sup>+</sup>].

**General procedure for the preparation of ferrocenyl BTDs 5a-5f by Sonogashira coupling reaction.**

To a stirred solution of respective alkynyl ferrocene (0.37 mmol), and ferrocenyl bromo-BTDs **3a/3b/3c** (0.34 mmol) in THF, and TEA (1:1, v/v) were added PdCl<sub>2</sub>(PPh<sub>3</sub>)<sub>2</sub> (10 mg, 0.014 mmol), and CuI (2 mg, 0.01 mmol) under an argon flow at room temperature. The reaction mixture was stirred for 6 h at 60°C, and then cooled to room temperature. The solvent was then evaporated under reduced pressure, and the mixture was purified by SiO<sub>2</sub> chromatography with DCM/Hexane (2:3, v/v) followed by recrystallization in DCM:methanol (1:1) to obtain colored solid.

**BTD 5a:** Red solid (149 mg, Yield: 70 %): mp > 300.0 °C; <sup>1</sup>H NMR (400 MHz, CDCl<sub>3</sub>, δ in ppm): 7.76 (d, 1H, *J* = 7.5 Hz), 7.73 (d, 1H, *J* = 7.3 Hz), 7.58 (d, 2H, *J* = 8.5 Hz), 7.48 (d, 2H, *J* = 8.8 Hz), 4.69 (t, 2H, *J* = 2 Hz), 4.64 (t, 2H, *J* = 1.8 Hz), 4.37 (t, 2H, *J* = 2 Hz), 4.32-4.30 (m, 7H), 4.04 (s, 5H); <sup>13</sup>C NMR (100 MHz, CDCl<sub>3</sub>, δ in ppm): 154.5, 154.4, 140.9, 132.3, 132.0, 131.8, 125.8, 119.6, 117.8, 116.6, 97.72, 97.68, 84.0, 82.0, 71.9, 70.2, 69.8, 69.51, 69.45, 66.6, 64.2; HRMS (ESI) *m/z* calcd for C<sub>36</sub>H<sub>24</sub>Fe<sub>2</sub>N<sub>2</sub>S 628.0355 [M<sup>+</sup>], found 628.0387 [M<sup>+</sup>]; UV/vis (DCM): λ<sub>max</sub> (ε [M<sup>-1</sup>cm<sup>-1</sup>]) 413 (38,250), 507 (22,677).

**BTD 5b:** Orange-red solid (138 mg, Yield: 65 %): mp 208.5-209.6 °C; <sup>1</sup>H NMR (400 MHz, CDCl<sub>3</sub>, δ in ppm): 7.80 (d, 1H, *J* = 7.5 Hz), 7.75-7.74 (m, 2H), 7.51-7.48 (m, 2H), 7.31 (t, 1H, *J* = 7.8 Hz), 4.69 (t, 2H, *J* = 1.8 Hz), 4.65 (t, 2H, *J* = 2 Hz), 4.34-4.31 (m, 9H), 4.06 (s, 5H); <sup>13</sup>C NMR (100 MHz, CDCl<sub>3</sub>, δ in ppm): 154.5, 154.4, 139.9, 132.7, 131.8, 129.5, 129.1, 128.5, 126.8, 122.6, 118.0, 116.3,



97.8, 97.3, 85.2, 84.1, 81.9, 72.0, 70.2, 69.7, 69.5, 69.2, 66.5, 64.1; HRMS (ESI)  $m/z$  calcd for  $C_{36}H_{24}Fe_2N_2S$  628.0355 [ $M^+$ ], found 628.0370 [ $M^+$ ]; UV/vis (DCM):  $\lambda_{max}$  ( $\epsilon$  [ $M^{-1}cm^{-1}$ ]) 409 (39,850), 504 (12,870).

**BTd 5c:** Red solid (137 mg, Yield: 62 %): mp > 300.0 °C;  $^1H$  NMR (400 MHz,  $CDCl_3$ ,  $\delta$  in ppm): 7.76 (d, 1H,  $J = 7.3$  Hz), 7.73 (d, 1H,  $J = 7.3$  Hz), 7.61 (d, 2H,  $J = 8$  Hz), 7.49 (d, 2H,  $J = 8$  Hz), 4.64 (t, 2H,  $J = 2$  Hz), 4.51 (t, 2H,  $J = 1.8$  Hz), 4.33-4.30 (m, 7H), 4.26-4.25 (m, 7H);  $^{13}C$  NMR (100 MHz,  $CDCl_3$ ,  $\delta$  in ppm): 154.38, 154.37, 132.6, 131.8, 131.7, 131.3, 124.6, 121.6, 118.1, 116.1, 98.0, 97.0, 91.2, 87.1, 85.5, 81.9, 72.0, 71.5, 70.2, 70.0, 69.5, 69.0, 64.8, 64.1; HRMS (ESI)  $m/z$  calcd for  $C_{38}H_{24}Fe_2N_2S$  652.0355 [ $M^+$ ], found 652.0364 [ $M^+$ ]; UV/vis (DCM):  $\lambda_{max}$  ( $\epsilon$  [ $M^{-1}cm^{-1}$ ]) 417(52950), 515 (sh).

**BTd 5d:** Orange solid (143 mg, Yield: 60 %): mp 210.5-211.4 °C;  $^1H$  NMR (400 MHz,  $CDCl_3$ ,  $\delta$  in ppm): 7.83 (d, 1H,  $J = 7.5$  Hz), 7.80 (d, 1H,  $J = 7.5$  Hz), 7.75 (t, 1H,  $J = 1.8$  Hz), 7.59 (d, 2H,  $J = 8.5$  Hz), 7.52-7.48 (m, 4H), 7.32 (t, 1H,  $J = 7.8$  Hz), 4.69 (t, 4H,  $J = 2$  Hz), 4.37 (t, 2H,  $J = 2$  Hz), 4.35 (t, 2H,  $J = 2$  Hz), 4.05-4.06 (m, 10H);  $^{13}C$  NMR (100 MHz,  $CDCl_3$ ,  $\delta$  in ppm): 154.44, 154.41, 141.0, 139.9, 132.6, 132.2, 132.1, 129.5, 129.1, 128.5, 126.8, 125.8, 122.5, 119.5, 117.5, 116.9, 114.1, 98.2, 97.6, 85.5, 85.1, 84.1, 83.9, 69.8, 69.7, 69.5, 69.2, 66.6, 66.5; HRMS (ESI)  $m/z$  calcd for  $C_{42}H_{28}Fe_2N_2S$  704.0688 [ $M^+$ ], found 704.0704 [ $M^+$ ]; UV/vis (DCM):  $\lambda_{max}$  ( $\epsilon$  [ $M^{-1}cm^{-1}$ ]) 421(46,400).

**BTd 5e:** Orange solid (148 mg, Yield: 60 %): mp 219.5-220.6 °C;  $^1H$  NMR (400 MHz,  $CDCl_3$ ,  $\delta$  in ppm): 7.84-7.80 (m, 2H), 7.75 (s, 1H), 7.62 (d, 2H,  $J = 7.8$  Hz), 7.51-7.49 (m, 4H), 7.32 (t, 1H,  $J = 7.8$  Hz), 4.69 (s, 2H), 4.52 (s, 2H), 4.35-4.20 (m, 9H), 4.06 (s, 5H);  $^{13}C$  NMR (100 MHz,  $CDCl_3$ ,  $\delta$  in ppm): 154.3, 144.8, 139.9, 132.52, 132.45, 131.9, 131.3, 129.5, 129.1, 128.5, 126.9, 124.8, 122.5, 121.5, 117.3, 117.1, 97.9, 97.4, 91.3, 86.9, 85.5, 84.1, 71.5, 70.0, 69.7, 69.2, 69.1, 66.5, 64.8, 60.6; HRMS (ESI)  $m/z$  calcd for  $C_{44}H_{28}Fe_2N_2S$  728.0668 [ $M^+$ ], found 728.0665 [ $M^+$ ]; UV/vis (DCM):  $\lambda_{max}$  ( $\epsilon$  [ $M^{-1}cm^{-1}$ ]) 423(54,630).

**BTd 5f:** Orange solid (151 mg, Yield: 61 %): mp > 300.0 °C;  $^1H$  NMR (400 MHz,  $CDCl_3$ ,  $\delta$  in ppm): 7.79 (s, 2H), 7.62 (d, 2H,  $J = 8.5$  Hz), 7.58 (d, 2H,  $J =$

8.5 Hz), 7.51-7.47 (m, 4H), 4.69 (t, 2H,  $J = 1.8$  Hz), 4.51 (t, 2H,  $J = 1.8$  Hz), 4.37 (t, 2H,  $J = 2$  Hz), 4.26-4.25 (m, 7H), 4.04 (s, 5H);  $^{13}\text{C}$  NMR (100 MHz,  $\text{CDCl}_3$ ,  $\delta$  in ppm): 154.4, 148.4, 132.5, 132.2, 132.1, 131.9, 131.4, 128.0, 125.9, 124.8, 123.7, 122.3, 121.5, 119.5, 116.8, 91.2, 85.5, 83.9, 81.5, 71.5, 70.0, 69.8, 69.6, 69.1, 66.6, 64.8; HRMS (ESI)  $m/z$  calcd for  $\text{C}_{44}\text{H}_{28}\text{Fe}_2\text{N}_2\text{S}$  728.0668 [ $\text{M}^+$ ], found 728.0664 [ $\text{M}^+$ ]; UV/vis (DCM):  $\lambda_{\text{max}}$  ( $\epsilon$  [ $\text{M}^{-1}\text{cm}^{-1}$ ]) 429 (52,500).

**General procedure for the preparation of Ferrocenyl BTDs 5g, and 5h by Stille coupling reaction.**

To a stirred solution of BTd **3a** (0.5 mmol) in toluene (20 ml) were added  $\text{Pd}(\text{PPh}_3)_4$  (0.05 mmol), and the respective stannyl derivative (0.25 mmol) under an argon flow at room temperature. The mixture was stirred for 15 h at 100 °C, and then allowed to cool to room temperature. The solvent was evaporated under reduced pressure, and the black residue was dissolved in dichloromethane (20 mL). This was washed with brine solution ( $2 \times 20$  mL). The aqueous layer was washed with more dichloromethane (20 mL), and the combined organic layers were dried with  $\text{Na}_2\text{SO}_4$ , filtered, and the dichloromethane was allowed to evaporate. The resulting residual solid was purified by column chromatography through silica gel (100-200 mesh) with DCM as the eluent. The desired compound eluted in DCM. The solvent was evaporated, and the solid was recrystallized from DCM:methanol (1:1) to give colored solid.

**BTd 5g:** Reddish-brown solid (106 mg, Yield: 30 %): mp > 300.0 °C;  $^1\text{H}$  NMR (400 MHz,  $\text{CDCl}_3$ ,  $\delta$  in ppm): 7.92 (d, 2H,  $J = 7.3$  Hz), 7.77 (d, 2H,  $J = 7.3$  Hz), 4.65 (t, 4H,  $J = 1.8$  Hz), 4.34-4.31 (m, 14H);  $^{13}\text{C}$  NMR (100 MHz,  $\text{CDCl}_3$ ,  $\delta$  in ppm): 154.38, 154.36, 133.2, 131.7, 118.8, 115.5, 92.8, 82.0, 72.0, 70.3, 69.6, 68.0, 64.0; HRMS (ESI)  $m/z$  calcd for  $\text{C}_{38}\text{H}_{22}\text{Fe}_2\text{N}_4\text{S}_2$  709.9981 [ $\text{M}^+$ ], found 710.0035 [ $\text{M}^+$ ]; UV/vis (DCM):  $\lambda_{\text{max}}$  ( $\epsilon$  [ $\text{M}^{-1}\text{cm}^{-1}$ ]) 443 (69,000), 540 (33,023).

**BTd 5h:** purple solid (96 mg, Yield: 25 %): mp > 300.0 °C;  $^1\text{H}$  NMR (400 MHz,  $\text{CDCl}_3$ ,  $\delta$  in ppm): 8.25 (s, 2H), 7.94 (d, 2H,  $J = 7.5$  Hz), 7.79 (d, 2H,  $J = 7.5$  Hz), 4.66 (t, 4H,  $J = 1.5$ ), 4.33-4.32 (m, 14H);  $^{13}\text{C}$  NMR (100 MHz,  $\text{CDCl}_3$ ,  $\delta$  in ppm): 155.2, 151.9, 140.8, 132.2, 128.9, 126.52, 125.3, 116.5, 96.8, 82.2, 72.0, 70.4,

69.5, 65.8, 60.4; HRMS (ESI)  $m/z$  calcd for  $C_{40}H_{24}Fe_2N_4S_3$  calcd 767.9858 [ $M^+$ ], found 767.9832 [ $M^+$ ]; UV/vis (DCM):  $\lambda_{max}$  ( $\epsilon$  [ $M^{-1}cm^{-1}$ ]) 489 (70,900), 542 (sh).

#### 4.9. Conclusion

In summary, donor–acceptor system was designed, where donor is ferrocene, and acceptor is benzothiadiazole, and synthesized by the Pd-catalyzed Sonogashira, and Stille coupling reaction. The modulation of the  $\pi$ -spacer group between the donor, and the acceptor units, and increasing the number of acceptor units results in significant perturbation in the photonic properties. The photophysical, and electrochemical properties of the BTDs exhibit strong donor–acceptor interaction. The detailed nonlinear optical characterization of these ferrocenyl substituted BTDs are currently ongoing in our laboratory.

#### 4.10. References

- [1] (a) Kato S., Furuya T., Kobayashi A., Nitani M., Ie Y., Aso Y., Yoshihara T., Tobita S., Nakamura Y. (2012),  $\pi$ -Extended thiadiazoles fused with thienopyrrole or indole moieties: synthesis, structures, and properties, *J. Org. Chem.*, 77, 7595–7606 (DOI: 10.1021/jo301458m). (b) Omer K. M., Ku S. Y., Wong K. T., Bard A. J. (2009), Green electrogenerated chemiluminescence of highly fluorescent benzothiadiazole and fluorene derivatives, *J. Am. Chem. Soc.*, 131, 10733-10741 (DOI: 10.1021/ja904135y). (c) Sonar P., Singh S. P., Li Y., Soh M. S., Dodabalapur A. (2010), A low-bandgap diketopyrrolopyrrole-benzothiadiazole-based copolymer for high-mobility ambipolar organic thin-film transistors, *Adv. Mater.*, 22, 5409-5413 (DOI: 10.1002/adma.201002973). (d) Li Y., Li A.-Y., Li B.-X., Huang J., Zhao L., Wang B.-Z., Li J.-W., Zhu X.-H., Peng J., Cao Y., Ma D.-G., Roncali J. (2009), Asymmetrically 4,7-disubstituted benzothiadiazoles as efficient non-doped solution-processable green fluorescent emitters, *Org. Lett.*, 11,

- 5318-5321 (DOI: 10.1021/ol9022563). (e) Kobayashi N., Inagaki S., Nemykin V. N., Nonomura T. (2001), A novel hemiporphyrine comprising three isoindoleimine and three thiadiazole units, *Angew. Chem., Int. Ed.*, 40, 2710-2712 (DOI: 10.1002/1521-3773(20010716)40:14<2710::AID-ANIE2710>3.0.CO;2-A).
- [2] (a) Kato S., Matsumoto T., Ishi-i T., Thiemann T., Shigeiwa M., Gorohmaru H., Maeda S., Yamashita Y., Mataka S. (2004), Strongly red-fluorescent novel donor- $\pi$ -bridge-acceptor- $\pi$ -bridge-donor (D- $\pi$ -A- $\pi$ -D) type 2,1,3-benzothiadiazoles with enhanced two-photon absorption cross-sections, *Chem. Commun.*, 2342-2343 (DOI: 10.1039/B410016F). (b) Neto B. A. D., Lapis A. A. M., Júnior, E. N., da S., Dupont J. (2013), 2,1,3-Benzothiadiazole and derivatives: synthesis, properties, reactions, and applications in light technology of small molecules, *Eur. J. Org. Chem.*, 228-255 (DOI: 10.1002/ejoc.201201161). (c) Kato S., Matsumoto T., Shigeiwa M., Gorohmaru H., Maeda S., Ishi-i T., Mataka S. (2006), Novel 2,1,3-benzothiadiazole-based red-fluorescent dyes with enhanced two-photon absorption cross-sections, *Chem.-Eur. J.*, 12, 2303-2317 (DOI: 10.1002/chem.200500921). (d) Wang J.-L., Tang Z.-M., Xiao Q., Ma Y., Pei J. (2009), Star-shaped D- $\pi$ -A conjugated molecules: synthesis and broad absorption bands, *Org. Lett.*, 11, 863-866 (DOI: 10.1021/ol802845w). (e) Lindner B. D., Engelhart J. U., Märken M., Tverskoy O., Appleton A. L., Rominger F., Hardcastle K. I., Enders M., Bunz U. H. F. (2012), Synthesis and optical properties of diaza- and tetraazatetracenes, *Chem.-Eur. J.*, 18, 4627-4633 (DOI: 10.1002/chem.201103227). (f) Aviram A., Ratner M. A. (1974), Molecular rectifiers, *Chem. Phys. Lett.*, 29, 277-283 (DOI:10.1016/0009-2614(74)85031-1).
- [3] (a) Tang Z. M., Lei T., Jiang K. J., Song Y. L., Pei J. (2010), Benzothiadiazole containing D- $\pi$ -A conjugated compounds for dye-sensitized solar cells: synthesis, properties, and photovoltaic

- performances, *Chem. Asian J.*, 5, 1911-1917 (DOI: 10.1002/asia.201000158). (b) Wu Y., Zhu W. (2013), Organic sensitizers from D- $\pi$ -A to D-A- $\pi$ -A: effect of the internal electron-withdrawing units on molecular absorption, energy levels and photovoltaic performances, *Chem. Soc. Rev.*, 42, 2039-2058 (DOI: 10.1039/C2CS35346F).
- [4] Wang J.-L., Xiao Q., Pei J. (2010), Benzothiadiazole-based D- $\pi$ -A- $\pi$ -D Organic dyes with tunable band gap: synthesis and photophysical properties, *Org. Lett.*, 12, 4164-4167 (DOI: 10.1021/ol101754q).
- [5] (a) Zhang H., Wan X., Xue X., Li Y., Yu A., Chen Y. (2010), Selective tuning of the HOMO-LUMO gap of carbazole-based donor-acceptor-donor compounds toward different emission colors, *Eur. J. Org. Chem.*, 1681-1687 (DOI: 10.1002/ejoc.200901167). (b) Bures F., Schweizer W. B., May J. C., Boudon C., Gisselbrecht J.-P., Gross M., Biaggio I., Diederich F. (2007), Property tuning in charge-transfer chromophores by systematic modulation of the spacer between donor and acceptor, *Chem.-Eur. J.*, 13, 5378-5387 (DOI: 10.1002/chem.200601735).
- [6] (a) Zhou E., Yamakawa S., Tajima K., Yang C., Hashimoto K. (2009), Synthesis and photovoltaic properties of diketopyrrolopyrrole-based donor-acceptor copolymers, *Chem. Mater.*, 21, 4055-4061 (DOI: 10.1021/cm901487f). (b) Hrobárik, P., Hrobáriková, V., Sigmundová, I., Zahradník, P., Fakis, M., Polyzos, I., Persephonis, P. (2011), Benzothiazoles with tunable electron-withdrawing strength and reverse polarity: a route to triphenylamine-based chromophores with enhanced two-photon absorption, *J. Org. Chem.*, 76, 8726-8736 (DOI: 10.1021/jo201411t). (c) Janowska I., Miomandre F., Clavier G., Audebert P., Zakrzewski J., Thi K. H., Ledoux-Rak I. (2006), Donor-acceptor-donor tetrazines containing a ferrocene unit: synthesis, electrochemical and spectroscopic properties, *J. Phys. Chem. A*, 110, 12971-12975 (DOI: 10.1021/jp062186f). (d) Lembo A., Tagliatesta P., Guldi D. M. (2006),

- Synthesis and photophysical investigation of new porphyrin derivatives with  $\beta$ -pyrrole ethynyl linkage and corresponding dyad with [60] fullerene, *J. Phys. Chem. A*, 110, 11424-11433 (DOI: 10.1021/jp062735h).
- (e) Zhu W., Wu G. S. (2001), Molecular design for octupolar nonlinear optical systems: an ab initio study of first hyperpolarizabilities of symmetrically heteroaromatic-substituted triazines, *J. Phys. Chem. A*, 105, 9568-9574 (DOI: 10.1021/jp0120559).
- (f) Zhu Y., Wolf M. O. (2000), Charge transfer and delocalization in conjugated (ferrocenylethynyl)oligothiophene complexes, *J. Am. Chem. Soc.*, 122, 10121-10125 (DOI: 10.1021/ja0008564).
- [7] (a) Sakurai H., Ritonga M. T. S., Shibatani H., Hirao T. (2005), Synthesis and characterization of p-phenylenediamine derivatives bearing an electron-acceptor unit, *J. Org. Chem.*, 70, 2754-2762 (DOI: 10.1021/jo048324j).
- (b) Dhanabalan A., van Duren J. K. J., van Hal P. A., van Dongen J. L. J., Janssen, R. A. J. (2001), Synthesis and characterization of a low bandgap conjugated polymer for bulk heterojunction photovoltaic cells, *Adv. Funct. Mater.*, 11, 255-262 (DOI: 10.1002/1616-3028(200108)11:4<255::AID-ADFM255>3.0.CO;2-I).
- (c) Zhang M., Tsao H. N., Pisula W., Yang C., Mishra A. K., Müllen K. (2007), Field-effect transistors based on a benzothiadiazole-cyclopentadithiophene copolymer, *J. Am. Chem. Soc.*, 129, 3472-3473 (DOI: 10.1021/ja0683537).
- [8] (a) Shi C., Yao Y., Yang Y., Pei Q. (2006), Regioregular copolymers of 3-alkoxythiophene and their photovoltaic application, *J. Am. Chem. Soc.*, 128, 8980-8986 (DOI: 10.1021/ja061664x).
- (b) Hou Q., Zhou Q. M., Zhang Y., Yang W., Yang R. Q., Cao Y. (2004), Synthesis and electroluminescent properties of high-efficiency saturated red emitter based on copolymers from fluorene and 4,7-di(4-hexylthien-2-yl)-2,1,3-benzothiadiazole, *Macromolecules*, 37, 6299-6305 (DOI: 10.1021/ma049204g).
- (c) Zhu Z., Waller D., Gaudiana R., Morana M.,

- Muhlbacher D., Scharber M., Brabec C. (2007), Panchromatic conjugated polymers containing alternating donor/acceptor units for photovoltaic applications, *Macromolecules*, 40, 1981-1986 (DOI: 10.1021/ma062376o). (d) Thomas K. R. J., Lin J. T., Velusamy M., Tao Y. T., Chuen C. H. (2004), Color tuning in benzo[1,2,5]thiadiazole-based small molecules by amino conjugation/deconjugation: bright red-light-emitting diodes, *Adv. Funct. Mater.*, 14, 83-90 (DOI: 10.1002/adfm.200304486).
- [9] (a) Gautam P., Dhokale B., Shukla V., Singh C. P., Bindra K. S., Misra R. (2012), Optical limiting performance of meso-tetraferrocenyl porphyrin and its metal derivatives, *J. Photochem. Photobiol. A. Chem.*, 239, 24-27 (DOI:10.1016/j.jphotochem.2012.04.020). (b) Jadhav T., Maragani R., Misra R., Sreeramulu V., Rao D. N., Mobin S. M. (2013), Design and synthesis of donor–acceptor pyrazabole derivatives for multiphoton absorption, *Dalton Trans.*, 42, 4340-4342 (DOI: 10.1039/C3DT33065F). (c) Maragani R., Thaksen J., Mobin S. M., Misra R. (2013), C<sub>3</sub> symmetric ferrocenyl triazines: synthesis, structure, and properties, *RSC Adv.*, 3, 2889-2892 (DOI: 10.1039/C2RA23153K).
- [10] (a) Gautam P., Dhokale B., Mobin S. M., Misra R. (2012), Ferrocenyl BODIPYs: synthesis, structure and properties, *RSC Adv.*, 2, 12105-12107 (DOI: 10.1039/C2RA21964F). (b) Dhokale B., Gautam P., Mobin S. M., Misra R. (2013), Donor–acceptor, ferrocenyl substituted BODIPYs with marvelous supramolecular interactions, *Dalton Trans.*, 42, 1512-1518 (DOI: 10.1039/C2DT31632C). (c) Sharma R., Maragani R., Mobin S. M., Misra R. (2013), Ferrocenyl substituted calixarenes: synthesis, structure and properties, *RSC Adv.*, 3, 5785-5788 (DOI: 10.1039/C3RA00146F).
- [11] Misra R., Gautam P., Sharma R., Mobin S. M. (2013), Donor– $\pi$ –acceptor– $\pi$ –donor ferrocenyl benzothiadiazoles: synthesis, structure, and properties, *Tetrahedron Lett.*, 54, 381-383 (DOI:10.1016/j.tetlet.2012.11.016).

- [12] Wang B., Tsang S., Zhang W., Tao Y., Wong M. S. (2011), Naphthodithiophene-2,1,3-benzothiadiazole copolymers for bulk heterojunction solar cells, *Chem. Commun.*, 47, 9471-9473 (DOI: 10.1039/C1CC13690A).
- [13] Ma X., Hua J., Wu W., Jin Y., Meng F., Zhan W., Tian H. (2008), A high-efficiency cyanine dye for dye-sensitized solar cells, *Tetrahedron* 2008, 64, 345-350 (DOI:10.1016/j.tet.2007.10.094).
- [14] Wang X., Sun Y., Chen S., Guo X., Zhang M., Li X., Li Y., Wang H. (2012), Effects of  $\pi$ -conjugated bridges on photovoltaic properties of donor- $\pi$ -acceptor conjugated copolymers, *Macromolecules*, 45, 1208-1216 (DOI: 10.1021/ma202656b).
- [15] (a) Chen S., Li Y., Yang W., Chen N., Liu H., Li Y. (2010), Synthesis and Tuning optical nonlinear properties of molecular crystals of benzothiadiazole, *J. Phys. Chem. C*, 114, 15109-15115 (DOI: 10.1021/jp103159b). (b) Anant P., Lucas N. T., Jacob J. (2008), A simple route toward the synthesis of bisbenzothiadiazole derivatives, *Org. Lett.*, 10, 5533-5536 (DOI: 10.1021/ol8022837). (c) Pop F., Amacher A., Avarvari N., Ding J., Daku L. M. L., Hauser A., Koch M., Hauser J., Liu S., Decurtins S. (2013), Tetrathiafulvalene-benzothiadiazoles as redox-tunable donor-acceptor systems: synthesis and photophysical study, *Chem.-Eur. J.*, 19, 2504-2514 (DOI: 10.1002/chem.201202742).
- [16] (a) Melinger J. S., Pan Y., Kleiman V. D., Peng Z., Davis B. L., McMorro D., Lu M. (2002), Optical and photophysical properties of light-harvesting phenylacetylene monodendrons based on unsymmetrical branching, *J. Am. Chem. Soc.*, 124, 12002-12012 (DOI: 10.1021/ja020380j). (b) Misra, R.; Kumar, R.; Chandrashekar, T. K.; Suresh, C. H.; Nag, A.; Goswami, D. (2006),  $22\pi$  Smaragdyrin molecular conjugates with aromatic phenylacetylenes and ferrocenes: syntheses, electrochemical, and photonic properties, *J. Am. Chem. Soc.*, 128, 16083-16091 (DOI: 10.1021/ja0628295).



- [17] Ziessel R., Retailleau P., Elliott K. J., Harriman A. (2009), Boron dipyrroin dyes exhibiting “push–pull–pull” electronic signatures, *Chem. –Eur. J.*, 15, 10369-10374 (DOI: 10.1002/chem.200901725).
- [18] Rao M. R., Kumar K. V. P., Ravikanth M. (2010), Synthesis of boron-dipyrromethene–ferrocene conjugates, *J. Organomet. Chem.*, 695, 863-869 (DOI:10.1016/j.jorganchem.2010.01.009).
- [19] (a) Fery-Forgues S., Delavaux-Nicot B. (2000), Ferrocene and ferrocenyl derivatives in luminescent systems, *J. Photochem. Photobiol. A*, 132, 137-159 (DOI:10.1016/S1010-6030(00)00213-6). (b) Dhokale B., Gautam P., Misra, R. (2012), Donor–acceptor perylenediimide–ferrocene conjugates: synthesis, photophysical, and electrochemical properties, *Tetrahedron Lett.*, 53, 2352-2354 (DOI:10.1016/j.tetlet.2012.02.107). (c) Nadtochenko V. A., Denisov N. N., Gak V. Y., Abramova N. V., Loim N. M. (1999), Photochemical and photophysical properties of meso-tetraferrocenylporphyrin. Quenching of meso-tetraphenylporphyrin by ferrocene, *Russ. Chem. Bull.*, 48, 1900-1903 (DOI: 10.1007/BF02494744). (d) Barlow S., Marder S. R. (2000), Electronic and optical properties of conjugated group 8 metallocene derivatives, *Chem. Commun.*, 1555-1562 (DOI: 10.1039/B004907G).
- [20] Sharma R., Gautam P., Mobin S. M., Misra R. (2013),  $\beta$ -Substituted ferrocenyl porphyrins: synthesis, structure, and properties, *Dalton Trans.*, 42, 5539-5545 (DOI: 10.1039/C3DT00003F).
- [21] Maragani R., Jadhav T., Mobin S. M., Misra R. (2012), Synthesis, structure, photophysical, and electrochemical properties of donor–acceptor ferrocenyl derivatives, *Tetrahedron*, 68, 7302-7308 (DOI:10.1016/j.tet.2012.06.094).
- [22] (a) Xu E., Zhong H., Lai H., Zeng D., Zhang J., Zhu W., Fang Q. (2010), A new polymeric light-emitting material with pure green emission: poly(fluorene-alt-quinoxaline) with benzothiadiazole groups in the side chain, *Macromol. Chem. Phys.*, 211, 651-656 (DOI:

- 10.1002/macp.200900486). (b) Watanabe M., Goto K., Fujitsuka M., Tojo S., Majima T., Shinmyozu T. (2010), 2,1,3-Benzothiadiazole dimers: preparation, structure, and transannular electronic interactions of syn- and anti-[2.2](4,7)benzothiadiazolophanes, *Bull. Chem. Soc. Jpn.*, 83, 1155-1161 (doi:10.1246/bcsj.20100085).
- [23] Poander L. E., Pandey L., Barlow S., Tiwari P., Risko C., Kippelen B., Bredas J. L., Marder S. R. (2011), Benzothiadiazole-dithienopyrrole donor-acceptor-donor and acceptor-donor-acceptor triads: synthesis and optical, electrochemical, and charge-transport properties, *J. Phys. Chem. C*, 115, 23149-23163 (DOI: 10.1021/jp208643k).
- [24] Watanabe M., Goto K., Shibahara M., Shinmyozu T. (2010), Synthesis, structure, and electronic and photophysical properties of two- and three-layered [3.3]paracyclophane-based donor-acceptor systems(1), *J. Org. Chem.*, 75, 6104-6114 (DOI: 10.1021/jo100688m).
- [25] Auger A., Muller A. J., Swarts J. C. (2007), Remarkable isolation, structural characterisation and electrochemistry of unexpected scrambling analogues of 5-ferrocenyl-10,20-diphenylporphyrin, *Dalton Trans.*, 3623-3633 (DOI: 10.1039/B706840A).
- [26] Patel D. G. D., Feng F., Ohnishi Y.-y., Abboud K. A., Hirata S., Schanze K. S., Reynolds J. R. (2012), It takes more than an imine: the role of the central atom on the electron-accepting ability of benzotriazole and benzothiadiazole oligomers, *J. Am. Chem. Soc.*, 134, 2599-2612 (DOI: 10.1021/ja207978v).
- [27] Gritzner G., Kuta G. J. (1984), Recommendations on reporting electrode potentials in nonaqueous solvents (recommendations 1983), *Pure Appl. Chem.*, 56, 461-466 (DOI: 10.1351/pac198456040461).



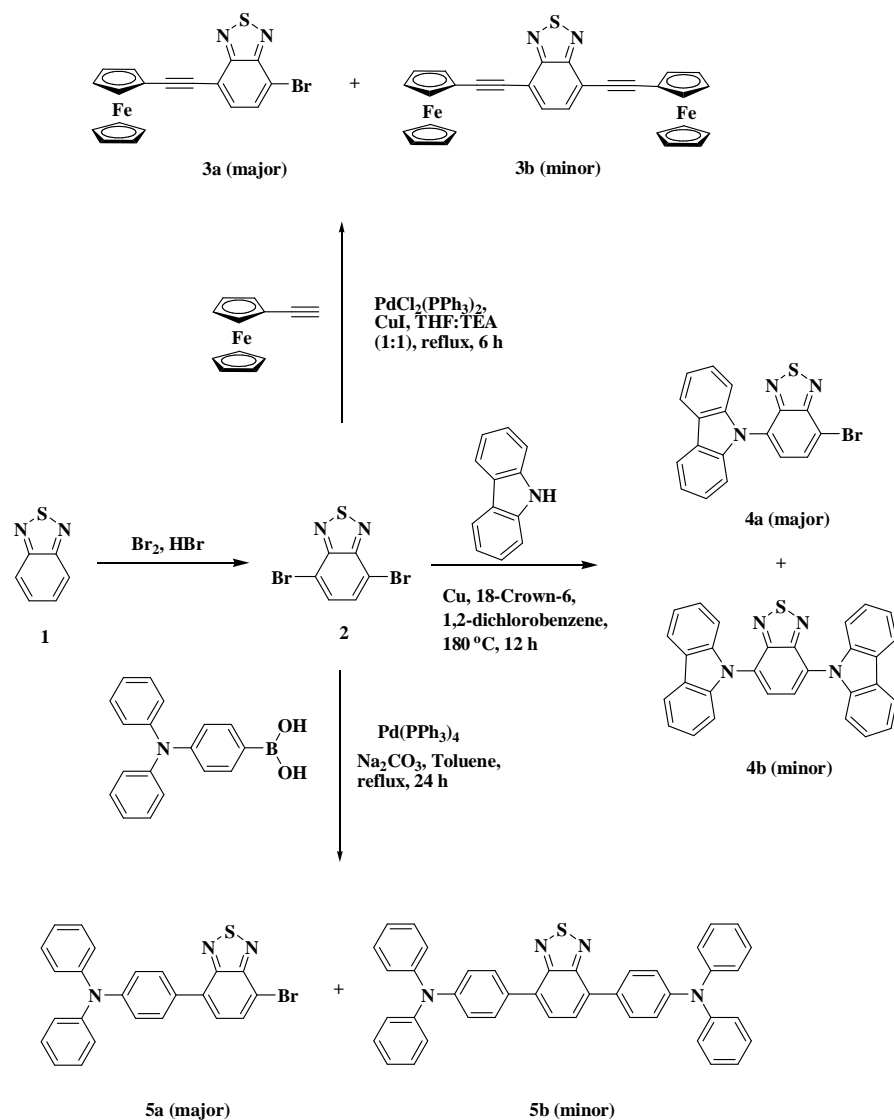
## Chapter 5

### Aryl-substituted unsymmetrical benzothiadiazoles

#### 5.1. Introduction

The design, and synthesis of organic  $\pi$ -conjugated donor–acceptor system continues to create great amount of interest because of their application in organic photovoltaics (OPV), and nonlinear optics (NLO).<sup>[1]</sup> The properties of the donor–acceptor system can be modulated either by increasing the donor and acceptor strength, or by varying the  $\pi$ -linker between the donor and the acceptor.<sup>[2]</sup> A wide variety of donor and acceptor has been used for the synthesis of D– $\pi$ –A type of systems.<sup>[3]</sup> 2,1,3-Benzothiadiazole (BTD) is a strong acceptor due to its high electron affinity.<sup>[4]</sup> Ferrocene is a strong electron donor and highly stable. Our group is interested in the design and synthesis of ferrocene based donor-acceptor molecular system for a variety of photonic applications.<sup>[5,6]</sup> Recently we have reported the synthesis of ferrocene substituted symmetrical and unsymmetrical BTD systems of type D– $\pi$ –A– $\pi$ –D, D– $\pi_1$ –A– $\pi_2$ –D and D– $\pi_1$ –A– $\pi_2$ –A– $\pi_1$ –D.<sup>[7,8]</sup> In continuation of this work, we were further interested in the design and synthesis of unsymmetrical BTDs having different donor/acceptor of varying strength and to see their effect on the donor–acceptor interaction. In this contribution, we wish to report unsymmetrical donor–acceptor systems of the type D<sub>1</sub>– $\pi$ –A– $\pi$ –D<sub>2</sub>, D<sub>1</sub>– $\pi$ –A<sub>1</sub>– $\pi$ –A<sub>2</sub>, D<sub>1</sub>–A– $\pi$ –D<sub>2</sub>, and D<sub>1</sub>–A<sub>1</sub>–A<sub>2</sub>–D<sub>2</sub>. Three sets of mono-bromobenzothiadiazoles **3a**, **4a**, and **5a** were designed, and synthesized by the Sonogashira, Suzuki, and Ullmann coupling reactions respectively. These mono-bromobenzothiadiazoles (**3a**, **4a**, and **5a**) were further subjected to Sonogashira cross-coupling reaction which resulted in unsymmetrical BTDs. The unsymmetrical benzothiadiazoles **7a**, and **8a** with monoethyne spacer were subjected to [2 + 2] cycloaddition reaction with tetracyanoethene (TCNE) followed by ring opening, which resulted 1,1,4,4-tetracyanobuta-1,3-diene (TCBD) bridged unsymmetrical benzothiadiazoles **9a**, and **9b**.

## 5.2. Results and Discussion

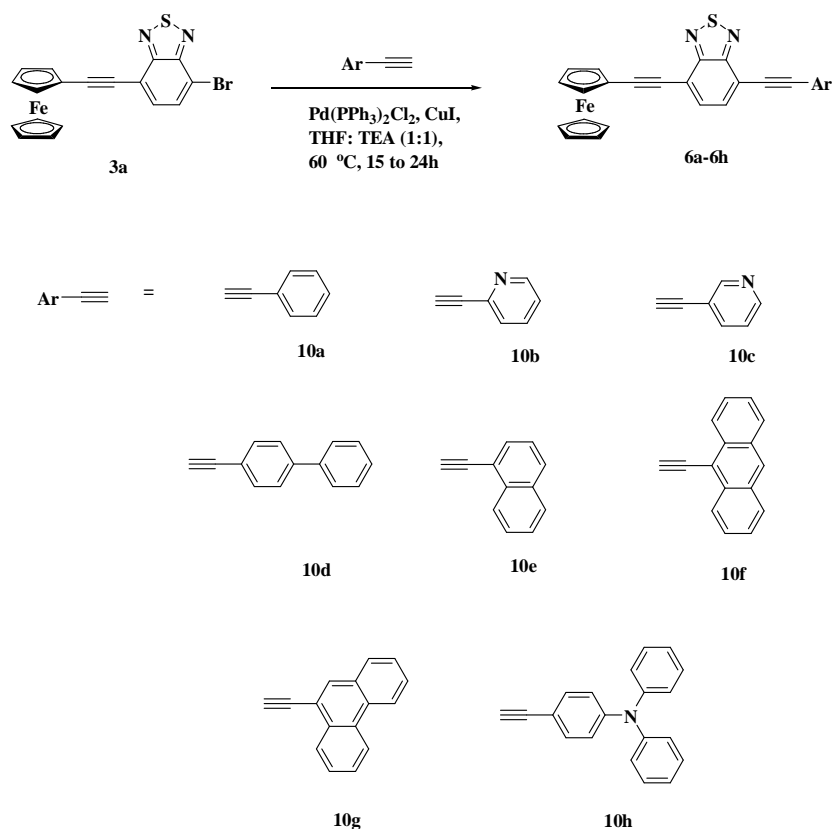


**Scheme 5.1.** Synthetic route for mono-bromobenzothiadiazoles **3a**, **4a**, and **5a**.

The synthesis of unsymmetrical benzothiadiazoles **6a–6h**, **7a–7c**, **8a–8c**, **9a**, and **9b** are outlined in Scheme 5.2, Scheme 5.3, and Scheme 5.4. The dibromo-BTD **2** was synthesized by the bromination reaction of the BTD **1**.<sup>[9]</sup> The Pd catalyzed Sonogashira coupling reaction of ethynylferrocene, and dibromo-BTD **2** resulted 4-Bromo-7-ferrocenylethynylbenzo[1,2,5]thiadiazole

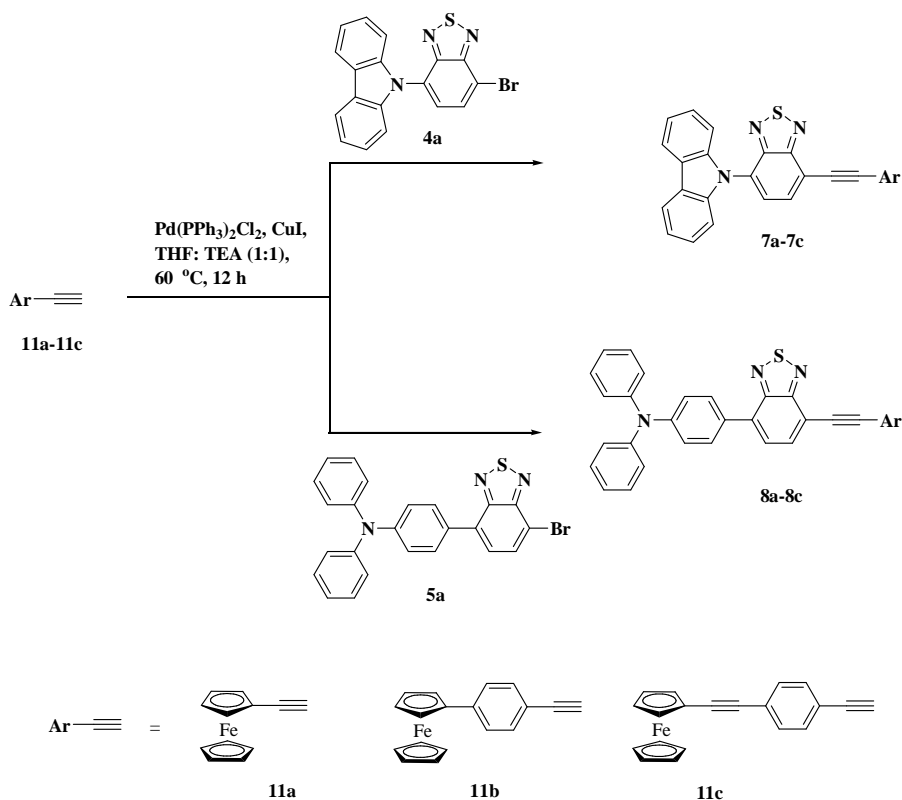
(**3a**) in 60% yield (Scheme 1).<sup>[8]</sup> The Ullmann coupling reaction of carbazole, and dibromo-BTD **2** resulted 4-(9-Carbazolyl)-7-bromo-2,1,3-benzothiadiazole (**4a**) in 40 % yield (Scheme 1).<sup>[10]</sup> The Pd-catalyzed Suzuki coupling reaction of the dibromo-BTD **2**, and 4-(*N,N*-Diphenylamino)-1-phenylboronic acid resulted [4-(7-Bromo-benzo[1,2,5]thiadiazol-4-yl)-phenyl]-diphenyl-amine (**5a**) in 50% yield (Scheme 1).<sup>[11]</sup>

The precursor **3a**, **4a**, and **5a** were further subjected to Sonogashira coupling reaction, which resulted unsymmetrical BTDs. In order to study the effect of the aryl substituents with enhanced conjugation on the unsymmetrical ferrocenyl-BTD a series of aromatic terminal alkynes were selected with one (**10a–10c**), two (**10d**, and **10e**), and three (**10f–10h**) aromatic rings. The Sonogashira cross-coupling reaction of the bromo-BTD **3a** with the respective aryl-acetylenes (**10a–10h**) resulted in BTDs **6a–6h** in 40–70% yield (Scheme 5.2).



**Scheme 5.2.** Synthesis of unsymmetrical benzothiadiazoles **6a–6h**.

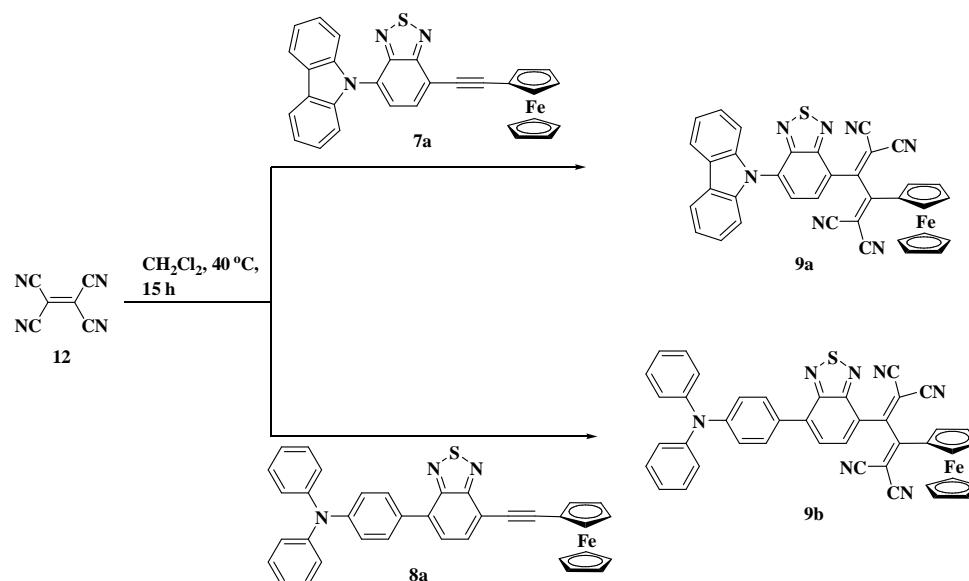
To explore the effect of variation of  $\pi$ -bridge a set of ethynyl substituted ferrocenes namely ethynylferrocene (**11a**), 4-ferrocenylphenylacetylene (**11b**), and 4-ethynyl-phenylethynylferrocene (**11c**) were synthesized, and subjected to Sonogashira cross-coupling reaction with 4-(9-Carbazolyl)-7-bromo-2,1,3-benzothiadiazole (**4a**), and [4-(7-Bromo-benzo[1,2,5]thiadiazol-4-yl)-phenyl]-diphenyl-amine (**5a**). The Sonogashira coupling of the BTDs **4a**, and **5a** with respective ferrocenyl-acetylenes resulted in compound **7a–7c**, and **8a–8c** in 60–70% yield respectively (Scheme 5.3).



**Scheme 5.3.** Synthesis of benzothiadiazoles **7a–7c**, and **8a–8c**.

The 1,1,4,4-tetracyanobuta-1,3-diene (TCBD) bridged unsymmetrical BTDs **9a** and **9b** were synthesized *via* [2 + 2] cycloaddition reaction of the ferrocenyl substituted BTDs **7a**, and **8a** with tetracyanoethene (**12**) to form an intermediate cyclobutene which subsequently undergoes ring opening (Scheme 5.4).<sup>[12]</sup> The purification of the unsymmetrical BTDs **6a–6h**, **7a–7c**, **8a–8c**, **9a**,

and **9b** were achieved by column chromatography. All the unsymmetrical BTDs were well characterized by  $^1\text{H}$  and  $^{13}\text{C}$  NMR and HRMS techniques. The BTD **6c**, **6g**, **7a**, and **7b** were also characterized by single-crystal X-ray diffraction.



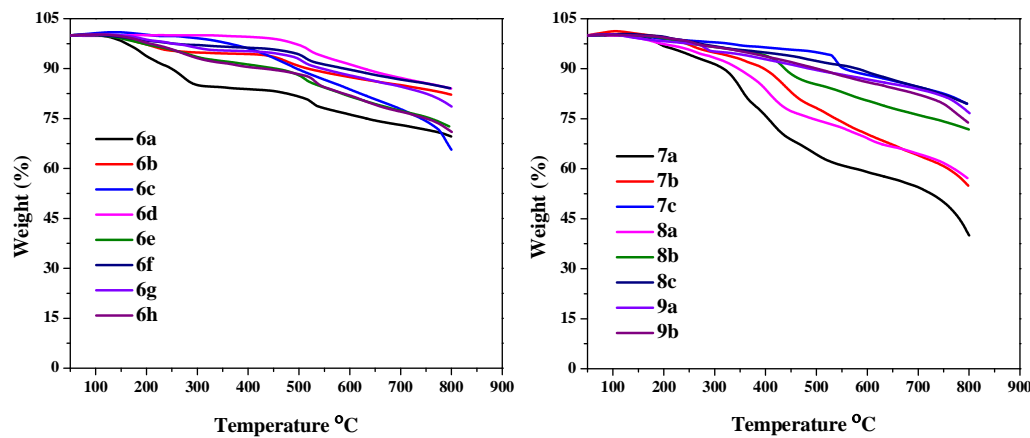
**Scheme 5.4.** Synthesis of benzothiadiazoles **9a** and **9b**.

### 5.3. Thermogravimetric analysis

The thermal properties of the unsymmetrical benzothiadiazoles **6a–6h**, **7a–7c**, **8a–8c**, and **9a–9b** were investigated by the thermogravimetric analysis (TGA) at a heating rate of  $10\text{ }^{\circ}\text{C min}^{-1}$ , under nitrogen atmosphere (Figure 5.1). The decomposition temperatures for 10% weight loss in the BTDs **6b–6h** was above  $450\text{ }^{\circ}\text{C}$ , whereas the BTD **6a** with the phenyl substituent shows the 10% weight loss at  $249\text{ }^{\circ}\text{C}$ . This reflects that the hetero-aryl, biaryl and the polycyclic aromatic substituted BTDs show higher thermal stability. The BTDs **7a–7c**, and **8a–8c** exhibit the 10% weight loss above  $300\text{ }^{\circ}\text{C}$ . The trend observed in the decomposition temperature follows the order  $8\text{c} > 7\text{c} > 8\text{b} > 7\text{b} > 8\text{a} > 7\text{a}$ . The extension of the  $\pi$ -bridge between the ferrocene and the BTD unit results in increased thermal stability. The incorporation of 1,1,4,4-tetracyanobuta-1,3-diene (TCBD) bridge results in greater thermal stability in BTDs **9a** and **9b** compared



to the ethyne bridged BTDs **7a** and **8a**. The decomposition temperatures for 10% weight loss is above 500 °C for TCBD bridged BTDs **9a** and **9b**.



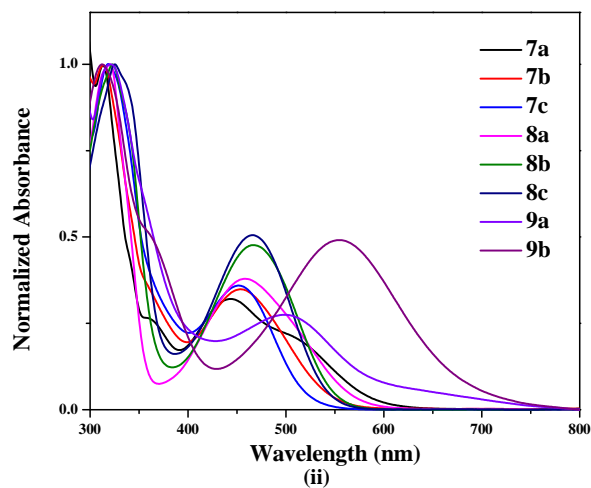
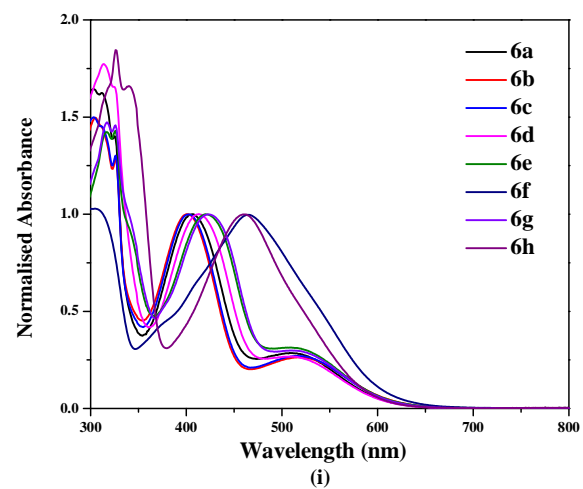
**Figure 5.1.** TGA plots of unsymmetrical BTDs **6a–6h**, **7a–7c**, **8a–8c**, and **9a–9b** at a heating rate of 10 °C min<sup>-1</sup>, under nitrogen atmosphere.

#### 5.4. Photophysical Properties

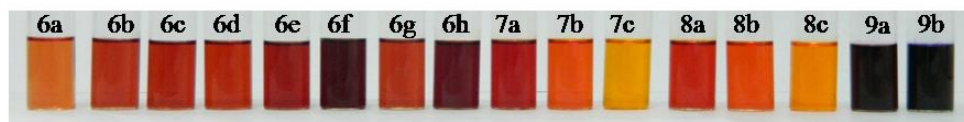
The UV–vis absorption spectra of the unsymmetrical benzothiadiazoles were recorded in dichloromethane at room temperature (Figure 5.2), and the data are compiled in Table 1. The unsymmetrical BTDs show the characteristic absorption band between 300–340 nm due to the BTD unit.<sup>[13]</sup>

The BTDs **6a–6h** shows the presence of lower energy absorption band between 399–465 nm, corresponding to the  $\pi \rightarrow \pi^*$  transition, and between 509–521 nm attributed to the charge-transfer (CT) transitions.<sup>[7,8,14]</sup> The red shift in the absorption maxima for the lower energy  $\pi \rightarrow \pi^*$  absorption band follows the order **6f** > **6h** > **6g** > **6e** > **6d** > **6a** > **6c** > **6b**. The magnitude in red shift observed for BTDs **6a–6h** is a function of the aryl substituent attached to the BTD core. A comparison of the absorption data reveals that the increase in the number of aromatic rings from one (**6a–6c**), two (**6d–6e**), and three (**6f–6h**) leads to a regular increase in the red shift of the absorption maxima due to enhancement of  $\pi$ -conjugation. The mode of conjugation in the aryl substituents also affects the absorption bands. The BTDs with naphthalene **6e**, and anthracene **6f** substituents

exhibit red shift compared to the biphenyl **6d**, and phenanthrene **6g** substituted BTDs respectively. The BTDs **6a-6d** exhibit distinct CT band between 509–515 nm, whereas **6e** and **6g** shows in form of shoulder between 512–521 nm. The lower energy electronic absorption maxima are broad in BTDs **6f**, and **6h** due to the overlap with the charge-transfer absorption.<sup>[8,15]</sup> The BTDs **7a-7c**, **8a-8c**, and **9a-9b** shows the lower energy absorption band between 443–554 nm. The BTD **7a** exhibit CT band as a shoulder at 520 nm. The BTDs **7b**, **7c**, **8a-8c**, and **9a-9b** exhibit broadening of the lower energy electronic absorption band which can be attributed to the overlap of the lower energy  $\pi \rightarrow \pi^*$  transition with the CT band. The lower energy electronic absorption band shows bathochromic shift with the enhancement of conjugation length. The incorporation of a 1,1,4,4-tetracyanobuta-1,3-diene (TCBD)  $\pi$ -bridge in BTDs **9a**, and **9b** results in substantial bathochromic shift of the lower energy electronic absorption band compared to BTDs **7a**, and **8a**. The trend in the bathochromic shift follows the order **9b** > **9a** > **8a** > **7a**. This reveals strong donor-acceptor interaction in TCBD  $\pi$ -bridge in BTDs **9a**, and **9b**. The effect of systematic variation of  $\pi$ -conjugation through aryl substitution, and  $\pi$ -bridge is also reflected from the colored solution of these unsymmetrical BTDs **6a-6h**, **7a-7c**, **8a-8c**, and **9a-9b** (Figure 5.3.). The emission studies of the unsymmetrical BTDs show complete quenching of the fluorescence.



**Figure 5.2.** Normalized electronic absorption spectra of (i) benzothiadiazoles **6a–6h**, and (ii) benzothiadiazoles **7a–7c**, **8a–8c**, and **9a–9b** dichloromethane at  $1.0 \times 10^{-6}$  M concentration.



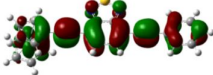
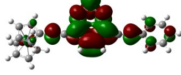
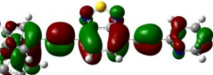
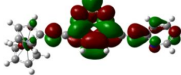
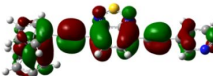
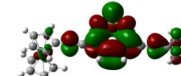

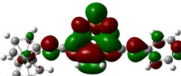
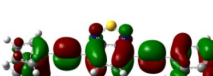
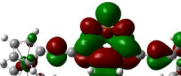

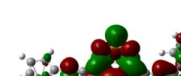

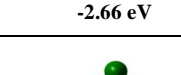
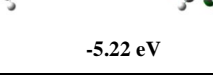

**Figure 5.3.** Unsymmetrical benzothiadiazoles **6a–6h**, **7a–7c**, **8a–8c**, and **9a–9b** at  $1 \times 10^{-4}$  M concentration in dichloromethane.

**Table 5.1.** Photophysical, and thermal properties of the benzothiadiazoles **6a–6h**, **7a–7c**, **8a–8c**, **9a**, and **9b**.

BTD	Photophysical data <sup>a</sup>		Td(°C) <sup>b</sup>	BTD	Photophysical data <sup>a</sup>		Td(°C) <sup>b</sup>
	$\lambda_{\text{abs}}$ (nm)	$\epsilon$ (M <sup>-1</sup> cm <sup>-1</sup> )			$\lambda_{\text{abs}}$ (nm)	$\epsilon$ (M <sup>-1</sup> cm <sup>-1</sup> )	
<b>Ferrocene</b>	-	-					
<b>6a</b>	406	32791	249	<b>7a</b>	443	35138	328
	509	9324			520	sh	
<b>6b</b>	399	85328	535	<b>7b</b>	453	47855	411
	511	22404					
<b>6c</b>	402	78216	506	<b>7c</b>	454	62777	604
	515	20963					
<b>6d</b>	413	55533	646	<b>8a</b>	458	37842	359
	512	14750					
<b>6e</b>	421	54400	471	<b>8b</b>	466	51474	449
	521	sh					
<b>6f</b>	465	67550	611	<b>8c</b>	467	84788	625
<b>6g</b>	423	58074	563	<b>9a</b>	502	46178	549
	514	sh					
<b>6h</b>	460	58729	462	<b>9b</b>	554	61482	543

<sup>a</sup>Absorbance measured in dichloromethane at  $1 \times 10^{-6}$  M concentration; sh = shoulder;  $\lambda_{\text{abs}}$ : absorption wavelength;  $\epsilon$ : extinction coefficient. <sup>b</sup>decomposition temperatures for 10% weight loss at a heating rate of  $10 \text{ }^{\circ}\text{C min}^{-1}$ , under nitrogen atmosphere.

## 5.5. Theoretical Calculations.

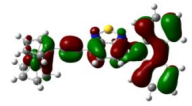
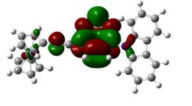
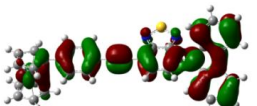
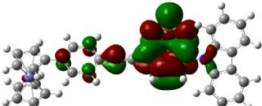
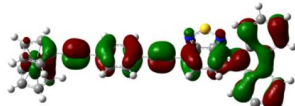
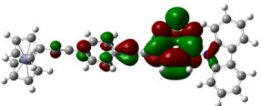
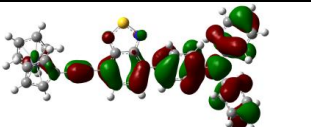
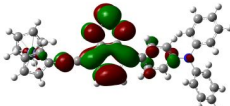
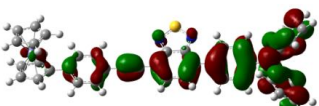
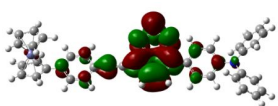
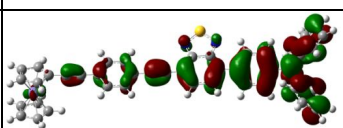
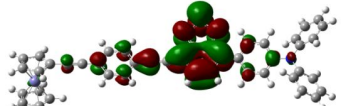
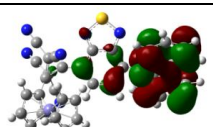
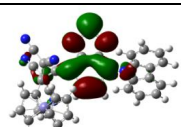
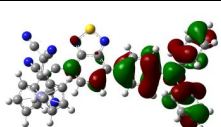
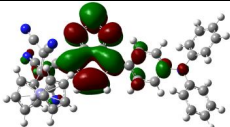
BTD	HOMO	LUMO	Band-gap (eV)
6a	 -5.29 eV	 -2.57 eV	2.72
6b	 -5.38 eV	 -2.65 eV	2.73
6c	 -5.41 eV	 -2.69 eV	2.72
6d	 -5.25 eV	 -2.58 eV	2.67
6e	 -5.23 eV	 -2.60 eV	2.63
6f	 -5.00 eV	 -2.66 eV	2.34
6g	 -5.22 eV	 -2.60 eV	2.62
6h	 -4.91 eV	 -2.48 eV	2.43

**Figure 5.4.** HOMO and LUMO frontier orbitals of unsymmetrical benzothiadiazoles **6a-6h** at the B3LYP/6-31G\*\* level for C, N, S, H, and Lanl2DZ level for Fe.

DFT calculations were performed on the unsymmetrical benzothiadiazoles **6a-6h**, **7a-7c**, **8a-8c**, and **9a-9b** to explore the effect of the aryl substituents on the electronic structure of the unsymmetrical ferrocenyl-BTDs. The contours of the HOMO, and LUMO of BTDs **6a-6h**, **7a-7c**, **8a-8c**, and **9a-9b** are shown in Figure 4, and 5.

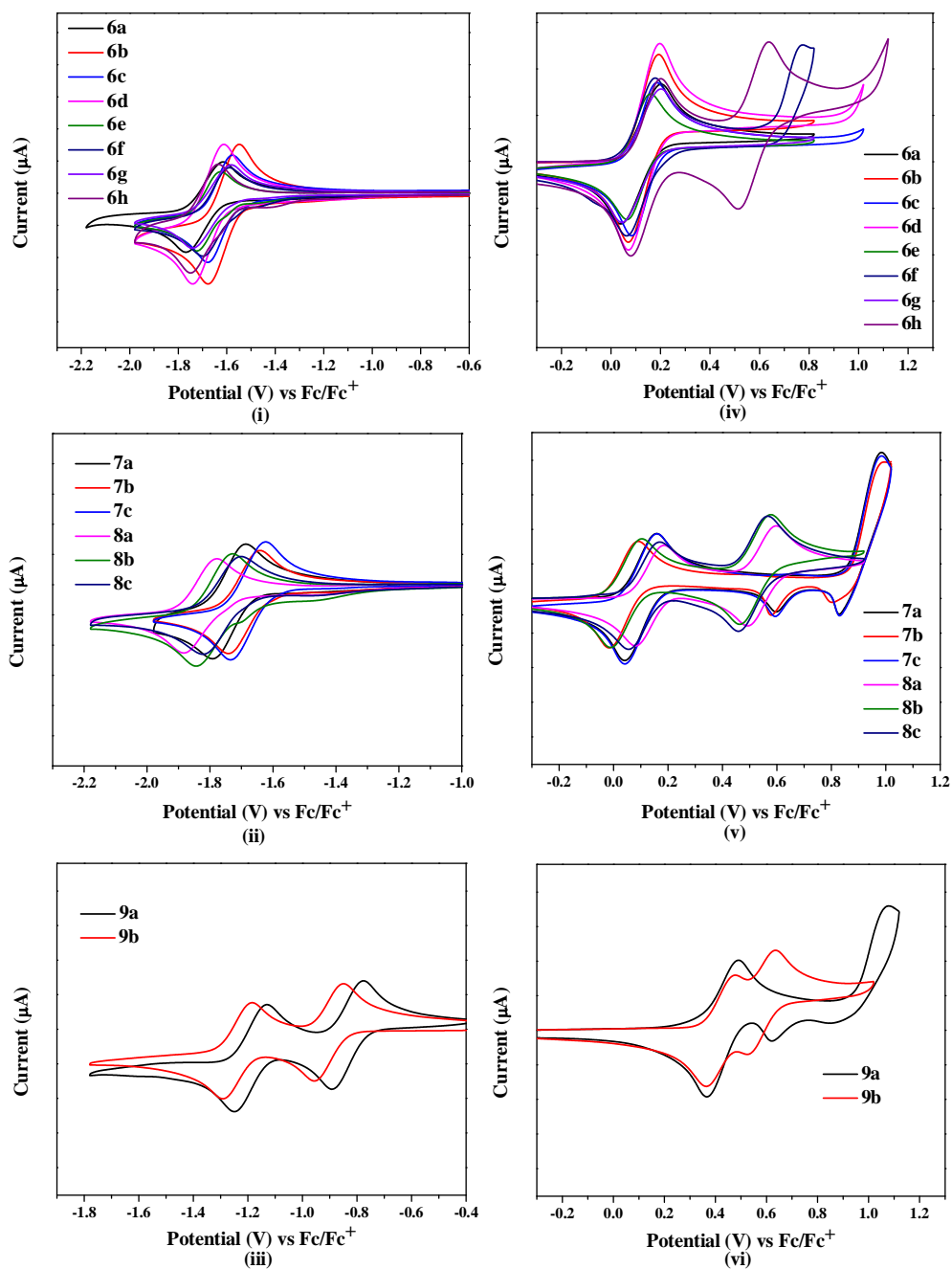
The HOMO orbitals are localized over the ferrocene, the aryl substituent, and the hydrocarbon portion of the BTD, whereas the LUMO orbitals are mainly concentrated on the BTD unit.<sup>[8,16]</sup> The comparison of the HOMOs of BTD **6d**, and **6e** reveals greater delocalization of the HOMO orbital on the naphthalene unit compared to biphenyl unit. Similarly the anthracene unit in BTD **6f** shows better delocalization in HOMO orbital, compared to the phenanthrene substituted BTD **6g**. The presence of electron rich substituents anthracene and triphenylamine on the BTD **6f** and **6g** lowers the contribution of ferrocene in the HOMO. The band gap in BTDs **6a-6h** follows the order **6b** > **6c**  $\cong$  **6a** > **6d** > **6e** > **6g** > **6h** > **6f**, which is reflected in their electronic absorption. The band gap in BTDs **7a-7c**, and **8a-8c** were found to be inversely proportional to the conjugation length. In the HOMO of BTD **8a-8c** the contribution of ferrocene unit is reduced with the extension of  $\pi$ -bridge. The band-gap in BTD **7a-7c**, and **8a-8c** follows the order **7a** > **7b** > **7c**, and **8a** > **8b** > **8c**. The observed trend supports the electronic absorption behavior of BTDs **7a-7c**, and BTDs **8a-8c**.

The 1,1,4,4-tetracyanobuta-1,3-diene (TCBD)  $\pi$ -bridge in **9a** and **9b** lower the band gap which results in bathochromic shift of the electronic absorption spectra. The trend in the energy gap follows the order **7a** > **8a** > **9a** > **9b**.

BTd	HOMO	LUMO	Band-gap (eV)
7a	 -5.30 eV	 -2.61 eV	2.69
7b	 -5.27 eV	 -2.65 eV	2.62
7c	 -5.28 eV	 -2.70 eV	2.57
8a	 -4.92 eV	 -2.40 eV	2.52
8b	 -4.91 eV	 -2.43 eV	2.48
8c	 -4.93 eV	 -2.47 eV	2.46
9a	 -5.82 eV	 -3.20 eV	2.62
9b	 -5.30 eV	 -2.93 eV	2.37

**Figure 5.5.** HOMO and LUMO frontier orbitals of unsymmetrical benzothiadiazoles **7a–7c**, **8a–8c**, **9a**, and **9b** at the B3LYP/6-31G\*\* level for C, N, S, H, and Lanl2DZ level for Fe.

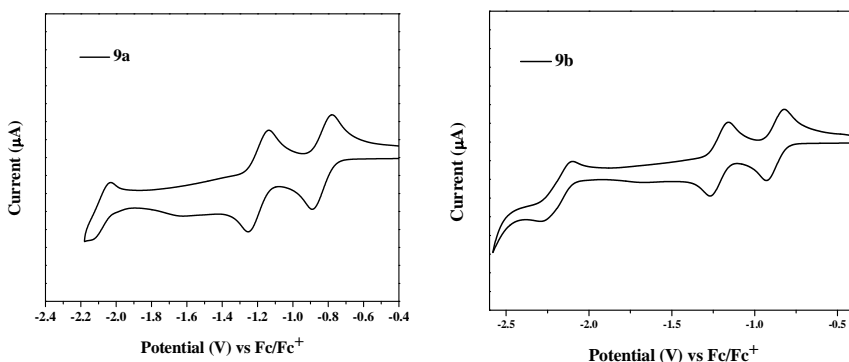
## 5.6. Electrochemical Properties



**Figure 5.6.** Cyclic voltammogram of unsymmetrical benzothiadiazoles **6a–6h**, **7a–7c**, **8a–8c**, **9a**, and **9b** representing the reduction wave (i, ii, and iii), and the oxidation wave (iv, v, and vi) at 0.01 M concentration in 0.1 M TBAPF<sub>6</sub> in dichloromethane recorded at a scan rate of 100 mVs<sup>-1</sup>.



The electrochemical behavior of the BTDs **6a–6h**, **7a–7c**, **8a–8c**, and **9a–9b** were explored by the cyclic voltammetric (CV) analysis in dry dichloromethane (DCM) solution at room temperature using tetrabutylammonium hexafluorophosphate (TBAPF<sub>6</sub>) as a supporting electrolyte. The electrochemical data are listed in Table 2, and the representative cyclic voltammograms are shown in Figure 5.6, and Figure 5.7. In general the unsymmetrical ferrocenyl-substituted BTDs show one reversible oxidation wave in the region 0.04–0.42 V, corresponding to the oxidation of ferrocene to ferrocenium ion. The BTDs **6a–6h**, **7a–7c**, **8a–8c**, and **9a–9b** exhibit one reversible reduction wave in the region –1.61 V to –2.15 V attributed to the acceptor benzothiadiazole unit.<sup>[7,8,12]</sup>



**Figure 5.7.** Cyclic voltammogram of BTD **9a** and **9b** representing the complete reduction waves at 0.01 M concentration in 0.1 M Bu<sub>4</sub>NPF<sub>6</sub> in dichloromethane recorded at 100 mVs<sup>-1</sup> scan speed.

The trend in the oxidation potential of the ferrocenyl moiety in the BTDs **6a–6h** follows the order **6h** > **6c** > **6b** > **6d** > **6a** > **6g** > **6e** > **6f**, whereas the BTDs **7a–7c**, **8a–8c**, and **9a–9b** follows the order **9b** > **9a** > **7a** > **7c** > **7b** > **8a** > **8c** > **8b**. The ferrocenyl moiety in the BTDs exhibit higher oxidation potentials compared to free ferrocene ( $E^\circ = 0.00$  V, as recommended by IUPAC), confirming the strong electronic communication between the ferrocene unit, and the BTD core.<sup>[8,17]</sup> 1,1,4,4-tetracyanobuta-1,3-diene (TCBD) is a strong electron withdrawing group which results in high oxidation of the ferrocene unit.<sup>[18]</sup>

In addition to the ferrocene oxidation wave a quasi-reversible oxidation wave due to the triphenylamine unit in BTDs **6h**, **8a–8c**, and **9b** is observed in the region 0.51–0.58 V.<sup>[19]</sup> The BTDs **7a–7c**, and **9a** exhibit two irreversible oxidation waves in the region 0.58–1.82 V attributed to the carbazole unit.<sup>[20]</sup>

The reduction potential for the BTDs **6a–6h**, **7a–7c**, and **8a–8c** shows less negative values compared to 2,1,3-Benzothiadiazole **1** (−1.98 V vs Fc/Fc<sup>+</sup> in DCM), indicating that the BTD rings in these ferrocenyl substituted compounds are easier to reduce than unsubstituted BTD.<sup>[7,8,21]</sup> The BTDs **9a**, and **9b** exhibit two reversible reduction waves in the region −0.83 V to −1.29 V attributed to the successive one-electron reductions of the dicyanovinyl (DCV) groups of the TCBD  $\pi$ -linker.<sup>[22]</sup> The third reduction wave in BTDs **9a**, and **9b** is assigned to the BTD unit and was observed at −2.08 V and −2.15 V respectively.

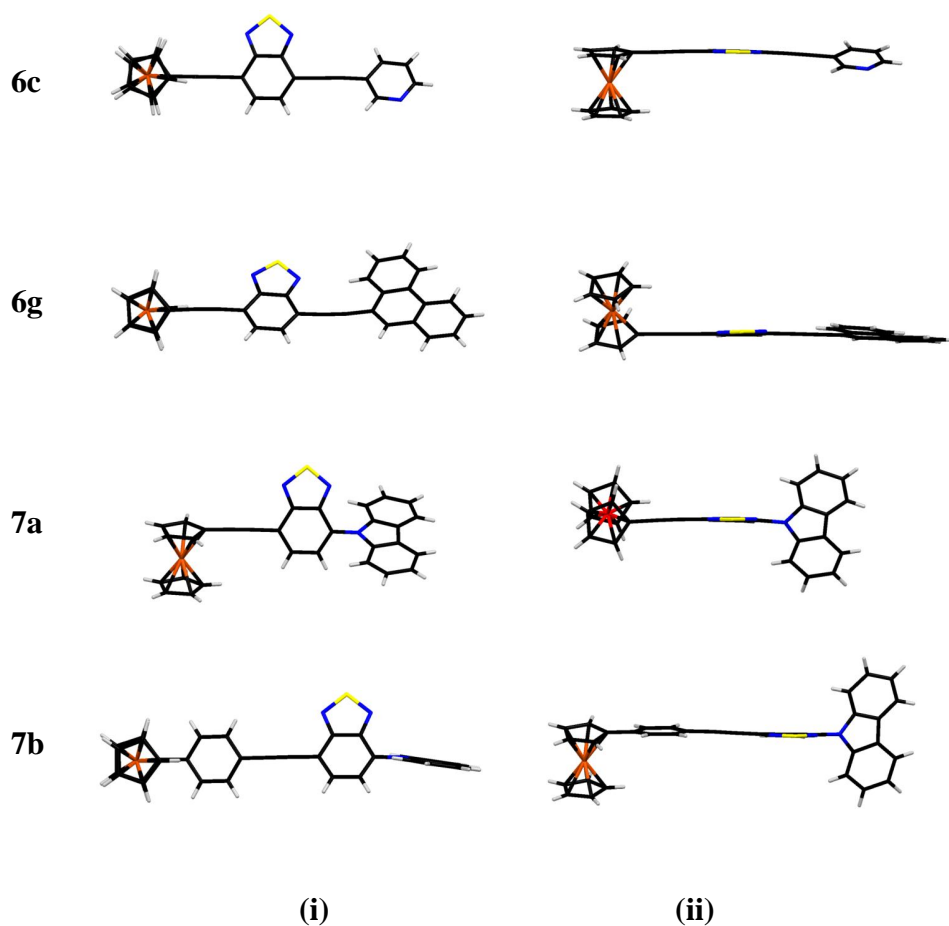
**Table 5.2.** Electrochemical data of unsymmetrical BTDs **6a–6h**, **7a–7c**, **8a–8c**, **9a**, and **9b**.

Compound	Electrochemical data <sup>a</sup>		Compound	Electrochemical data <sup>a</sup>	
	E <sub>ox</sub> (V) <sup>b</sup>	E <sub>red</sub> (V) <sup>b</sup>		E <sub>ox</sub> (V) <sup>b</sup>	E <sub>red</sub> (V) <sup>b</sup>
<b>Ferrocene</b>	0.00	-	<b>Ferrocene</b>	0.00	-
<b>6a</b>	0.12	-1.69	<b>7a</b>	0.10, 0.60, 0.82	-1.73
<b>6b</b>	0.13	-1.61	<b>7b</b>	0.04, 0.58, 0.80	-1.69
<b>6c</b>	0.14	-1.62	<b>7c</b>	0.10, 0.59, 0.82	-1.68
<b>6d</b>	0.13	-1.67	<b>8a</b>	0.13, 0.54	-1.82
<b>6e</b>	0.11	-1.66	<b>8b</b>	0.02, 0.52	-1.78
<b>6f</b>	0.11	-1.64	<b>8c</b>	0.11, 0.51	-1.76
<b>6g</b>	0.12	-1.66	<b>9a</b>	0.42, 0.62, 0.82	-0.83, -1.19, -2.08
<b>6h</b>	0.52, 0.95	-1.69	<b>9b</b>	0.41, 0.58	-0.85, -1.29, -2.15

<sup>a</sup>Recorded by cyclic voltammetry, in 0.1M solution of TBAPF<sub>6</sub> in DCM at 100 mVs<sup>-1</sup> scan rate, vs Fc/Fc<sup>+</sup> at 25°C. <sup>b</sup>For the irreversible redox process, the peak potential is quoted.

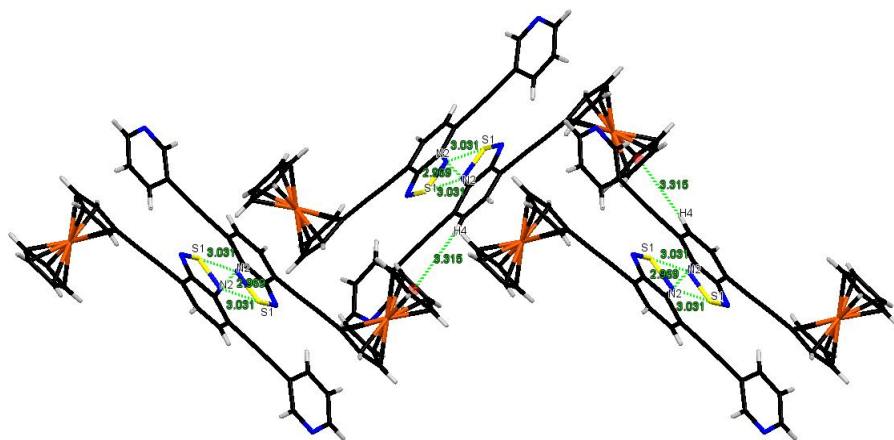
## 5.7. X-ray analysis

The single crystal of the unsymmetrical BTDs **6c**, **6g**, **7a**, and **7b** were obtained via slow diffusion of ethanol into the chloroform solution at room temperature. The BTDs **6c**, and **7a** crystallizes in the monoclinic space group *P*2<sub>1</sub>/*c*, whereas the BTDs **6g** crystallizes in the monoclinic space group *P*2<sub>1</sub>/*n*. The BTD **7b** crystallizes in triclinic space group *P*  $\bar{1}$ . Figure 5.8 shows the single crystal X-ray structure of **6c**, **6g**, **7a**, and **7b**.



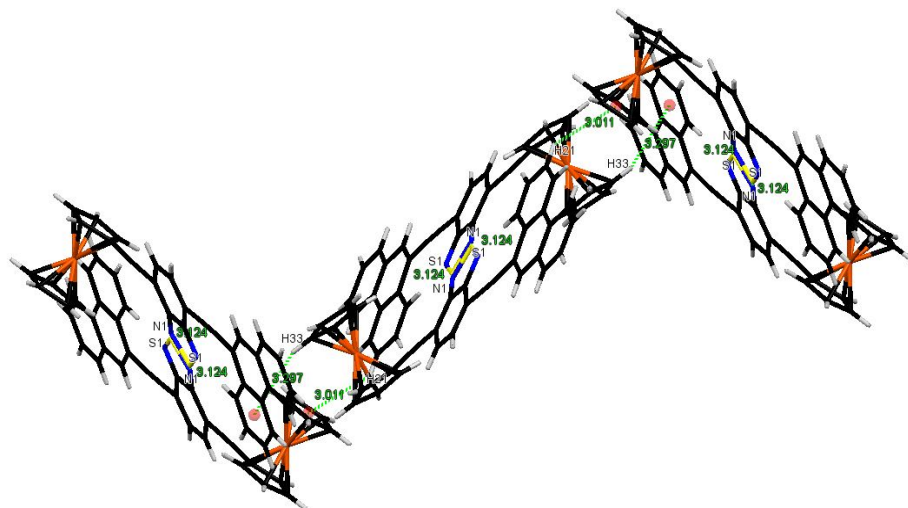
**Figure 5.8.** Single-crystal X-ray structure of ferrocenyl BTDs **6c**, **6g**, **7a**, and **7b**; (i) front view and (ii) side view. Solvent molecule (Chloroform) is omitted from **7a** for clarity.

The BTD core shows planar structure in the unsymmetrical BTDs **6c**, **6g**, **7a**, and **7b**. The cyclopentadienyl rings of the ferrocenyl moiety shows eclipsed skew conformation in BTD **6c**, and eclipsed conformation in BTDs **6g**, **7a**, and **7b**. The dihedral angle between the planes containing the BTD core, and the cyclopentadienyl ring of ferrocene units was found to be  $9.44^\circ$  in **6c**,  $41.06^\circ$  in **6g**,  $70.66^\circ$  in **7a**, and  $24.35^\circ$ .



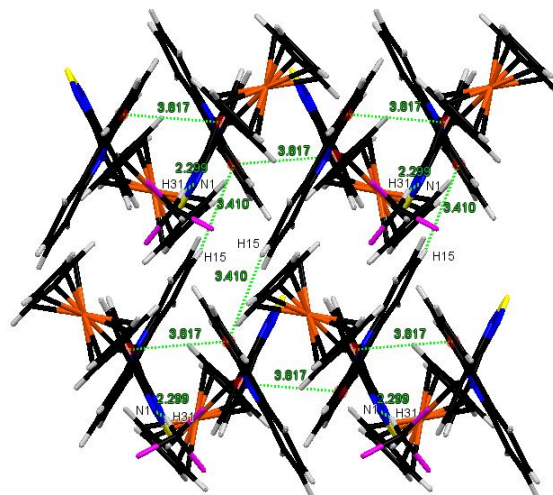
**Figure 5.9.** Packing diagram of ferrocenyl BTB **6c** forming 2D zigzag chain along *a*-axis.

The packing diagram of BTB **6c** exhibits short S1...N2 (3.031(2) Å), and N2...N2 (2.969(5) Å) interhydroatom contacts between the BTB rings, which leads to the formation of dimer in head-to-head fashion.<sup>[4a,8,23]</sup> The dimer units are interlinked through C-H... $\pi$  interaction C4H4...C21-C25 (3.315(2) Å) to form a 2D zigzag chain (Figure 5.9.).



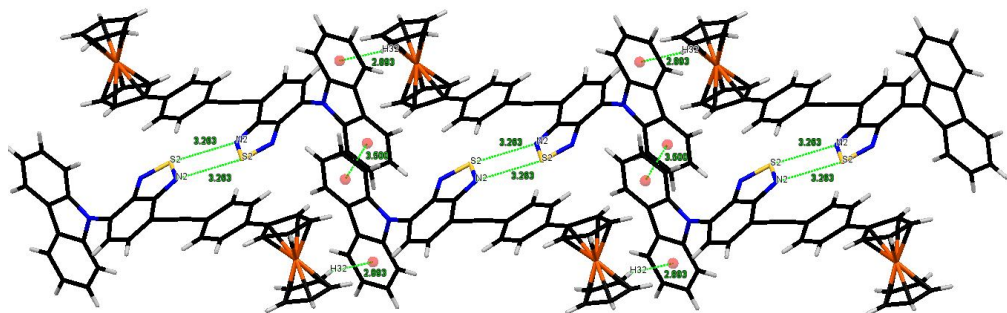
**Figure 5.10.** Packing diagram of ferrocenyl BTB **6g** forming 2D zigzag chain along *a*-axis.

The packing diagram of BTD **6g** exhibits short S1...N2 (3.124(5) Å) interhetroatom contacts between the BTD rings, resulting in the formation of dimer in head-to-head fashion.<sup>4a,8,23</sup> The dimer units are interlinked through C–H... $\pi$  interaction C21H21...C30-C34 (3.011(3) Å) to form a 2D zigzag chain (Figure 5.10.).



**Figure 5.11.** Packing diagram of ferrocenyl BTD **7a** forming 2D sheet along *a*-axis.

The packing diagram of **7a** shows  $\pi$ ... $\pi$  stacking interaction C7-C12...C1-C6 (3.817(2) Å) between the carbazole, and the BTD units which lead to the formation of a 1D polymeric chain. These chains are interlinked in anti fashion via intermolecular C–H... $\pi$  interaction C15H15...C7-C12 (3.410(3) Å) to form a 2D sheet like structure (Figure 5.11).



**Figure 5.12.** Packing diagram of ferrocenyl BTB **7b** forming 2D sheet along *b*-axis.

The packing diagram of BTB **7b** exhibits short S2...N2 (3.263(5) Å) interhydrogen contacts between the BTB rings, which leads to the formation of dimer in head-to-head fashion.<sup>[4a,8,23]</sup> These dimers show  $\pi\cdots\pi$  stacking interaction C21-C26...C21-C26 (3.500(2) Å) between two adjacent carbazole units of the dimer. The dimer units are interlinked through C-H... $\pi$  interaction C32H32...C15-C20 (2.893(4) Å) to form a 1D polymeric chain (Figure 5.12.).

**Table S1.** Crystal data and structure refinement for **6c**, **6g**, **7a** and **7b**.

Parameter	<b>6c</b>	<b>6g</b>	<b>7a</b>	<b>7b</b>
<b>Empirical formula</b>	C <sub>12.50</sub> H <sub>7.50</sub> Fe <sub>0.50</sub> N <sub>1.50</sub> S <sub>0.50</sub>	C <sub>13.60</sub> H <sub>8</sub> Fe <sub>0.40</sub> N <sub>0.80</sub> S <sub>0.40</sub>	C <sub>31</sub> H <sub>20</sub> Cl <sub>3</sub> Fe N <sub>3</sub> S	C <sub>36</sub> H <sub>23</sub> Fe N <sub>3</sub> S
<b>Formula weight</b>	222.65	217.77	628.76	585.48
<b>Temperature</b>	150(2) K	150(2) K	150(2) K	150(2)
<b>Wavelength(Å)</b>	1.5418 Å	1.5418	0.71073 Å	0.71073
<b>Crystal system, space group</b>	Monoclinic, <i>P</i> 2 <sub>1</sub> / <i>c</i>	Monoclinic, <i>P</i> 2 <sub>1</sub> / <i>n</i>	Monoclinic, <i>P</i> 2 <sub>1</sub> / <i>c</i>	Triclinic, <i>P</i> $\bar{1}$
<i>a</i> / (Å)	10.7116(2)	14.4585(3)	20.1248(3)	8.3665(5)
<i>b</i> / (Å)	19.3310(3)	7.53930(10)	8.14360(10)	12.8349(7)
<i>c</i> / (Å)	10.3975(2)	23.5366(4)	16.4453(3) Å	13.9064(8)
$\alpha$ / (°)	90	90	90	92.895(5)
$\beta$ / (°)	115.994(2)	96.619(2)	93.0960(10)	90.071(5)
$\gamma$ / (°)	90	90	90	92.334(4)
<b>Volume</b>	1935.17(6) Å <sup>3</sup>	2548.55(8) Å <sup>3</sup>	2691.26(7) Å <sup>3</sup>	1490.16(15) Å <sup>3</sup>
<b>Z, Calculated density (mg m<sup>-3</sup>)</b>	8, 1.528	10, 1.419	4, 1.552	2, 1.305
<b>Absorption coefficient /(mm<sup>-1</sup>)</b>	7.389	5.711	0.964	0.605
<b>F(000)</b>	912	1120	1280	604
<b>Crystal size</b>	0.23 × 0.18 × 0.13 mm	0.23 × 0.18 × 0.13 mm	0.26 × 0.21 × 0.16 mm	0.33 × 0.26 × 0.21 mm
<b><math>\theta</math> range for data collection/(°)</b>	4.57 to 72.08	3.42 to 72.01	2.95 to 25.00	2.96 to 25.00
<b>Limiting indices</b>	-13 ≤ <i>h</i> ≤ 12, -23 ≤ <i>k</i> ≤ 23, -9 ≤ <i>l</i> ≤ 12	-17 ≤ <i>h</i> ≤ 17, -9 ≤ <i>k</i> ≤ 6, -28 ≤ <i>l</i> ≤ 28	-21 ≤ <i>h</i> ≤ 23, -9 ≤ <i>k</i> ≤ 9, -19 ≤ <i>l</i> ≤ 19	-9 ≤ <i>h</i> ≤ 9, -15 ≤ <i>k</i> ≤ 14, -11 ≤ <i>l</i> ≤ 16
<b>Reflections collected / unique</b>	12330 / 3760	16801 / 4953 [R(int) = 0.0234]	23046 / 4735 [R(int) = 0.0289]	11604 / 5228 [R(int) = 0.0244]
<b>Completeness to theta</b>	72.08 98.7%	θ = 25.00 100.0%	25.00 99.9%	25.00 99.8%
<b>Absorption correction</b>	Semi-empirical from equivalents	Semi-empirical from equivalents	Semi-empirical from equivalents	Semi-empirical from equivalents
<b>Max. and min. transmission</b>	0.4468 and 0.2813	0.5239 and 0.3534	0.8611 and 0.7877	0.8834 and 0.8253
<b>Refinement method</b>	Full-matrix least-squares on F <sup>2</sup>	Full-matrix least-squares on F <sup>2</sup>	Full-matrix least-squares on F <sup>2</sup>	Full-matrix least-squares on F <sup>2</sup>
<b>Data / restraints / parameters</b>	3760 / 0 / 271	4953 / 0 / 343	4735 / 0 / 352	5228 / 0 / 370
<b>Goodness-of-fit on F<sup>2</sup></b>	1.054	1.018	1.027	1.107
<b>Final R indices [I &gt; 2σ(I)]</b>	R <sub>1</sub> = 0.0308, wR <sub>2</sub> = 0.0824	R <sub>1</sub> = 0.0323, wR <sub>2</sub> = 0.0849	R <sub>1</sub> = 0.0302, wR <sub>2</sub> = 0.0718	R <sub>1</sub> = 0.0443, wR <sub>2</sub> = 0.1367
<b>R indices (all data)</b>	R <sub>1</sub> = 0.0332, wR <sub>2</sub> = 0.0841	R <sub>1</sub> = 0.0423, wR <sub>2</sub> = 0.0910	R <sub>1</sub> = 0.0356, wR <sub>2</sub> = 0.0755	R <sub>1</sub> = 0.0521, wR <sub>2</sub> = 0.1441
<b>Largest diff. peak and hole (e Å<sup>-3</sup>)</b>	0.194 and -0.445	0.285 and -0.344	0.298 and -0.368	0.346 and -0.233
<b>CCDC number</b>	959150	959151	959148	959149



## 5.8. Experimental details

$^1\text{H}$  NMR spectra were recorded using a 400 MHz spectrometer. Chemical shifts are reported in delta ( $\delta$ ) units, expressed in parts per million (ppm) downfield from tetramethylsilane using residual protonated solvent as an internal standard ( $\text{CDCl}_3$ , 7.26 ppm;  $(\text{CD}_3)_2\text{CO}$ , 2.05).  $^{13}\text{C}$  NMR spectra were recorded using a 100 MHz spectrometer. Chemical shifts are reported in delta ( $\delta$ ) units, expressed in parts per million (ppm) downfield from tetramethylsilane using the solvent as an internal standard ( $\text{CDCl}_3$ , 77.0 ppm;  $(\text{CD}_3)_2\text{CO}$ , 29.8;  $\text{DMSO}-d_6$ , 39.5 ppm). The  $^1\text{H}$  NMR splitting patterns have been described as “s, singlet; bs, broad singlet; d, doublet; t, triplet; dd (doublet of doublets), dt (doublet of triplets), and m, multiplet”. UV-visible absorption spectra of all compounds were recorded in DCM. Cyclic voltamograms (CVs) were recorded on electrochemical analyzer using Glassy carbon as working electrode, Pt wire as the counter electrode, and Saturated Calomel Electrode (SCE) as the reference electrode. The scan rate was  $100\text{ mVs}^{-1}$  for CV. A solution of tetrabutylammoniumhexafluorophosphate ( $\text{TBAPF}_6$ ) in  $\text{CH}_2\text{Cl}_2$  (0.1 M) was employed as the supporting electrolyte. DCM was freshly distilled from  $\text{CaH}_2$  prior to use. All potentials were experimentally referenced against the saturated calomel electrode couple but were then manipulated to be referenced against  $\text{Fc}/\text{Fc}^+$  as recommended by IUPAC.<sup>[24]</sup> Under our conditions, the  $\text{Fc}/\text{Fc}^+$  couple exhibited  $E^\circ = 0.38\text{ V}$  versus SCE. HRMS was recorded on TOF-Q mass spectrometer. The density functional theory (DFT) calculation were carried out at the B3LYP/6-31G\*\* level for C, N, S, H, and Lan12DZ level for Fe in the Gaussian 09 program.<sup>[25]</sup>

### General procedure for the preparation of BTDs 6a-6c by Sonogashira coupling reaction.

To a stirred solution of respective aryl alkyne (**10a–10h**) (0.37 mmol), and ferrocenyl bromo-BTDs **3a** (0.34 mmol) in THF, and TEA (1:1, v/v) were added  $\text{PdCl}_2(\text{PPh}_3)_2$  (10 mg, 0.014 mmol), and CuI (2 mg, 0.01 mmol) under an argon flow at room temperature. The reaction mixture was stirred for 15 h to 24 h at

60°C, and then cooled to room temperature. The solvent was then evaporated under reduced pressure, and the mixture was purified by SiO<sub>2</sub> chromatography with DCM/Hexane (2:3, v/v) followed by recrystallization in chloroform:ethanol (1:1) to obtain **6a-6h** as colored solid.

Compound **6a**: Deep-red solid (73 mg, Yield: 48 %): mp 200.0-201.5 °C; <sup>1</sup>H NMR (400 MHz, (CD<sub>3</sub>)<sub>2</sub>CO,  $\delta$  in ppm): 7.89 (d, 1H,  $J$  = 7.3 Hz), 7.84 (d, 1H,  $J$  = 7.3 Hz), 7.69-7.66 (m, 2H), 7.50-7.47 (m, 3H), 4.65 (t, 2H,  $J$  = 1.8 Hz), 4.40 (t, 2H,  $J$  = 1.8 Hz), 4.32 (s, 5H); <sup>13</sup>C NMR (100 MHz, DMSO-*d*<sub>6</sub>,  $\delta$  in ppm): 153.7, 134.3, 132.8, 131.8, 131.5, 131.4, 128.7, 128.5, 121.7, 117.1, 115.2, 96.3, 85.6, 81.8, 71.4, 69.9, 69.5, 63.6 ; HRMS (ESI)  $m/z$  calcd for C<sub>26</sub>H<sub>16</sub>FeN<sub>2</sub>S 444.0378 [M]<sup>+</sup>, found 444.0376 [M]<sup>+</sup>; UV/vis (DCM):  $\lambda_{\max}$  ( $\epsilon$  [M<sup>-1</sup>cm<sup>-1</sup>]) 406 (32791), 509 (9324).

Compound **6b**: Deep-red solid (76 mg, Yield: 50 %): mp 225.5-226.5 °C; <sup>1</sup>H NMR (400 MHz, (CD<sub>3</sub>)<sub>2</sub>CO,  $\delta$  in ppm): 7.97 (d, 1H,  $J$  = 7.5 Hz), 7.92-7.86 (m, 3H), 7.73(dt, 1H,  $J$  = 7.8 Hz,  $J$  = 1 Hz), 7.46-7.42 (m, 1H), 4.65 (t, 2H,  $J$  = 2.0 Hz), 4.41 (t, 2H,  $J$  = 2.0 Hz), 4.32 (s, 5H); <sup>13</sup>C NMR (100 MHz, DMSO-*d*<sub>6</sub>,  $\delta$  in ppm): 150.4, 145.9, 139.0, 136.9, 132.1, 131.9, 127.6, 124.2, 111.1, 108.4, 106.2, 101.9, 98.0, 92.7, 82.3, 71.5, 70.0, 69.7, 63.3; HRMS (ESI)  $m/z$  calcd for C<sub>25</sub>H<sub>15</sub>FeN<sub>3</sub>S 446.0409 [M+H]<sup>+</sup>, found 446.0407 [M + H]<sup>+</sup>; UV/vis (DCM):  $\lambda_{\max}$  ( $\epsilon$  [M<sup>-1</sup>cm<sup>-1</sup>]) 399 (85328), 511 (22404).

Compound **6c**: Deep-red solid (91 mg, Yield: 60 %): mp > 300 °C; <sup>1</sup>H NMR (400 MHz, CDCl<sub>3</sub>,  $\delta$  in ppm): 8.90 (bs, 1H), 8.62-8.60 (m, 1H), 7.95 (dt, 1H,  $J$  = 8 Hz;  $J$  = 1.8 Hz), 7.80 (d, 1H,  $J$  = 7.6 Hz), 7.75 (d, 1H,  $J$  = 7.3), 4.66 (t, 2H,  $J$  = 1.8 Hz), 4.34 (t, 2H,  $J$  = 2.0 Hz), 4.31 (s, 5H); <sup>13</sup>C NMR (100 MHz, DMSO-*d*<sub>6</sub>,  $\delta$  in ppm): 153.6, 138.6, 135.9, 133.4, 133.1, 132.0, 131.8, 117.6, 114.4, 113.7, 113.2, 108.0, 104.5, 100.8, 95.3, 71.4, 69.9, 63.2; HRMS (ESI)  $m/z$  calcd for C<sub>25</sub>H<sub>15</sub>FeN<sub>3</sub>S 446.0363 [M+H]<sup>+</sup>, found 446.0360 [M + H]<sup>+</sup>; UV/vis (DCM):  $\lambda_{\max}$  ( $\epsilon$  [M<sup>-1</sup>cm<sup>-1</sup>]) 402 (85328), 515 (20963).

Compound **6d**: deep-red solid (124 mg, Yield: 70 %): mp 191.5-192.5 °C; <sup>1</sup>H NMR (400 MHz, (CD<sub>3</sub>)<sub>2</sub>CO,  $\delta$  in ppm): 7.92 (d; 1H;  $J$  = 7.5 Hz), 7.85 (d, 1H,  $J$  =

7.5 Hz), 7.81-7.73 (m, 6H), 7.52-7.48 (m, 2H), 7.43-7.39 (m, 2H), 4.65 (t, 2H,  $J = 2.0$  Hz), 4.40 (t, 2H,  $J = 1.8$  Hz), 4.32 (s, 5H);  $^{13}\text{C}$  NMR (100 MHz,  $\text{CDCl}_3$ ,  $\delta$  in ppm): 154.25, 154.22, 141.5, 140.0, 132.4, 132.2, 131.7, 128.7, 127.6, 126.9, 121.3, 117.7, 116.2, 97.8, 97.0, 86.0, 81.9, 72.8, 71.6, 70.9, 65.8; HRMS (ESI)  $m/z$  calcd for  $\text{C}_{32}\text{H}_{20}\text{FeN}_2\text{S}$  520.0692  $[\text{M}]^+$ , found 520.0692  $[\text{M}]^+$ ; UV/vis (DCM):  $\lambda_{\text{max}}$  ( $\epsilon$  [ $\text{M}^{-1}\text{cm}^{-1}$ ]) 413 (55533), 512 (14750).

Compound **6e**: Deep-red solid (117 mg, Yield: 70%): mp 199.0-200.5 °C;  $^1\text{H}$  NMR (400 MHz,  $(\text{CD}_3)_2\text{CO}$ ,  $\delta$  in ppm): 8.76 (d, 1H,  $J = 8.3$  Hz), 8.06-8.02 (m, 3H), 7.94-7.88 (m, 2H), 7.77-7.73 (m, 1H), 7.67-7.58 (m, 2H), 4.66 (t, 2H,  $J = 1.8$  Hz), 4.41 (t, 2H,  $J = 1.8$  Hz), 4.33 (s, 5H);  $^{13}\text{C}$  NMR (100 MHz,  $\text{CDCl}_3$ ,  $\delta$  in ppm): 154.0, 153.7, 132.7, 132.6, 131.7, 131.2, 130.1, 129.0, 127.7, 126.6, 126.0, 125.7, 124.7, 119.6, 117.4, 115.7, 97.2, 94.7, 90.0, 81.4, 71.5, 69.9, 69.4, 63.9; HRMS (ESI)  $m/z$  calcd for  $\text{C}_{30}\text{H}_{18}\text{FeN}_2\text{S}$  494.0535  $[\text{M}]^+$ , found 494.0533  $[\text{M}]^+$ ; UV/vis (DCM):  $\lambda_{\text{max}}$  ( $\epsilon$  [ $\text{M}^{-1}\text{cm}^{-1}$ ]) 421 (54400), 521 (sh).

Compound **6f**: Deep-red solid (120 mg, Yield: 65%): mp 192.5-193.8 °C;  $^1\text{H}$  NMR (400 MHz,  $(\text{CD}_3)_2\text{CO}$ ,  $\delta$  in ppm): 8.99-8.96 (m, 2H), 8.72 (s, 1H), 8.21-8.17 (m, 2H), 7.94 (d, 1H,  $J = 7.5$  Hz), 7.79-7.75 (m, 2H), 7.66-7.62 (m, 2H), 4.68 (t, 2H,  $J = 1.8$  Hz), 4.42 (t, 2H,  $J = 1.8$  Hz), 4.34 (s, 5H);  $^{13}\text{C}$  NMR (100 MHz,  $\text{CDCl}_3$ ,  $\delta$  in ppm): 154.4, 154.2, 132.6, 131.7, 131.6, 130.9, 128.5, 127.3, 127.2, 126.8, 126.6, 125.6, 123.0, 117.6, 116.4, 116.3, 97.6, 96.8, 94.2, 81.9, 71.9, 70.3, 69.7, 63.8; HRMS (ESI)  $m/z$  calcd for  $\text{C}_{34}\text{H}_{20}\text{FeN}_2\text{S}$  544.0692  $[\text{M}]^+$ , found 544.0694  $[\text{M}]^+$ ; UV/vis (DCM):  $\lambda_{\text{max}}$  ( $\epsilon$  [ $\text{M}^{-1}\text{cm}^{-1}$ ]) 465 (67550).

Compound **6g**: Deep-red solid (74 mg, Yield: 40 %): mp 201.5-202.4 °C;  $^1\text{H}$  NMR (400 MHz,  $(\text{CD}_3)_2\text{CO}$ ,  $\delta$  in ppm): 8.93-8.86 (m, 3H), 8.32 (s, 1H), 8.10-8.05 (m, 2H), 7.91 (d, 1H,  $J = 7.3$ ), 7.88-7.76 (m, 3H), 7.74-7.71 (m, 1H), 4.67 (t, 2H,  $J = 2.0$  Hz), 4.42 (t, 2H,  $J = 2.0$  Hz), 4.34 (s, 5H);  $^{13}\text{C}$  NMR (100 MHz,  $\text{CDCl}_3$ ,  $\delta$  in ppm): 154.3, 154.1, 140.0, 132.2, 132.1, 131.5, 130.7, 130.6, 130.2, 129.7, 128.4, 127.6, 127.1, 127.0, 126.8, 122.5, 122.3, 118.8, 117.7, 115.9, 97.6, 95.2, 89.8, 81.7, 71.9, 70.3, 69.6, 63.5; HRMS (ESI)  $m/z$  calcd for  $\text{C}_{34}\text{H}_{20}\text{FeN}_2\text{S}$  544.0692  $[\text{M}]^+$ , found 544.0708  $[\text{M}]^+$ ; UV/vis (DCM):  $\lambda_{\text{max}}$  ( $\epsilon$  [ $\text{M}^{-1}\text{cm}^{-1}$ ]) 423 (58074), 514 (sh).

Compound **6h**: Deep-red solid (114 mg, Yield: 55 %): mp 182.0-183.0 °C; <sup>1</sup>H NMR (400 MHz, (CD<sub>3</sub>)<sub>2</sub>CO,  $\delta$  in ppm): 7.85-7.80 (m, 2H), 7.55-7.51 (m, 2H), 7.39-7.35 (m, 2H), 7.17-7.13 (m, 2H), 7.03-7.00 (m, 2H), 4.64 (t, 2H,  $J$  = 1.8 Hz), 4.39 (t, 2H,  $J$  = 2.0 Hz), 4.32 (s, 5H); <sup>13</sup>C NMR (100 MHz, CDCl<sub>3</sub>,  $\delta$  in ppm): 154.0, 153.9, 148.1, 146.5, 132.4, 131.6, 131.4, 129.0, 124.8, 123.4, 121.2, 116.9, 116.3, 114.6, 97.4, 97.0, 84.6, 81.5, 71.5, 69.9, 69.1, 63.9; HRMS (ESI)  $m/z$  calcd for C<sub>38</sub>H<sub>25</sub>FeN<sub>3</sub>S 611.1114 [M]<sup>+</sup>, found 611.1115 [M]<sup>+</sup>; UV/vis (DCM):  $\lambda_{\max}$  ( $\epsilon$  [M<sup>-1</sup>cm<sup>-1</sup>]) 460 (58729).

**General procedure for the preparation of BTDs 7a-7c, and 8a-8c by Sonogashira coupling reaction.**

To a stirred solution of respective alkynyl ferrocene (0.37 mmol), and bromo-BTDs **4a/5a** (0.34 mmol) in THF, and TEA (1:1, v/v) were added PdCl<sub>2</sub>(PPh<sub>3</sub>)<sub>2</sub> (10 mg, 0.014 mmol), and CuI (2 mg, 0.01 mmol) under an argon flow at room temperature. The reaction mixture was stirred for 12 h at 60°C, and then cooled to room temperature. The solvent was then evaporated under reduced pressure, and the mixture was purified by SiO<sub>2</sub> chromatography with DCM/Hexane (2:3, v/v) followed by recrystallization in Chloroform:Ethanol (1:1) to obtain **7a-7c**, and **8a-8c** as colored solid.

Compound **7a**: Red solid (121 mg, Yield: 70 %): mp 185.5-186.5 °C; <sup>1</sup>H NMR (400 MHz, (CD<sub>3</sub>)<sub>2</sub>CO,  $\delta$  in ppm): 8.26-8.24 (m, 2H), 8.09 (d, 1H,  $J$  = 7.5 Hz), 7.99 (d, 1H,  $J$  = 7.5 Hz), 7.41-7.37 (m, 2H), 7.33-7.28 (m, 4H), 4.69 (t, 2H,  $J$  = 1.8 Hz), 4.42 (t, 2H,  $J$  = 2.0 Hz), 4.35 (s, 5H); <sup>13</sup>C NMR (100 MHz, CDCl<sub>3</sub>,  $\delta$  in ppm): 155.9, 151.2, 140.9, 131.9, 129.4, 127.7, 125.9, 123.9, 120.6, 120.4, 117.5, 110.3, 97.2, 81.46, 72.7, 71.3, 70.6, 65.3; HRMS (ESI)  $m/z$  calcd for C<sub>30</sub>H<sub>19</sub>FeN<sub>3</sub>S 509.0644 [M]<sup>+</sup>, found 509.0666 [M]<sup>+</sup>; UV/vis (DCM):  $\lambda_{\max}$  ( $\epsilon$  [M<sup>-1</sup>cm<sup>-1</sup>]) 443 (35138), 520 (sh).

Compound **7b**: Orange solid (129 mg, Yield: 65%): mp 198.0-199.5 °C; <sup>1</sup>H NMR (400 MHz, (CD<sub>3</sub>)<sub>2</sub>CO,  $\delta$  in ppm): 8.27-8.24 (m, 2H), 8.18 (d, 1H,  $J$  = 7.5 Hz), 8.04 (d, 1H,  $J$  = 7.5 Hz), 7.70- 7.68 (m, 2H), 7.64-7.62 (m, 2H), 7.42-7.37 (m, 2H), 7.34-7.30 (m, 4H), 4.86 (t, 2H,  $J$  = 1.8 Hz), 4.42 (t, 2H,  $J$  = 1.8 Hz), 4.07 (s, 5H); <sup>13</sup>C NMR (100 MHz, DMSO-*d*<sub>6</sub>,  $\delta$  in ppm): 155.4, 150.7, 141.1, 140.5,

133.1, 131.7, 129.2, 128.2, 126.1, 123.1, 120.5, 120.4, 118.7, 115.8, 110.8, 96.6, 85.6, 83.3, 69.6, 69.64, 66.6; HRMS (ESI)  $m/z$  calcd for  $C_{36}H_{23}FeN_3S$  585.0957  $[M]^+$ , found 585.0952  $[M]^+$ ; UV/vis (DCM):  $\lambda_{max}$  ( $\epsilon$  [ $M^{-1}cm^{-1}$ ]) 453 (47855).

Compound **7c**: Orange solid (124 mg, Yield: 60%): mp 220.5-221.2 °C;  $^1H$  NMR (400 MHz,  $(CD_3)_2CO$ ,  $\delta$  in ppm): 8.27-8.26 (m, 2H), 8.20 (d, 2H,  $J = 7.5$  Hz), 8.06 (d, 2H,  $J = 7.5$  Hz), 7.73-7.71 (m, 2H), 7.61-7.59 (m, 2H), 7.42-7.38 (m, 2H), 7.34-7.30 (m, 2H), 4.56 (t, 2H,  $J = 1.8$  Hz), 4.34 (t, 2H,  $J = 2.0$  Hz), 4.28 (s, 5H);  $^{13}C$  NMR (100 MHz,  $DMSO-d_6$ ,  $\delta$  in ppm): 155.2, 150.5, 140.3, 133.1, 131.6, 131.2, 129.4, 127.9, 125.9, 124.0, 123.0, 120.9, 120.3, 120.1, 115.3, 110.5, 95.5, 91.4, 86.9, 84.9, 71.1, 69.7, 69.0, 63.8; HRMS (ESI)  $m/z$  calcd for  $C_{38}H_{23}FeN_3S$  609.0957  $[M]^+$ , found 609.0956  $[M]^+$ ; UV/vis (DCM):  $\lambda_{max}$  ( $\epsilon$  [ $M^{-1}cm^{-1}$ ]) 454(62777).

Compound **8a**: Red solid (120 mg, Yield: 68%): mp 180.5-181.6 °C;  $^1H$  NMR (400 MHz,  $(CD_3)_2CO$ ,  $\delta$  in ppm): 8.03-8.01 (m, 2H), 7.89 (d, 1H,  $J = 7.5$  Hz), 7.84 (d, 1H,  $J = 7.5$  Hz), 7.38-7.34 (m, 4H), 7.18-7.10 (m, 8H), 4.63 (t, 2H,  $J = 1.8$  Hz), 4.38 (t, 2H,  $J = 1.8$  Hz), 4.32 (s, 5H);  $^{13}C$  NMR (100 MHz,  $CDCl_3$ ,  $\delta$  in ppm): 155.3, 153.1, 148.3, 147.2, 133.2, 132.4, 130.3, 129.8, 129.3, 126.7, 124.9, 123.3, 122.6, 115.7, 95.5, 81.9, 71.9, 70.3, 69.4, 64.8; HRMS (ESI)  $m/z$  calcd for  $C_{36}H_{23}FeN_3S$  587.1114  $[M]^+$ , found 587.1114  $[M]^+$ ; UV/vis (DCM):  $\lambda_{max}$  ( $\epsilon$  [ $M^{-1}cm^{-1}$ ]) 458 (37842).

Compound **8b**: orange solid (140 mg, Yield: 62 %): mp 202.0-203.5 °C;  $^1H$  NMR (400 MHz,  $(CD_3)_2CO$ ,  $\delta$  in ppm): 8.04 (d, 2H,  $J = 9.0$  Hz), 7.98 (d, 1H,  $J = 7.5$  Hz), 7.89 (d, 1H,  $J = 7.5$  Hz), 7.65 (d, 2H,  $J = 8.5$  Hz), 7.58 (d, 2H,  $J = 8.0$  Hz), 7.38-7.34 (m, 4H), 7.18-7.10 (m, 8H), 4.84 (t, 2H,  $J = 2.0$  Hz), 4.41 (t, 2H,  $J = 2.0$  Hz), 4.06 (s, 5H);  $^{13}C$  NMR (100 MHz,  $CDCl_3$ ,  $\delta$  in ppm): 155.4, 153.1, 148.3, 147.3, 140.5, 133.9, 132.9, 131.8, 130.2, 130.0, 129.3, 126.6, 125.9, 125.0, 123.4, 122.6, 119.9, 115.2, 96.2, 85.8, 70.6, 70.2, 67.1; HRMS (ESI)  $m/z$  calcd for  $C_{42}H_{29}FeN_3S$  663.1427  $[M]^+$ , found 663.1426  $[M]^+$ ; UV/vis (DCM):  $\lambda_{max}$  ( $\epsilon$  [ $M^{-1}cm^{-1}$ ]) 466(51474).

Compound **8c**: Orange solid (152 mg, Yield: 65 %): mp 189.5-190.5 °C;  $^1H$  NMR (400 MHz,  $(CD_3)_2CO$ ,  $\delta$  in ppm): 8.04 (d, 2H,  $J = 9$  Hz), 8.00 (d, 1H,  $J =$

7.28 Hz), 7.90 (d, 1H,  $J = 7.28$  Hz), 7.67 (d, 2H,  $J = 8.80$  Hz), 7.57 (d, 2H,  $J = 8.52$  Hz), 7.39-7.35 (m, 4H), 7.18-7.11 (m, 8H), 4.55 (t, 2H,  $J = 1.8$  Hz), 4.33 (t, 2H,  $J = 2.0$  Hz), 4.27 (s, 5H);  $^{13}\text{C}$  NMR (100 MHz,  $\text{CDCl}_3$ ,  $\delta$  in ppm): 154.9, 152.5, 147.9, 146.7, 145.3, 141.8, 133.8, 132.8, 131.3, 130.7, 129.5, 128.9, 126.0, 124.4, 123.0, 121.9, 114.0, 109.7, 96.3, 94.3, 93.2, 87.1, 73.4, 70.8, 69.4, 64.9; HRMS (ESI)  $m/z$  calcd for  $\text{C}_{44}\text{H}_{29}\text{FeN}_3\text{S}$  687.1427  $[\text{M}]^+$ , found 687.1426  $[\text{M}]^+$ ; UV/vis (DCM):  $\lambda_{\text{max}}$  ( $\epsilon$  [ $\text{M}^{-1}\text{cm}^{-1}$ ]) 467 (84788).

### General procedure for the preparation of BTDs **9a-9b**.

TCNE (77 mg, 0.60 mmol) was added to a solution of **7a/8a** (0.30 mmol) in DCM (60 mL) at room temperature. The mixture was refluxed at 40 °C for 15 h. The solvent was removed in vacuo, and the product was purified by  $\text{SiO}_2$  chromatography with DCM as the eluent to yield **9a/9b** as a dark colored solid.

Compound **9a**: Purple solid (134 mg, Yield: 70 %): mp 279.5-280.5 °C;  $^1\text{H}$  NMR (400 MHz,  $(\text{CD}_3)_2\text{CO}$ ,  $\delta$  in ppm): 8.76 (d, 1H,  $J = 7.5$  Hz), 8.31 (d, 2H,  $J = 7.3$  Hz), 7.40-7.29 (m, 4H), 7.24-7.12 (m, 2H), 5.46-5.45 (m, 1H), 5.07-5.05 (m, 1H), 5.01-5.00 (m, 1H), 4.92-4.91 (m, 1H), 4.39 (s, 5H);  $^{13}\text{C}$  NMR (100 MHz,  $\text{CDCl}_3$ ,  $\delta$  in ppm): 171.0, 160.9, 152.1, 150.5, 140.0, 135.2, 131.9, 126.0, 125.5, 124.3, 124.2, 122.8, 121.3, 120.2, 113.8, 111.4, 110.7, 110.5, 90.5, 79.3, 75.9, 74.8, 74.2, 73.0, 72.4, 70.7, 65.5; HRMS (ESI)  $m/z$  calcd for  $\text{C}_{36}\text{H}_{19}\text{FeN}_7\text{S}$  637.0767  $[\text{M}]^+$ , found 637.0774  $[\text{M}]^+$ ; UV/vis (DCM):  $\lambda_{\text{max}}$  ( $\epsilon$  [ $\text{M}^{-1}\text{cm}^{-1}$ ]) 502 (46178).

Compound **9b**: Deep-green solid (172 mg, Yield: 80 %): mp 222.5-223.5 °C;  $^1\text{H}$  NMR (400 MHz,  $(\text{CD}_3)_2\text{CO}$ ,  $\delta$  in ppm): 8.52 (d, 1H,  $J = 7.8$  Hz), 8.10-8.07 (m, 3H), 7.40-7.36 (m, 4H), 7.19-7.10 (m, 8H), 5.40-5.38 (m, 1H), 5.00-4.99 (m, 1H), 4.89-4.87 (m, 1H), 4.85-4.83 (m, 1H), 4.35 (s, 5H);  $^{13}\text{C}$  NMR (100 MHz,  $\text{CDCl}_3$ ,  $\delta$  in ppm): 171.3, 164.8, 161.5, 152.9, 151.4, 149.3, 146.4, 139.3, 132.0, 130.3, 129.2, 127.8, 125.3, 125.2, 125.1, 123.9, 121.8, 121.1, 111.7, 101.3, 89.0, 82.1, 79.2, 75.5, 74.5, 74.2, 72.7, 72.1, 70.6, 64.6; HRMS (ESI)  $m/z$  calcd for  $\text{C}_{42}\text{H}_{27}\text{FeN}_7\text{S}$  715.1237  $[\text{M}]^+$ , found 715.1240  $[\text{M}]^+$ ; UV/vis (DCM):  $\lambda_{\text{max}}$  ( $\epsilon$  [ $\text{M}^{-1}\text{cm}^{-1}$ ]) 554 (61482).

## 5.9. Conclusion

In summary, a series of aryl substituted benzothiadiazole derivatives were designed and synthesized by the Pd-catalyzed Sonogashira cross-coupling reaction. The photophysical and electrochemical properties show strong electronic communication. The enhancement of conjugation *via*  $\pi$ -bridge resulted in the red shift of the absorption bands in BTDs **7a-7c**, **8a-8c**, and **9a-9b**. The modulation of the donor and acceptor strength results in lowering of the band gap. The detailed nonlinear optical characterization of these ferrocenyl substituted unsymmetrical BTDs are currently ongoing in our laboratory.

## 5.10. References

- [1] (a) Sonar P., Singh S. P., Li Y., Soh M. S., Dodabalapur A. (2010), A low-bandgap diketopyrrolopyrrole-benzothiadiazole-based copolymer for high-mobility ambipolar organic thin-film transistors, *Adv. Mater.*, 22, 5409-5413 (DOI: 10.1002/adma.201002973). (b) Kato S., Furuya T., Kobayashi A., Nitani M., Ie Y., Aso Y., Yoshihara T., Tobita S., Nakamura Y.,  $\pi$ -Extended thiadiazoles fused with thienopyrrole or indole moieties: synthesis, structures, and properties, *J. Org. Chem.*, 77, 7595-7606 (DOI: 10.1021/jo301458m). (c) Omer K. M., Ku S. Y., Wong K. T., Bard A. J. (2009), Green electrogenerated chemiluminescence of highly fluorescent benzothiadiazole and fluorene derivatives, *J. Am. Chem. Soc.*, 131, 10733-10741 (DOI: 10.1021/ja904135y). (d) Li Y., Li A.-Y., Li B.-X., Huang J., Zhao L., Wang B.-Z., Li J.-W., Zhu X.-H., Peng J., Cao Y., Ma D.-G., Roncali J. (2009), Asymmetrically 4,7-disubstituted benzothiadiazoles as efficient non-doped solution-processable green fluorescent emitters, *Org. Lett.*, 11, 5318-5321 (DOI: 10.1021/ol9022563). (e) Wang J.-L., Tang Z.-M., Xiao Q., Ma Y., Pei J. (2009), Star-shaped D- $\pi$ -A conjugated molecules: synthesis and broad absorption bands, *Org. Lett.*, 11, 863-866 (DOI: 10.1021/ol802845w). (f) Kato S., Matsumoto T., Ishi-i T., Thiemann T., Shigeiwa M., Gorohmaru H., Maeda S., Yamashita Y., Mataka S. (2004), Strongly red-fluorescent

novel donor- $\pi$ -bridge-acceptor- $\pi$ -bridge-donor (D- $\pi$ -A- $\pi$ -D) type 2,1,3-benzothiadiazoles with enhanced two-photon absorption cross-sections, *Chem. Commun.*, 2342-2343 (DOI: 10.1039/B410016F). (g) Neto B. A. D., Lapis A. A. M., Júnior E. N. da S., Dupont J. (2013), 2,1,3-benzothiadiazole and derivatives: synthesis, properties, reactions, and applications in light technology of small molecules, *Eur. J. Org. Chem.*, 228-255 (DOI: 10.1002/ejoc.201201161). (h) Kato S., Matsumoto T., Shigeiwa M., Gorohmaru H., Maeda S., Ishi-i T., Mataka S. (2006), Novel 2,1,3-Benzothiadiazole-based red-fluorescent dyes with enhanced two-photon absorption cross-sections, *Chem.-Eur. J.*, 12, 2303-2317 (DOI: 10.1002/chem.200500921). (i) Kobayashi N., Inagaki S., Nemykin V. N., Nonomura T. (2001), A novel hemiporphyrine comprising three isoindoleimine and three thiadiazole units, *Angew. Chem., Int. Ed.*, 40, 2710-2712 (DOI: 10.1002/1521-3773(20010716)40:14<2710::AID-ANIE2710>3.0.CO;2-A). (j) Lindner B. D., Engelhart J. U., Märken M., Tverskoy O., Appleton A. L., Rominger F., Hardcastle K. I., Enders M., Bunz U. H. F. (2012), Synthesis and optical properties of diaza- and tetraazatetracenes, *Chem.-Eur. J.*, 18, 4627-4633 (DOI: 10.1002/chem.201103227). (k) Aviram A., Ratner M. A. (1974), Molecular rectifiers, *Chem. Phys. Lett.*, 29, 277-283 (DOI:10.1016/0009-2614(74)85031-1).

- [2] (a) Wang J.-L., Xiao Q., Pei J. (2010), Benzothiadiazole-based D- $\pi$ -A- $\pi$ -D Organic dyes with tunable band gap: Synthesis and photophysical properties, *Org. Lett.*, 12, 4164-4167 (DOI: 10.1021/ol101754q). (b) Zhang H., Wan X., Xue X., Li Y., Yu A., Chen Y. (2010), Selective tuning of the HOMO-LUMO gap of carbazole-based donor-acceptor-donor compounds toward different emission colors, *Eur. J. Org. Chem.*, 1681-1687 (DOI: 10.1002/ejoc.200901167). (c) Bures F., Schweizer W. B., May J. C., Boudon C., Gisselbrecht J.-P., Gross M., Biaggio I., Diederich F. (2007), Property tuning in charge-transfer chromophores by



systematic modulation of the spacer between donor and acceptor, *Chem.–Eur. J.*, 13, 5378–5387 (DOI: 10.1002/chem.200601735).

- [3] (a) Tang Z. M., Lei T., Jiang K. J., Song Y. L., Pei J. (2010), Benzothiadiazole containing D– $\pi$ –A conjugated compounds for dye-sensitized solar cells: synthesis, properties, and photovoltaic performances, *Chem.–Asian J.*, 5, 1911–1917 (DOI: 10.1002/asia.201000158). (b) Wu Y., Zhu W. (2013), Organic sensitizers from D– $\pi$ –A to D–A– $\pi$ –A: effect of the internal electron-withdrawing units on molecular absorption, energy levels and photovoltaic performances, *Chem. Soc. Rev.*, 42, 2039–2058 (DOI: 10.1039/C2CS35346F).
- [4] (a) Chen S., Li Y., Yang W., Chen N., Liu H., Li Y. (2010), Synthesis and Tuning optical nonlinear properties of molecular crystals of benzothiadiazole, *J. Phys. Chem. C*, 114, 15109–15115 (DOI: 10.1021/jp103159b). (b) Tambara K., Pantoş G. D. 2012, Supramolecular chemistry of donor–acceptor interactions, *Annu. Rep. Prog. Chem., Sect. B: Org. Chem.*, 108, 186–201 (DOI: 10.1039/C2OC90016E). (c) Polander L. E., Pandey L. S., Barlow S., Tiwari S. P., Risko C., Kippelen B., Brédas J., Marder S. R. (2011), Benzothiadiazole-dithienopyrrole donor–acceptor–donor and acceptor–donor–acceptor triads: synthesis and optical, electrochemical, and charge-transport properties, *J. Phys. Chem. C*, 115, 23149–23163 (DOI: 10.1021/jp208643k). (d) Shi C. J., Yao Y., Yang Y., Pei Q. B. (2006), Regioregular copolymers of 3-alkoxythiophene and their photovoltaic application, *J. Am. Chem. Soc.*, 128, 8980–8986 (DOI: 10.1021/ja061664x). (e) Hou Q., Zhou Q. M., Zhang Y., Yang W., Yang R. Q., Cao Y. (2004), Synthesis and electroluminescent properties of high-efficiency saturated red emitter based on copolymers from fluorene and 4,7-di(4-hexylthien-2-yl)-2,1,3-benzothiadiazole, *Macromolecules*, 2004, 37, 6299–6305 (DOI: 10.1021/ma049204g). (f) Zhu, Z.; Waller, D.; Gaudiana, R.; Morana, M., Mühlbacher D., Scharber M., Brabec C. (2007), Panchromatic conjugated polymers containing alternating

- donor/acceptor units for photovoltaic applications, *Macromolecules*, 40, 1981-1986 (DOI: 10.1021/ma062376o). (g) Thomas K. R. J., Lin J. T., Velusamy M., Tao Y. T., Chuen C. H. (2004), Color tuning in benzo[1,2,5]thiadiazole-based small molecules by amino conjugation/deconjugation: bright red-light-emitting diodes, *Adv. Funct. Mater.*, 14, 83-90 (DOI: 10.1002/adfm.200304486).
- [5] (a) Gautam P., Dhokale B., Shukla V., Singh C. P., Bindra K. S., Misra R. (2012), Optical limiting performance of meso-tetraferrocenyl porphyrin and its metal derivatives, *J. Photochem. Photobiol., A*, 239, 24–27 (DOI:10.1016/j.jphotochem.2012.04.020). (b) Jadhav T., Maragani R., Misra R., Sreeramulu V., Rao D. N., Mobin S. M. (2013), Design and synthesis of donor–acceptor pyrazabole derivatives for multiphoton absorption, *Dalton Trans.*, 42, 4340-4342 (DOI: 10.1039/C3DT33065F). (c) Maragani R., Thaksen J., Mobin S. M., Misra R. (2013), *RSC Adv.*, 3, 2889-2892 (DOI: 10.1039/C2RA23153K).
- [6] (a) Gautam P., Dhokale B., Mobin S. M., Misra R. (2012), Ferrocenyl BODIPYs: synthesis, structure and properties, *RSC Adv.*, 2, 12105-12107 (DOI: 10.1039/C2RA21964F). (b) Dhokale B., Gautam P., Mobin S. M., Misra R. (2013), Donor–acceptor, ferrocenyl substituted BODIPYs with marvelous supramolecular interactions, *Dalton Trans.*, 42, 1512-1518 (DOI: 10.1039/C2DT31632C). (c) Sharma R., Maragani R., Mobin S. M., Misra R. (2013), Ferrocenyl substituted calixarenes: synthesis, structure and properties, *RSC Adv.*, 3, 5785-5788 (DOI: 10.1039/C3RA00146F).
- [7] Misra R., Gautam P., Sharma R., Mobin S. M. (2013), Donor– $\pi$ –acceptor– $\pi$ –donor ferrocenyl benzothiadiazoles: synthesis, structure, and properties, *Tetrahedron Lett.*, 54, 381-383 (DOI:10.1016/j.tetlet.2012.11.016).
- [8] Misra R., Gautam P., Jadhav T., Mobin S. M. (2013), Donor–acceptor ferrocenyl-substituted benzothiadiazoles: synthesis, structure, and properties, *J. Org. Chem.*, 78, 4940-4948 (DOI: 10.1021/jo4005734).
- [9] Wang B., Tsang S., Zhang W., Tao Y., Wong M. S. (2011), Naphthodithiophene-2,1,3-benzothiadiazole copolymers for bulk

- heterojunction solar cells, *Chem. Commun.* 47, 9471-9473 (DOI: 10.1039/C1CC13690A).
- [10] Karpicz R., Puzinas S., Krotkus S., Kazlauskas K., Jursenas S., Grazulevicius J. V., Grigalevicius S., Gulbinas V. (2011), Impact of intramolecular twisting and exciton migration on emission efficiency of multifunctional fluorene-benzothiadiazole-carbazole compounds, *J. Chem. Phys.*, 134, 204508-204516 (DOI: 10.1063/1.3594047).
- [11] Velusamy M., Justin Thomas K. R., Lin J. T., Hsu Y.-C., Ho K.-C. (2005), Organic dyes incorporating low-band-gap chromophores for dye-sensitized solar cells, *Org. Lett.*, 7, 1899-1902 (DOI: 10.1021/ol050417f).
- (12) Chen S., Li Y., Liu C., Yang W., Li Y. (2011), Strong charge-transfer chromophores from [2+2] cycloadditions of TCNE and TCNQ to peripheral donor-substituted alkynes, *Eur. J. Org. Chem.*, 32, 6445-6451 (DOI: 10.1002/ejoc.201101009).
- [13] (a) Wang J. L., Tang Z. M., Xiao Q., Ma Y. G., Pei J. (2008), Energy transfer in new D- $\pi$ -A conjugated dendrimers: their synthesis and photophysical properties, *Org. Lett.* 2008, 10, 4271-4274 (DOI: 10.1021/ol801671w). (b) Zhang H., Wan X., Xue X., Li Y., Yu A., Chen Y. (2010), Selective tuning of the HOMO-LUMO gap of carbazole-based donor-acceptor-donor compounds toward different emission colors, *Eur. J. Org. Chem.*, 1681-1687 (DOI: 10.1002/ejoc.200901167). (c) Xu E., Zhong H., Du J., Zeng D., Ren S., Sun J., Fang Q. (2009), The synthesis and properties of novel  $\pi$ -conjugated 2,1,3-benzothiadiazole oligomers, *Dyes Pigm.*, 80, 194-198 (DOI:10.1016/j.dyepig.2008.07.008). (d) Tao Y.-M., Li H.-Y., Xu Q.-L., Zhu Y.-C., Kang L.-C., Zheng Y.-X., Zuo J.-L., You X.-Z. (2011), Synthesis and characterization of efficient luminescent materials based on 2,1,3-benzothiadiazole with carbazole moieties, *Synth. Met.*, 161, 718-723 (DOI:10.1016/j.synthmet.2011.01.020).

- [14] Vieira A. A., Cristiano R., Bortoluzzi A. J., Gallardo H. (2008), Luminescent 2,1,3-benzothiadiazole-based liquid crystalline compounds, *J. Mol. Struct.* 2008, 875, 364-371 (DOI:10.1016/j.molstruc.2007.05.006).
- [15] Ziessel R., Retailleau P., Elliott K. J., Harriman A. (2009), Boron dipyrroin dyes exhibiting “push–pull–pull” electronic signatures, *Chem.–Eur. J.*, 15, 10369-10374 (DOI: 10.1002/chem.200901725).
- [16] (a) Watanabe M., Goto K., Fujitsuka M., Tojo S., Majima T., Shinmyozu T. (2010), 2,1,3-Benzothiadiazole dimers: preparation, structure, and transannular electronic interactions of syn- and anti-[2.2](4,7)benzothiadiazolophanes, *Bull. Chem. Soc. Jpn.*, 83, 1155-1161 (doi:10.1246/bcsj.20100085). (b) Xu E., Zhong H., Lai H., Zeng D., Zhang J., Zhu W., Fang Q. (2010), A new polymeric light-emitting material with pure green emission: poly(fluorene-alt-quinoxaline) with benzothiadiazole groups in the side chain, *Macromol. Chem. Phys.*, 211, 651-656 (DOI: 10.1002/macp.200900486).
- [17] (a) Maragani R., Jadhav T., Mobin S. M., Misra R. (2012), Synthesis, structure, photophysical, and electrochemical properties of donor–acceptor ferrocenyl derivatives, *Tetrahedron*, 68, 7302-7308 (DOI:10.1016/j.tet.2012.06.094). (b) Misra R., Kumar R., Chandrashekar T. K., Suresh C. H., Nag A., Goswami D. (2006), 22 $\pi$ -Smaragdyrin molecular conjugates with aromatic phenylacetylenes and ferrocenes: syntheses, electrochemical, and photonic properties, *J. Am. Chem. Soc.*, 128, 16083-16091 (DOI: 10.1021/ja0628295).
- [18] Niu S., Ulrich G., Retailleau P., Ziessel R. (2011), BODIPY-bridged push–pull chromophores: optical and electrochemical properties, *Tetrahedron Lett.*, 52, 4848-4853 (DOI:10.1016/j.tetlet.2011.07.028).
- [19] (a) Lambert C., Gaschler W., Schmäzlin E., Meerholz K., Bräuchle C. (1999), Subchromophore interactions in tricyanovinyl-substituted triarylamine— a combined experimental and computational study, *J. Chem. Soc., Perkin Trans. 2* 1999, 577-588 (DOI: 10.1039/A808009G). (b) Tsai M.-H., Lin H.-W., Su H.-C., Ke T.-H., Wu C.-c., Fang F.-C., Liao Y.-L.,

- Wong K.-T., Wu C.-I. (2006), Highly efficient organic blue electrophosphorescent devices based on 3,6-bis(triphenylsilyl)carbazole as the host material, *Adv. Mater.*, 18, 1216-1220 (DOI: 10.1002/adma.200502283). (c) Tang X., Liu W., Wu J., Lee C.-S., You J., Wang P. (2010), Synthesis, crystal structures, and photophysical properties of triphenylamine-based multicyno derivatives, *J. Org. Chem.*, 75, 7273-7278 (DOI: 10.1021/jo101456v).
- [20] Kato S.-I., Noguchi H., Kobayashi A., Yoshihara T., Tobita S., Nakamura Y. (2012), Bicarbazoles: systematic structure–property investigations on a series of conjugated carbazole dimers, *J. Org. Chem.*, 77, 9120-9133 (DOI: 10.1021/jo3016538).
- [21] (a) Rao M. R., Kumar K. V. P., Ravikanth M. (2010), Synthesis of boron-dipyrromethene–ferrocene conjugates, *J. Organomet. Chem.*, 695, 863–869 (DOI:10.1016/j.jorganchem.2010.01.009). (b) Watanabe M., Goto K., Shibahara M., Shinmyozu T. (2010), Synthesis, structure, and electronic and photophysical properties of two- and three-layered [3.3]paracyclophane-based donor–acceptor systems(1), *J. Org. Chem.*, 75, 6104-6114 (DOI: 10.1021/jo100688m)..
- [22] Kivala M., Boudon C., Gisselbrecht J.-P., Seiler P., Gross M., Diederich F. (2007), Charge-transfer chromophores by cycloaddition–retro-electrocyclization: multivalent systems and cascade reactions, *Angew. Chem., Int. Ed.*, 46, 6357-6360 (DOI: 10.1002/anie.200701733).
- [23] (a) Pop F., Amacher A., Avarvari N., Ding J., Daku L. M. L., Hauser A., Koch M., Hauser J., Liu S., Decurtins S. (2013), Tetrathiafulvalene–benzothiadiazoles as redox-tunable donor–acceptor systems: Synthesis and photophysical study, *Chem.–Eur. J.*, 19, 2504-2514 (DOI: 10.1002/chem.201202742). (b) Anant P., Lucas N. T., Jacob J. (2008), A simple route toward the synthesis of bisbenzothiadiazole derivatives, *Org. Lett.*, 10, 5533-5536 (DOI: 10.1021/ol8022837).

- [24] Gritzner G., Kuta G. J. (1984), Recommendations on reporting electrode potentials in nonaqueous solvents (Recommendations 1983), *Pure Appl. Chem.*, 56, 461-466 (DOI: 10.1351/pac198456040461).
- [25] (a) Frisch M. J., Trucks G. W., Schlegel H. B., Scuseria G. E., Robb M. A., Cheeseman J. R., Scalmani G., Barone V., Mennucci B., Petersson G. A., Nakatsuji H., Caricato M., Li X., Hratchian H. P., Izmaylov A. F., Bloino J., Zheng G., Sonnenberg J. L., Hada M., Ehara M., Toyota K., Fukuda R., Hasegawa J., Ishida M., Nakajima, T., Honda, Y., Kitao O., Nakai H., Vreven T., Montgomery J. A. Jr., Peralta J. E., Ogliaro F., Bearpark M., Heyd J. J., Brothers E., Kudin K. N., Staroverov V. N., Kobayashi R., Normand J., Raghavachari K., Rendell A., Burant J. C., Iyengar S. S., Tomasi J., Cossi M., Rega N., Millam N. J., Klene M., Knox J. E., Cross J. B., Bakken V., Adamo C., Jaramillo J., Gomperts R., Stratmann, R. E., Yazyev O., Austin A. J., Cammi R., Pomelli C., Ochterski J. W., Martin R. L., Morokuma K., Zakrzewski V. G., Voth G. A., Salvador P., Dannenberg J. J., Dapprich S., Daniels A. D., Farkas O., Foresman J. B., Ortiz J. V., Cioslowski J., Fox D. J. (2009), *Gaussian 09*, revision A.02; Gaussian, Inc.: Wallingford, CT, 2009. (b) Lee C., Yang W., Parr R. G. (1988), Development of the Colle-Salvetti correlation-energy formula into a functional of the electron density, *Phys. Rev. B*, 37, 785-789 (10.1103/PhysRevB.37.785). (c) Becke A. D. (1993), Density-functional thermochemistry. III. The role of exact exchange, *J. Chem. Phys.* 1993, 98, 1372-1377 (DOI: 10.1063/1.464913).



## Chapter 6

### Tuning of the HOMO–LUMO gap of symmetrical and unsymmetrical benzothiadiazoles

#### 6.1. Introduction

$\pi$ -Functional donor–acceptor (D–A) molecular systems are of significant interest because of their potential applications in multi-photon absorption, organic field effect transistors (OFETs), organic light emitting diodes (OLEDs) and organic photovoltaics (OPVs).<sup>[1]</sup> The electronic and photonic properties of the D–A system is a function of the HOMO–LUMO gap.<sup>[2]</sup> The HOMO–LUMO gap in D– $\pi$ –A systems can be tuned either by altering the strength of D/A units or by varying the  $\pi$ -bridge.<sup>[3]</sup> Literature reveals that a variety of donors (triphenylamine, carbazole, *etc.*) have been attached with electron acceptor (benzothiadiazole, diketopyrrolopyrrole, *etc.*) to generate low HOMO–LUMO gap molecular systems.<sup>[4]</sup> Our group is interested in the design and synthesis of D–A molecular systems for various applications.<sup>[5]</sup>

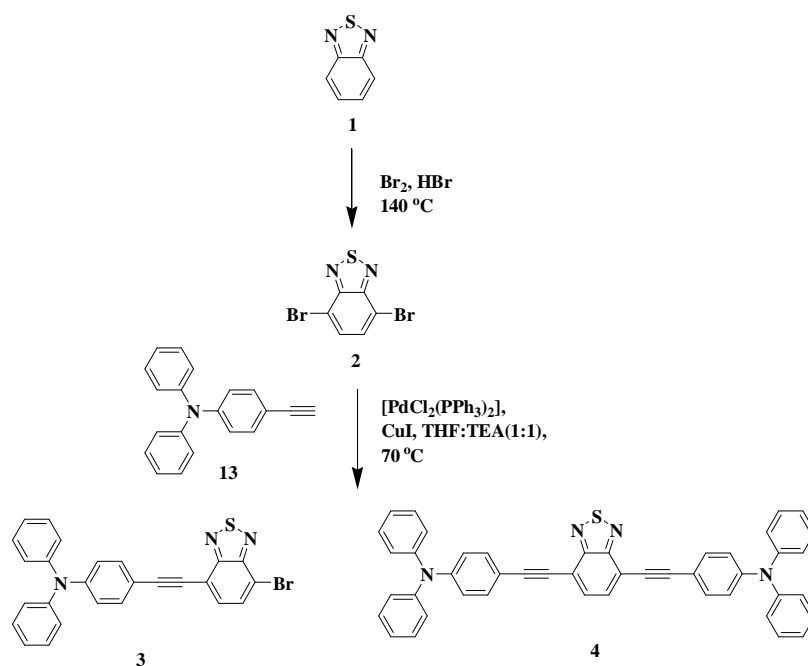
The reaction of electron deficient tetracyanoethylene (TCNE) and 7,7,8,8-tetracyanoquinodimethane (TCNQ) with electron rich acetylenic donors results in strong intramolecular charge-transfer (ICT) chromophores. The D–A systems incorporating these cyano-based acceptors have proved to be efficient candidates in organic photovoltaics and nonlinear optics.<sup>[6]</sup> Diederich and coworkers reacted TCNE and TCNQ with a variety of acetylenic donors and synthesized charge-transfer chromophores *via* [2 + 2] cycloaddition–retroelectrocyclization process.<sup>[7]</sup> Shoji *et al.* reported the synthesis and properties of TCNE and TCNQ derivatives of azulene based molecular system.<sup>[8]</sup> Li group described the synthesis and nonlinear optical (NLO) properties of *N,N*-dimethylaniline-substituted benzothiadiazole (BTD) systems. Their [2 + 2] cycloaddition–retroelectrocyclization with TCNE and TCNQ resulted in strong charge-transfer (CT) molecular system.<sup>[9]</sup>



Benzothiadiazole is a strong acceptor owing to its high electron affinity and have been extensively utilized for the design of low HOMO–LUMO gap molecular systems.<sup>[10]</sup> Recently we have reported a series of low band gap symmetrical and unsymmetrical ferrocenyl substituted BTDs.<sup>[11]</sup> Triphenylamine and carbazole are strong electron donors and their derivatives have been explored for various optoelectronic applications.<sup>[1f,12]</sup> We were interested to explore the band gap of triphenylamine and carbazole substituted symmetrical and unsymmetrical BTDs and to see the effect of acceptor strength on their photophysical properties. In this contribution, we wish to report symmetrical and unsymmetrical donor–acceptor molecular systems of the type D–A<sub>1</sub>–A<sub>2</sub>–A<sub>1</sub>–D, D– $\pi$ –A–D, D<sub>1</sub>– $\pi$ –A–D<sub>2</sub>, D–A<sub>1</sub>–A<sub>2</sub>–D and D<sub>1</sub>–A<sub>1</sub>–A<sub>2</sub>–D<sub>2</sub>. Triphenylamine substituted BTDs **3** and **4** were synthesized by the Pd-catalyzed Sonogashira cross-coupling reaction of dibromo-BTD **2** with 4-ethynyltriphenylamine (**13**). The unsymmetrical BTDs **5** and **6** were synthesized by the Ullmann and Suzuki coupling reactions of BTD **3** with carbazole **14** and triphenylamine-4-boronic acid **15** respectively. The BTDs **4**, **5** and **6** were further subjected to the [2 + 2] cycloaddition–retroelectrocyclization reaction with tetracyanoethylene (TCNE) and 7,7,8,8-tetracyanoquinodimethane (TCNQ), which resulted symmetrical and unsymmetrical BTDs **7–12**.

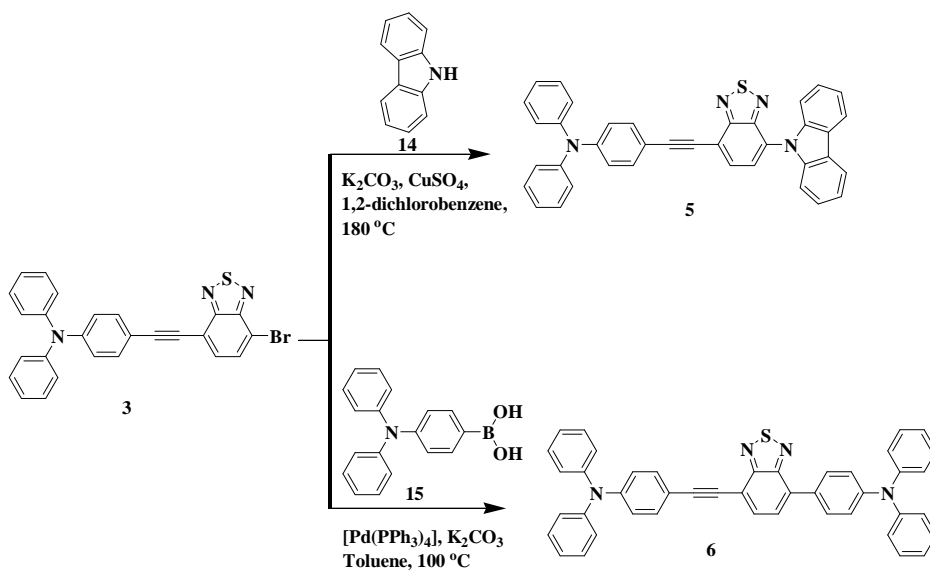
## 6.2. Results and discussion

The synthesis of symmetrical and unsymmetrical benzothiadiazoles **5–12** are shown in Scheme 6.2, Scheme 6.3 and Scheme 6.4. The dibromo-BTD **2** was synthesized by the bromination reaction of BTD **1**.<sup>[13]</sup> The Pd-catalyzed Sonogashira cross-coupling reaction of dibromo-BTD **2** with one equivalent of 4-ethynyltriphenylamine (**13**) resulted [4-(7-bromo-benzo[1,2,5]thiadiazol-4-ylethynyl)-phenyl]-diphenylamine (**3**) and 4,7-bis{2-[4-(*N,N*-diphenylamino)phenyl]ethynyl}-2,1,3-benzothiadiazole (**4**) in 50% and 30% yields respectively (Scheme 6.1).<sup>[14]</sup>



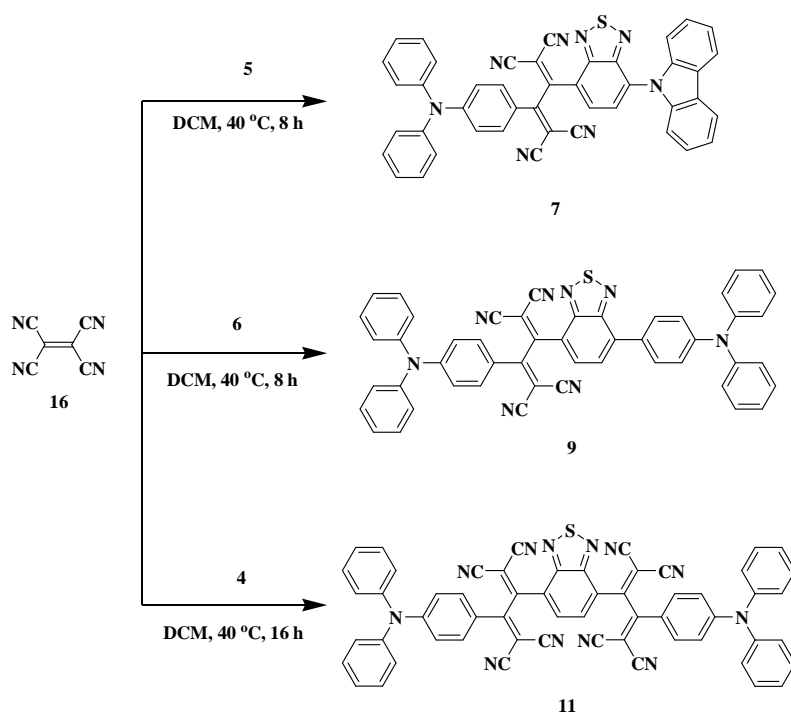
**Scheme 6.1.** Synthesis of benzothiadiazoles **3** and **4**.

The Ullmann and Suzuki coupling reaction of monobromo-BTD **3** with carbazole (**14**) and triphenylamine-4-boronic acid (**15**) resulted BTDs **5** and **6** in 40% and 65% yields respectively (Scheme 6.2).<sup>[15,16]</sup>



**Scheme 6.2.** Synthesis of benzothiadiazoles **5** and **6**.

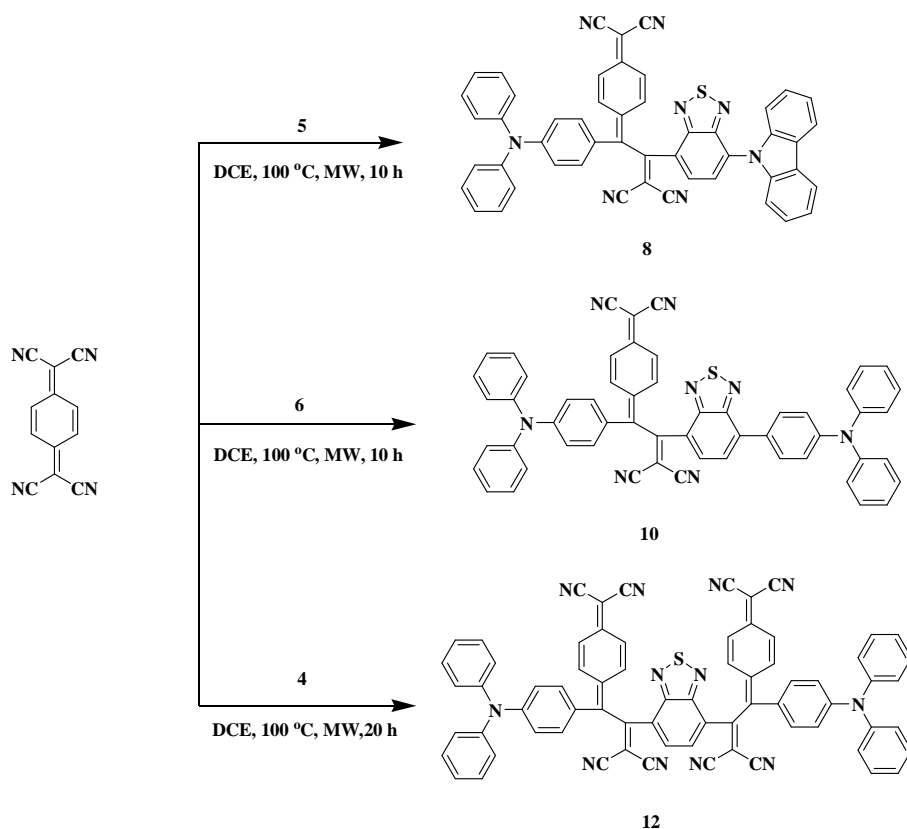
The tetracyanobutadiene (TCBD) and dicyanoquinodimethane (DCNQ) linked BTDs **7–12** were synthesized *via* the [2 + 2] cycloaddition–retroelectrocyclization reaction of the BTDs **4–6** bearing acetylene linkage with tetracyanoethene (TCNE) **16** and 7,7,8,8-tetracyanoquinodimethane (TCNQ) **17** (Scheme 6.3 and Scheme 6.4).<sup>[9b]</sup> The reaction of BTDs **5** and **6** with one equivalent of TCNE resulted BTDs **7** and **9** in 75% and 80% yields respectively. The reaction of BTD **4** with two equivalents of TCNE resulted BTD **11** in 85% yield.



**Scheme 6.3.** Synthesis of benzothiadiazoles **7**, **9** and **11**.

The reactions of 7,7,8,8-tetracyanoquinodimethane (TCNQ) with the acetylene linked BTDs **4**, **5** and **6** were sluggish in nature.<sup>[17]</sup> To overcome this hurdle the reactions were carried out under the microwave irradiation.<sup>[18]</sup> The reaction of BTDs **5** and **6** with one equivalent of TCNQ in 1,2-dichloroethane (DCE) at 100 °C under microwave irradiation for 10 h resulted BTDs **8** and **10** in 70% and 65% yields respectively. The reaction of BTD **4** with two equivalents of TCNQ in DCE at 100 °C under microwave irradiation for 20 h resulted BTD **12** in

50% yield. The reactions carried out under microwave irradiation showed improved yields along with reduced time period.<sup>[9b]</sup>

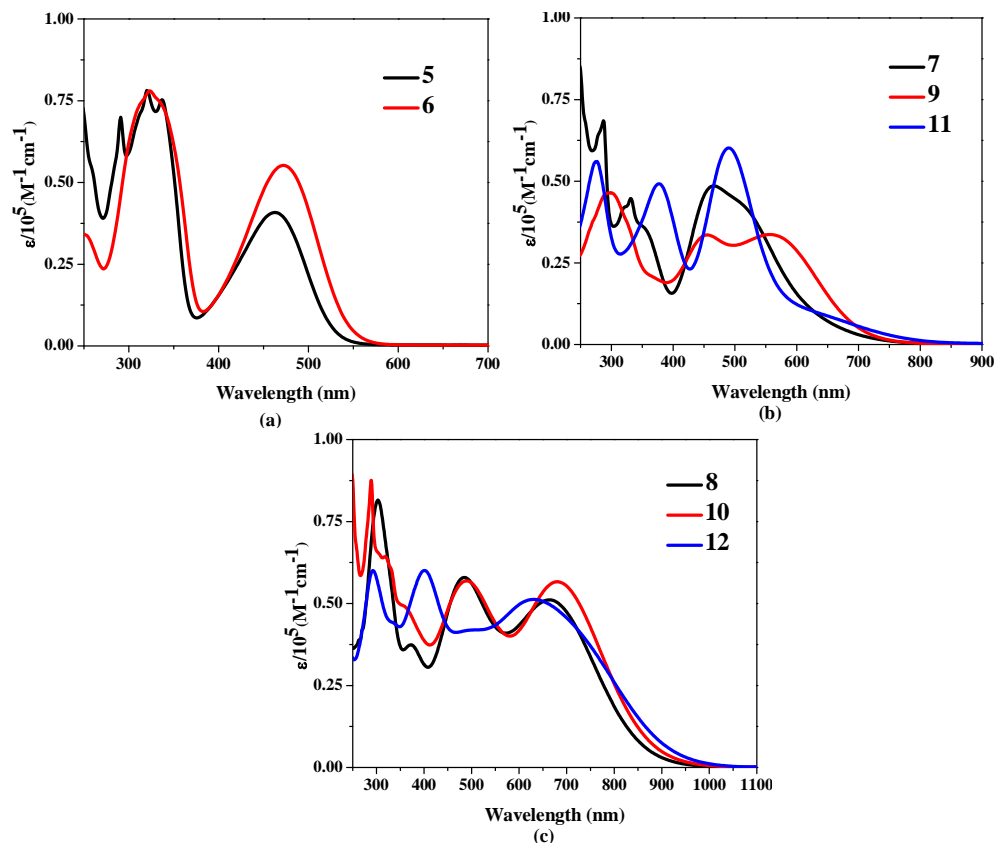


**Scheme 6.4.** Synthesis of benzothiadiazoles **8**, **10** and **12**.

The purification of BTDs **5–12** were achieved by column chromatography. Benzothiadiazoles **5–12** were well characterized by  $^1\text{H}$ ,  $^{13}\text{C}$  NMR, and HRMS techniques. The  $^1\text{H}$  NMR spectra of unsymmetrical BTDs **5–10** show a characteristic doublet between 8.30–7.66 ppm corresponding to two protons of benzothiadiazole. The  $^1\text{H}$  NMR spectra of symmetrical BTDs **11** and **12** exhibit singlet for two benzothiadiazole protons at 8.07 ppm and 8.45 ppm respectively. Benzothiadiazoles **5–12** are readily soluble in common organic solvents such as chloroform, dichloromethane, toluene, tetrahydrofuran, acetone, *etc.*

### 6.3. Photophysical properties

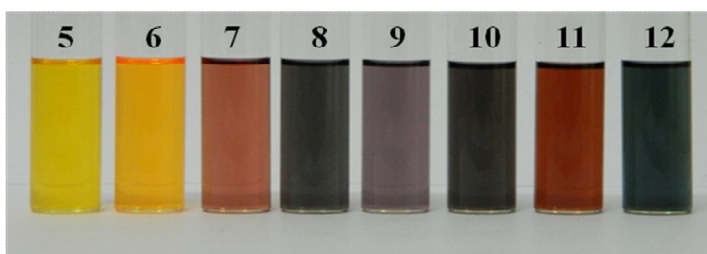
The electronic absorption spectra of the benzothiadiazoles (BTDs) **5–12** were recorded in dichloromethane (Figure 6.1) and the data are listed in Table 6.1. BTDs **5–12** exhibit strong absorption band between 250–350 nm, corresponding to  $\pi \rightarrow \pi^*$  transition.<sup>[10,19]</sup>



**Figure 6.1.** Electronic absorption spectra of benzothiadiazoles **5–12** in dichloromethane at  $1.0 \times 10^{-5}$  M concentration.

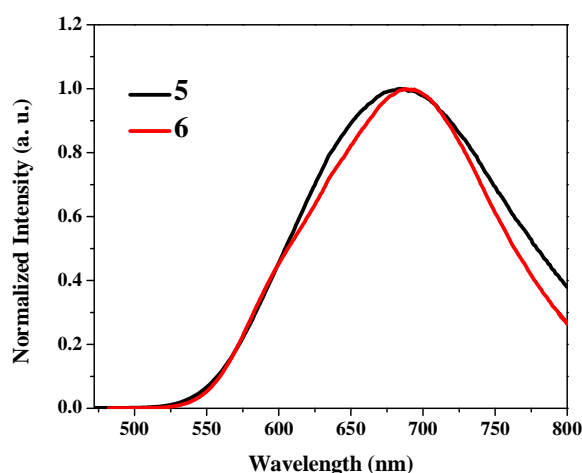
The absorption spectra of BTDs **5** and **6** exhibit charge transfer (CT) band at 464 nm and 473 nm respectively.<sup>[1e,14b]</sup> The incorporation of the tetracyanobutadiene (TCBD) and dicyanoquinodimethane (DCNQ) acceptor unit result in multi-CT bands in BTDs **7–12**.<sup>9b</sup> This indicates strong donor-acceptor interaction in the BTDs **7–12** with TCBD and DCNQ linkers. The presence of strong CT transition result in intense color solution of BTDs **7–12** in

dichloromethane (Figure 6.2.).The trend observed in the optical HOMO-LUMO gap values exhibit the order **5** > **6** > **7** > **9** > **11** > **8** > **10** > **12**. This reveals that the optical HOMO-LUMO gap values were significantly lowered in the DCNQ linked BTDs followed by the TCBD and acetylene linked BTDs. Incorporation of two TCBD and DCNQ linkages in BTDs **11** and **12** results in lower optical HOMO-LUMO gap values. Therefore HOMO-LUMO gap in these BTDs are function of acceptor strength.



**Figure 6.2.** Benzothiadiazoles **5–12** at  $1 \times 10^{-5}$  M concentration in dichloromethane.

The BTDs **5** and **6** exhibit broad fluorescence spectra in dichloromethane (Figure 6.3.).<sup>[9a]</sup> The fluorescence emission wavelengths  $\lambda_{em}$  for BTDs **5** and **6** were observed at 684 nm and 691 nm respectively (Table 6.1.).



**Figure 6.3.** Emission spectra of BTD **5** and **6** at 0.1 absorption, excited at 462 nm and 473 nm respectively in dichloromethane.


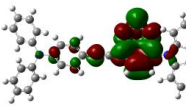
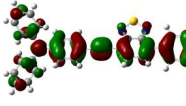
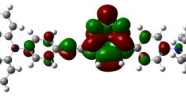
**Table 6.1.** Photophysical, electrochemical and thermal stability data of benzothiadiazoles **5–12**.

BTd	Photophysical data					T <sub>d</sub> (°C) <sup>d</sup>
	$\lambda_{\text{abs}}$ (nm) <sup>a</sup>	$\epsilon$ (M <sup>-1</sup> cm <sup>-1</sup> )	$\lambda_{\text{em}}$ (nm) <sup>a</sup>	Optical Gap (eV) <sup>b</sup>	HOMO-LUMO Gap (eV) <sup>c</sup>	
<b>5</b>	320	78087	684	2.20	2.44	352
	464	40765				
<b>6</b>	323	77978	691	2.19	2.42	165
	473	55191				
<b>7</b>	287	68633	-	1.68	2.46	373
	332	44590				
	466	48688				
	518	sh				
<b>8</b>	303	81366	-	1.34	2.31	458
	484	57868				
	665	51092				
<b>9</b>	298	46557	-	1.66	2.40	331
	454	33497				
	560	33770				
<b>10</b>	288	87541	-	1.31	2.18	343
	491	56994				
	683	56612				
<b>11</b>	276	56010	-	1.57	2.03	298
	377	49125				
	490	60218				
<b>12</b>	293	60054	-	1.27	1.86	275
	401	60163				
	637	51366				

<sup>a</sup> Absorbance measured in dichloromethane at  $1 \times 10^{-5}$  M concentration; sh = shoulder;  $\lambda_{\text{abs}}$ : absorption wavelength;  $\lambda_{\text{em}}$ : emission wavelength;  $\epsilon$ : extinction coefficient. <sup>b</sup> determined from onset wavelength of the UV/Vis absorption; <sup>c</sup> calculated from theoretical study; <sup>d</sup> decomposition temperatures for 5% weight loss under N<sub>2</sub> atmosphere at heating rate of 10 °C min<sup>-1</sup>

#### 6.4. Theoretical calculations

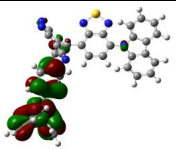
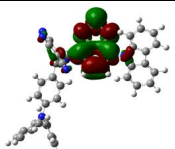

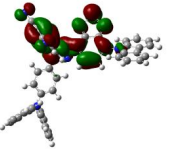
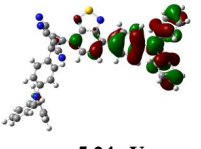
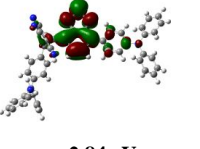
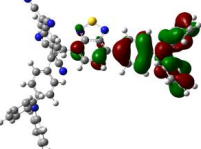
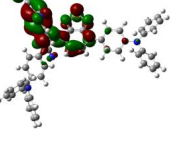
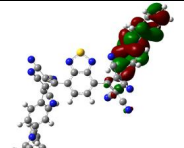
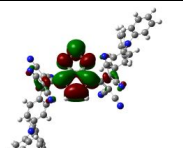
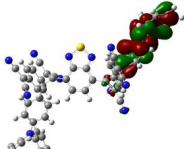
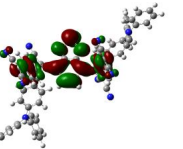
In order to explore the effect of acceptors on the electronic structure and the HOMO-LUMO gap of the benzothiadiazoles **5–12** density functional theory (DFT) calculations were performed at the B3LYP/6-31G\*\* level.<sup>20</sup> The contours of the HOMO, and LUMO of BTds **5–12** are shown in Figure 6.4 and Figure 6.5.

<u>BTD</u>	<u>HOMO</u>	<u>LUMO</u>
5	 -5.02 eV	 -2.58 eV
6	 -4.79 eV	 -2.36 eV

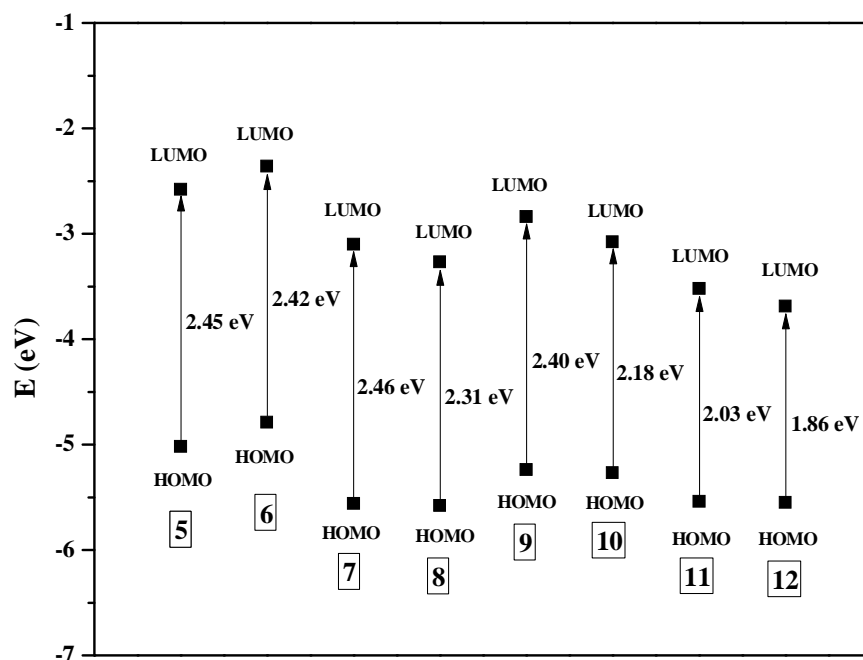
**Figure 6.4.** HOMO and LUMO frontier orbitals of benzothiadiazoles **5** and **6** at the B3LYP/6-31G\*\* level for C, N, S, and H.

The HOMO is contributed by the aryl donors and the hydrocarbon portion of the benzothiadiazole in BTDs **5** and **6**.<sup>[11b]</sup> The HOMO in BTDs **7**, **8**, **11** and **12** are delocalized over the triphenylamine donor adjacent to the TCBD and DCNQ units. On the other hand the HOMO in BTDs **9** and **10** is localized on the triphenylamine donor directly linked to the benzothiadiazole core. The LUMO orbitals in BTDs **5–12** are concentrated over the benzothiadiazole, TCBD and DCNQ acceptors units. The energy level diagram of the frontier orbitals are shown in Figure 6.6. The presence of strong acceptors (TCBD and DCNQ) in BTDs **7–12** lowers the LUMO level, which leads to low HOMO-LUMO gap and red shift in the electronic absorption.



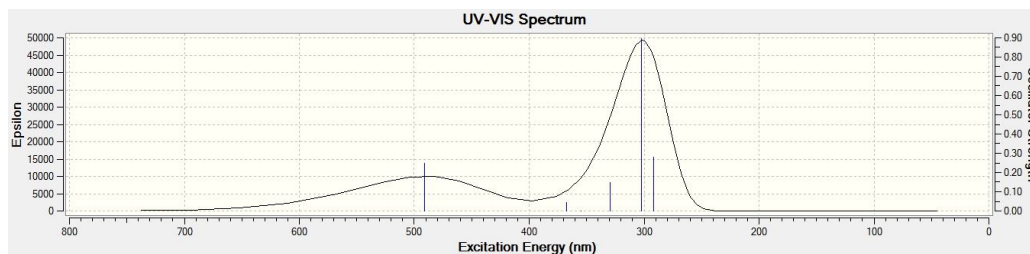
<u>BTD</u>	<u>HOMO</u>	<u>LUMO</u>
7	 -5.56 eV	 -3.10 eV
8	 -5.58 eV	 -3.27 eV
9	 -5.24 eV	 -2.84 eV
10	 -5.27 eV	 -3.08 eV
11	 -5.54 eV	 -3.52 eV
12	 -5.55 eV	 -3.69 eV

**Figure 6.5.** HOMO and LUMO frontier orbitals of benzothiadiazoles **7–12** at the B3LYP/6-31G\*\* level for C, N, S, and H.



**Figure 6.6.** Energy diagram of the frontier orbitals of benzothiadiazole **5–12** estimated by DFT calculations.

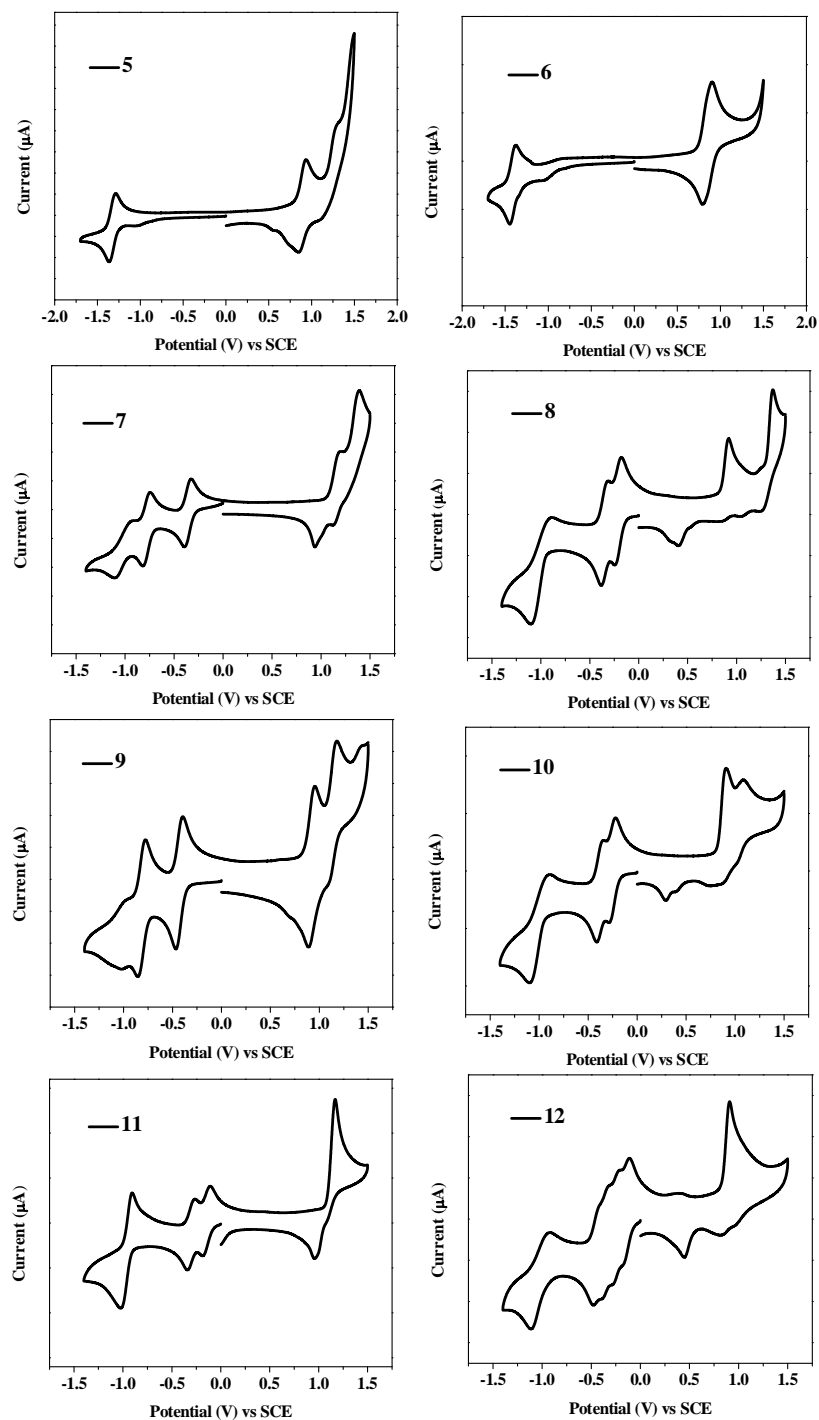
Time-dependent DFT calculation was performed on BTD **7** in dichloromethane to understand the absorption properties. The contributions to the molecular orbitals in the UV/Vis absorption were determined on the basis of their oscillator strength ( $f$ ). The TD-DFT calculation shows that, the lower energy band at 490 nm in the absorption spectrum (Figure 6.7.) show a preferential contribution from HOMO→LUMO and HOMO-1→LUMO.



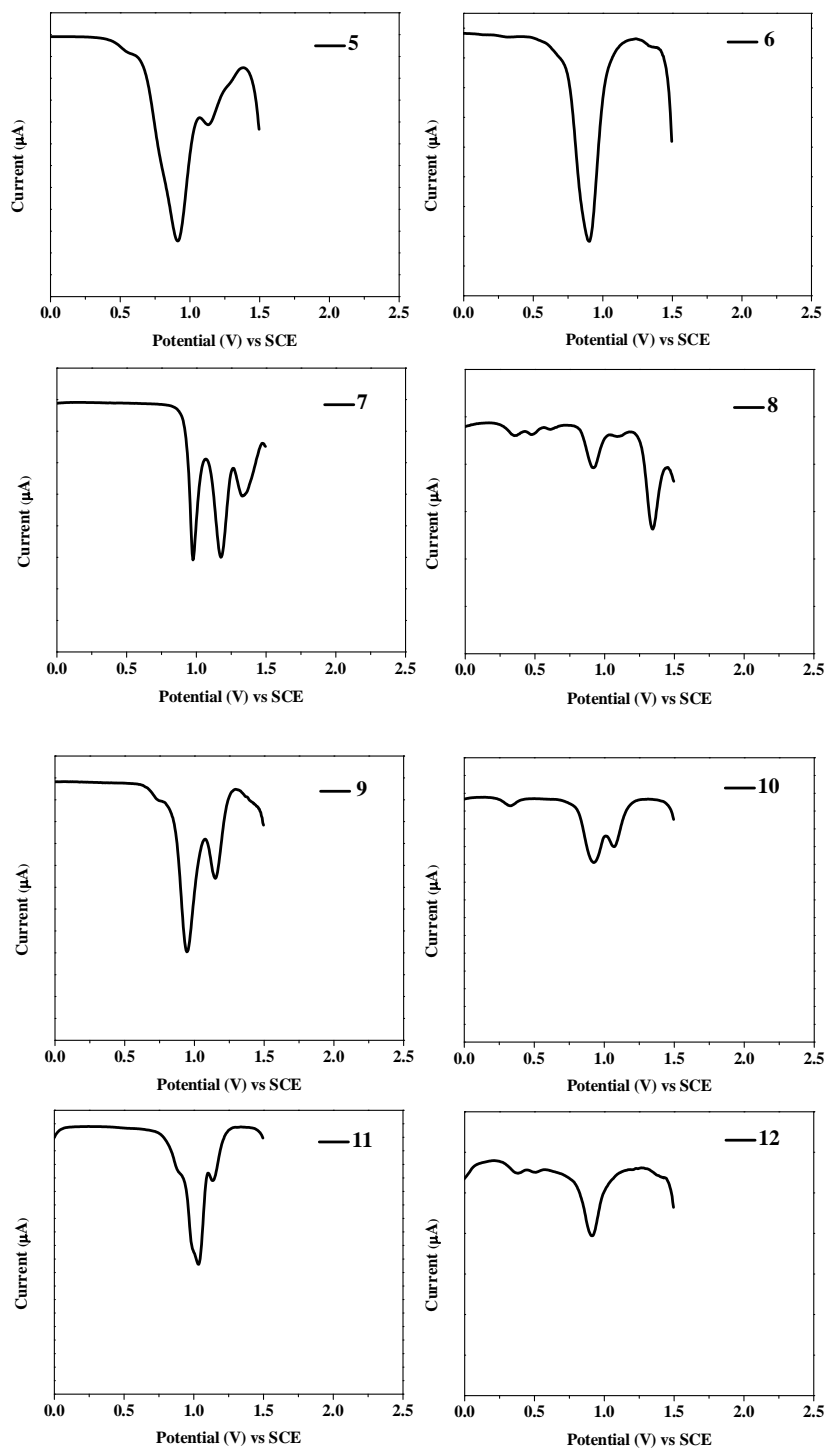
**Figure 6.7.** Simulated UV-visible optical absorption spectra of BTD **7** at the TDDFT/CAM-B3LYP/6-31G\*\* level for C, N, H, and S in dichloromethane.

## 6.5. Electrochemical properties

The electrochemical properties of the BTDs **5–12** were explored by the cyclic voltammetry (CV) and differential pulse voltammetry (DPV). All the measurements were performed in dry dichloromethane (DCM) solution at room temperature using tetrabutylammonium hexafluorophosphate (TBAPF<sub>6</sub>) as a supporting electrolyte. The electrochemical data and cyclic voltammetric HOMO–LUMO gap values are listed in Table 6.2, and the cyclic voltammograms are shown in Figure 6.8.<sup>[10a]</sup> BTDs **5–12** show irreversible oxidation waves attributed to the donor aryl groups in the region 0.84 to 1.34 V. The BTDs **5** and **6** exhibit one reversible reduction wave corresponding to the benzothiadiazole acceptor unit at –1.32 V and –1.41 V respectively.<sup>[11a]</sup> The BTDs **7, 9** and **11** exhibit three reversible reduction waves in the region of –0.15 V to –1.03 V. The first and second reduction waves are attributed to the successive one-electron reductions of the dicyanovinyl (DCV) groups of the TCBD unit in BTDs **7** and **9**.<sup>[21]</sup> BTD **11** undergoes simultaneous electrochemical reduction of the two TCBD groups and exhibits the reduction waves at –0.15 and –0.30 V. The third reduction wave in BTDs **7, 9** and **11** in the region of –0.96 V to –1.03 V is assigned to the benzothiadiazole unit.<sup>[11c]</sup> BTDs **8** and **10** exhibit three reversible reduction wave in the region of –0.21 V to –0.99 V corresponding to the electrochemical reduction of the DCNQ and the benzothiadiazole acceptor unit, whereas BTD **12** exhibit multiple reversible reduction wave in the region of –0.12 to –1.06 V due to the two DCNQ unit and the benzothiadiazole unit.<sup>[9b]</sup> The comparison of first reduction potential of BTDs **5–12** reflects that the DCNQ linked BTDs **8, 10** and **12** were easier to reduce than TCBD linked BTDs **7, 9** and **11**, which can be attributed to the strong electron accepting nature of the DCNQ unit.<sup>[22]</sup> The presence of TCBD and DCNQ linkage facilitates the reduction of BTDs **7–12** compared to acetylene linked BTDs **5** and **6**. The electrochemical and optical HOMO–LUMO gaps are in good agreement and exhibit the same trend.



**Figure. 6.8.** Cyclic voltammograms of benzothiadiazoles **5** and **7** at 0.01 M concentration in 0.1 M TBAPF<sub>6</sub> in dichloromethane recorded at a scan rate of 100 mV s<sup>-1</sup>.



**Figure 6.9.** Differential pulse voltammogram of benzothiadiazoles **5–12** at 0.01 M concentration in 0.1 M TBAPF<sub>6</sub> in dichloromethane (representing the oxidation waves).

**Table 6.2.** Electrochemical data of benzothiadiazoles **5–12**.

Compound	Electrochemical data <sup>a</sup>		
	E <sub>ox</sub> (V)	E <sub>red</sub> (V)	HOMO-LUMO Gap (eV) <sup>b</sup>
<b>Ferrocene</b>	0.38	-	
<b>5</b>	0.91 <sup>c</sup> 1.13 <sup>c</sup>	-1.32	2.24
<b>6</b>	0.84	-1.41	
<b>7</b>	0.97 <sup>c</sup> 1.18 <sup>c</sup>	-0.36 -0.83	2.22 1.72
<b>8</b>	0.92 <sup>c</sup> 1.34 <sup>c</sup>	-1.03 -0.21 -0.35	1.37
<b>9</b>	0.94 <sup>c</sup> 1.15 <sup>c</sup>	-0.43 -0.81 -1.02	1.70
<b>10</b>	0.92 <sup>c</sup> 1.07 <sup>c</sup>	-0.22 -0.36 -0.99	1.35
<b>11</b>	1.04 <sup>c</sup>	-0.15 -0.30 -0.96	1.58
<b>12</b>	0.91 <sup>c</sup>	-0.12 -0.22 -0.35 -0.45 -1.06	1.30

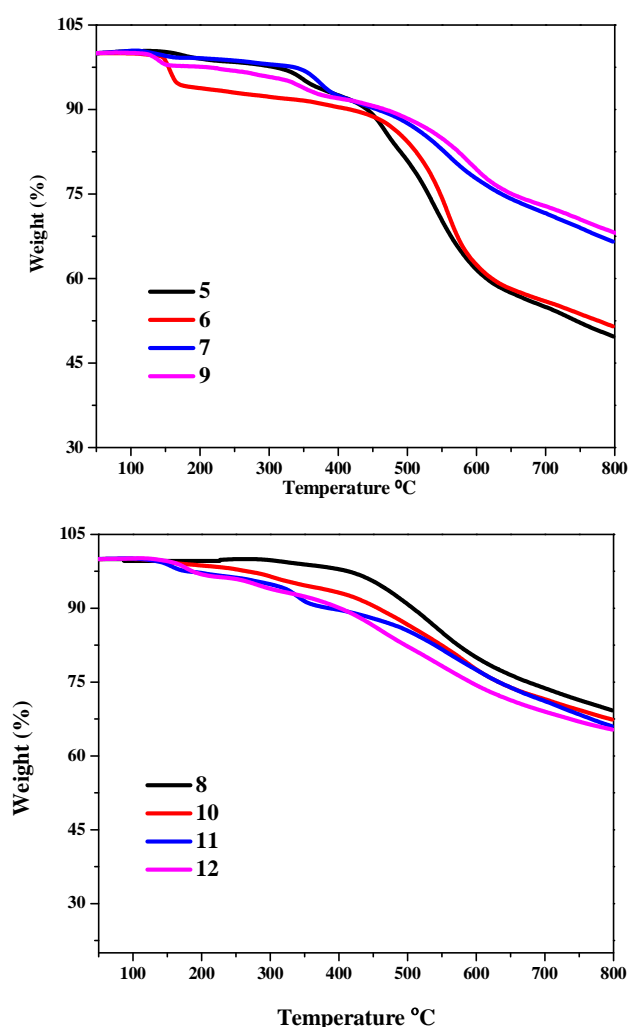
<sup>a</sup> recorded by cyclic voltammetry in 0.1 M solution of TBAPF<sub>6</sub> in DCM at 100 mV s<sup>-1</sup> scan rate versus SCE electrode, <sup>b</sup> electrochemical HOMO–LUMO gap; <sup>c</sup> assigned by differential pulse voltammetry.

## 6.6. Thermal stability

Thermal stability is significant for practical applications of organic chromophores. In order to have an elementary idea about the thermal stability of BTDs **5–12** thermogravimetric analysis (TGA) were carried out at a heating rate of 10 °C min<sup>-1</sup>, under a nitrogen atmosphere (Figure 6.10.) and the decomposition temperatures (T<sub>d</sub>) for 5% weight loss are listed in Table 6.1. The BTD **6**, **9** and **10** exhibit T<sub>d</sub> values at 165 °C, 331 °C and 343 °C whereas BTDs **5**, **7** and **8** exhibit T<sub>d</sub> values at 352 °C, 373 °C and 458 °C respectively. The BTDs **11** and **12** with two TCBD and DCNQ units exhibit the T<sub>d</sub> values above 298 °C and 275 °C

respectively. The trend in thermal stability follows the order  $8 > 7 > 5 > 10 > 9 > 11 > 12 > 6$ . This indicates the following: (a) The carbazole substituted BTDs **5**, **7** and **8** exhibit better thermal stability compared to their respective analogous triphenylamine substituted BTDs **6**, **9** and **10**. This may be due to the reduced conformational flexibility by the planar carbazole unit.<sup>[23]</sup> (b) The BTDs **7–10** with one TCBD or DCNQ unit were thermally more stable compared to BTDs **11** and **12** with two TCBD and DCNQ units.

The thermal stability results and observed trend may be useful to improve the thermal stability of such type of D–A systems.



**Figure 6.10.** TGA plots of BTDs **5–12** at a heating rate of  $10\text{ }^{\circ}\text{C min}^{-1}$ , under nitrogen atmosphere.

## 6.7. Experimental section

$^1\text{H}$  NMR spectra were recorded using a 400 MHz spectrometer. The NMR spectra were recorded at room temperature (298 K). Chemical shifts are reported in delta ( $\delta$ ) units, expressed in parts per million (ppm) downfield from tetramethylsilane using residual protonated solvent as an internal standard  $\{\text{CDCl}_3, 7.26 \text{ ppm}; (\text{CD}_3)_2\text{CO}, 2.05 \text{ ppm}\}$ .  $^{13}\text{C}$  NMR spectra were recorded using a 100 MHz spectrometer. Chemical shifts are reported in delta ( $\delta$ ) units, expressed in parts per million (ppm) downfield from tetramethylsilane using the solvent as internal standard  $\{\text{CDCl}_3, 77.0 \text{ ppm}; (\text{CD}_3)_2\text{CO}, 29.8 \text{ ppm}\}$ . The  $^1\text{H}$  NMR splitting patterns have been described as “s, singlet; d, doublet; and m, multiplet”. UV/Visible absorption spectra of all compounds were recorded in DCM. The density functional theory (DFT) and calculation were carried out at the B3LYP/6-31G\*\* level and for C, N, S, H and Time-dependent DFT calculation was performed on BTD **7** at CAM-B3LYP/6-31G\*\* level for C, N, H, and S in dichloromethane in the Gaussian 09 program. Cyclic voltammograms and differential pulse voltammograms were recorded on electrochemical analyzer using Glassy carbon as working electrode, Pt wire as the counter electrode, and Saturated Calomel Electrode (SCE) as the reference electrode. The scan rate was  $100 \text{ mVs}^{-1}$  for CV. A solution of tetrabutylammonium hexafluorophosphate ( $\text{TBAPF}_6$ ) in DCM (0.1 M) was employed as the supporting electrolyte. DCM was freshly distilled from  $\text{CaH}_2$  prior to use. All potentials were experimentally referenced against the saturated calomel electrode couple. Under our conditions, the  $\text{Fc}/\text{Fc}^+$  couple exhibited  $E^\circ = 0.38 \text{ V}$  versus SCE. HRMS was recorded on TOF-Q mass spectrometer. All microwave reactions were performed on CEM discover microwave instrument (Model No.–908,010). The method used to measure the reaction temperature during microwave heating is external sensor type.

**Preparation of BTDs **3** and **4** by Sonogashira coupling reaction:** To a stirred solution of 4-ethynyltriphenylamine (3.7 mmol), and dibromo-BTD **2** (3.7 mmol) in THF, and TEA (1:1, v/v) were added  $[\text{PdCl}_2(\text{PPh}_3)_2]$  (100 mg, 0.14 mmol), and CuI (20 mg, 0.1 mmol) under an argon flow at room temperature. The reaction



mixture was stirred for 12 h at 70 °C, and then cooled to room temperature. The solvent was then evaporated under reduced pressure, and the mixture was purified by SiO<sub>2</sub> chromatography with DCM/hexane (2:3, v/v) to obtain compound **3** as orange solid (0.89 g; Yield 50 %). Further elution with DCM/hexane (3:2) gave compound **4** as deep red solid (0.74 g; Yield 30 %). The <sup>1</sup>H NMR and <sup>13</sup>C NMR data were consistent with earlier reports.<sup>[14]</sup>

**Preparation of BTDs 5:** Carbazole **14** (0.67 g, 4.0 mmol), bromo-BTD **3** (1.45 g, 3.0 mmol), anhydrous potassium carbonate (1.66 g, 12.0 mmol), cupric sulfate (91 mg, 0.63 mmol), and 1,2-dichlorobenzene (10 mL) were added to a round bottom flask, degassed, and flushed with N<sub>2</sub>. The reaction mixture was heated at 180 °C for 2 days, and then cooled to room temperature. After that dichloromethane and water were added. The organic phase was washed with water and then dried over Na<sub>2</sub>SO<sub>4</sub>. After removal of the solvent, the residue was purified by SiO<sub>2</sub> column chromatography, using DCM:hexane (1:1) mixture as eluent to afford compound **5**. Orange solid (685 mg, Yield: 40 %). (SiO<sub>2</sub>, hexane–DCM, 1 : 1). Mp 220.5–221.5 °C. <sup>1</sup>H NMR (400 MHz, ((CD<sub>3</sub>)<sub>2</sub>CO,  $\delta$  in ppm) 8.26–8.24 (m, 2H), 8.13 (d, 1H,  $J$  = 7.5 Hz), 8.02 (d, 1H,  $J$  = 7.5 Hz), 7.58 (d, 2H,  $J$  = 8.8 Hz), 7.41–7.28 (m, 10H), 7.18–7.14 (m, 6H), 7.06–7.03 (m, 2H). <sup>13</sup>C NMR (100 MHz, CDCl<sub>3</sub>,  $\delta$  in ppm) 156.0, 151.2, 148.7, 147.0, 141.0, 133.0, 132.1, 129.7, 129.5, 127.7, 126.0, 125.2, 124.0, 123.9, 121.8, 120.6, 120.4, 117.2, 114.8, 110.4, 97.7, 84.4. HRMS (ESI-TOF, positive):  $m/z$  [M + Na]<sup>+</sup> calcd for C<sub>38</sub>H<sub>24</sub>N<sub>4</sub>SN<sub>a</sub>, 591.1614, found 591.1615. UV/Vis (DCM)  $\lambda_{\text{max}}$  ( $\epsilon$  [M<sup>-1</sup>cm<sup>-1</sup>]) 320 (78087), 464 (40765).

**Preparation of BTD 6:** To a stirred mixture of triphenylamine-4-boronic acid **15** (1.45 g, 5.0 mmol), bromo-BTD **3** (2.41 g, 5.0 mmol), Toluene (5 ml), THF (5 ml) and H<sub>2</sub>O (1 ml) were added [Pd(PPh<sub>3</sub>)<sub>4</sub>] (0.075 g, 0.75 mmol), Na<sub>2</sub>CO<sub>3</sub> (0.73 g, 5 mmol). The reaction mixture was heated at reflux for 24 h and then water was added to quench the reaction. The product was extracted with diethyl ether. The organic layer was collected, dried over anhydrous Na<sub>2</sub>SO<sub>4</sub> and evaporated under vacuum. The solid was adsorbed on silica gel and purified by column chromatography, using DCM:hexane (1:1) mixture as eluent to afforded

compound **6**. Red solid (2.1 g, Yield: 65 %). Mp 153.0–154.0 °C. <sup>1</sup>H NMR (400 MHz, (CDCl<sub>3</sub>, δ in ppm) 7.90–7.86 (m, 2H), 7.83 (d, 1H, *J* = 7.3, H), 7.67 (d, 1H, *J* = 7.3, H), 7.53–7.50 (m, 2H), 7.32–7.27 (m, 8H), 7.22–7.17 (m, 6H), 7.15–7.12 (m, 4H), 7.10–7.02 (m, 6H). <sup>13</sup>C NMR (100 MHz, CDCl<sub>3</sub>, δ in ppm) 155.4, 153.2, 148.4, 148.3, 147.3, 147.1, 133.6, 132.9, 132.6, 130.4, 129.9, 129.41, 129.36, 126.7, 125.1, 125.0, 123.7, 123.4, 122.7, 122.0, 115.5, 115.4, 96.4, 85.0. HRMS (ESI-TOF, positive): *m/z* [M + H]<sup>+</sup> calcd for C<sub>44</sub>H<sub>31</sub>N<sub>4</sub>S 647.2264, found 647.2262. UV/Vis (DCM) λ<sub>max</sub> (ε [M<sup>-1</sup>cm<sup>-1</sup>]) 323 (77978), 473 (55191).

**General procedure for the preparation of BTDs 7 and 9:** TCNE (39.0 mg, 0.30 mmol) was added to a solution of compound **5/6** (0.30 mmol) in DCM (50 mL). The mixture was refluxed at 40 °C for 8 h. The solvent was removed in vacuo, and the product was purified by SiO<sub>2</sub> column chromatography with DCM as the eluent to yield **7/9** as a dark colored solid.

**BTd 7:** Black solid (0.16 mg, Yield: 75 %). Mp 184.0–185.0 °C. <sup>1</sup>H NMR (400 MHz, (CDCl<sub>3</sub>, δ in ppm) 8.30 (d, 1H, *J* = 7.8 Hz), 8.18–8.16 (m, 2H), 8.02 (d, 1H, *J* = 7.8 Hz), 7.77–7.74 (m, 2H), 7.44–7.36 (m, 8H), 7.30–7.28 (m, 3H), 7.24–7.21 (m, 5H), 6.70–6.93 (m, 2H). <sup>13</sup>C NMR (100 MHz, CDCl<sub>3</sub>, δ in ppm) 164.0, 163.7, 153.7, 152.7, 150.8, 144.6, 140.2, 136.0, 133.4, 132.3, 130.1, 126.9, 126.6, 126.3, 125.6, 124.7, 123.3, 122.2, 121.8, 120.6, 118.1, 113.6, 113.0, 111.8, 111.0, 110.9, 91.9, 79.6. HRMS (ESI-TOF, positive): *m/z* [M + Na]<sup>+</sup> calcd for C<sub>44</sub>H<sub>24</sub>N<sub>8</sub>SNa 719.1731, found 719.1737. UV/Vis (DCM) λ<sub>max</sub> (ε [M<sup>-1</sup>cm<sup>-1</sup>]) 287 (68633), 466 (48688), 518 (sh).

**BTd 9:** Black solid (0.19 g, Yield: 80 %). Mp 171.0–173.0 °C. <sup>1</sup>H NMR (400 MHz, (CDCl<sub>3</sub>, δ in ppm) 8.15 (d, 1H, *J* = 7.8 Hz), 7.96–7.92 (m, 2H), 7.81 (d, 1H, *J* = 7.8 Hz), 7.70–7.66 (m, 2H), 7.39–7.31 (m, 8H), 7.26–7.11 (m, 14H), 6.91–6.87 (m, 2H). <sup>13</sup>C NMR (100 MHz, CDCl<sub>3</sub>, δ in ppm) 164.5, 164.4, 153.4, 153.3, 152.1, 149.8, 146.8, 144.7, 140.2, 133.5, 132.2, 130.7, 130.0, 129.55, 128.1, 126.9, 126.4, 125.7, 125.4, 124.3, 122.4, 122.3, 121.4, 118.0, 113.7, 113.0, 112.1, 111.3, 90.1, 79.7. HRMS (ESI-TOF, positive): *m/z* [M + Na]<sup>+</sup> calcd for

C<sub>50</sub>H<sub>30</sub>N<sub>8</sub>SNa 797.2206, found 797.2204; UV/Vis (DCM)  $\lambda_{\text{max}}$  ( $\epsilon$  [M<sup>-1</sup>cm<sup>-1</sup>]) 298 (46557), 454 (33497), 560 (33700).

**Preparation of BTD 11.** TCNE (77 mg, 0.60 mmol) was added to a solution of compound **4** (0.30 mmol) in DCM (50 mL) at room temperature. The mixture was refluxed at 40 °C for 16 h. The solvent was removed in vacuo, and the product was purified by SiO<sub>2</sub> chromatography with DCM as the eluent to yield compound **11** as a dark colored solid. Black solid (0.24 g, Yield: 85 %). Mp >300 °C; <sup>1</sup>H NMR (400 MHz, (CDCl<sub>3</sub>,  $\delta$  in ppm) 8.07 (s, 2H), 7.64–7.60 (m, 4H), 7.40–7.35 (m, 8H), 7.27–7.26 (m, 1H), 7.25–7.23 (m, 3H), 7.18–7.16 (m, 8H), 6.88–6.86 (m, 4H). <sup>13</sup>C NMR (100 MHz, CDCl<sub>3</sub>,  $\delta$  in ppm) 162.6, 162.0, 154.0, 151.0, 144.3, 131.9, 131.0, 130.1, 129.2, 126.9, 126.8, 120.6, 118.1, 113.4, 113.3, 111.0, 110.4, 94.6, 79.5. HRMS (ESI-TOF, positive):  $m/z$  [M + Na]<sup>+</sup> calcd for C<sub>58</sub>H<sub>30</sub>N<sub>12</sub>SNa 949.2329, found 949.2327. UV/Vis (DCM)  $\lambda_{\text{max}}$  ( $\epsilon$  [M<sup>-1</sup>cm<sup>-1</sup>]) 276 (56010), 377 (49125), 490 (60218).

**General procedure for the preparation of BTDs 8 and 10.** TCNQ (61 mg, 0.30 mmol) was added to a solution of **5/6** (0.30 mmol) in 1,2-dichloroethane (DCE) (4 mL) in a microwave tube. The mixture was reacted under microwave condition at 100 °C for 10 h. The solvent was removed in vacuo, and the product was purified by SiO<sub>2</sub> chromatography with DCM:ethylacetate (9:1) as the eluent to yield compound **8/10** as a dark colored solid.

**BTD 8:** Black solid (0.16 g, Yield: 70 %). Mp 208.5–209.5 °C. <sup>1</sup>H NMR (400 MHz, (CDCl<sub>3</sub>,  $\delta$  in ppm) 8.17–8.15 (m, 2H), 8.04 (d, 1H,  $J$  = 7.5 Hz), 7.92 (d, 1H,  $J$  = 7.5 Hz), 7.51–7.48 (m, 1H), 7.42–7.27 (m, 12H), 7.23–7.13 (m, 9H), 6.94–6.90 (m, 2H); <sup>13</sup>C NMR (100 MHz, CDCl<sub>3</sub>,  $\delta$  in ppm) 167.4, 154.9, 152.9, 151.6, 150.8, 145.3, 140.3, 135.7, 134.9, 134.7, 134.4, 132.4, 129.9, 126.8, 126.62, 126.56, 126.52, 126.2, 126.0, 125.9, 125.7, 124.6, 121.6, 120.6, 119.1, 114.03, 114.01, 112.6, 112.0, 110.6, 91.7, 75.2. HRMS (ESI-TOF, positive):  $m/z$  [M + Na]<sup>+</sup> calcd for C<sub>50</sub>H<sub>28</sub>N<sub>8</sub>SNa 795.2050, found 795.2047. UV/Vis (DCM)  $\lambda_{\text{max}}$  ( $\epsilon$  [M<sup>-1</sup>cm<sup>-1</sup>]) 303 (81366), 484 (57868), 665 (51092).

**BTD 10:** Black solid (0.17 g, Yield: 65 %). Mp 200.5–201.5 °C; <sup>1</sup>H NMR (400 MHz, (CDCl<sub>3</sub>,  $\delta$  in ppm) 7.93–7.90 (m, 3H), 7.74 (d, 1H,  $J$  = 7.8 Hz), 7.48–7.45

(m, 1H), 7.36–7.29 (m, 9H), 7.23–7.10 (m, 18H), 6.91–6.87 (m, 2H).  $^{13}\text{C}$  NMR (100 MHz,  $\text{CDCl}_3$ ,  $\delta$  in ppm) 168.2, 153.9, 153.2, 152.3, 151.5, 151.3, 149.6, 146.8, 145.3, 139.0, 135.9, 134.6, 133.9, 132.7, 130.5, 129.9, 129.5, 128.3, 127.3, 126.5, 125.9, 125.8, 125.7, 125.5, 125.3, 124.2, 121.6, 119.0, 114.2, 114.1, 112.9, 112.3, 90.4, 74.6. HRMS (ESI-TOF, positive)  $m/z$   $[\text{M} + \text{H}]^+$  calcd for  $\text{C}_{56}\text{H}_{35}\text{N}_8\text{S}$  851.2700, found 851.2701. UV/Vis (DCM)  $\lambda_{\text{max}}$  ( $\epsilon$  [ $\text{M}^{-1}\text{cm}^{-1}$ ]) 288 (87541), 491 (56994), 683 (56612).

**Preparation of BTD 12.** TCNQ (123 mg, 0.60 mmol) was added to a solution of **4** (0.30 mmol) in 1,2-dichloroethane (DCE) (4 mL) in a microwave tube. The mixture was reacted under microwave condition at 100 °C for 20 h. The solvent was removed in vacuo, and the product was purified by  $\text{SiO}_2$  chromatography with DCM:ethylacetate (9:1) as the eluent to yield compound **12** as a dark colored solid. Black solid (0.16 g, Yield: 50 %). Mp 204.0–205.0 °C;  $^1\text{H}$  NMR (400 MHz,  $(\text{CD}_3)_2\text{CO}$ ,  $\delta$  in ppm) 8.45 (s, 2H), 8.01–7.98 (m, 2H), 7.58–7.56 (m, 2H), 7.41–7.28 (m, 16H), 7.22–7.18 (m, 4H), 7.10–7.08 (m, 8H), 6.79 (d, 4H,  $J$  = 8.8 Hz).  $^{13}\text{C}$  NMR (100 MHz,  $(\text{CD}_3)_2\text{CO}$ ,  $\delta$  in ppm) 166.7, 154.9, 152.3, 152.1, 151.6, 146.5, 137.3, 137.2, 136.2, 134.9, 132.7, 132.4, 130.7, 127.2, 126.7, 126.4, 126.0, 119.7, 114.8, 113.4, 113.1, 94.7, 74.9. HRMS (ESI-TOF, positive):  $m/z$   $[\text{M} + \text{Na}]^+$  calcd for  $\text{C}_{70}\text{H}_{38}\text{N}_{12}\text{SNa}$  1101.2955, found 1101.2957. UV/Vis (DCM)  $\lambda_{\text{max}}$  ( $\epsilon$  [ $\text{M}^{-1}\text{cm}^{-1}$ ]) 293 (60054), 401 (60163), 637 (51366).

## 6.8. Conclusion

In summary a series of symmetrical and unsymmetrical donor-substituted benzothiadiazoles were synthesized. The number and nature of acceptor units perturbs the photonic properties, HOMO–LUMO gap and thermal stability of the benzothiadiazoles. The electronic absorption and computational calculation indicate substantial lowering of the HOMO–LUMO gap by the incorporation of cyano-based dicyanoquinodimethane (DCNQ) and tetracyanobutadiene (TCBD) groups in the benzothiadiazoles. The TCBD and DCNQ linkage of donor-substituted benzothiadiazole facilitates the reduction of the acceptor BTD unit and results in non-emissive nature of these molecular systems which confirms the

strong donor–acceptor interaction. The thermal stability of the benzothiadiazoles can be enhanced by the incorporation of planar carbazole donor. The presence of single TCBD or DCNQ improves the thermal stability. The results obtained in this study will be useful for design and synthesis of materials with low HOMO–LUMO gap and improved thermal stability for various optoelectronic applications. These low HOMO–LUMO gap molecular systems are potential candidate for organic photovoltaics. The study towards organic photovoltaic applications of these BTDs are currently ongoing in our laboratory.

## 6.9. References

- [1] (a) He G. S., Tan L.-S., Zheng Q., Prasad P. N. (2008), Multiphoton absorbing materials: molecular designs, characterizations, and applications *Chem. Rev.*, 108, 1245-1330 (DOI: 10.1021/cr050054x). (b) Liangwab M., Chen J. (2013), Arylamine organic dyes for dye-sensitized solar cells, *Chem. Soc. Rev.*, 42, 3453-3488 (DOI: 10.1039/C3CS35372A). (c) Mishra A., Fischer M. K. R., Bauerle P. (2009), Metal-free organic dyes for dye-sensitized solar cells: from structure: property relationships to design rules, *Angew. Chem., Int. Ed.*, 48, 2474-2499 (DOI: 10.1002/anie.200804709). (d) Neto B. A. D., Lapis A. A. M., Júnior E. N., da S., Dupont J. (2013), 2,1,3-Benzothiadiazole and derivatives: synthesis, properties, reactions, and applications in light technology of small molecules, *Eur. J. Org. Chem.*, 228-255 (DOI: 10.1002/ejoc.201201161). (e) Thomas K. R. J., Lin J. T., Velusamy M., Tao Y. T., Chuen C. H. (2004), Color tuning in benzo[1,2,5]thiadiazole-based small molecules by amino conjugation/deconjugation: bright red-light-emitting diodes, *Adv. Funct. Mater.*, 14, 83-90 (DOI: 10.1002/adfm.200304486). (f) Kato S., Matsumoto T., Ishi-i T., Thiemann T., Shigeiwa M., Gorohmaru H., Maeda S., Yamashitad Y. and Mataka S. (2004), Strongly red-fluorescent novel donor– $\pi$ -bridge–acceptor– $\pi$ -bridge–donor (D– $\pi$ –A– $\pi$ –D) type 2,1,3-benzothiadiazoles with enhanced two-photon absorption cross-sections, *Chem. Commun.*, 2342-2343 (DOI: 10.1039/B410016F). (g) Zhang M.,

- Tsao H. N., Pisula W., Yang C., Mishra A. K., Müllen K. (2007), Field-effect transistors based on a benzothiadiazole–cyclopentadithiophene copolymer, *J. Am. Chem. Soc.*, 129, 3472–3473 (DOI: 10.1021/ja0683537). (h) Sonar P., Singh S. P., Li Y., Soh M. S., Dodabalapur A. (2010), A Low-bandgap diketopyrrolopyrrole-benzothiadiazole-based copolymer for high-mobility ambipolar organic thin-film transistors, *Adv. Mater.*, 22, 5409–5413 (DOI: 10.1002/adma.201002973). (i) Zhang W.-S., Wang D., Cao H., Yang H. (2014), Energy level tunable pre-click functionalization of [60]fullerene for nonlinear optics” *Tetrahedron*, 70, 573-577 (DOI: 10.1016/j.tet.2013.12.018). (j) Wang J. -L., Tang Z. -M., Xiao Q., Ma Y., Pei J. (2009), Star-shaped D- $\pi$ -A conjugated molecules: synthesis and broad absorption bands, *Org. Lett.*, 11, 863-866 (DOI: 10.1021/ol802845w). (k) Poander L. E., Pandey L., Barlow S., Tiwari P., Risko C., Kippelen B., Bredas J. L., Marder S. R. (2011), Benzothiadiazole-dithienopyrrole donor–acceptor–donor and acceptor–donor–acceptor triads: synthesis and optical, electrochemical, and charge-transport properties, *J. Phys. Chem. C*, 115, 23149-23163 (DOI: 10.1021/jp208643k). (l) Omer K. M., Ku S. Y., Wong K. T., Bard A. J. (2009), Green electrogenerated chemiluminescence of highly fluorescent benzothiadiazole and fluorene derivatives, *J. Am. Chem. Soc.*, 131, 10733-10741 (DOI: 10.1021/ja904135y).
- [2] (a) Zhang Q. T., Tour J. M. (1998), Alternating donor/acceptor repeat units in polythiophenes. Intramolecular charge transfer for reducing band gaps in fully substituted conjugated polymers, *J. Am. Chem. Soc.*, 120, 5355-5362 (DOI: 10.1021/ja972373e). (b) Gohier F., Frère P., Roncali J. (2013), 3-Fluoro-4-hexylthiophene as a building block for tuning the electronic properties of conjugated polythiophenes, *J. Org. Chem.*, 78, 1497-1503 (DOI: 10.1021/jo302571u).

- [3] (a) Štefko M., Tzirakis M. D., B. Breiten, M.-O. Ebert, O. Dumele, Schweizer W. B., Gisselbrecht J.-P., Boudon C., Beels M. T., Biaggio I., Diederich F. (2013), Donor–acceptor (D–A)-substituted polyyne chromophores: modulation of their optoelectronic properties by varying the length of the acetylene spacer, *Chem. –Eur. J.*, 19, 12693–12704 (DOI: 10.1002/chem.201301642). (b) van Mullekom H. A. M., Vekemans J. A. J. M., Meijer E. W. (1998), Band-gap engineering of donor–acceptor-substituted  $\pi$ -conjugated polymers, *Chem. –Eur. J.*, 4, 1235–1243 (DOI: 10.1002/(SICI)1521-3765(19980710)4:7<1235::AID-CHEM1235>3.0.CO;2-4). (c) Wang J.-L., Xiao Q., Pei J. (2010), Benzothiadiazole-based D– $\pi$ -A– $\pi$ -D organic dyes with tunable band gap: synthesis and photophysical properties, *Org. Lett.*, 12, 4164–4167 (DOI: 10.1021/ol101754q). (d) Bures F., Schweizer W. B., May J. C., Boudon C., Gisselbrecht J. -P., Gross M., Biaggio I., Diederich F. (2007), Property tuning in charge-transfer chromophores by systematic modulation of the spacer between donor and acceptor, *Chem.–Eur. J.*, 13, 5378–5387 (DOI: 10.1002/chem.200601735). (e) Moonen N. N. P., Pomerantz W. C., Gist R., Boudon C., Gisselbrecht J.-P., Kawai T., Kishioka A., Gross M., Irie M., Diederich F. (2005), Donor-substituted cyanoethynylethenes:  $\pi$ -conjugation and band-gap tuning in strong charge-transfer chromophores, *Chem. –Eur. J.*, 11, 3325–3341 (DOI: 10.1002/chem.200500082).
- [4] (a) Lin L.-Y., Chen Y.-H., Huang Z.-Y., Lin H.-W., Chou S.-H., Lin F., Chen C.-W., Liu Y.-H., Wong K.-T. (2011), A low-energy-gap organic dye for high-performance small-molecule organic solar cells, *J. Am. Chem. Soc.*, 133, 15822–15825 (DOI: 10.1021/ja205126t). (b) Wang J.-L., Tang Z.-M., Xiao Q., Ma Y., Pei J. (2010), Benzothiadiazole-based D– $\pi$ -A– $\pi$ -D organic dyes with tunable band gap: synthesis and photophysical properties, *Org. Lett.*, 10, 4271–4274 (DOI: 10.1021/ol101754q). (c) Dou L., Gao J., Richard E., You J., Chen C. -C., Cha K. C., He Y., Li G., Yang, Y. (2012), Systematic investigation of benzodithiophene- and

- diketopyrrolopyrrole-based low-bandgap polymers designed for single junction and tandem polymer solar cells, *J. Am. Chem. Soc.*, 134, 10071-10079 (DOI: 10.1021/ja301460s). (d) Sonar P., Ng G. -M., Lin G. T. T., Dodabalapur A., Chen Z.-K. (2010), Solution processable low bandgap diketopyrrolopyrrole (DPP) based derivatives: novel acceptors for organic solar cells, *J. Mater. Chem.*, 2010, 20, 3626-3636 (DOI: 10.1039/B924404B). (e) Blouin N., Michaud A., Leclerc M. (2007), A low-bandgap poly(2,7-Carbazole) derivative for use in high-performance solar cells *Adv. Mater.*, 19, 2295-2300 (10.1002/adma.200602496).
- [5] (a) Jadhav T., Maragani R., Misra R., Sreeramulu V., Rao D. N., Mobin S. M. (2013), Design and synthesis of donor–acceptor pyrazabole derivatives for multiphoton absorption, *Dalton Trans.*, 42, 4340-4342 (10.1039/C3DT33065F). (b) Gautam P., Dhokale B., Mobin S. M., Misra R. (2012), Ferrocenyl BODIPYs: synthesis, structure and properties, *RSC Adv.*, 2012, 2, 12105-12107 (DOI: 10.1039/C2RA21964F). (c) Gautam P., Dhokale B., Shukla V., Singh C. P., Bindra K. S., Misra, R. (2012), Optical limiting performance of meso-tetraferrocenyl porphyrin and its metal derivatives, *J. Photochem. Photobiol., A*, 239, 24-27 (DOI: 10.1016/j.jphotochem.2012.04.020).
- [6] (a) Kivala M., Diederich F. (2009), Acetylene-derived strong organic acceptors for planar and nonplanar push–pull chromophores, *Acc. Chem. Res.*, 42, 235-248 (DOI: 10.1021/ar8001238). (b) Kato S., Diederich F. (2010), Non-planar push–pull chromophores, *Chem. Commun.*, 46, 1994-2006 (DOI: 10.1039/B926601A). (c) Kivala M., Stanoeva T., Michinobu T., Frank B., Gescheidt G., Diederich F. (2008), One-electron-reduced and -oxidized stages of donor-substituted 1,1,4,4-tetracyanobuta-1,3-dienes of different molecular architectures, *Chem.–Eur. J.*, 14, 7638-7647 (DOI: 10.1002/chem.200800716). (d) Michinobu T., May J. C., Lim J. H., Boudon C., Gisselbrecht J.-P., Seiler P., Gross M., Biaggio I., Diederich, F. (2005), A new class of organic donor–acceptor molecules with large



third-order optical nonlinearities, *Chem. Commun.*, 737-739 (DOI: 10.1039/B417393G); (e) Michinobu T., Boudon I., Gisselbrecht J.-P., Seiler P., Frank B., Moonen N. N. P., Gross M., Diederich F. (2006), Donor-substituted 1,1,4,4-tetracyanobutadienes (TCBDs): new chromophores with efficient intramolecular charge-transfer interactions by atom-economic synthesis, *Chem.-Eur. J.*, 12, 1889-1905 (DOI: 10.1002/chem.200501113). (f) Leliège A., Blanchard P., Rousseau T., Roncali J. (2011), Triphenylamine/Tetracyanobutadiene-based D-A-D  $\pi$ -conjugated systems as molecular donors for organic solar cells, *Org. Lett.*, 13, 3098-3101 (DOI: 10.1021/ol201002j). (g) Michinobu T., Satoh N., Cai J., Li Y., Han L. (2014), Novel design of organic donor-acceptor dyes without carboxylic acid anchoring groups for dye-sensitized solar cells, *J. Mater. Chem. C*, 2, 3367-3372 (DOI: 10.1039/C3TC32165G). (h) Esembeson B., Scimeca M. L., Michinobu T., Diederich F., Biaggio I. (2008), A high-optical quality supramolecular assembly for third-order integrated nonlinear optics, *Adv. Mater.*, 2008, 20, 4584-4587 (DOI: 10.1002/adma.200801552).

- [7] (a) Yamada M., Schweizer W. B., Schoenebeck F., Diederich F. (2010), Unprecedented thermal rearrangement of push-pull-chromophore-[60]fullerene conjugates: formation of chiral 1,2,9,12-tetrakis-adducts, *Chem. Commun.*, 46, 5334-5336 (DOI: 10.1039/C0CC00881H). (b) Jordan M., Kivala M., Boudon C., Gisselbrecht J.-P., Schweizer W. B., Seiler P., Diederich F. (2011), Switching the regioselectivity in cycloaddition-retro-electrocyclizations between donor-activated alkynes and the electron-accepting olefins TCNE and TCNQ, *Chem.-Asian J.*, 6, 396-401 (DOI: 10.1002/asia.201000539). (c) Kivala M., Boudon C., Gisselbrecht J.-P., Seiler P., Gross M., Diederich, F. (2007), A novel reaction of 7,7,8,8-tetracyanoquinodimethane (TCNQ): charge-transfer chromophores by [2 + 2] cycloaddition with alkynes, *Chem. Commun.* 2007, 4731-4733 (DOI: 10.1039/B713683H).

- [8] (a) Shoji T., Ito S., Okujima T., Morita N. (2012), Synthesis of push-pull chromophores by the sequential [2 + 2] cycloaddition of 1-azulenylbutadiynes with tetracyanoethylene and tetrathiafulvalene *Org. Biomol. Chem.*, 10, 8308-8313 (DOI: 10.1039/C2OB26028J). (b) Shoji T., Ito S., Toyota K., Iwamoto T., Yasunami M., Morita N. (2009), Reactions between 1-ethynylazulenes and 7,7,8,8-tetracyanoquinodimethane (TCNQ): preparation, properties, and redox behavior of novel azulene-substituted redox-active chromophores, *Eur. J. Org. Chem.*, 4316-4324 (DOI: 10.1002/ejoc.200900539).
- [9] (a) Chen S., Li Y., Yang W., Chen N., Liu H., Li Y. (2010), Synthesis and tuning optical nonlinear properties of molecular crystals of benzothiadiazole *J. Phys. Chem. C*, 114, 15109-15115 (DOI: 10.1021/jp103159b). (b) Chen S., Li Y., Liu C., Yang W., Li Y. (2011), Strong Charge-Transfer Chromophores from [2 + 2] Cycloadditions of TCNE and TCNQ to peripheral donor-substituted alkynes, *Eur. J. Org. Chem.*, 32, 6445-6451 (DOI: 10.1002/ejoc.201101009).
- [10] (a) Zhang H., Wan X., Xue X., Li Y., Yu A., Chen Y. (2010), Selective Tuning of the HOMO-LUMO gap of carbazole-based donor-acceptor-donor compounds toward different emission colors, *Eur. J. Org. Chem.*, 1681-1687 (DOI: 10.1002/ejoc.200901167). (b) Qian G., Dai B., Luo M., Yu D., Zhan J., Zhang Z., Ma D., Wang Z. Y. (2008), Band gap tunable, donor-acceptor-donor charge-transfer heteroquinoid-based chromophores: near infrared photoluminescence and electroluminescence *Chem. Mater.*, 20, 6208-6216 (DOI: 10.1021/cm801911n). (c) Zhou J., Xie S., Amond E. F., Becker M. L. (2013), Tuning energy levels of low bandgap semi-random two acceptor copolymers, *Macromolecules*, 46, 3391-3394 (DOI: 10.1021/ma400531v).
- [11] (a) Misra R., Gautam P., Sharma R., Mobin S. M. (2013), Donor- $\pi$ -acceptor- $\pi$ -donor ferrocenyl benzothiadiazoles: synthesis, structure, and properties, *Tetrahedron Lett.*, 54, 381-383 (DOI: 10.1016/j.tetlet.2012.11.011).

- 10.1016/j.tetlet.2012.11.016). (b) Misra R., Gautam P., Jadhav T., Mobin S. M. (2013), Donor–acceptor ferrocenyl-substituted benzothiadiazoles: synthesis, structure, and properties, *J. Org. Chem.*, 78, 4940–4948 (DOI: 10.1021/jo4005734). (c) Misra R., Gautam P., Mobin S. M. (2013), Aryl-substituted unsymmetrical benzothiadiazoles: synthesis, structure, and properties, *J. Org. Chem.*, 78, 12440-12452 (DOI: 10.1021/jo402111q).
- [12] (a) Roquet S., Cravino A., Leriche P., Aleveque O., Frere P., Roncali J. (2006), Triphenylamine–thienylenevinylene hybrid systems with internal charge transfer as donor materials for heterojunction solar cells, *J. Am. Chem. Soc.*, 128, 3459-3466 (DOI: 10.1021/ja058178e). (b) Xu W., Peng B., Chen J., Liang M., Cai, F. (2008), New triphenylamine-based dyes for dye-sensitized solar cells, *J. Phys. Chem. C*, 112, 874-880 (DOI: 10.1021/jp076992d). (c) Moonsin P., Prachumrak N., Namuangruk S., Jungsuttiwong S., Keawin T., Sudyoadsuk T., Promarak V. (2013), Novel bis(fluorenyl)benzothiadiazole-cored carbazole dendrimers as highly efficient solution-processed non-doped green emitters for organic light-emitting diodes, *Chem. Commun.*, 49, 6388-6390 (DOI: 10.1039/C3CC42931H).
- [13] Wang B., Tsang S., Zhang W., Tao Y., Wong M. S. (2011), Naphthodithiophene-2,1,3-benzothiadiazole copolymers for bulk heterojunction solar cells, *Chem. Commun.*, 47, 9471-9473 (DOI: 10.1039/C1CC13690A).
- [14] (a) Ma X. M., Hua J. L., Wu W. J., Tian H. (2008), A high-efficiency cyanine dye for dye-sensitized solar cells *Tetrahedron*, 64, 345-350 (DOI: 10.1016/j.tet.2007.10.094). (b) Kato S., Matsumoto T., Shigeiwa M., Gorohmaru H., Maeda S., Ishi-I T., Mataka S. (2006), Novel 2,1,3-benzothiadiazole-based red-fluorescent dyes with enhanced two-photon absorption cross-sections *Chem.–Eur. J.*, 12, 2303-2317 (DOI: 10.1002/chem.200500921).

- [15] Xie Y., Ding Y., Li X., Wang C., Hill J. P., Ariga K., Zhang W., Zhu W., (2012), Selective, sensitive and reversible “turn-on” fluorescent cyanide probes based on 2,2'-dipyridylaminoanthracene–Cu<sup>2+</sup> ensembles *Chem. Commun.*, 48, 11513-11515 (DOI: 10.1039/C2CC36140J).
- [16] Velusamy M., Thomas K. R. J., Lin J. T., Hsu Y.-C., Ho K.-C. (2005), Organic dyes incorporating low-band-gap chromophores for dye-sensitized solar cells, *Org. Lett.*, 7, 1899-1902 (DOI: 10.1021/ol050417f).
- [17] Reutenauer P., Kivala M., Jarowski P. D., Boudon C., Gisselbrecht J.-P., Gross M., Diederich, F. (2007), New strong organic acceptors by cycloaddition of TCNE and TCNQ to donor-substituted cyanoalkynes, *Chem. Commun.*, 4898-4900 (DOI: 10.1039/B714731G).
- [18] Yuan Y., Michinobu T., Ashizawa M., Mori T. (2011), Microwave-assisted TCNE/TCNQ addition to poly(thienyleneethynylene) derivative for construction of donor–acceptor chromophores, *J. Polym. Sci., Part A: Polym. Chem.*, 49, 1013-1020 (DOI: 10.1002/pola.24515).
- [19] (a) Xu E., Zhong H., Du J., Zeng D., Ren S., Sun J., Fang Q. (2009), The synthesis and properties of novel  $\pi$ -conjugated 2,1,3-benzothiadiazole oligomers, *Dyes Pigm.*, 80, 194-198 (DOI: 10.1016/j.dyepig.2008.07.008).  
 (b) Tao Y.-M., Li H.-Y., Xu Q.-L., Zhu Y.-C., Kang L.-C., Zheng Y.-X., Zuo J.-L., You X.-Z. (2011), Synthesis and characterization of efficient luminescent materials based on 2,1,3-benzothiadiazole with carbazole moieties, *Synth. Met.*, 161, 718-723 (DOI: 10.1016/j.synthmet.2011.01.020).
- [20] (a) Frisch M. J., Trucks G. W., Schlegel H. B., Scuseria G. E., Robb M. A., Cheeseman J. R., Scalmani G., Barone V., Mennucci B., Petersson G. A., Nakatsuji H., Caricato M., Li X., Hratchian H. P., Izmaylov A. F., Bloino J., Zheng G., Sonnenberg J. L., Hada M., Ehara M., Toyota K., Fukuda R., Hasegawa J., Ishida M., Nakajima, T., Honda, Y., Kitao O., Nakai H., Vreven T., Montgomery J. A. Jr., Peralta J. E., Ogliaro F., Bearpark M., Heyd J. J., Brothers E., Kudin K. N., Staroverov V. N.,

- Kobayashi R., Normand J., Raghavachari K., Rendell A., Burant J. C., Iyengar S. S., Tomasi J., Cossi M., Rega N., Millam N. J., Klene M., Knox J. E., Cross J. B., Bakken V., Adamo C., Jaramillo J., Gomperts R., Stratmann, R. E., Yazyev O., Austin A. J., Cammi R., Pomelli C., Ochterski J. W., Martin R. L., Morokuma K., Zakrzewski V. G., Voth G. A., Salvador P., Dannenberg J. J., Dapprich S., Daniels A. D., Farkas O., Foresman J. B., Ortiz J. V., Cioslowski J., Fox D. J. (2009), *Gaussian 09*, revision A.02; Gaussian, Inc.: Wallingford, CT, 2009. (b) Lee C., Yang W., Parr R. G. (1988), Development of the Colle-Salvetti correlation-energy formula into a functional of the electron density, *Phys. Rev. B*, 37, 785-789 (10.1103/PhysRevB.37.785). (c) Becke A. D. (1993), Density-functional thermochemistry. III. The role of exact exchange, *J. Chem. Phys.* 1993, 98, 1372-1377 (DOI: 10.1063/1.464913).
- [21] Kivala M., Boudon C., Gisselbrecht J. -P., Seiler P., Gross M., Diederich F. (2007), Charge-transfer chromophores by cycloaddition–retro-electrocyclization: multivalent systems and cascade reactions, *Angew. Chem., Int. Ed.*, 46, 6357-6360 (DOI: 10.1002/anie.200701733).
- [22] Shoji T., Maruyama M., Shimomura E., Maruyama A., Ito S., Okujima T., Toyota K., Morita N. (2013), Synthesis, properties, and redox behavior of tetracyanobutadiene and dicyanoquinodimethane chromophores bearing two azulenyl substituents, *J. Org. Chem.*, 78, 12513-12524 (DOI: 10.1021/jo402104n).
- [23] Niu H., Kang H., Cai J., Wang C., Bai X., Wang W. (2011), Novel soluble polyazomethines with pendant carbazole and triphenylamine derivatives: preparation, characterization, and optical, electrochemical and electrochromic properties, *Polym. Chem.*, 2, 2804-2817 (DOI: 10.1039/C1PY00237F).

## Chapter 7

### Reversible mechanochromism in unsymmetrical benzothiadiazoles

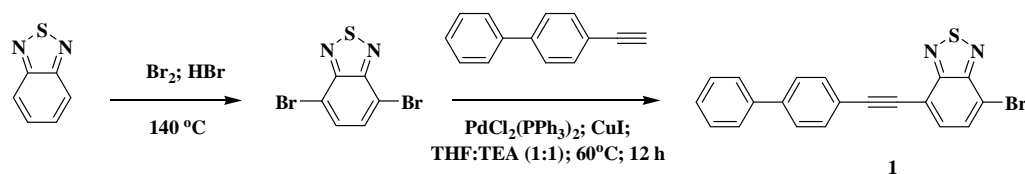
#### 7.1. Introduction

In recent years research on organic mechanochromic materials has gained momentum due to their applications in mechano-sensors, optical storage, rewritable media, and security ink.<sup>[1]</sup> Mechanochromic materials exhibit reversible solid-state emission in response to external stimuli such as grinding, pressing, fuming and annealing.<sup>[1a]</sup> The reversibility in solid-state emission is associated to the phase transitions between crystalline and amorphous state.<sup>[2]</sup> A variety of donor–acceptor organic molecular system have been explored for mechanochromism.<sup>[3]</sup> Recently we reported mechanochromism in tetraphenylethene substituted phenanthroimidazoles.<sup>[4]</sup>

2,1,3-Benzothiadiazole (BTD) is a strong acceptor owing to its high electron affinity.<sup>[5]</sup> Our group is involved in the design and synthesis of symmetrical and unsymmetrical donor-substituted BTDs.<sup>[6]</sup> In this contribution we wish to report the synthesis, photophysical and reversible mechanochromic response of dipyriddyamine substituted unsymmetrical BTD. The design of the dipyriddyamine substituted unsymmetrical BTD is based on the following considerations: 1) possibility of potential intermolecular hydrogen bonding interactions *via* the *N*-atoms of dipyriddyamine unit. 2) The orientation of the two pyridyl rings of the dipyriddyamine unit can provide twisted arrangement to endorse non-parallel packing in solid state. 3) The incorporation of BTD acceptor results in strongly luminescent systems.<sup>[7]</sup>

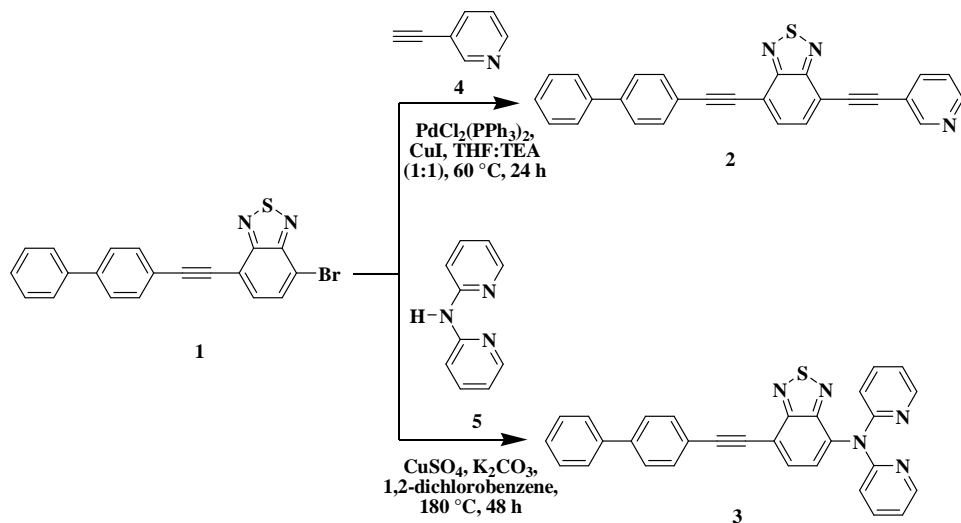
#### 7.2. Results and discussion

The synthetic route to the push–pull BTDs **2** and **3** are shown in Scheme 2. The Pd-catalyzed Sonogashira cross-coupling reaction of dibromo-BTD with 4-ethynylbiphenyl resulted BTD **1** in 52% yield (Scheme 1).



**Scheme 1** Synthesis of BTD **1**.

In order to study the effect of orientation of pyridyl rings on the mechanochromic behavior, we designed BTD **2** and **3** with acetylene linked pyridyl unit and *N*-linked dipyridylamine unit respectively. The Pd-catalyzed Sonogashira cross-coupling reaction of BTD **1** with 3-ethynylpyridine resulted BTD **2** in 78% yield. The Ullmann coupling reaction of BTD **1** with dipyridylamine in the presence of  $\text{CuSO}_4$  and  $\text{K}_2\text{CO}_3$  in dichlorobenzene at 180 °C for 48 h resulted BTD **3** in 65% yield. The BTDs **2** and **3** were well characterized by  $^1\text{H}$ ,  $^{13}\text{C}$  NMR and HRMS techniques.

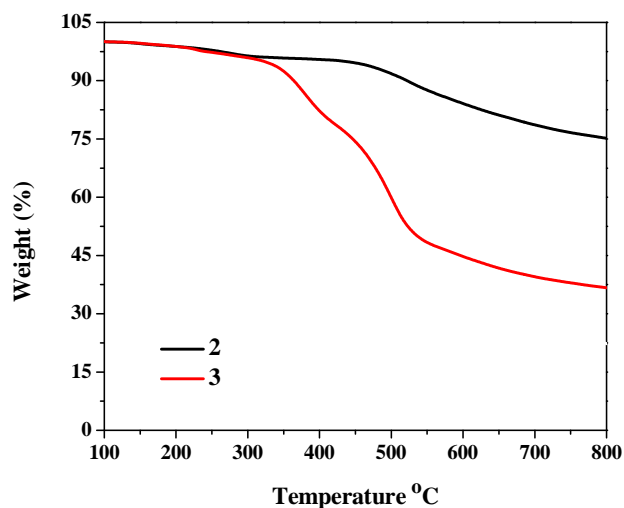


**Scheme 2** Synthesis of BTDs **2** and **3**.

### 7.3. Thermal properties

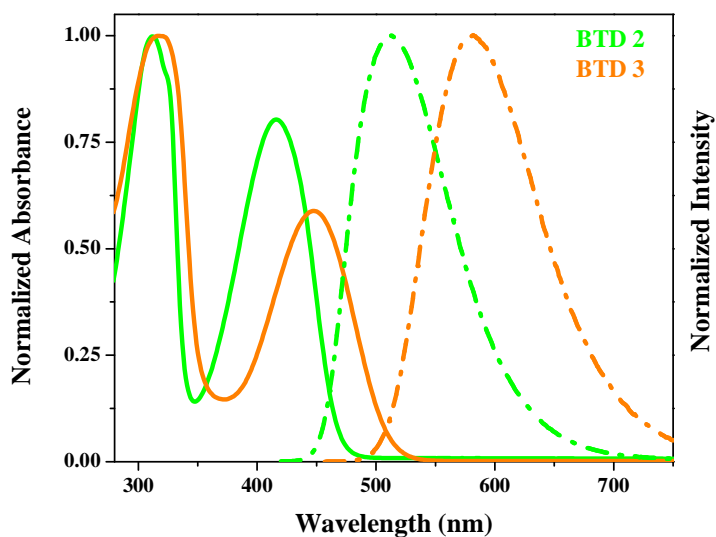
The thermal stability of the push–pull BTDs **2** and **3** were studied using thermogravimetric analysis (TGA) at a heating rate of 10 °C min<sup>-1</sup>, under nitrogen atmosphere (Figure 7.1.). The decomposition temperatures (5% weight loss) for

BTD **2** and **3** were 430 °C and 321 °C respectively. The pyridyl-substituted BTD **2** exhibits higher thermal stability compared to dipyridylamine-substituted BTD **3**.



**Figure 7.1.** TGA plots of **2** and **3** at a heating rate of 10 °C min<sup>-1</sup>, under nitrogen atmosphere.

#### 7.4. Photophysical propeties



**Figure 7.2.** Electronic absorption and emission spectra of BTD **2** and **3**.

The electronic absorption and emission spectra of BTDs **2** and **3** were recorded in dichloromethane at room temperature (Figure 7.2.) and the data are compiled in Table 7.1. The BTDs **2** and **3** exhibit strong absorption between 300–



320 nm, corresponding to  $\pi \rightarrow \pi^*$  transition and a charge transfer (CT) band between 399–450 nm.<sup>[8]</sup> There is a large red shift (~65 nm) in the low energy transition of BTD **3** compared to BTD **2**, reflecting strong electronic communication between dipyridylamine and BTD moiety. The BTDs **2** and **3** emit green and orange fluorescence at the wavelength of ~513 nm and ~578 nm respectively.


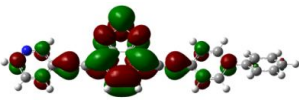

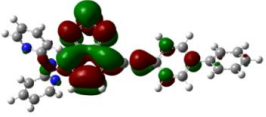
**Table 7.1.** Photophysical data of BTD **2** and **3**.

BTD	Photophysical data				
	In dichloromethane solution				
	$\lambda_{\text{abs}}$ (nm)	$\epsilon$ (M <sup>-1</sup> cm <sup>-1</sup> )	$\lambda_{\text{em}}$ (nm)	Stoke's shift (nm)	$\Phi_F$
<b>2</b>	312	50437	513	96	0.47
	417	40382			
<b>3</b>	319	90273	578	130	0.14
	448	52841			

$\Phi_F$  calculated with Quinine sulfate ( $\Phi = 0.55$ ) in 0.1M H<sub>2</sub>SO<sub>4</sub> as standard.

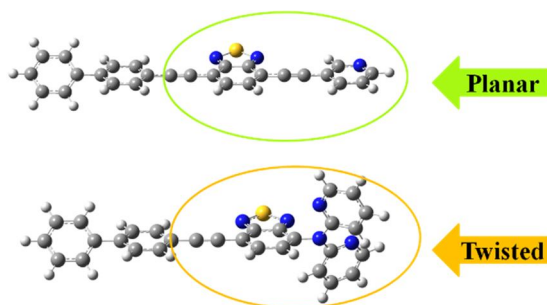
## 7.5. Theoretical calculations

In order to explore the electronic structure of the BTDs **2** and **3** density functional theory (DFT) calculations were performed at the B3LYP/6-31G\*\* level. In BTD **2** and **3** the HOMO is localized on the electron donating biphenyl, pyridyl, dipyridylamine and the hydrocarbon portion of the BTD unit and LUMO on the electron withdrawing BTD unit reflecting strong donor–acceptor interaction (Figure 7.3.). The incorporation of dipyridylamine in BTD **3** results in lowering of the HOMO–LUMO gap, leading to red shift of the absorption spectrum.

BTD	HOMO	LUMO
2	 -5.51 eV	 -2.72 eV
3	 -5.17 eV	 -2.48 eV

**Figure 7.3.** HOMO and LUMO frontier orbitals of BTD **2** and **3**.

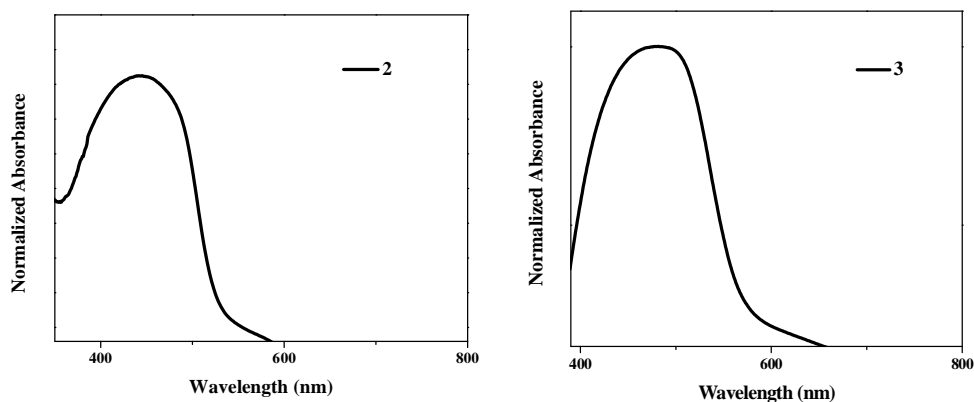
DFT optimized structure of BTD **2** and **3** exhibits planar and non-planar alignment of the pyridyl rings with respect to BTD core respectively. This indicates that the incorporation of dipyridylamine results in twisted arrangement to endorse non-parallel packing in solid state (Figure 7.4.).



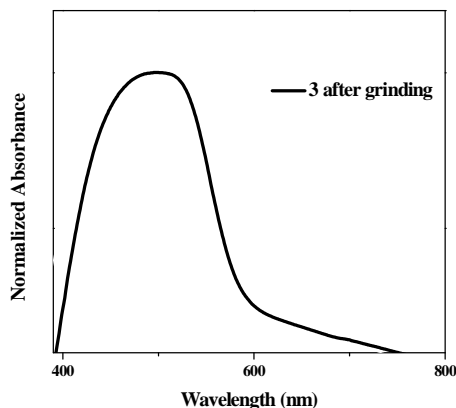
**Figure 7.4.** DFT optimized structure of BTDs **2** (top) and **3** (bottom).

## 7.6. Mechanochromic properties

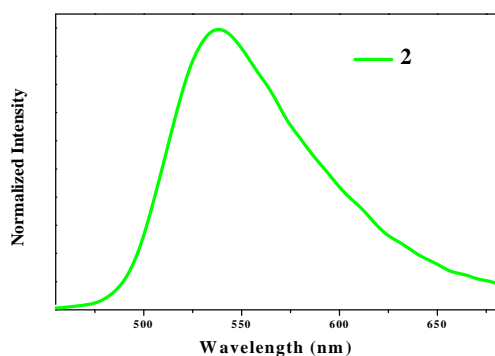
The mechanochromic properties of unsymmetrical BTDs **2** and **3** were studied by the absorption and emission studies. The crystalline samples of BTDs **2** and **3** absorb at 443 and 481 nm respectively (Figure 7.5.). Upon grinding, the sample of BTD **2** shows no change in the absorption behavior whereas BTD **3** exhibits red-shifted absorption at 498 nm (Figure 7.6).



**Figure 7.5.** Normalized absorbance of the solid sample of BTD **2** and **3** as prepared.



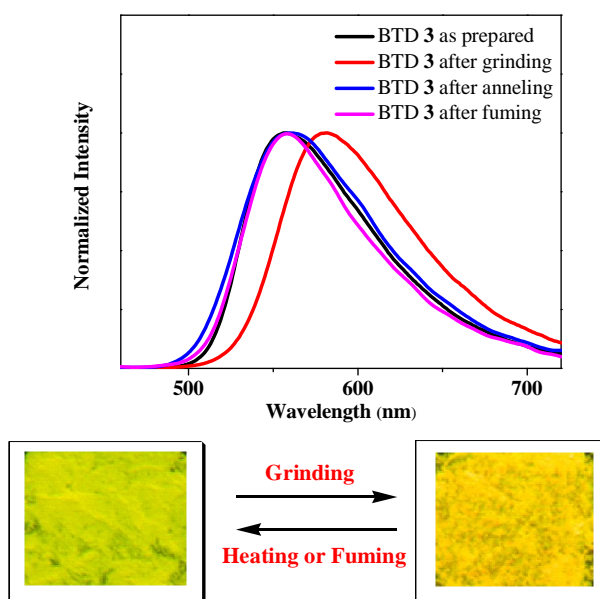
**Figure 7.6.** Normalized absorbance of the sample of BTD **3** after grinding.



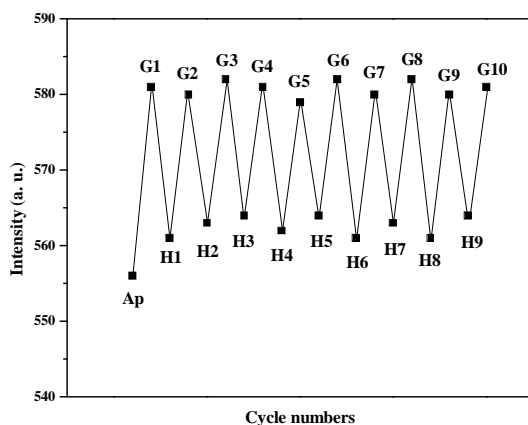
**Figure 7.7.** Normalized emission of the solid sample of BTD **2**.

The solid samples of BTD **2** show greenish-yellow emission at 538 nm whereas BTD **3** exhibits yellow emission at 556 nm (Figure 7.7. and 7.8.). The

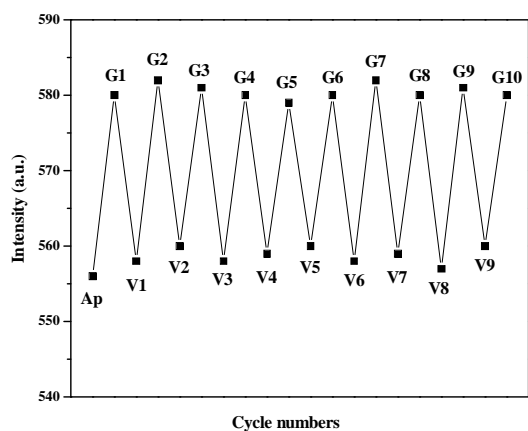
solid sample of BTD **3** upon grinding using a spatula or a pestle exhibits drastic change in the emission behavior and the emission peak at 556 nm was red shifted to 581 nm (Figure. 7.8.). The solid sample of BTD **2** exhibits no change in the emission upon grinding. The mechanochromic effect of BTD **3** can be reverted to its original color either by annealing or fuming with dichloromethane vapor (Figure 7.8). The grinded sample of BTD **3** upon annealing at 150 °C for 35 min or fuming with dichloromethane vapor for 4 min restored the original yellow emission (Figure 7.8., 7.9 and 7.10).



**Figure 7.8.** Solid state emission spectra and fluorescence colour change induced upon grinding the solid sample of BTD **3**.



**Figure 7.9.** BTD **3** as prepared (**Ap**) and repeated switching of the solid-state fluorescence by repeated grinding (**G**) and heating (**H**) cycles.



**Figure 7.10.** BTD **3** as prepared (**Ap**) and repeated switching of the solid-state fluorescence by repeated grinding (**G**) and fuming (**V**) cycles.

## 7.7. X-ray analysis

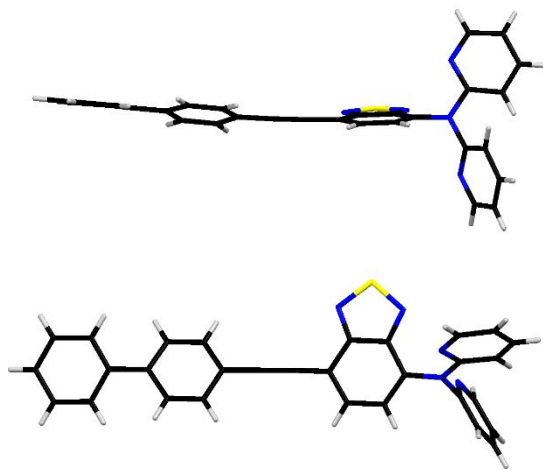
The single crystal of BTD **3** was obtained *via* slow diffusion of ethanol into the dichloromethane solution at room temperature. BTD **3** crystallizes in the monoclinic space group  $P2_1/c$  and exhibits twisted structural arrangement (Figure 7.11. and 7.12.). The dihedral angle between the planes containing the BTD core and the pyridyl rings of dipyridylamine unit was found to be  $69.90^\circ$  and  $82.82^\circ$ . The crystal data, important bond lengths and bond angles are listed in the Table 7.2 and 7.3.

**Table 7.2.** Crystal data and structure refinement for **BTD 3**.

<b>Empirical formula</b>	C <sub>30</sub> H <sub>19</sub> N <sub>5</sub> S
<b>Formula weight</b>	481.56
<b>Temperature</b>	273(2) K
<b>Wavelength(A)</b>	1.5418 Å
<b>Crystal system, space group</b>	Monoclinic, <i>P</i> 2 <sub>1</sub> / <i>c</i>
<b><i>a</i>/ (Å)</b>	20.8735(5)
<b><i>b</i>/ (Å)</b>	11.8292(3)
<b><i>c</i>/ (Å)</b>	9.8383(3)
<b><math>\alpha</math> / (°)</b>	90
<b><math>\beta</math> / (°)</b>	101.978(3)
<b><math>\gamma</math> / (°)</b>	90
<b>Volume</b>	2376.35(11) Å <sup>3</sup>
<b>Z, Calculated density (mg m<sup>-3</sup>)</b>	4, 1.346
<b>Absorption coefficient /(mm<sup>-1</sup>)</b>	1.438
<b>F(000)</b>	1000
<b>Crystal size</b>	0.22 x 0.18 x 0.14 mm
<b><math>\theta</math> range for data collection/(°)</b>	4.32 to 71.98
<b>Limiting indices</b>	-25<= <i>h</i> <=24, -14<= <i>k</i> <=10, -12<= <i>l</i> <=11
<b>Reflections collected / unique</b>	15657 / 4584 [R(int) = 0.0256]
<b>Completeness to theta</b>	$\theta$ = 25.00; 99.5%
<b>Absorption correction</b>	Semi-empirical from equivalents
<b>Max. and min. transmission</b>	0.8240 and 0.7426
<b>Refinement method</b>	Full-matrix least-squares on F <sup>2</sup>
<b>Data / restraints / parameters</b>	4584 / 0 / 400
<b>Goodness-of-fit on F<sup>2</sup></b>	1.057
<b>Final R indices [I&gt;2sigma(I)]</b>	R1 = 0.0452, wR2 = 0.1274
<b>R indices (all data)</b>	R1 = 0.0529, wR2 = 0.1393
<b>Largest diff. peak and hole (eÅ<sup>-3</sup>)</b>	0.312 and -0.397
<b>CCDC Number</b>	1020099

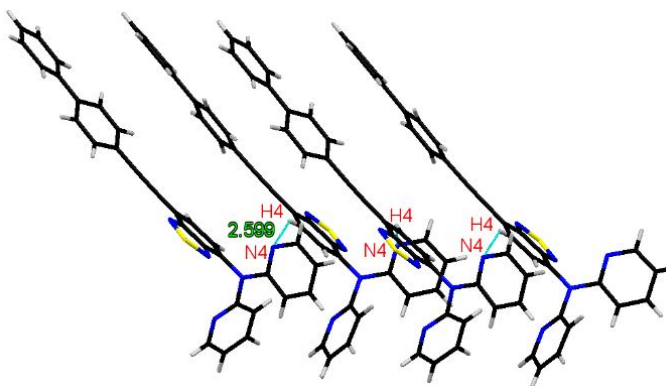
**Table 7.3.** Selected bond length and bond angle of BTD **3**.

Bond lengths [Å]		Bond angles [°]	
S(1)-N(2)	1.6035(18)	N(2)-S(1)-N(1)	101.64(8)
S(1)-N(1)	1.6086(17)	C(1)-N(1)-S(1)	105.76(12)
N(1)-C(1)	1.341(2)	C(6)-N(2)-S(1)	106.07(12)
N(2)-C(6)	1.339(2)	N(1)-C(1)-C(2)	126.49(15)
C(2)-N(5)	1.416(2)	N(1)-C(1)-C(6)	113.32(15)
C(21)-N(5)	1.429(2)	C(3)-C(2)-N(5)	121.05(16)
C(21)-N(3)	1.320(2)	N(5)-C(2)-C(1)	121.69(15)
C(25)-N(3)	1.347(3)	N(2)-C(6)-C(5)	125.63(15)
C(26)-N(4)	1.336(2)	N(2)-C(6)-C(1)	113.21(15)
C(26)-N(5)	1.394(2)	N(3)-C(21)-C(22)	123.75(17)
N(4)-C(30)	1.350(3)	N(3)-C(21)-N(5)	115.47(15)
		C(22)-C(21)-N(5)	120.77(17)
		N(3)-C(25)-C(24)	123.5(2)
		N(3)-C(25)-H(25)	118.3
		N(4)-C(26)-C(27)	123.23(16)



**Figure 7.11.** Crystal structure of **3** side view (above) and top view (below).

The packing diagram of BTD **3** exhibits H-bonding interaction N4...H4 (2.59 Å) between the dipyridylamine nitrogen (N4) and the BTD hydrogen H4. The H-bonding interaction between the dipyridylamine and BTD results in twisted arrangement in the crystalline state.

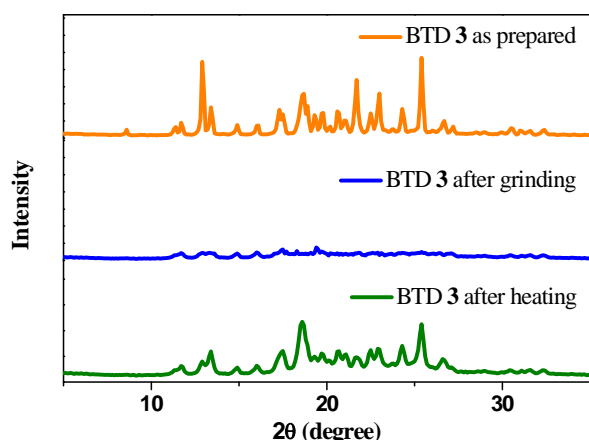


**Figure 7.12.** Packing diagram of BTD **3** along the *b*-axis.

### 7.7. PXRD analysis

In order to gain insight into the mechanism of mechanochromism in BTD **3** powder X-ray diffraction (PXRD) analysis was performed (Figure 7.13.). The BTD **3** exhibit intense and sharp diffraction peaks before grinding reflecting the crystalline character. The BTD **3** sample show very weak diffraction peaks upon grinding suggesting the transition to amorphous state.<sup>[9]</sup> The ground sample of BTD **3** exhibits sharp diffraction peaks when subjected to heating or fuming indicating the transformation to the crystalline phase. This study clearly concludes that the mechanochromism in BTD **3** is associated with the morphology change from the crystalline state to the amorphous state and *vice versa*.





**Figure 7.13.** Powder-XRD patterns of BTD 3

## 7.8. Experimental section

Chemicals were used as received unless otherwise indicated. All oxygen or moisture sensitive reactions were performed under nitrogen/argon atmosphere.  $^1\text{H}$  NMR (400 MHz), and  $^{13}\text{C}$  NMR (100 MHz) spectra were recorded on the Bruker Avance (III) 400 MHz instrument by using  $\text{CDCl}_3$ . Chemical shifts for  $^1\text{H}$  NMR spectra are reported in delta ( $\delta$ ) units, expressed in parts per million (ppm) downfield from tetramethylsilane using residual protonated solvent as an internal standard  $\{\text{CDCl}_3, 7.26 \text{ ppm}\}$ . Chemical shifts for  $^{13}\text{C}$  NMR spectra are reported in delta ( $\delta$ ) units, expressed in parts per million (ppm) downfield from tetramethylsilane using the solvent as internal standard  $\{\text{CDCl}_3, 77.0 \text{ ppm}\}$ . The  $^1\text{H}$  NMR splitting patterns have been described as “s, singlet; d, doublet; t, triplet and m, multiplet”. Thermogravimetric analyses were performed on the Metler Toledo Thermal Analysis system. UV-visible absorption spectra were recorded on a Carry-100 Bio UV-visible Spectrophotometer. Emission spectra were taken in a fluoromax-4p fluorimeter from Horiba Yovin (model: FM-100). The excitation and emission slits were 2/2 nm for the emission measurements. All of the measurements were done at 25 °C. The density functional theory (DFT) calculation were carried out at the B3LYP/6-31G\*\* level for C, N, S, H in the Gaussian 09 program. HRMS was recorded on Bruker-Daltonics, micrOTOF-Q II mass spectrometer. The XRD measurements were performed using Rigaku SmartLab, Automated Multipurpose

X-ray diffractometer. The X-rays were produced using a sealed tube and the wavelength of the X-ray was 0.154 nm (Cu K-alpha).

#### **Preparation of benzothiazole 1.**

To a stirred solution of the 4-ethynylbiphenyl (1 mmol), and dibromo-BTD **1** (1 mmol) in THF, and TEA (1:1, v/v) were added  $\text{PdCl}_2(\text{PPh}_3)_2$  (10 mg, 0.014 mmol) and CuI (2 mg, 0.01 mmol) under an argon flow at room temperature. The reaction mixture was stirred for 12 h at 60 °C, and then cooled to room temperature. The solvent was then evaporated under reduced pressure, and the mixture was purified by  $\text{SiO}_2$  chromatography with DCM/hexane (1:3, v/v), followed by recrystallization in DCM:hexane (1:3) to obtain **1**. Pale yellowish solid (203 mg, Yield: 52%):  $^1\text{H}$  NMR (400 MHz,  $\text{CDCl}_3$ ,  $\delta$  in ppm): 7.85 (d, 1H,  $J = 7.5$  Hz), 7.75–7.72 (m, 2H), 7.68 (d, 1H, 7.5 Hz), 7.65–7.62 (m, 4H), 7.49–7.44 (m, 2H), 7.40–7.36 (m, 1H);  $^{13}\text{C}$  NMR (100 MHz,  $\text{CDCl}_3$ ,  $\delta$  in ppm): 154.1, 153.1, 141.8, 140.1, 132.7, 132.4, 132.0, 128.9, 127.8, 127.1, 127.0, 121.2, 116.7, 114.6, 96.8, 85.2; HRMS (ESI-TOF)  $m/z$  calcd for  $\text{C}_{20}\text{H}_{11}\text{BrN}_2\text{S} + \text{Na}$ : 412.9719  $[\text{M} + \text{Na}]^+$ , found 412.9683  $[\text{M} + \text{Na}]^+$ .

#### **Preparation of benzothiadiazole 2.**

To a stirred solution of the 3-ethynylpyridine (1 mmol), **1** (1 mmol) in THF, and TEA (1:1, v/v) were added  $\text{PdCl}_2(\text{PPh}_3)_2$  (10 mg, 0.014 mmol) and CuI (2 mg, 0.01 mmol) under an argon flow at room temperature. The reaction mixture was stirred for 24 h at 60 °C, and then cooled to room temperature. The solvent was then evaporated under reduced pressure, and the mixture was purified by  $\text{SiO}_2$  chromatography with DCM/hexane (2:2, v/v) to obtain **2**. Yellowish green solid (322 mg, Yield: 78%):  $^1\text{H}$  NMR (400 MHz,  $\text{CDCl}_3$ ,  $\delta$  in ppm): 8.91 (s, 1H), 8.63 (m, 1H), 7.98–7.95 (m, 1H), 7.86–7.82 (m, 2H), 7.77–7.74 (m, 2H), 7.67–7.63 (m, 4H), 7.49–7.45 (m, 2H), 7.41–7.34 (m, 2H);  $^{13}\text{C}$  NMR (100 MHz,  $\text{CDCl}_3$ ,  $\delta$  in ppm): 154.3, 154.2, 152..5, 149.2, 141.9, 140.1, 138.7, 132.8, 132.4, 132.2, 128.9, 127.8, 127.1, 127.0, 123.1, 121.2, 119.8, 117.9, 116.2, 97.9, 93.6, 88.4, 85.9, HRMS (ESI-TOF)  $m/z$  calcd for  $\text{C}_{27}\text{H}_{15}\text{N}_3\text{S} + \text{H}$ : 414.1059  $[\text{M} + \text{H}]^+$ , found 414.1058  $[\text{M} + \text{H}]^+$ .

#### **Preparation of benzothiadiazole 3.**

2,2'-Dipyridylamine (4.0 mmol), **1** (3.0 mmol), anhydrous potassium carbonate (12.0 mmol), cupric sulfate (0.63 mmol), and 1,2-dichlorobenzene (10 mL) were added to a round bottom flask, degassed, and flushed with N<sub>2</sub>. The reaction mixture was heated at 180 °C for 48 h, and then cooled to room temperature. Dichloromethane and water were added. The organic phase was washed with water and then dried over Na<sub>2</sub>SO<sub>4</sub>. After removal of the solvent, the residue was purified by SiO<sub>2</sub> column chromatography, using DCM: Ethylacetate (9:1) mixture as eluent to afford **3**. Yellow solid (313 mg, Yield: 65%); <sup>1</sup>H NMR (400 MHz, (CDCl<sub>3</sub>, δ in ppm): 8.30-8.28 (m, 2H), 7.81 (d, 1H, *J* = 7.8 Hz), 7.75-7.72 (m, 2H), 7.66-7.61 (m, 6H), 7.49-7.45 (m, 2H), 7.41-7.35 (m, 2H), 7.14-7.12 (m, 2H), 7.03-6.99 (m, 2H); <sup>13</sup>C NMR (100 MHz, CDCl<sub>3</sub>, δ in ppm): 157.5, 156.1, 151.5, 148.6, 141.4, 140.3, 137.8, 137.6, 133.3, 132.3, 128.9, 127.7, 127.04, 127.0, 125.6, 121.7, 119.1, 117.2, 114.2, 95.5, 86.1; HRMS (ESI-TOF) *m/z* calcd for C<sub>30</sub>H<sub>19</sub>N<sub>5</sub>S + H: 482.143 [M + H]<sup>+</sup>, found 482.143 [M + H]<sup>+</sup>.

## 7.9. Conclusions

In summary unsymmetrical push–pull benzothiadiazoles **2** and **3** were synthesized by the Pd-catalyzed Sonogashira and Cu-catalyzed Ullmann coupling reactions. The photophysical, computational and single crystal X-ray studies reveal that the planar and non-planar orientation of the pyridyl rings with respect to the benzothiadiazole core in BTD **2** and **3** effectively alters the mechanochromic behavior. The dipyridylamine-substituted BTD **3** shows reversible mechanochromic response between yellow (crystalline state) and orange (amorphous state) color. The results obtained in this study will help to understand the design criteria and the mechanism behind mechanochromism. Currently our group is synthesizing BTD based new mechanochromic materials with different color contrast for various applications.

## 7.10. References

- [1] (a) Chi Z., Zhang X., Xu B., Zhou X., Ma C., Zhang Y., Liua S., Xu J. (2012), Recent advances in organic mechanofluorochromic materials,

- Chem. Soc. Rev.*, 41, 3878-3896 (DOI: 10.1039/C2CS35016E). (b) Nagura K., Saito S., Yusa, H., Yamawaki H., Fujihisa H., Sato H., Shimoikeda Y., Yamaguchi S. (2013), Distinct responses to mechanical grinding and hydrostatic pressure in luminescent chromism of tetrathiazolylthiophene, *J. Am. Chem. Soc.*, 135, 10322-10325 (DOI: 10.1021/ja4055228). (c) Li R., Xiao S., Li Y., Lin Q., Zhang R., Zhao J., Yang C., Zou K., Li D., Yi T. (2014), Polymorphism-dependent and piezochromic luminescence based on molecular packing of a conjugated molecule, *Chem. Sci.*, 5, 392-3928 (DOI: 10.1039/C4SC01243G). (d) Zhao N., Yang Z., Lam J. W. Y., Sung H. H. Y., Xie N., Chen S., Su H., Gao M., Williams I. D., Wong K. S., Tang B. Z. (2012), Benzothiazolium-functionalized tetraphenylethene: an AIE luminogen with tunable solid-state emission, *Chem. Commun.*, 48, 8637-8639 (DOI: 10.1039/C2CC33780K). (e) Wang J., Mei J., Hu R., Sun J. Z., Qin A., Tang B. Z. (2012), Click synthesis, aggregation-induced emission, E/Z isomerization, self-organization, and multiple chromisms of pure stereoisomers of a tetraphenylethene-cored luminogen, *J. Am. Chem. Soc.*, 134, 9956-9966 (DOI: 10.1021/ja208883h).
- [2] (a) Kwon M. S., Gierschner J., Yoon S. J., Park S. Y. (2012), Unique piezochromic fluorescence behavior of dicyanodistyrylbenzene based donor-acceptor-donor triad: mechanically controlled photo-induced electron transfer (eT) in molecular assemblies, *Adv. Mater.*, 24, 5487-5492 (DOI: 10.1002/adma.201202409). (b) Qi Q., Zhang J., Xu B., Li B., Zhang S. X.-A., Tian W. (2013), Mechanochromism and polymorphism-dependent emission of tetrakis(4-(dimethylamino)phenyl)ethylene, *J. Phys. Chem. C*, 117, 24997-25003 (DOI: 10.1021/jp407965a).
- [3] (a) Zhao N., Li M., Yan Y. L., Lam J. W. Y., Zhang Y. L., Zhao Y. S., Wong K. S., Tang, B. Z. (2013), A tetraphenylethene-substituted pyridinium salt with multiple functionalities: synthesis, stimuli-responsive emission, optical waveguide and specific mitochondrion imaging, *J. Mater. Chem. C*, 1, 4640-4646 (DOI: 10.1039/C3TC30759J). (b) Zhang X., Chi Z.,

- Zhang Y., Liu S., Xu J. (2013), Recent advances in mechanochromic luminescent metal complexes, *J. Mater. Chem. C*, 1, 3376-3390 (DOI: 10.1039/C3TC30316K). (c) Tzeng B.-C., Chang T.-Y., Wei S.-L., Sheu H.-S., Reversible phase transformation and mechanochromic luminescence of Zn<sup>II</sup>-dipyridylamide-based coordination frameworks, *Chem.–Eur. J.*, 18, 5105-5112 (DOI: 10.1002/chem.201103405). (d) Han T., Zhang Y., Feng X., Lin Z., Tong B., Shi J., Zhi J., Dong Y. (2013), Reversible and hydrogen bonding-assisted piezochromic luminescence for solid-state tetraaryl-butadiene, *Chem. Commun.*, 49, 7049-7051 (DOI: 10.1039/C3CC42644K). (e) Tzeng B.-C., Chang T.-Y., Sheu H.-S. (2010), Reversible phase transformation and luminescent mechanochromism of Zn<sup>II</sup>-based coordination frameworks containing a dipyridylamide ligand, *Chem.–Eur. J.*, 16, 9990-9993 (DOI: 10.1002/chem.201001346). (f) Dou C., Chen D., Iqbal J., Yuan Y., Zhang H., Wang Y. (2011), Multistimuli-responsive benzothiadiazole-cored phenylene vinylene derivative with nanoassembly properties, *Langmuir*, 27, 6323-6329 (DOI: 10.1021/la200382b). (g) Zhang X., Ma Z., Yang Y., Zhang X., Jia X., Wei Y. (2014), Fine-tuning the mechanofluorochromic properties of benzothiadiazole-cored cyano-substituted diphenylethene derivatives through D–A effect, *J. Mater. Chem. C*, 2, 8932-8938 (DOI: 10.1039/C4TC01457J).
- [4] Misra R., Jadhav T., Dhokale B., Mobin S. M. (2014), Reversible mechanochromism and enhanced AIE in tetraphenylethene substituted phenanthroimidazoles, *Chem. Commun.*, 50, 9076-9078 (DOI: 10.1039/C4CC02824D).
- [5] Chen S., Li Y., Yang W., Chen N., Liu H., Li Y. (2010), Synthesis and tuning optical nonlinear properties of molecular crystals of benzothiadiazole, *J. Phys. Chem. C*, 114, 15109-15115 (DOI: 10.1021/jp103159b).
- [6] (a) Misra R., Gautam P., Jadhav T., Mobin S. M. (2013), Donor–acceptor ferrocenyl-substituted benzothiadiazoles: synthesis, structure, and properties, *J. Org. Chem.*, 78, 4940-4948 (DOI: 10.1021/jo4005734). (b)

- Misra R., Gautam P., Mobin S. M. (2013), Aryl-substituted unsymmetrical benzothiadiazoles: synthesis, structure, and properties, *J. Org. Chem.*, 78, 12440-12452 (DOI: 10.1021/jo402111q). (c) Misra R., Gautam P. (2014), Tuning of the HOMO–LUMO gap of donor-substituted symmetrical and unsymmetrical benzothiadiazoles, *Org. Biomol. Chem.*, 12, 5448–5457 (DOI: 10.1039/C4OB00629A). (d) Misra R., Gautam P., Sharma R., Mobin S. M. (2013), Donor– $\pi$ –acceptor– $\pi$ –donor ferrocenyl benzothiadiazoles: synthesis, structure, and properties, *Tetrahedron Lett.*, 54, 381-383 (DOI:10.1016/j.tetlet.2012.11.016).
- [7] Moonsin P., Prachumrak N., Namuangruk S., Jungsuttiwong S., Keawin T., Sudyoadsuk T., Promarak V. (2013), Novel bis(fluorenyl)benzothiadiazole-cored carbazole dendrimers as highly efficient solution-processed non-doped green emitters for organic light-emitting diodes, *Chem. Commun.*, 49, 6388-6390 (DOI: 10.1039/C3CC42931H).
- [8] (a) Zhang H., Wan X., Xue X., Li Y., Yu A., Chen Y. (2010), Selective tuning of the HOMO–LUMO gap of carbazole-based donor–acceptor–donor compounds toward different emission colors, *Eur. J. Org. Chem.*, 1681-1687 (DOI: 10.1002/ejoc.200901167). (b) Kato S., Matsumoto T., Shigeiwa M., Gorohmaru H., Maeda S., Ishi-i T., Mataka S. (2006), Novel 2,1,3-benzothiadiazole-based red-fluorescent dyes with enhanced two-photon absorption cross-sections, *Chem. Eur. J.*, 12, 2303-2317 (DOI: 10.1002/chem.200500921). (c) Kato S., Matsumoto T., Ishi-i T., Thiemann T., Shigeiwa M., Gorohmaru H., Maeda S., Yamashita Y., Mataka S. (2004), Strongly red-fluorescent novel donor– $\pi$ –bridge–acceptor– $\pi$ –bridge–donor (D– $\pi$ –A– $\pi$ –D) type 2,1,3-benzothiadiazoles with enhanced two-photon absorption cross-sections, *Chem. Commun.*, 2342-2343 (DOI: 10.1039/B410016F). (d) Li Y., Liu T., Liu H., Tian M.-Z., Li Y. (2014), Self-assembly of intramolecular charge-transfer compounds into functional molecular systems, *Acc. Chem. Res.*, 47, 1186-1198 (DOI: 10.1021/ar400264e).

- [9] Xue P., Yao B., Sun J., Xu Q., Chen P., Zhang Z., Lu R. (2014), Phenothiazine-based benzoxazole derivatives exhibiting mechanochromic luminescence: the effect of a bromine atom, *J. Mater. Chem. C*, 2, 3942-3950 (DOI: 10.1039/C4TC00061G).

## Chapter 8

### Conclusions and future scope

#### 8.1. Conclusions

The benzothiadiazole (BTD) unit is a strong acceptor and its derivatives exhibit strong absorption.<sup>[1]</sup> The photonic properties of BTD derivatives can be tuned by variation in the nature of substituents.<sup>[2]</sup> We have functionalized BTD with various donor/acceptor units in symmetrical and unsymmetrical fashion to tune photonic properties.<sup>[3]</sup>

In Chapter 3, the BTDs were functionalized with ferrocenyl donor unit at the 4- and 7-positions through various  $\pi$ -linkers. The photonic properties of ferrocenyl-substituted BTDs are a function of the  $\pi$ -linkers between the BTD acceptor and the ferrocene donor. The nature of  $\pi$ -linker determine the strength of D–A and charge-transfer interaction.<sup>[4]</sup>

In Chapter 4, symmetrical and unsymmetrical ferrocenyl-substituted BTDs were designed and synthesized. The photophysical, and electrochemical behavior of the ferrocenyl-substituted benzothiadiazoles show strong donor–acceptor interaction. These D–A systems exhibit significant perturbation in the photonic properties upon modulation of the  $\pi$ -spacer between the donor and the acceptor units, and increasing the number of acceptor units. The results indicate that increase in the number of acceptor benzothiadiazole unit, results in the lowering of the energy gap, which leads to the bathochromic shift of the absorption spectrum.<sup>[5]</sup>

In Chapter 5, a series of aryl-substituted unsymmetrical benzothiadiazole derivatives were designed and synthesized. The photophysical and electrochemical properties show strong electronic communication. The enhancement of conjugation *via* a  $\pi$ -bridge resulted in the red shift of the absorption bands in these aryl-substituted BTDs. The incorporation of the 1,1,4,4-tetracyanobuta-1,3-diene group in benzothiadiazoles results in significant lowering of the HOMO–LUMO gap and enhanced thermal stability. Our results provide the rationale to design low HOMO–LUMO gap materials for various optoelectronic applications.<sup>[6]</sup>



In chapter 6, a series of symmetrical and unsymmetrical donor-substituted benzothiadiazoles were synthesized. The number and nature of acceptor units perturbs the photonic properties, HOMO–LUMO gap and thermal stability of the benzothiadiazoles. The electronic absorption and computational calculation indicates substantial lowering of the HOMO–LUMO gap by the incorporation of cyano-based dicyanoquinodimethane (DCNQ) and tetracyanobutadiene (TCBD) groups in the benzothiadiazoles. The TCBD and DCNQ linkage of donor-substituted benzothiadiazole facilitates the reduction of the acceptor BTD unit and results in non-emissive nature of these molecular systems, which confirms the strong donor–acceptor interaction. The thermal stability of the benzothiadiazoles can be enhanced by the incorporation of a planar carbazole donor, single TCBD or DCNQ linkage.<sup>[7]</sup>

In chapter 7, unsymmetrical push–pull benzothiadiazoles were synthesized. The photophysical, computational and single crystal X-ray studies reveal that the planar and non-planar orientation of the pyridyl rings with respect to the benzothiadiazole core effectively alters the mechanochromic behavior. The incorporation of dipyridyl unit results in reversible mechanochromism with color contrast between yellow (crystalline state) and orange (amorphous state). The powder-XRD studies clearly concludes that the mechanochromism in dipyridylamine-substituted BTDs is associated with the morphology change from the crystalline state to the amorphous state and *vice versa*.<sup>[8]</sup>

## 8.2. Future scope

The thesis highlights a smart methodology for designing low HOMO–LUMO gap donor-acceptor small molecules. The HOMO–LUMO gap of the donor-acceptor molecules can be tuned by enhancement of conjugation length and increasing the donor/acceptor strength. The increase of donor/acceptor strength results in significant tuning of the optical (HOMO–LUMO) gap as compared to enhancement of conjugation length. The incorporation of strong cyano-based acceptor units (TCNE and TCNQ) in the donor–acceptor BTDs results strong intramolecular charge-transfer extending in the near infrared region. These strongly absorbing

small molecules are promising candidates for donor materials in bulk heterojunction solar cells.<sup>[9]</sup>

The BTD derivatives exhibit strong solid-state emission. The incorporation of non-planar dipyridylamine unit in the BTD core results in the phenomenon of reversible mechanochromism. The results can be utilized to design BTD-based molecules with reversible mechanochromic behavior.<sup>[10]</sup>

### 8.3. References

- [1] Chen S., Li Y., Yang W., Chen N., Liu H. and Li Y. (2010), Synthesis and Tuning Optical Nonlinear Properties of Molecular Crystals of Benzothiadiazole, *J. Phys. Chem. C*, 114, 15109-15115 (DOI: 10.1021/jp103159b).
- [2] Parker T. C., Patel D. G., Moudgil K., Barlow S., Risko C., Brédas, J.-L., Reynolds J. R., Marder S. R. (2015), Heteroannulated acceptors based on benzothiadiazole, *Mater. Horiz.*, 2, 22-36 (DOI: 10.1039/c4mh00102h).
- [3] Gautam, P., Maragani, R., Misra, R. (2015), Aryl-substituted symmetrical and unsymmetrical benzothiadiazoles, *RSC Adv.*, 5, 18288-18294 (DOI: 10.1039/C4RA15424J).
- [4] Misra R.,\* Gautam P., Sharma R., Mobin S. M. (2013), Donor- $\pi$ -acceptor- $\pi$ -donor ferrocenyl benzothiadiazoles: synthesis, structure, and properties, *Tetrahedron Lett.*, 54, 381-383 (DOI: 10.1016/j.tetlet.2012.11.016).
- [5] Misra R., Gautam P., Jadhav T., Mobin S. M. (2013), Donor-acceptor ferrocenyl-substituted benzothiadiazoles: synthesis, structure, and properties, *J. Org. Chem.*, 78, 4940-4948 (DOI: 10.1021/jo4005734).
- [6] Misra R., Gautam P., Mobin S. M. (2013), Aryl-substituted unsymmetrical benzothiadiazoles: synthesis, structure, and properties, *J. Org. Chem.*, 78, 12440-12452 (DOI: 10.1021/jo402111q).
- [7] Misra R.,\* Gautam P. (2014), Tuning of the HOMO-LUMO gap of donor-substituted symmetrical and unsymmetrical benzothiadiazoles, *Org. Biomol. Chem.*, 12, 5448-5457 (DOI: 10.1039/c4ob00629a).

- [8] Gautam P., Maragani, R., Mobin S. M., Misra R.\* (2014), Reversible mechanochromism in dipyridylamine-substituted unsymmetrical benzothiadiazoles, *RSC Adv.*, 4, 52526-52529 (DOI: 10.1039/C4RA09921D).
- [9] Gautam P., Misra R., Siddiqui S. A., Sharma G. D. (2015), Unsymmetrical donor-acceptor-acceptor- $\pi$ -donor type benzothiadiazole-based small molecule for a solution processed bulk heterojunction organic solar cell, *ACS Appl. Mater. Interfaces*, 7, 10283-10292 (DOI: 10.1021/acsami.5b02250).
- [10] Jadhav T., Dhokale B., Misra R. (2015), Effect of the cyano group on solid state photophysical behavior of tetraphenylethene substituted benzothiadiazoles. *J. Mater. Chem. C*, 3, 9063-9068 (DOI: 10.1039/C5TC01871D)